The copyright of this thesis vests in the author. No quotation from it or information derived from it is to be published without full acknowledgement of the source. The thesis is to be used for private study or non-commercial research purposes only.

Published by the University of Cape Town (UCT) in terms of the non-exclusive license granted to UCT by the author.

University of Cape Town

# The effect of particulate-induced hydrodynamic stress on the bioleaching of chalcopyrite by a *Sulfolobus* sp.

By

**Sashnee B. Raja**

University of Cape Town

Thesis presented for the Degree of

**DOCTOR OF PHILOSOPHY**

In the Department of Chemical Engineering

**UNIVERSITY OF CAPE TOWN**

December 2005

**The effect of particulate-induced hydrodynamic stress on the bioleaching of chalcopyrite by a *Sulfolobus* sp.**

**Sashnee B. Raja**

Department of Chemical Engineering, University of Cape Town, Private Bag Rondebosch, 7700

July 2005

In slurry reactors, hydrodynamic stress originates primarily from interactions between particles and cells in the reactor. This form of stress has been shown to negatively affect the process performance. The present study centres on slurry reactors utilised in the bioleaching industry. The micro-organisms employed in these processes include mesophilic micro-organisms and, more recently, thermophilic microbes which have shown much promise for improving the rate and extent of leaching particularly of recalcitrant minerals such as chalcopyrite. The drawback to using high temperature microbes is that these thermoacidophiles, unlike their mesophilic counterparts, are Gram-negative Archaea, not bacteria, hence they do not possess resilient cell walls and are more prone to hydrodynamic induced injury.

In an effort to gain a more in-depth understanding of the effects of hydrodynamic-mediated stress on thermophilic bioleaching micro-organisms, a chalcopyrite-quartzite system was considered for the present study. The effect of increasing hydrodynamic stress in the presence of 3 % chalcopyrite was investigated by (i) increasing quartzite concentration in units of 3 % by mass (0 through to 18 % w/v) at a constant impeller tip speed (1.97 m $s^{-1}$) and (ii) increasing the impeller tip speed (1.67 through to 2.13 m $s^{-1}$) at two quartzite loadings (0 and 9 % w/v. The process performance was monitored by measuring changes in pH, redox potential, and cell, iron and copper concentrations. The effect at a cellular level and the biological response was determined by observing changes in the morphology, metabolic activity, viability and protein composition of the cells with increasing hydrodynamic stress.

The results of the solids loadings and impeller speed experiments showed that bioleaching was progressively impaired with increasing quartzite loading and impeller speed. The overall rate and extent of microbial growth and iron and copper solubilisation declined with increasing hydrodynamic stress. The results for the solids loading experiments showed that the critical solids loading beyond which hydrodynamic stress had a significant effect on process performance was 9 % quartzite. At an 18 % quartzite loading the system approached failure. The results for the impeller speed experiments showed that there was a positive effect of an increase in metabolic activity of the culture on increasing impeller speed in the absence of quartzite and negative effect on increasing impeller speed at a 9 % quartzite loading. At a 9 % solids loading, the positive effects of improved mass transfer at the increased agitation rates were outweighed by the negative effects of increased hydrodynamic stress.

University of Cape Town

Further analysis of the growth and redox potential data from the solids loading experiments was conducted. Specific death rate constants were derived from the growth data and modelled as a function of solids loading yielding the following model:

$$k_{d1} = 4.61 \times 10^{-5} \Phi^{1.66}$$

Further analysis of redox potential data was conducted using the method of Rawlings *et al.* (1999), adapted by Petersen and Dixon (2005). The basis of the analysis is that the operating redox potential in a bioleaching system may be predicted if the leaching kinetics, described by the mineral ferric consumption and the microbial ferric supply, are known. In the present study the analysis method was able to predict the changes in the redox potential observed for the solids loading experiments successfully.

In addition to a decreased overall process performance, the effect of hydrodynamic stress was also examined at a cellular level. Selected samples from the solids loading and impeller speed experiments were analysed for changes in (i) morphology (ii) metabolic activity, (iii) membrane integrity and (iv) protein composition. Morphological changes observed using phase contrast and scanning electron microscopy included decreases in cell size and the presence of leaking and ghost cells. At the highest intensity of hydrodynamic stress (18 % quartzite) no healthy cells, only cell clumps and cell debris were observed. A quantitative analysis of cell size profiles showed a decrease in the mode of the cell-number based size distribution with increasing solids loading confirming the decrease in cell size with increased stress. The metabolic activity of the cell, measured by the oxygen utilisation rate of the cultures, also decreased on increasing the quartzite concentration. Furthermore, the metabolic activity at each solids loading declined with time due to nutrient limitation induced by passivation of the chalcopyrite. Differential fluorescence staining showed that cell membrane integrity was also compromised with increasing quartzite loading. The percentage of cells with permeabilised membranes increased on increasing the quartzite loading from 0 through to 18 % quartzite. A possible bio-response was identified in a preliminary investigation into the production of stress proteins induced by hydrodynamic stress. SDS PAGE analysis showed the up-regulation of a protein at 45 kDa when the solids loading was increased from 0 to 12 % quartzite.

In bioprocesses early warning signals of system failure are important. Assessment of the various indicators used in this study, at process performance, as well as at a cellular level, enabled the identification of possible early warning signals. Indicators such as metabolic activity and cell size which are sensitive to increasing stress conditions were identified for use as potential early indicators of reduced system performance.

University of Cape Town

**DECLARATION**

I declare that this thesis is my own, unaided work. It is being submitted for the Degree of Doctor of Philosophy in the University of Cape Town. It has not been submitted before for any degree or examination in any other university.

University of Cape Town

_____

_____ day of _____ 2005

**Dedicated to my family…**

My wonderful parents Mr and Mrs Raja, my precious sisters, Kalvenie akka and Kimenthra akka, my irreplaceable brother Ashwina, my aunt Rani, my patient and caring brother-in-law Sagaylan, my sister-in-law Shamanthree… and last, but certainly not least, to a very extraordinary young lady, my niece, Santhuri.

University of Cape Town

# Acknowledgements

**Thank you** to my supervisor Prof. Sue Harrison for her help and guidance in writing this thesis, for lessons learned and financial support.

To Shehnaaz and Giles, words cannot express my gratitude my dear friends. **Thank you!**

**Thank to my endearing friends** Andrew, Brendan, Elaine, Georgie, Gillian, Hannes, Jo-Ann, Madelyn, Nicola, Robert, Rose, Sanet, Vihitha and Zoë for laughs, love and years of endless support. A thank you also to Hilary and Robert Searby… for fine food and fine company!

**Thank you** Ritva for all your support and for being so patient and understanding.

**Thank you** Chris du Plessis and Dave Dew for the opportunity to work at the BHP Billtion laboratories and for looking after me so well during my stay.

**A heartfelt thank you to:**

Sue J (what would Bios do without you!), Jochen Petersen, Geoff Hansford, Peter Gaylard and Megan Clarke

**I would like to express my sincere gratitude to the following people:**

Alan and Chris at the Electron Microscope Unit at the University of Pretoria.
Dr Dirk Lang from the Anatomy Department at the University of Cape Town
Mrs Helen Divey from the Chemical Engineering Department at the University of Cape Town
Joachim and Peter from the Chemical Engineering workshop at the University of Cape Town
Dr Juwa Nyirenda from the Department of Statistics at the University of Cape Town
Dr George Lindsey from the Molecular and cellular Biology Department at the University of Cape Town
Mr Essack Abib from the Soil Science Department at the University of Kwa-Zulu Natal
Celeste and Di from the Microbiology department at the University of Kwa-Zulu Natal
Andrew Kessler
Ankia Wagner

**Thank you to**

The National Research foundation and BHP Billiton for financial support

**And finally to**

The Bio Group (past and present) and to those who dwell in the post-doc office…. Thank you guys!

University of Cape Town

# Summary

Microbial bioprocesses find wide application in the fine chemical and pharmaceutical industry, in mineral processing, remediation systems and in waste treatment to name a few. In these bioprocesses, cells are exposed to various physicochemical and mechanical stresses. Common examples of physicochemical stresses include changes in temperature (heat and cold shock), pH, osmolarity, redox potential, pressure, salinity, oxygen, nutrient starvation and product inhibition. In stirred tank reactors, mechanical stress (e.g. hydrodynamic stress) originates from mixing (through agitation) due to rotation of the impeller, aeration and the presence of solids. Mixing enables inter-phase mass transfer, suspension of solid particles and the promotion of heat transfer. Injury to cells during system operation occurs due to cell-cell, cell-vessel component, cell-bubble (bubble shear), cell-eddy (fluid shear) and in slurry systems, cell-solid interactions. Thus a fine balance is required in order to attain adequate mixing without inducing cell injury.

The present study centres on slurry reactors utilised in the bioleaching industry. In these solids-containing systems, cell-solid interactions prevail over fluid and bubble-shear. Increasing the solids loading in biological mineral slurry increases process productivity. However, increasing the solids loading can increase the hydrodynamic stress effect. Further to this, higher solids concentrations require increased agitation rates in order to attain complete solids suspension. Increased agitation rates up to a critical rate may have a positive influence on the metabolic activity of the micro-organisms due to improved mass transfer. However, above the critical rate the positive effect is outweighed by the increase in the solid-cell-solid collision frequency which contributes significantly towards hydrodynamic stress. Stress to cells has an effect at the process performance level as well as at the cellular level. In bioleach reactors, at the process performance level, investigators have observed decreases in the rate and extent of growth and metal solubilisation. While at the cellular level, changes in morphology, viability and cell envelope integrity were identified.

High temperature bioleaching processes are favoured over those operated at mesophilic temperature due to factors such as increased reaction rates at the higher temperatures. An understanding of the hydrodynamic stress capacity of the thermophilic micro-organisms is thus vital to the bioleaching industry. The resistance of micro-organisms to stress is primarily dictated by their physiology. Micro-organisms such as the mesophilic bioleaching bacteria, *Leptospirillum* sp. and *Acidithiobacillus* spp. possess true cell walls re-enforced by peptidoglycan and thus are less susceptible to hydrodynamic cell injury. The cells wall of the Gram-negative Archaea such as those used in high-temperature tank bioleaching processes, do not contain re-enforcing macromolecules, instead the cell wall, termed an S-layer, comprises only glycoproteins. Mesophilic tank leaching systems have been shown to fail at mineral loadings higher than 20 % (Rossi, 2001). Initially this

University of Cape Town

failure was attributed to the high oxygen demand of the system at the increased mineral loadings (Dispirito *et al.*, 1981; Bailey and Hansford, 1994; Loia, 1994) but later studies showed that the hydrodynamic stress due to the increased solids loading was the reason for reactor failure (Pearce, 1993; Deveci, 2002; Witne and Phillips, 2001). Thus, if the mesophilic bioleach systems utilising bacteria with re-enforced cell walls fail at solids concentrations above 20 % then it is expected that the thermophilic bioleach systems would fail at even lower solids loadings.

Previous work by Nemati and Harrison (2000) on the bioleaching of pyrite by the thermophilic archaeon, *Sulfolobus metallicus*, in a stirred reactor showed that increasing the pyrite concentration resulted in reduced process performance, and at the highest solids loading tested (18 % w/v pyrite) reactor failure occurred. Sissing (2002) also investigated hydrodynamic stress in a pyrite slurry but increased the solids concentration by adding inert quartzite particles instead of mineral particles. In this way the negative physicochemical effects associated with increasing the mineral concentration were avoided. The investigation showed that when the solids concentration was increased without increasing the mineral load, the reactor failed at 27 % w/v (3 % pyrite and 24 % inert quartzite) total solids. Furthermore, increasing the impeller tip speed above 1.97 m $s^{-1}$ also caused reactor failure.

The current study is based on a system akin to that of Sissing (2002) except that chalcopyrite was the mineral of choice. Chalcopyrite was chosen due to its economic importance in the bioleaching industry and because the mineral is notoriously recalcitrant to either biological or chemical leaching. This recalcitrance stems primarily from passivation of the mineral resulting in nutrient limitation which causes physiological stress to the leaching micro-organisms. In the present study the effect of increasing the solids loading and agitation rate on the bioleaching of chalcopyrite by *Sulfolobus* culture in a chalcopyrite-quartzite slurry system was investigated. Process performance was monitored by measuring changes in the pH, redox potential, cell concentration and iron and copper solubilisation. The effect at a cellular level was measured by observing changes in morphology, metabolic activity, viability and protein composition of the micro-organisms.

Bioleaching was progressively impaired with increasing quartzite loading from 0 through to 18 % w/v with significant impairment above 9 % quartzite. The decline in process performance was characterised by:

(i) A decline in the rate of pH decrease with increasing solids loading and at an 18 % quartzite concentration the pH increased instead of decreasing. This revealed inhibition of the bioleaching process.

University of Cape Town

(ii) A reduction in the redox potential at all quartzite concentrations. The extent of reduction was proportional to the quartzite concentration.

(iii) A decrease in the rate and extent of growth, and iron and copper solubilisation with increasing quartzite loading. No growth was observed at an 18 % quartzite loading however leaching continued though at a highly reduced rate.

(iv) A decrease in the yield coefficient, $Y_{x/s}$. Energy derived from the oxidation of iron may have been directed to cell repair mechanisms instead of growth, resulting in a reduced biomass yield on substrate.

The critical solids loading beyond which the bioleaching process was significantly impaired was determined to be 9 % quartzite. Increasing the quartzite concentration from 9 to 15 % caused a progressive decrease in the system performance. At an 18 % quartzite concentration the system approached failure.

Increasing the impeller tip speed had a similar effect to increasing solids loading except that at a 0 % quartzite concentration, an increase in the impeller tip speed from 1.67 to 1.97 m $s^{-1}$ resulted in an increase in the metabolic activity of the micro-organisms due to improved mass transfer. However, the overall extent of iron and copper solubilisation did not improve. Increasing the solids loading to 9 % quartzite with a simultaneous increase in the impeller tip speed from 1.67 to 1.97 m $s^{-1}$ resulted in a decline in the process performance as measured by a decrease in the rate and extent of growth, and iron and copper solubilisation. A further increase in the impeller tip speed to 2.13 m $s^{-1}$ resulted in system failure. No growth was observed, instead cell death occurred.

The growth and redox potential data from solids loading experiments was further analysed in an attempt at predictive modelling. The specific death rate constant in the growth phase ($k_{d1}$) was calculated from the growth data and the following model describing the relationship between $k_{d1}$ and solids loading was elucidated:

$$k_{d1} = 4.61 \times 10^{-5} \Phi^{1.66}$$

The model fitted the data with a correlation coefficient of 0.98. The exponent of $\Phi$ was close to 2, indicating that solid-cell-solid collision was the dominant mechanism of cell damage. Further analysis of redox potential data using the approach of Petersen and Dixon (2005) showed that this method of analysis could be used to predict the variation in redox potential data over time for the solids loading experiments. The analysis, based on changes in the ferric supply by the *Sulfolobus* culture and the chalcopyrite ferric demand, explained changes in redox potential observed in the solids loading experiments and showed that it was possible to improve chalcopyrite leaching by reducing the microbial ferrous iron oxidation capacity of the culture.

University of Cape Town

The effect of hydrodynamic stress was also considered at a cellular level. Selected samples from the solids loading and impeller speed experiments were analysed for changes in (i) morphology using phase contrast and scanning electron microscopy, and the CellFacts particle analyser (ii) metabolic activity in terms of the oxygen utilisation rate, (iii) membrane integrity as measured by the uptake of the fluorescence stain, propidium iodide and (iv) protein composition of the cells using sodium dodecyl sulphate polyacrylamide gel electrophoresis.

A range of morphological types was identified on varying the intensity of hydrodynamic stress. These varied from phase dark round cells (negligible stress) to small and tiny cells, leaking cells and ghost cells resulting from damage to the cell envelope (mild to intermediate stress) and complete cell disruption resulting in the presence of cell debris (intense stress). Changes in cell size with increased solids loading were analysed quantitatively using cell-number based cell size distributions. The decrease in the mode of the size distribution with increasing solids loading confirmed that the overall cell size decreased with increased stress. Evidence was also presented to show that cell clumping (in the 2-5 μm cell diameter range) increased with increasing solids loading from 0 to 18 % quartzite. This result corroborated the phase contrast micrographs showing cell clumping at the same solids loading.

Oxygen utilisation rate was used to measure the metabolic activity of the culture on exposure to increasing solids loading. It was shown that culture metabolic activity decreased with time as well as with increasing solids loading. The decrease in metabolic activity with time may have resulted from nutrient limitation due to mineral passivation while the decrease with solids loading was due to increased hydrodynamic stress. The increased level of propidium iodide uptake by *Sulfolobus* cells with increasing solids loading demonstrated the loss of membrane integrity as the severity of stress increased. An increase in solids loading was accompanied by a change in the proportions of green, orange and red fluorescence. At a 0 % quartzite loading, no apparent loss of membrane integrity was observed. At a 12 % quartzite loading, more than 50 % of the cells had compromised membranes while at an 18 % quartzite loading, all cell membranes were compromised. Furthermore, cell clumps were visible exclusively at an 18 % solids loading.

In the solids loading experiments, the possibility of system recovery during long-term exposure to hydrodynamic stress was discussed. A preliminary investigation of protein composition of cells, under mild and intermediate intensities of hydrodynamic stress, yielded SDS PAGE gels showing the down-regulation of a 26 kDa protein and the up-regulation of a 45 kDa protein with increased solids loading. These results suggest that a stress protein may have been up-regulated under conditions of increased hydrodynamic stress and this points towards a possible mechanism of counteracting hydrodynamic stress and thus resulting in system recovery. Furthermore, combining

University of Cape Town

the results of the cell size analysis, i.e. a reduction in cell size with increased stress, with the protein analysis, it is postulated that the micro-organisms diverted energy for growth to resistance against stress, possibly in the form of stress proteins.

This study confirms that the bioleaching system performance was highest at low solids loadings and impeller tip speeds and that nutrient stress compounded the effect of hydrodynamic stress. The micro-organisms were shown to respond actively to stress in several ways including (i) decreasing cell size and (ii) the up-regulation of possible stress proteins. Operating conditions that increase the resilience of cells (e.g. stress proteins) to hydrodynamic stress need to be identified. In addition, indicators sensitive to changes in process conditions may be used as early warning signals of decreasing system performance. In the present study these indicators were identified as cell size and metabolic activity.

University of Cape Town

# Table of Contents



University of Cape Town

University of Cape Town

**CHAPTER 3: MATERIALS AND METHODS**



University of Cape Town

University of Cape Town

University of Cape Town

University of Cape Town

University of Cape Town

# List of Figures



University of Cape Town

University of Cape Town

University of Cape Town

University of Cape Town

University of Cape Town

University of Cape Town

University of Cape Town

University of Cape Town

University of Cape Town

# List of Tables



University of Cape Town

University of Cape Town

University of Cape Town

# Abbreviations and Nomenclature

## ABBREVIATIONS

| | |
|---|---|
| AL | conventional airlift |
| APS | ammonia persulphate |
| cs | cold shock |
| CPD | critical point drying |
| CSTR | continuously stirred tank reactor |
| CUR | carbon dioxide utilisation rate (μl $CO_2$ $min^{-1}$) |
| hs | heat shock |
| HSPs | heat shock proteins |
| LDH | lactate dehydrogenase |
| Lk | linking number (the number of times two closed strands are linked or, the number of times that one DNA strand winds around another) |
| MAb | monoclonal antibody |
| MAL | modified airlift |
| MS | mechanosenstive |
| NAG | N-acetyl-D-glucosamine |
| NAM | N-acetyl-muramic acid |
| OUR | oxygen utilisation rate (μl $O_2$ $min^{-1}$) |
| PPI | peptidyl-prolyl *cis-trans* isomerases |
| PBT | pitched blade turbine |
| Rf | relative migration distance of a protein (m) |
| rRNA | ribosomal RNA |
| RT | Rushton turbine |
| smHSP | small heat shock protein |
| S-layers | surface layers |
| SEM | scanning electron microscopy |
| SDS | sodium dodecyl sulphate |
| SDS PAGE | sodium dodecyl sulphate polyacrylamide gels |
| STR | stirred tank reactor |
| TF55 | thermophilic factor 55 |

University of Cape Town

## NOMENCLATURE

| | |
|---|---|
| a | weibull parameter (cells $ml^{-1}$) |
| $a$ | gas-liquid interfacial area per unit volume of fluid ($m^2\ m^{-3}$) |
| b | weibull parameter (μm) |
| A | total area of the chamber (1 $mm^2$) |
| $C_{AL}$ | oxygen concentration in the broth (gmol $m^{-3}$) |
| $C^*_{AL}$ | solubility of oxygen in the broth at saturation (gmol $m^{-3}$) |
| $C_{crit}$ | critical oxygen concentration (gmol $m^{-3}$) |
| $CS_T$ | collision severity based on eddy velocity ($J.s^{-1}$) |
| $C_N$ | cell concentration (cells $ml^{-1}$) |
| $c_L$ | number of cells counted in the large squares |
| $\overline{C}_{t1-t2}$ | average cell concentration over the time period $t_1$ to $t_2$ (cells $ml^{-1}$) |
| $C_N$ | biomass concentration at time t (cells $ml^{-1}$) |
| $C_{N0}$ | initial biomass concentration (cells $ml^{-1}$) |
| $C_1$ | concentration of $Fe^{2+}$ ($g\ l^{-1}$) |
| $C_2$ | concentration of $K_2Cr_2O_7$ ($g\ l^{-1}$) |
| $\%C_{2-5\mu m}$ | percentage of cells in the 2 to 5 μm range |
| $Cellconc._{2-5\mu m}$ | concentration of cells in the 2 to 5 μm range (cells $ml^{-1}$) |
| $Cellconc._{0-5\mu m}$ | concentration of cells in the 0 to 5 μm range (cells $ml^{-1}$) |
| $d_r$ | dilution ratio |
| $d_p$ | particle diameter (m) |
| D | depth of the chamber (0.02 mm) |
| g | gravitational acceleration (9.81 m $s^{-2}$) |
| $k_L$ | liquid-phase mass-transfer coefficient (m $s^{-1}$) |
| $k_La$ | mass transfer coefficient ($s^{-1}$) |
| $k$ | disruption rate constant ($s^{-1}$) |
| k | first order rate constant ($s^{-1}$) |
| $k_d$ | the specific cell death rate ($h^{-1}$) |
| $k_{d1}$ | specific cell death rate in the growth phase ($h^{-1}$) |
| $k_{d2}$ | the cell death rate during the death phase ($h^{-1}$) |
| L | distance from the tip of the torque arm to the centre of the torque table (0.1 m) |
| $m_s$ | the maintenance coefficient (mol $Fe^{2+}$ $molC^{-1}\ h^{-1}$) |
| m | the mass reading on the load cell (kg) |
| M | molar mass of iron ($g\ mol^{-1}$) |
| n | number of observations |

University of Cape Town

| | |
|---|---|
| N | impeller tip speed (m $s^{-1}$) |
| $N_L$ | number of large squares where cell were counted |
| $N_T$ | total number of large squares = 16 |
| $N_{Fe}$ | number of moles of iron (mol) |
| $N_A$ | rate of oxygen transfer per unit volume of fluid (gmol $m^{-3}s^{-1}$) |
| $[O_2]_1$ | oxygen concentration at time $t_1$ (µl $l^{-1}$) |
| $[O_2]_2$ | oxygen concentration at time $t_2$ (µl $l^{-1}$) |
| P/V | power input into the system per unit volume ($W/m^3$) |
| $P_{t1}$ | the concentration of iron or copper at time $t_1$ (g $l^{-1}$) |
| $P_{t2}$ | the concentration of iron or copper at time $t_2$ (g $l^{-1}$) |
| $pHBase_{24h}$ | the pH value for the baseline reactor at 24 h |
| $pHExp_{24h}$ | the pH value for the experimental reactor at 24 h |
| $q_{O2}$ | Specific oxygen utilisation rate (µl$O_2$ $cell^{-1}$ $min^{-1}$) |
| $q_{Fe^{2+}}$ | the specific iron oxidation rate (mol $Fe^{2+}$ $molC^{-1}$ $h^{-1}$) |
| $R_f$ | relative migration distance of a protein (m) |
| $r_{O_2}$ | OUR (µl $min^{-1}$) |
| t | time (h) |
| $t_1$ | time 1 (min) |
| $t_2$ | time 2 (min) |
| $V$ | volume of gas (l) |
| $V_2$ | titre volume (l) |
| $V_{sol}$ | sample volume (l) |
| $\bar{x}$ | average of n measurements |
| $X_0$ | mode of the size distribution curve (µm) |
| $x_1$ | the OUR or cell, iron or copper concentration at time $t_1$ (µl$O_2$ $min^{-1}$,cells $ml^{-1}$, g $l^{-1}$ respectively) |
| $x_2$ | the OUR or cell, iron or copper concentration at time $t_2$ (µl$O_2$ $min^{-1}$,cells $ml^{-1}$, g $l^{-1}$ respectively) |
| $X_{max}$ | maximum cell concentration (cells $ml^{-1}$) |
| $X_{t1}$ | the concentration of cells at time $t_1$ (cells $ml^{-1}$) |
| $X_{t2}$ | the concentration of cells at time $t_2$ (cells $ml^{-1}$) |
| $Y_{x/s}$ | biomass yield coefficient (cells g $Fe^{-1}$) |
| $Y_{SX}^{max}$ | the maximum yield on substrate (mol $Fe^{2+}$ $molC^{-1}$) |

University of Cape Town

# Greek symbols

| | |
|---|---|
| $\alpha$ | constant |
| $\beta$ | constant |
| $\alpha$ | volume fraction of cells |
| $\varepsilon$ | turbulent energy dissipation rate per unit volume (W $m^{-3}$) |
| $\Phi$ | solids loading (w/w or w/v) |
| $\Phi_T$ | total solids volume fraction |
| $\eta$ | size of the smallest eddies is given by the Kolmogorov-scale of turbulence (m) |
| $\mu$ | the specific growth rate ($h^{-1}$) and is a function of physiological factors such as temperature, pH, nutrient availability, and ferrous and ferric iron concentration |
| $\mu$ | (Section 4.9.1.1; Eqn. 4.13) maximum specific growth rate in the absence of stress ($h^{-1}$) |
| $\mu_{app}$ | apparent or measured specific growth rate ($h^{-1}$) |
| $\mu_{max}$ | maximum specific growth rate ($h^{-1}$) |
| $\mu_{max\ exp}$ | maximum specific growth rate ($h^{-1}$) |
| $\mu_{viable\ cells}$ | specific growth rate based on the viable cell concentration ($h^{-1}$) |
| $\nu$ | kinematic fluid viscosity ($m^2\ s^{-1}$) |
| $\varrho_p$ | particle density (kg $m^{-3}$) |
| $\sigma$ | standard deviation |
| $\tau$ | shear stress (dynes $cm^{-2}$) |

University of Cape Town

# Glossary

**Abiotic** – sterile, without microbial action

**Aconitase** production, the key enzyme in lysine biosynthesis – an enzyme in the citric acid cycle for oxidative metabolism

**Adenosine triphosphate (ATP)** – a nucleotide that serves as the basic energy source for most metabolic activities

**Archaea** - A unique group of microorganisms, genetically and metabolically different from bacteria. They appear to be the survivors of an ancient group of organisms that bridged the gap in evolution between bacteria and the eukaryotes

**Autophosphorylation** - Addition of a phosphate to a protein by virtue of its own enzymic activity

**Biofilm** - A layered culture of microorganisms growing on a surface that they have created themselves by secreting polysaccharides and glycoproteins

**Biooxidation** – the microbially-assisted oxidation of minerals

**Chaperonins** - Subset of chaperone proteins (Cytoplasmic proteins of both prokaryotes and eukaryotes that bind to nascent or unfolded polypeptides and ensure correct folding or transport) found in prokaryotes, mitochondria and plastids

**Chemiosmosis** - A theoretical mechanism of energy transduction, coupling one enzyme catalysed reaction to another using the transmembrane flow of an intermediate species.

**Chemolithotrophic** – the use of an inorganic mineral as the electron donor for microbial metabolism

**Chirality** – "handedness", a structural characteristic of a molecule that makes it impossible to superimpose it on its mirror image, a feature produced by the physical orientation of its constituents

**Chitin** - A tough, protective, semitransparent substance, primarily a nitrogen-containing polysaccharide, forming the principal component of arthropod exoskeletons and the cell walls of certain fungi

**Coal depyritisation** – the removal of pyrite and pyritic sulphur from coal

**Coccoid** – spherical

**Cold shock** - a stress applied to microbial systems by a sudden decrease in the temperature

***Crenarchaeota*** - A kingdom in the domain Archaea comprised of thermoacidophilic, sulphur-dependent organisms.

**Eddies** - A current, as of water or air, moving contrary to the direction of the main current, especially in a circular motion, characteristic of turbulent fluid flow

**Ester** - Any of a class of organic compounds corresponding to the inorganic salts and formed from an organic acid and an alcohol, usually with the elimination of water

**Ether** - Any of a class of organic compounds in which two hydrocarbon groups are linked by an oxygen atom

**Eubacteria** - A major subdivision of the prokaryotes (includes all except Archaebacteria.

**Eukaryotes** - Organism whose cells have chromosomes with nucleosomal structure and separated from the cytoplasm by a two membrane nuclear envelope and compartmentalisation of a function in distinct cytoplasmic organelles.

University of Cape Town

**Extracytoplasmic** – activities that occur outside the cell membrane

**Extremophiles** – microbes capable of living under conditions outside the range generally considered viable for life

**Geotextile fibre** - A planar, permeable, synthetic textile material, which may be non-woven, knitted or woven, used in contact with soil and/or other materials in geotechnical and civil engineering applications

**'Ghost' cell** – a cell that has lost its cell contents, an empty cell

**Glucan** - A polysaccharide, such as cellulose, that is a polymer of glucose

**Glycoprotein** - a conjugated protein in which the non-protein group is a carbohydrate

**Glycosidic bonds** - A type of covalent chemical bond that joins two simple sugars via an oxygen atom

**Heat shock** – a stress applied to microbial systems by a sudden increase in the temperature

**Hybridoma** - A cell hybrid in which a tumour cell forms one of the original source cells, the resulting hybrid cells continue to grow and divide like the neoplastic (tumourous) parent.

**Hydrophobicity** - Not readily absorbing water or being adversely affected by water

**Hyperosmotic** – a solution that contains a higher concentration of solutes (higher osmotic pressure) than another

**Hyperthermophilic** - Describes an organism that lives in a very high-temperature environment (well over 50 degrees C)

**Isoprenoid** - A polymer whose carbon skeleton consists wholly or partly of isoprene units joined end to end

**Lactate dehydrogenase** – the enzyme that catalyses the formation and removal of lactate whose extracellular presence is often used as an indication of cell death and/or the release of cytoplasmic constituents

**'Leaky' cell** – a cell with a compromised cell membrane causing leakage of cytoplasmic elements

**Linking number** - A property of a long biopolymer (such as duplex DNA) equal to the number of twists (related to the frequency of turns around the central axis of the helix) plus the writhing number (the number of times the axis of a DNA helix crosses itself while the molecule is in the process of **supercoiling**).

**Mannan** – polysaccharide found in plant and yeast cell

**Mechanosensitive (MS) ion channels** - channels through the cell membrane whose gating mechanism responses to mechanical force

**Mesophiles** - Organism living in the temperature range around that of warm-blooded animals, usually between 20-45 °C

**Microcarriers** - small solid or in some cases immiscible liquid spheres, on which cells may be grown in suspension culture

**Mixotrophic** – capable of utilising both organic and inorganic carbon

**Monoclonal antibody** - A substance, usually a protein, which can be synthesised in the laboratory in pure form by a single clone (population) of cells

**Monolayer** – a cell culture that grows as a layer of cells one cell thick

**N-acetyl-D-glucosamine (NAG)** a constituent of polysaccharides like **peptidoglycan and chitin** in cell walls and membranes

**N-acetyl-muramic acid (NAM)** – another constituent of **peptidoglycan**, found in bacterial cell membranes

University of Cape Town

**Osmolarity** - The osmotic concentration of a solution expressed as number of moles of impermeable particles of solute per litre of solution

**Osmoprotectants** - substances and mechanisms that act to protect a cell against the detrimental effects of osmotic stresses

**Passivation** - the formation of a passive surface layer that hinders surface reaction

**Peptidoglycan** - A polymer found in the cell walls of prokaryotes that consists of polysaccharide and peptide chains in a strong molecular network. Also called mucopeptide, murein

**Periplasm** – the space between the cell membrane and the cell wall

**Permeabilisation** – (the action of making (a cell membrane) permeable, capable of allowing previously prevented elements to pass through)

**Phylogenetic** – related to the evolutionary development and history of a species or higher taxonomic grouping of organisms

**Proteasome** - Proteolytic complexes that degrade cytosolic and nuclear proteins.

**Proteolytic systems** – enzyme systems that break down proteins by hydrolysis of the peptide bonds to form smaller polypeptides

**Pseudomurein** – (or pseudopeptidoglycan ) an archaeal cell wall material similar to peptidoglycan, containing N-acetyltalosaminouronic acid instead of NAM, and L- instead of D-amino acids

**Pyrometallurgy** - An ore-refining process, such as smelting, dependent on the action of heat.

**Solfatara field** - A volcanic area or vent which yields only sulphur vapours, steam, and the like

**Sparging** - To introduce air or gas into (a liquid).

**Sporopollenin** – A protein polymer of carotenoids, found in the exine of the pollen wall, extremely resistant to chemical and enzymatic degradation

**Supercoiling** - In circular DNA or closed loops of DNA, twisting of the DNA about its own axis changes the number of turns of the double helix.

**Supracellular structures** – a structure above the level of a cell or cells

**Supraoptimal temperatures** – temperatures above a microbe's optimal growth temperature

**Thermoacidophiles** – microbes capable of living at high temperatures and low pH

**Thermoprotectants** - substances and mechanisms that act to protect a cell against the detrimental effects of thermal stresses

**Thermosome** - a chaperonin protein strongly induced by heat shock

**Turbohypobiosis** - decrease of biological activity caused by an increased intensity of turbulence

**Turgor** - The pressure within cells, derived from osmotic pressure differences between the inside and outside of the cell giving rise to mechanical rigidity of the cells

**Xenobiotics** - Chemical substances that are foreign to the biological system

University of Cape Town

# Chapter 1: Introduction

## 1.1 BACKGROUND

Slurry reactor systems are widely applied in the bioprocessing industry. Organisms immobilised on support materials are used in biotransformations and for the production of specialised bioproducts, while micro-organisms in mineral slurries are exploited for their metal oxidation or reduction capability. The optimisation of these bioprocesses requires an understanding of the key factors affecting productivity. One of these key factors is the impact of the particulate phase on the micro-organisms in slurry reactors. In the field of bioleaching the understanding of the impact of hydrodynamic stress in these systems remains low. The biological leaching of minerals is a key emerging technology for which discrete niche applications exist where it provides advantage over existing technologies. For example, conventional mineral treatment processes such as roasting or smelting produce sulphur dioxide and other undesirable pollutants (Rawlings, 2002).

Comparative studies of bioleaching have shown that faster leaching rates and greater extents of leaching can be obtained using temperatures at which thermophilic microbial cultures thrive instead of the conventional mesophilic micro-organisms (Brierley, 1990; Clark and Norris 1996). High temperature leaching in excess of 60°C has proven especially advantageous in the bioleaching of recalcitrant sulphide minerals. Chalcopyrite is an example of a recalcitrant mineral with limited technologies for its cost-effective exploitation. Whereas leaching of chalcopyrite at mesophilic temperatures does not allow sufficient extraction, economically favourable rates and extents of metal extraction are achievable under thermophilic conditions. In order to exploit the advantages of high temperature leaching, it is necessary to understand the resilience of these high temperature systems to stresses incurred during the leach process. In particular, the tank bioleaching system requires the micro-organisms present to function in a well agitated and aerated slurry environment into which substantial energy dissipation is required to ensure adequate mass transfer and solids suspension.

Several authors have shown that in mesophilic bioleaching systems, the presence of high concentrations of suspended solids may lower oxidation rates, increase lag times and decrease the ultimate extent of oxidation (Beyer *et al.*, 1986; Pearce, 1993; Deveci, 2002). The various factors proposed to cause these phenomena include oxygen and carbon dioxide availability, low bacteria-to-solids ratio, mechanical damage or inhibition of the bacteria, inhibition of bacterial attachment and the accumulation of toxic leach products. Cell wall strength is pivotal in maintaining cell integrity under conditions of high mechanical stress. Most eubacterial cell walls contain peptidoglycan. Peptidoglycan, a polysaccharide cross-linked by peptide side chains, is primarily

University of Cape Town

responsible for the strength of the cell wall. The cell walls of extremely thermophilic Archaea lack peptidoglycan and consist only of protein or glycoprotein subunits (Brock and Madigan, 1991). This difference in cell wall structure is expected to decrease the resilience of the thermophilic iron and sulphide oxidizers (Archaea) to mechanical damage in comparison to mesophilic (eubacteria) iron and sulphide oxidizers.

A high solids loading is desirable in any leaching system to maximise the use of reactor volume through increased productivity. High impeller tip speeds are necessary to provide sufficient mass transfer of oxygen and carbon dioxide as well as to facilitate mixing and solids suspension. Particulate solids present in the reactor, the impeller tip speed and the impeller type induce mechanical stress to the micro-organisms in slurry reactors such as those used in bioleaching systems. Consequently process optimisation is only possible when a balance is attained between cell injury induced by hydrodynamic forces and adequate nutrient supply.

## 1.2 RESEARCH TO DATE

Over the past 11 years a broad scope of studies have been conducted by the Bioprocess Engineering Unit at the University of Cape Town on hydrodynamic cell damage in slurry systems. These investigations have progressed from the use of a model system comprised of a non-growing *Saccharomyces cerevisiae* culture in quartzite slurries to the study of growing thermo-acidophilic cultures in mineral and mineral-quartzite slurries. The yeast-quartzite system provided an ideal system to describe and model cell damage in inert slurries. In studies conducted by Pearce (1993) and Scholtz-Brown (1998) on stationary phase yeast cells, empirical models describing cell disruption as a function of solids loading, incompletely and completely suspended solids, impeller speed and impeller type were elucidated. In addition, mechanistic models were developed that described the mechanism by which solids present in the slurry reactor damage cells. Lamaignére (2002) expanded the study of the *S. cerevisiae*-quartzite model system by using growing yeast cultures. The author determined the effect of increasing quartzite concentration, impeller tip speed and impeller type on process conditions. The model describing the correlation between the death rate and increased solids loading and impeller tip speed was extended in the growing yeast study to describe the death rate constant as a function of solids loading and speed in the growth phase (Lamaignére, 2002). Further to this, the change in morphological characteristics of yeast cells under conditions of hydrodynamic stress was also reported. These data pointed toward the existence of possible repair mechanisms in the organisms. Studies were extended to the thermoacidophile *S. metallicus* grown in the presence of pyrite only and a combination of pyrite and inert silica. Nemati and Harrison (2000) and Nemati *et al.* (2000) investigated the effect of increasing solids loading and varying particle size on process performance in archaeal-pyrite slurries. The disadvantages of using a

University of Cape Town

mineral-only slurry to assess the effects of hydrodynamic stress were highlighted in this work and thus further investigations described by Sissing (2002) and Sissing and Harrison (2003) were carried out in a pyrite-quartzite system. The pyrite-quartzite system provided a model system for mineral bioleaching slurries where the effects of increased hydrodynamic stress could be investigated in the absence of added physiological stress induced by increasing the mineral concentration (Sissing and Harrison, 2003). Process parameters such as growth rates, iron solubilisation rates and extents of leaching as a function of solids loading, impeller speed and inoculum state were considered. This work as well as the studies by Nemati and Harrison (2000) and Nemati *et al.* (2000) in which solids loadings were manipulated through the addition of pyrite provide an excellent basis for the current investigation. The current project was carried out to determine the effects of agitation rate and solids loading on a *Sulfolobus* culture in the presence of chalcopyrite. Variation of solids loading was achieved by the addition of inert quartzite.

## 1.3 SCOPE OF THE THESIS

The present study aims to further describe the cellular stress experienced by thermoacidophilic micro-organisms in mineral bioleaching slurry reactors, with special reference to chalcopyrite, by not only investigating the effects of hydrodynamic stress on process performance, as presented in the studies of thermoacidophilic micro-organisms in pyrite systems, but also by examining the microbial responses at a cellular level. Solids concentration and impeller speed were chosen as the hydrodynamic stress factors because they are important process considerations in commercial-scale bioleaching systems. Chalcopyrite was the mineral of choice because it presents a particular problem in the mineral industry due to its recalcitrance to biological and chemical leaching. Passivation of the mineral causes a decrease in the leaching rate leading to nutrient limitation in the bioleaching system. This creates an interesting scenario where the hydrodynamic as well as physiological (nutrient) stress capacity of the organisms can be tested and the critical solids concentration and energy dissipation in terms of impeller tip speed can be determined.

University of Cape Town

In order to describe the effects of hydrodynamic stress in the slurry reactor successfully, a number of key questions are posed in this study. These include:

(i) Under which conditions does significant cellular stress occur?

(ii) What is maximum amount of stress that can be tolerated by the cells, albeit in a laboratory system?

(iii) How does the extent of damage affect the rate of dissolution of the chalcopyrite concentrate?

(iv) What is the nature of the stress response at a cellular level?

(v) Are morphological changes associated with cellular damage?

(vi) Is the protein expression within the cell modified in response to exposure to stress to cause the overproduction of specific proteins or production of new proteins during stress conditions?

An important point to note is that a laboratory-scale reactor was used for this study and this may have implications with regards to scale-up. However, in this study the primary aim was not to determine the magnitude of hydrodynamic stress at a laboratory scale but to determine the nature and relative effect of hydrodynamic stress and the biological response and not to. This information will provide insight into how to handle these stresses when they prevail in bioleaching slurry reactors.

## 1.4 STRUCTURE OF THE THESIS

The dissertation begins with an overview of literature pertaining to the causes, the effects and the responses of organisms to stress with particular reference to hydrodynamic stress (Part A). In Part B of the literature review, a brief outline of bioleaching processes is given followed by a discussion on the effect of hydrodynamic stress in these systems. Chapter 3 provides detail on the experimental protocol, reactor setup and analytical methods utilised in the study. In Chapter 4 the effects of (i) increasing quartzite concentration (ii) increasing impeller speed and (iii) simultaneously increasing solids loading and impeller speed on the leaching of chalcopyrite by a *Sulfolobus* culture is presented. Chapter 4 begins with a discussion on variability of the *Sulfolobus* culture, reproducibility of the experiments as well as results obtained for abiotic leach experiments. This section is followed by a description of the chemical and biological processes that occur during leaching of chalcopyrite. In the next section the effect of increasing solids loading and impeller tip speed independently on the process performance presented. Growth and metal solubilisation rates as well as extents of leaching are discussed. The results are presented as raw data and normalised data. The results were normalised to enable comparison between different experimental runs. The concluding section of Chapter 4 presents further analysis of growth and redox potential data from the solids loading experiments. Here, the applicability of empirical models developed in the yeast-quartzite systems to the archaeal-mineral-quartzite system is elucidated. Furthermore, the change in redox potential over time observed at quartzite loading for the solids loading experiments is examined using the kinetics of the bioleaching of chalcopyrite by a *Sulfolobus* sp.. Finally, in Chapter 5 the biological response to increased hydrodynamic trauma is investigated. Changes in morphology, metabolic activity, viability and protein expression of the micro-organisms with increasing hydrodynamic stress are discussed. The dissertation culminates in Chapter 6 which presents the final conclusions and recommendations of the study. In addition, recommendations for future work pertaining to an improved understanding of hydrodynamic stress and bioleaching in chalcopyrite systems are discussed.

University of Cape Town

# Chapter 2: Literature Review

## 2.1 INTRODUCTION

Biological systems hold great value in industry. Prokaryotic and eukaryotic cells are used in the production of antibiotics and enzymes, in bio-transformations, in mineral processing and in waste treatment to name a few. During production, cells are exposed to various physicochemical and mechanical (e.g. hydrodynamic) stresses. In large-scale equipment, hydrodynamic stress is caused through sub-processes such as agitation, aeration, pumping and solid-liquid separation processes and in some processes the stress is compounded by the presence of solids in the reactor (Bronnenmeier and Märkl, 1982). Depending on the severity of the hydrodynamic stress, the effect on the micro-organisms can range from minor cell envelope damage to complete cell disruption and this, as with physicochemical stresses, can impair process performance.

The resilience of micro-organisms to hydrodynamic stress is largely dependent on three factors (i) the structure of the cell envelope, (ii) the size of the micro-organisms and (iii) the physiological status of the cells. Bacteria and yeast possess highly resilient cell walls that can, in most cases, withstand severe hydrodynamic stress. However some micro-organisms such as the Gram-negative Archaea have less resilient cell walls comprising only protein or glycoprotein subunits. These micro-organisms are fragile and susceptible to even mild hydrodynamic trauma. Large cells are more prone to the effects of hydrodynamic stress than small cells because they interact with a greater range of eddy sizes and thus a greater amount of energy is dissipated in larger cells. In general, small cells tend to be entrained within fluid eddies and because the flow within eddies is laminar, the shear effects of eddy-cell interactions are minimal. Micro-organisms that are physiologically stressed respond differently to hydrodynamic stress than those cells growing under optimal conditions (Bronnenmeier and Märkl, 1982). Nutrient stress as well as temperature and pH stresses have been shown to influence a micro-organism's susceptibility to hydrodynamic stress.

In the thermophilic tank bioleaching of mineral concentrates, micro-organisms are exposed to severe physiological and hydrodynamic stress. Physiological stress arises primarily from a decrease in pH, an increase in metal concentrations and nutrient limitation in the case of chalcopyrite due to passivation of the mineral. Hydrodynamic stress arises primarily from the optimisation of mass transfer and solids suspension through intensive mixing and aeration which compounds the detrimental effect of the presence of particulate solids in the reactor. Mesophilic tank bioleaching systems have failed at oxidisable solids concentration above 20 %. In the past

University of Cape Town

this failure has been attributed to reduced oxygen availability. Recently studies have shown that the failure could be as a result of a combination of oxygen limitation and hydrodynamic stress. Mesophilic bioleaching micro-organisms are prokaryotes with resilient cell walls. The micro-organisms involved in thermophilic bioleaching possess cell walls of reduced structural integrity and thus it is proposed that the thermophilic bioleaching system will fail at a lower solids concentration than the mesophilic system. To design bioleaching plants, it is important to know the stress capacity of the micro-organisms involved in the process and thus the study of the effect of hydrodynamic and physiological stress is imperative in defining the process requirements for the biological systems.

The literature review that follows is divided into two parts. In Part A, cellular stress in biological systems is considered. The first section covers the sources of hydrodynamic stress in the bioleaching stirred tank reactor (STR) and the mechanisms of hydrodynamic stress within the STR. The second section deals with the structure of micro-organisms with emphasis on the cell envelope as the first line of defense against hydrodynamic stress. This section is followed by a discussion on the negative impact of hydrodynamic stress on micro-organisms followed by a review of literature studies on the effect of hydrodynamic stress in solids-free and solids-containing systems and the effect of compounding stresses. In Part B of the review, bioleaching in stirred tank reactors is considered. The first section covers the role of bioleaching in the mining industry followed by a short discussion on the bioleaching process and large scale bioleaching operations. In the second section the micro-organisms involved in bioleaching are reviewed with particular reference to the genus *Sulfolobus* due to its relevance to the current study. Finally, a detailed review of literature available on hydrodynamic stress within tank bioleaching systems is presented.

University of Cape Town

# PART A

# CELLULAR STRESS IN BIOLOGICAL SYSTEMS

## 2.2 CELLULAR STRESS IN STIRRED TANK REACTORS

There are many causes of stress in stirred tank reactors. These include physicochemical and mechanical stressors (Cherry and Papoutsakis, 1986; Macario *et al.*, 1999). Common physicochemical stresses include sub-optimal temperature, pH, redox potential, pressure, osmotic potential, salinity, oxygen, nutrient starvation, and product inhibition (Brock and Madigan, 1991; Craig *et al*, 1993; Hei and Clark, 1994; Jobin *et al* 1997; de Macario and Macario, 2003). Within the domain Archaea, examples of physicochemical stresses that have been investigated include: hyper- and hypo-osmolarity, pressure, ethanol, UV light, copper, pH, ammonia and phosphate starvation (Macario *et al*, 1999). Mechanical stress in stirred tank reactors arises from the movement of fluid caused by mixing and aeration. In the active bioleaching of finely milled concentrates, stirred tank reactors are commonly used. The primary stressor in these systems is mechanical stress; however physicochemical stresses also prevail. In this section, the origin of hydrodynamic stress will be considered primarily in such STR systems followed by a discussion on the mechanism of hydrodynamic stress to the micro-organisms.

University of Cape Town

### 2.2.1 REACTOR CONSIDERATIONS IN STIRRED TANK REACTORS

In this section, reactor considerations within STRs are discussed with emphasis on the sub-processes that contribute to cellular stress and are of relevance to bioleaching systems. Mixing, gas-liquid mass transfer and the role of solids are examined. These contribute to the energy input into the system which leads to hydrodynamic stress. Furthermore, these processes are interlinked with mixing as the primary cause of hydrodynamic stress in the STR and its effect is compounded by intensive aeration (to promote gas-liquid mass transfer) and the presence of solids.

#### 2.2.1.1 Description of stirred tank reactors

Stirred tank bioreactors are typically operated as two-phase or three phase systems. Biological two-phase systems are characterised by liquid and gas phases while biological three-phase systems are characterised by solid, liquid and gas phases. In three-phase (slurry) systems, the solid phase may be microcarriers on to which cells or enzymes are immobilised or, in the case of mineral slurries, mineral particles which form both the biological nutrient supply as well as an immobilisation surface. The liquid phase consists of nutrients, planktonic cells and waste

products. In aerobic systems, the gas phase is made up of air or combinations of air and other gases. Figure 2.1 illustrates the typical components of a biological stirred tank slurry reactor. On considering bulk properties, the biomass phase may be considered as part of the liquid phase, whereas on considering properties at the micro-scale, the biomass forms a second solid phase. Hydrodynamic stress in the STR originates from agitation due to rotation of the impeller, aeration and the presence of solids.

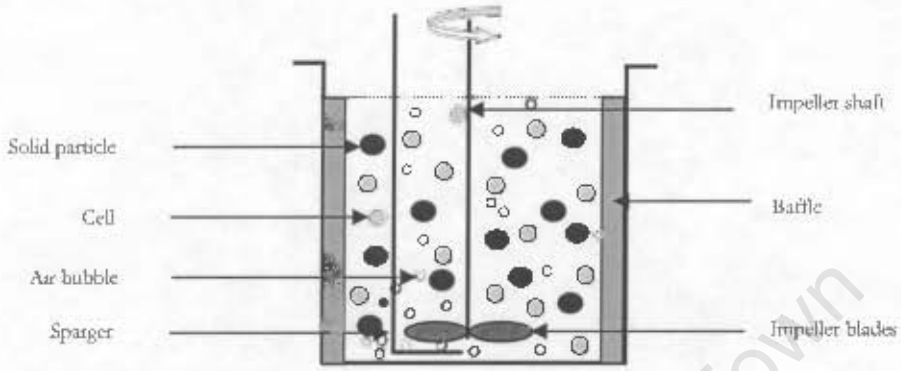


**Figure 2.1:** Typical components of a biological stirred tank slurry reactor.

University of Cape Town

### 2.2.1.2 Agitation

To maintain a homogenous environment, the phases within the reactor require good contacting through mixing. Mixing enables (i) mass transfer of nutrients from the liquid and gas phases and the solid surface to the cells and waste materials away from the cells, (ii) suspension of solid particles and (iii) promotion of heat transfer. The overall reactor performance may decline because of the appearance of zones of the fluid with insufficient nutrients or non-optimal temperature or pH (Abu-Reesh and Kargi, 1991; Namdev *et al.*, 1994; Deveci, 2002).

In addition to its positive effects, mixing can lead to unfavourable hydrodynamic conditions that cause cell stress and, in extreme cases, cell death. In order to attain proper mixing, fluid flow must be turbulent (Doran, 1997). The kinetic energy in turbulent flow is directed into regions of rotational flow called eddies. Eddies are broken down by the action of the stirrer into decreasing sizes. The size of the smallest eddies is given by the Kolmogorov-scale of turbulence, $\eta$ (Kunas and Papoutsakis, 1990).

In the STR, mixing is attained by rotation of the impellet and the flow region with the highest turbulence is the impeller stream (Rao and Brodkey, 1972). The most common impeller types used in bioreactors are radial and axial flow impellers. The blades of axial flow impellers form an angle of less than 90° to the plane of rotation and promote axial motion. Radial-flow impellers have blades at 90° to the plane of rotation. These impellers provide good gas dispersion thereby

aiding gas-liquid mass transfer, whereas axial flow impellers provide good solids suspension. The basic impeller designs and flow patterns for a radial- and axial-flow impeller, maximising dispersion and suspension respectively, are shown in Figure 2.2.

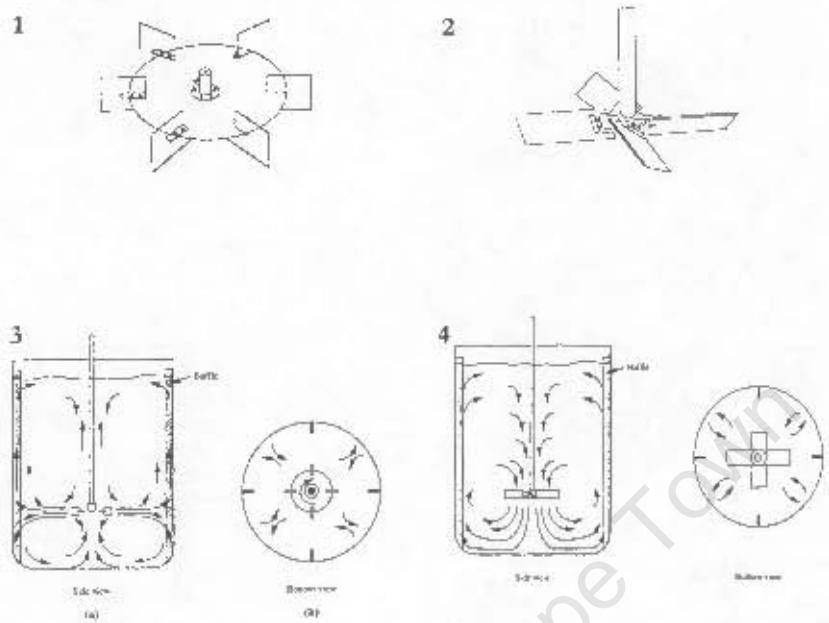


**Figure 2.2:** (1) radial (Rushton) and (2) axial (pitched-blade) flow impellers. Flow patterns produced by (3) radial- and (4) axial-flow impellers in baffled tanks (sourced from Doran, 1997).

The hydrodynamic shear produced by the impeller depends on the impeller design and agitation rate. High shear develops in the vicinity of the impeller blades with the highest incidence of cell damage conditions occurring at the turbine tip (Bronnenmeier and Märkl, 1982). Radial flow impellers create a high shear environment, while axial flow impellers generate less shear. Thus to achieve optimal mixing under low shear conditions, axial flow impellers are advantageous over radial flow impellers (Junker *et al*., 1998; Myers and Bakker, 1998). Recently, new types of impellers that provide increased pumping efficiency with high gas handling capabilities and low shear have been developed. These include hydrofoil impellers such as the Lightnin A315 (Figure 2.3) and Prochem Maxflo T impellers. Hydrofoil impellers have been shown to induce a stronger axial flow and produce higher relative pumping efficiencies than pitched blade turbines (Bakker and van den Akker, 1990). The success of the hydrofoil impellers lies in their high solidity ratio, which is defined as the ratio of the total blade area to the projected, or swept, area of the impeller.

University of Cape Town

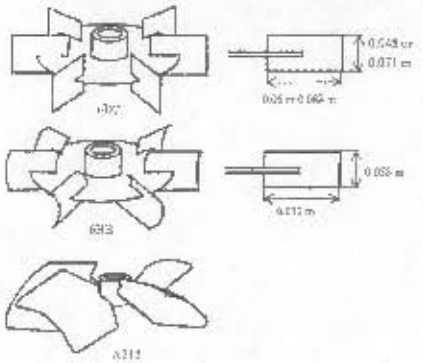

**Figure 2.3:** Comparison of (a) six-bladed Rushton turbine; (b) six-bladed hollow blade disk turbine and (c) Lightnin A315 impeller types (sourced from Otomo *et al.*, 2003).

#### 2.2.1.3 Gas-liquid mass transfer

The mass transfer of oxygen and carbon dioxide is an important consideration in the thermophilic bioleaching STR because the energy-producing oxidation reactions of ferrous to ferric iron and sulphur to sulphate require oxygen, while carbon dioxide is required as a source of carbon to build biomass. It thus follows that oxygen and carbon dioxide limitation will cause physiological stress to the micro-organisms. Limitation of gas-liquid mass transfer will be considered further through oxygen transfer.

Due to the sparingly soluble nature of oxygen, especially at elevated temperatures, intensive mixing and aeration are required to improve oxygen mass transfer and this promotes hydrodynamic cell damage. As gas bubbles move through the liquid phase during the mixing process (Figure 2.4), bubbles are dispersed while bubble collapse occurs at the liquid surface (Lu *et al*, 1992). The gas diffuses from the bubble across the interfacial area into the solution in response to the concentration driving force. An expression for rate of oxygen transfer from gas to liquid is given by:

$$N_A = k_L a\left(C^*_{AL} - C_{AL}\right) \qquad \text{...Eqn. 2.1}$$

where $N_A$ is the rate of oxygen transfer per unit volume of fluid (gmol $m^{-3}s^{-1}$), $k_L$ is the liquid-phase mass-transfer coefficient ($m\ s^{-1}$), $a$ is the gas-liquid interfacial area per unit volume of fluid ($m^2\ m^{-3}$), $C_{AL}$ is the oxygen concentration in the broth (gmol $m^{-3}$), and $C^*_{AL}$ (gmol $m^{-3}$) represents the solubility of oxygen in the broth at saturation. The efficiency of gas-liquid mass transfer depends to a large extent on the characteristics of bubbles in the liquid medium (Doran, 1997).

The difference ($C^*_{AL} - C_{AL}$) between the maximum (saturated) and actual oxygen concentrations in the liquid represents the concentration-difference driving force for mass transfer. The

University of Cape Town

solubility of oxygen, even at ambient temperature, is low. This low solubility guarantees that the concentration difference ($C^*_{AL} - C_{AL}$) is always very small. A critical oxygen concentration $C_{crit}$ is required above which the rate of microbial growth and metabolism is independent of the dissolved oxygen concentration. Meeting this requirement further decreases the concentration driving force.

The temperature of the aerobic bioprocess affects both the solubility of oxygen ($C^*_{AL}$) and the mass-transfer coefficient ($k_L$). Increasing temperature causes $C^*_{AL}$ to decrease, so that the driving force for mass transfer ($C^*_{AL}$-$C_{AL}$) is reduced. At the same time, diffusivity of oxygen in the liquid film surrounding the bubbles is increased. As the mass transfer coefficient is the quotient of this diffusivity and the boundary thickness, this results in an increase in $k_L$. For temperatures between 10°C and 40°C, the effect of temperature on diffusivity and thereby $k_L$ is more dominant, hence an increase in temperature is more likely to increase the rate of oxygen transfer. Above 40°C, the solubility of oxygen decreases significantly, adversely affecting the driving force and rate of mass transfer.

#### 2.2.1.4 Solids suspension and related effects

Particulate solids may be present in a reactor for a number of reasons, the most significant of which are (i) as immobilisation surfaces for the cells e.g. in animal cell microcarrier cultures, (ii) as a supply of nutrients e.g. in mineral bioprocessing, and (iii) in bead mills for the disruption of cells to recover intracellular products. Through mixing, the solid particulates interact with each other, cells in the reactor and the reactor components. These interactions cause hydrodynamic stress to the organisms and thus the complete suspension of solids is desired at low power inputs and low levels of turbulence (Chisti and Moo-Young, 1996).

In addition to promoting hydrodynamic stress, the presence of solids can also influence gas-liquid mass transfer in the reactor. Several investigators have reported the reduction of mass transfer due to the presence of solids. Solids are postulated to affect the mass transfer coefficient by either modifying the interfacial turbulence at low solids concentration or by a diffusion-blocking effect. The specific interfacial area $a$ is affected by an increase in the apparent viscosity and by altered bubble coalescence rates. A decrease in gas hold up at high solids concentrations was observed by Mills *et al.* (1987), van Weert *et al.* (1995) and Derksen *et al.* (2000). Mills *et al.* (1987) investigated the change in the mass transfer coefficient ($k_La$) in slurries containing glass beads (66 μm diameter) and 0.1 M NaCl. The presence of particles reduced the $k_La$ by 63 % at a solids concentration of 40 % v/v. A 60 % decrease in $k_La$ in a 40 % v/v quartzite slurry (< 50 μm) was reported by van Weert *et al.* (1995), comparing favourably with the results of Mills *et al.* (1987). Derksen *et al.* (2000) studied bubble size and gas hold-up in finer quartzite slurries ($d_{50}$ 13 μm)

University of Cape Town

than those used by Mills *et al.* (1987). They reported that in an aerated system, as the solids fraction increased from 0 to 15 % v/v, $k_La$ decreased by 40 %. Boon *et al* (1992) showed that the volumetric $k_La$ decreased with increasing solids hold-up in coal slurries (< 100 μm). The authors found a 40 to 50 % decrease in $k_La$ at a volumetric solids hold-up of 28 %. The results of Boon *et al.* (1992) for coal compare favourably with those of Mills *et al.* (1987) and Derksen *et al.* (2000) for quartzite. However, in studying the effect of solids on mass transfer, it is important to take into consideration the oxygen consumption by solids such as pyrite and coal.

### 2.2.2 THE MECHANISM OF HYDRODYNAMIC STRESS IN STIRRED TANK REACTORS

Hydrodynamic stress can be defined as stress (to organisms) that originates from the movement of fluid. In biological reactors, this movement results from mixing and aeration of the fluid (sometimes bearing solids) within the system. If there are no nutrient and mass transfer limitations, cell injury in a hydrodynamic environment results from the application of mechanical stresses (Garcia-Briones and Chalmers, 1994). Hydrodynamic conditions in the stirred tank reactor are usually characterised by agitation intensity and aeration intensity (Toma *et al.*, 1991). During these processes, various interactions occur between the micro-organisms themselves, the abiotic reactor components and, if present, the particulate phase. These interactions can lead to cell stress and even cell death. Figure 2.1 illustrated the components common to most biological slurry reactors. From this diagram we can predict the interactions that may occur in a stirred tank slurry bioreactor. These are shown in Table 2.1.

University of Cape Town

**Table 2.1:** Interactions between cells and components of the slurry reactor vessel.

| High frequency stress interactions | Low frequency stress interactions |
|---|---|
| Particle-cell-particle | Cell-impeller blades |
| Particle-cell | Cell-vessel wall |
| Cell-bubble | Cell-baffle |
| Cell-fluid | |
| Cell-cell | |

These interactions result in (Cherry and Papoutsakis, 1986; Dunlop and Namdev, 1994; Michaels *et al.*, 1996; Doran, 1997):

(i) Shear stress occurring near solid objects in the vessel, especially in the impeller region,

(ii) Interactions between cells and turbulent eddies,

(iii) Attrition caused when the cell is caught between two solid particles entrained in the liquid medium,

(iv) Attrition from a particle rubbing against a cell,

(v) Collisions between cells, collision of cells with the impeller, and collision of cells with stationary surfaces in the vessel,

(vi) Shear stress affecting cells as bubbles rise through the liquid, and

(vii) Cell injury caused by compression waves generated due to bubbles bursting at the liquid surface.

In solids-free reactors, interactions between cells and bubbles and cells and turbulent eddies are considered most likely to damage cells (Cherry and Papoutsakis, 1986). In solids-containing, aerated reactors, the collisions between cells and solid phase particles are the predominant cause of cell injury (Scholtz-Brown, 1998).

#### 2.2.2.1 Interaction between cells and turbulent eddies

Cell damage has been associated and correlated with the relevant size of Komolgorov-scale turbulent eddies, $\eta$ (m). Investigators have shown that cell damage becomes severe when Kolmogorov–scale eddies are similar in size to the size of the cell (freely suspended cells) or microcarrier (attached cells) (Kunas and Papoutsakis, 1990). The Kolmogorov eddy size can be calculated from Eqn. 2.2.

$$\eta = (\nu^3/\varepsilon)^{1/4} \qquad \ldots\text{Eqn. 2.2}$$

where $\nu$ = kinematic fluid viscosity ($m^2\ s^{-1}$)

$\varepsilon$ = turbulent energy dissipation rate per unit volume ($W\ m^{-3}$)

If the cells are small relative to turbulent eddies, they tend to be captured or entrained in the eddies. As fluid motion within eddies is laminar, if the density of the cell is similar to the suspending fluid, there is little motion of the cell relative to the eddy. Hence the shear effects of eddy-cell interactions are minimal. Excessive agitation leads to formation of eddies with size small enough and of sufficient energy to cause damage to cells. The typical size of the smallest eddies in a 2 litre STR and a 100 $m^3$ STR was determined by Zhang *et al.* (1995) and Einsele (1978) to be 9 and 16 μm respectively. The characteristic size of microbial cells range from 0.5 to 5 μm indicating that shear stress due to eddy-cell interactions are an important consideration in STRs. In Figure 2.4, Cherry and Papoutsakis (1986) best illustrate the interaction between eddies and cells or particles (microcarriers). Figure 2.4 (a) shows microcarriers captured in large eddies and moving with the streamline flow while Figure 2.4 (b) shows the interaction between smaller eddies of opposing rotation and the microcarrier, simultaneously causing high levels of shear on the bead surface. Cells immobilised on the surface of micro-carriers or aggregates of comparable

University of Cape Town

size to turbulent eddies will be deformed in a turbulent regime due to work performed on the cells in this region (Dunlop and Namdev, 1994).

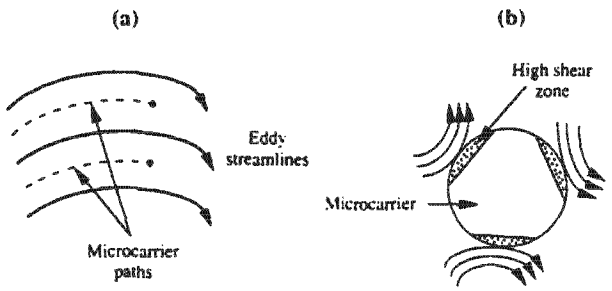


**Figure 2.4:** Eddy-microcarrier interactions (sourced from Cherry and Papoutsakis, 1986).

#### 2.2.2.2 Interaction between cells and bubbles

It has been proven extensively that the cell damage mechanisms resulting from gas sparging into bioreactors are associated primarily with bubbles bursting at the surface of the liquid and, to a lesser extent bubbles bursting within the bulk liquid (Kunas and Papoutsakis, 1990; Lu *et al*, 1992; Zhang *et al.*, 1992; Boulton-Stone and Blake, 1993; Illing and Harrison, 1999). Kunas and Papoutsakis (1990) showed that in a STR at agitation rates between 150 and 600 rpm, hybridoma cell damage was due to bubbles bursting at the liquid surface. Only at agitation rates above approximately 600 to 700 rpm did cell damage due to fluid forces (cell-eddy interactions) in the absence of bubbles play a role. Michaels *et al.* (1996) studied the effects of bubble break-up within the bulk liquid on animal cell damage in an STR. They postulated that at lower agitation intensities (below 200 to 250 rpm), bubble breakage in the bulk caused cell damage.

Breakage of the thin bubble film and rapid flow from the bubble rim back into the liquid generate high shear stress capable of damaging certain types of cells. A large number of hydrophobic substances, especially micro-organisms, tend to accumulate in the thin layer of liquid at the air-liquid interface. The contributing factors for cell-gas adhesion include: electrostatic forces, van der Waals forces, chemical interactions between the cell surface and the air-liquid interface, and hydrophobic interactions (Chattopadhyay *et al.*, 1995). It is proposed that cells are damaged by the rapid acceleration of the bubble film after rupture and the high levels of shear stress in the boundary layer associated with bubble jet formation. The location of a cell relative to a rupturing bubble can be classified into two regions: (i) cells adsorbed to the bubble film when the film breaks and (ii) cells adsorbed to or very near to the bubble cavity wall (Chalmers and Bavarian, 1991). Cells adsorbed to, or in the thin liquid layer surrounding a rupturing bubble, will be subjected to extremely high hydrodynamic forces, which are probably sufficient to disrupt them.

University of Cape Town

#### 2.2.2.3 Interaction between cells and solids

In the presence of solids, the particle-cell-particle damage mechanism predominates over the damage due to eddies and bubble shear (Pearce, 1993; Scholtz-Brown, 1998; Nemati and Harrison, 2000; Lamaignére, 2002; Deveci, 2002). During the solids suspension process, solids can either have a grinding effect (incompletely suspended solids or a high concentration of solids) on the cells or collisions can occur between cells and completely suspended solid particles (Scholtz-Brown, 1998). The extent of collision damage is expected to be a function of solids concentration and the impeller agitation rate (Scholtz *et al.*, 1997; Deveci, 2002; Nemati and Harrison, 2000). Collision damage is also affected by the size, shape and density of the particles (Pearce, 1993; Nemati *et al.*, 2000; Deveci, 2004).

It may be deduced that the frequency of the particle-particle collisions at a given agitation condition would ultimately govern the extent of cell damage. The increase in solids concentration or agitation speed or both gives rise to the increase in the probability and thereby frequency of the collisions between particles (Cherry and Papoutsakis, 1986, 1988). Collision frequency is extremely sensitive to the particle size and decreases with increasing the particle size under the same agitation conditions. However as the particle size becomes finer, the particle mass and terminal settling velocity will decrease with an increasing tendency of the finer particles to completely follow the fluid motion in eddy streamlines (Cherry and Papoutsakis, 1986, Kusters *et al.*, 1997). This could lead to the decrease in the probability and frequency of particle-particle encounters (Deveci, 2004). Pearce (1993) also supported this argument. Further, she argued that larger particles have greater kinetic energy than smaller particles and thus greater momentum. As a minimum force event is required to effect cell damage, smaller particles are unable to disrupt cells and only damage cells. However, for the same mass or volume concentration of solids, the number of particles increases with decreasing particle diameter, thus increasing the frequency of collisions between particles.

Several studies have been conducted in order to determine the mechanisms of damage when cells are grown in the presence of solid particulates. These studies could broadly be classified as microcarrier systems where cells are attached to microcarrier beads, yeast slurries where cells are grown in the presence of inert particles, and mineral slurries where cells are grown in the presence of mineral particles that serve as the energy source for the micro-organisms.

Cherry and Papoutsakis (1988) investigated the physical mechanisms of damage using growing primary bovine embryonic kidney cells attached to microcarrier beads in a STR. Three mechanisms of damage in the solids-containing system were hypothesised based on fluid mechanics. These were (i) collisions of a cell-covered microcarrier with other beads, (ii) collisions

University of Cape Town

of the cell covered microcarrier with parts of the reactor (primarily the impeller), and (iii) interaction of the microcarrier with turbulent eddies. When microcarrier beads collide, a physiologically significant amount of energy is released to the cell. Stathopoulos and Hellums (1985), reported that an applied shear stress $\tau$ of 10 dynes $cm^{-2}$ or more reduced the viability of flat monolayers of human embryonic kidney cells. The collision severity (CS) between particles and cells where the Kolmogorov microscale is of a similar size to the cells can be expressed as the product of the frequency and kinetic energy of collisions per cell (Eqn. 2.3). Collisions between beads and internal reactor components have a similar effect to bead-bead collisions. The important difference is that the kinetic energy of the collision is much higher.

$$CS_T = \frac{(\varepsilon v)^{\frac{3}{4}} \pi^2 \rho_p \alpha d_p^{\ 2}}{72} \qquad \text{...Eqn. 2.3}$$

where $CS_T$ = collision severity based on eddy velocity ($J.s^{-1}$)

$\varepsilon$ = rate of turbulent energy dissipation per mass of liquid ($W\ m^{-3}$)

$v$ = relative velocity of cells ($m\ s^{-1}$)

$\varrho_P$ = particle density ($kg\ m^{-3}$)

$\alpha$ = volume fraction of cells

$d_p$ = particle diameter (m)

Pearce (1993) conducted a study on the effect of hydrodynamic stress on stationary phase cells of *Saccharomyces cerevisiae* in a model yeast slurry system. The author found that disruption of the yeast cells occurred in the presence of solids. A first order rate equation was found to describe the disruption of the cells and the disruption rate constant ($k$) of the cells was dependent on the concentration of solids particles, particle size and impeller tip speed. For impeller speeds between 115 and 770 rpm, $k$ increased to 0.0024 $s^{-1}$ thereafter $k$ remained constant up to an impeller speed of 1090 rpm. The disruption rate constant followed a power law curve in the impeller speed range 115 to 540 rpm thereafter the model deviated from the data. This indicated that different disruption mechanisms dominated at impeller speeds below and above 540 rpm. The extent of disruption at low impeller speeds (< 380 rpm) was due to incomplete suspension of solids in the lower region of the reactor. Scholtz-Brown (1998) continued the studies of Pearce (1993) and investigated the effect of completely and incompletely suspended particulates on stationary phase cells of *S. cerevisiae*. Considering the incompletely suspended solids system, Scholtz-Brown (1998) identified two regions. The upper region where the solids are completely suspended and cells are disrupted by collisions between cells and one or more solid particles and the lower region where the solids are not fully suspended and the cells are disrupted by the grinding action of the adjacent solid particles. The author proposed that the cell disruption in the experiments with completely

University of Cape Town

suspended solids was found to occur mainly in the impeller region due to solid-cell-solid collisions, solid-cell collisions and solid-cell-reactor collisions. Experiments showed that collisions between the cell and two solid particles was the dominant mechanism of cell disruption. A modified mass transfer-type equation, Eqn. 2.4, describing the first order disruption rate constant as a function of power input per unit volume and the volume fraction of suspended solids, was derived for the completely suspended solids system (Scholtz *et al.*, 1997):

$$k = 7.11 \times 10^{-5} (P/V)^{0.56} \Phi_T^{1.64} \quad \ldots \text{Eqn. 2.4}$$

where $P/V$ = power input into the system per unit volume ($W/m^3$)

$\Phi_T$ = total solids volume fraction

The exponent of $\Phi_T$ can be related to the types of collisions that are responsible for cell disruption. The solid-cell-solid disruption mechanism is expressed as $c\Phi^2$ (Hinze, 1971 and Abrahamson, 1975 cited by Scholtz *et al.*, 1997). The cell-solid collision and solid-cell-reactor collision mechanisms are represented by $c\Phi$. In Eqn. 2.4, the exponent of $\Phi_T$ is closer to 2 than to 1 indicating that solid-cell-solid collisions are the dominant disruption mechanism in the yeast slurry system investigated.

Deveci (2002, 2004) investigated cell damage of mesophilic acidophiles in quartzite slurries. Several parameters including particle loading (0 to 30 % w/w), particle size (< 45 μm to -180+125 μm) and particle shape (spherical and irregular) were studied. The author showed that, as observed in the yeast-quartzite studies, hydrodynamic shear alone as a characteristic function of impeller type and speed has very limited effect on the bacterial cells during mixing in STRs, but mechanical damage occurs, to a more significant extent, via the attrition by solid particles and promoted by the intensity of agitation. In an attempt to determine the mechanism of damage to the cells, Deveci (2002) calculated the size of the smallest eddies generated in the presence of solids. In the presence of solids the smallest eddy size is greater (approximately 3 fold) than in the absence of solids. At 30 % w/w and an impeller tip speed of 3.35 m $s^{-1}$, this was approximated to 59 μm in the bulk fluid and 28 μm around the impeller zone. Thus, due to the relatively small size of the cells (0.5-1.5 μm) compared to the smallest eddy size, turbulent shear effects were considered negligible. However, this conclusion is only valid for planktonic cells and not for cells attached to the solids. Deveci (2001) also showed, as found by Scholtz-Brown (1998) and Pearce (1993), that collisions between cells and internal reactor components were minimal and thus concluded that the mechanism of damage was particle-cell-particle collisions.

University of Cape Town

## 2.3 THE STRUCTURE OF MICRO-ORGANISMS

A review of the structure of micro-organisms contributes to the understanding of their susceptibility to, and the structural defences they possess against, hydrodynamic stress. Four aspects of cell anatomy are important as barriers to mechanical stress. These are (Prokop and Bajpai, 1992):

(i) The cell envelope (comprised of membrane and wall) which forms the physical barrier against hydrodynamic forces;
(ii) The cytoskeleton which absorbs the energy generated by turbulence;
(iii) The cell size which determines the magnitude of kinetic energy absorbed by the cell; and
(iv) The presence of mechanisms to receive fluid mechanical stimuli.

Further consideration will be given to the cell envelopes of bacteria, yeasts and Archaea, due to the implications of the dissimilar structure and composition of the cell walls and membranes of micro-organisms belonging to these phylogenetic domains on their resistance to mechanical stress.

### 2.3.1 THE CELL ENVELOPE

The cell envelope is the only physical barrier between the micro-organism and the surrounding environment. In general, cell envelopes of prokaryotic bacteria and eukaryotic unicellular yeast consist of a cell membrane, a cell wall and in some micro-organisms, a surface layer while the cell envelopes of Archaea comprise a cell membrane and a cell wall (Figures 2.5a and 2.5b). The cell wall provides structural support and determines the cell shape (Brock and Madigan, 1991) while the plasma membrane is a highly selective barrier enabling the micro-organism to concentrate specific metabolites and excrete waste material.

University of Cape Town

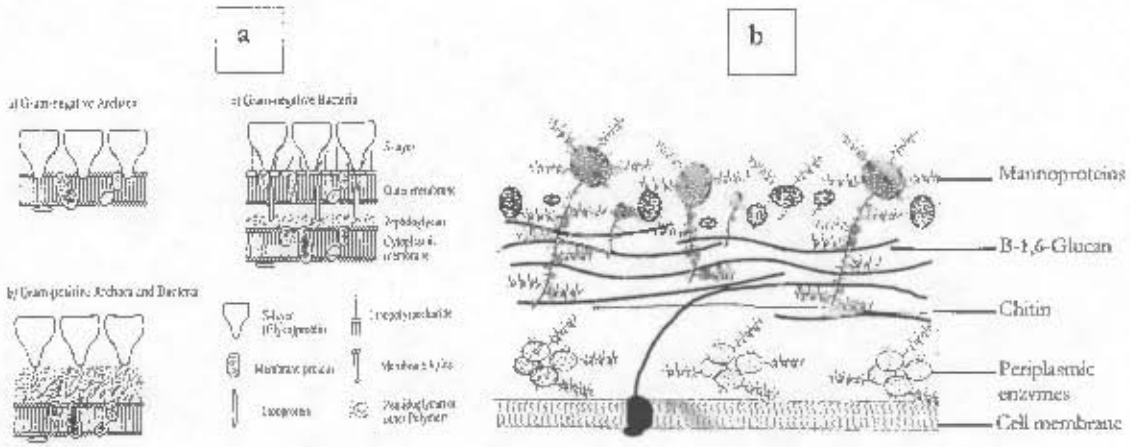


Figure 2.5: Schematic illustrations of the cell walls of (a) bacteria and Archaea, and (b) yeast (sourced from Schuster and Sleytr, 2000 and Walker, 1998).

### 2.3.1.1 The cell wall

The structure of the bacterial cell wall is used to distinguish between two groups of bacteria, Gram-positive and Gram-negative. Gram-positive cells possess a single, thick peptidoglycan layer outside of the plasma membrane. The cell wall of Gram-positive bacteria comprises 50 to 80 % peptidoglycan, presenting a greater structural resistance to fracture. The Gram-negative bacteria have a thin peptidoglycan layer outside the plasma membrane that is surrounded by an outer membrane. The rigid peptidoglycan layer is primarily responsible for the strength of the bacterial cell wall (Brock and Madigan, 1991). The peptidoglycan structure is similar in all bacteria and is composed of linear polysaccharide chains of alternating N-acetyl-D-glucosamine (NAG) and N-acetyl-muramic acid (NAM) residues joined by β-(1-4) glycosidic bonds. The chains are cross-linked by a tetra peptide of basic structure L-alanyl-D-glutamyl-L-$R_3$-D-alanine attached to the $C_3$ lactic acid side chains of the NAM residue. The resultant macromolecular structure provides the cell wall with tensile strength (Holtje and Glaunet, 1990).

The yeast cell wall is relatively thick and is 15 to 25 % of the total dry mass of the cell. The cell wall consists predominantly of three macromolecules: lipids, proteins and polysaccharides (mannan, glucan and chitin). Polysaccharides are the most abundant constituents accounting for 80 to 90 % of the wall by mass. Glucan and mannan are the predominant polysaccharides and render strength to the yeast cell wall.

There are two cell wall types in Archaea. The Gram-positive Archaea have a similar cell wall structure to the Gram-positive bacteria with a rigid peptidoglycan layer. The cell walls of the Gram-negative Archaea do not possess the rigid peptidoglycan layer. Their cell wall consists only

University of Cape Town

of one or two surface layers (S-layers) composed of protein or glycoprotein subunits in a two-dimensional crystalline arrangement (König, 1988; Baumeister and Lembke, 1992, Pum *et al* 1999). A possible explanation for the lack of peptidoglycan in Gram-negative Archaea is that some of the enzymes required for peptidoglycan biosynthesis do not function either at pH 2 or at high temperature (Michel *et al.*, 1980; König, 1988). In addition, cell envelopes with a high degree of rigidity are not required for life at high temperatures and low pH values. The S-layer is closely associated with the cytoplasmic membrane and covers the entire cell surface (Baumester and Lembke, 1992). Most S-layers are composed of single, high molecular-weight polypeptide species (protein or glycoprotein) with apparent molecular masses of 40 to 220 kDa (Messner, 1996; Pum *et al.*, 1999). S-layer subunits are usually held to each other and to the underlying wall by weak bonding forces: electrostatic interactions. Consequently, relatively mild extraction procedures can be used for their removal.

#### 2.3.1.2 The cell membrane

The bacterial and yeast plasma membrane is an 8 nm thick bilayer composed mostly of phospholipids and sterols. The archaeal membrane lacks fatty acids and instead has hydrocarbon moieties bonded to glycerol by ether linkages instead of ester linkages. There are four fundamental differences between the archaeal, and bacterial and yeast membranes: (i) chirality of glycerol, (ii) ether linkage, (iii) isoprenoid chains, and (iv) branching of side chains. Their ability to survive in extreme conditions is probably due to the unique structure of the archaeal membrane lipids. For example, at temperatures above the optimal temperature of growth, the membranes of bacteria and yeast become excessively fluid resulting in leaky membranes. In contrast, the Archaea are able to adapt the fluidity of their membrane and thus maintain the normal membrane permeability (van den Vossenberg, 1999).

#### 2.3.1.3 Differences between the cell envelopes of bacteria, yeast and Archaea

Table 2.2a lists examples of the major differences between the cell envelopes of bacteria, Archaea and yeasts. The Gram-negative Archaea have chemically different cell membranes and chemically and structurally different walls to bacteria and yeast. It is clear that the cell wall of the Archaea lacks the macromolecules that provide rigidity to the cell walls of bacteria and yeast, thus rendering these micro-organisms more susceptible to the effects of mechanical stress. The effect of a less rigid cell wall or the lack of a cell wall on an organism's capacity to tolerate hydrodynamic stress capacity is more clearly seen in Table 2.2b. The organisms are compared on the basis of their susceptibility to hydrodynamic stress based on the results of a study by Märkl *et al.* (1991). Organisms containing macromolecules such as murein and cellulose which confer rigidity to the cell wall were less susceptible to the effects of hydrodynamic stress than those organisms without a cell wall or with only glycoprotein- or protein-containing cell walls.

University of Cape Town

**Table 2.2a:** Some of the major differentiating and common molecular traits among the bacteria, Gram-negative Archaea and yeast (adapted from Martinac and Kloda, 2003).

| Trait | Bacteria | Gram-Negative Archaea | Yeast |
|---|---|---|---|
| Cell size | ≈ 1 μm | ≈ 1 μm | ≈ 10 μm |
| Cell wall | Peptidoglycan | Protein or glycoprotein S-layers | Glucan, mannan and protein |
| Membrane lipids | Ester linked, straight chains fatty acids | Ether linked, branched hydrocarbons | Ester linked, straight chains fatty acids |
| Cytoskeleton | Absent | Absent | Present |

**Table 2.2b:** Organisms arranged by virtue of their susceptibility to hydrodynamic shear stress (adapted from Märkl *et al.*, 1991).

| Organism | Group | Cell wall thickness (nm) | Cell wall constituent |
|---|---|---|---|
| | **Least susceptible to hydrodynamic stress** | | |
| *Chlorella* | Green algae | 100-120 | Cellulose, pectin, sporopollenin |
| *Methanobacterium* | Methane bacteria | 10-15 | Pseudomurein |
| *Synechococcus* | Cyanobacteria | 20-30 | Murein |
| | **Most susceptible to hydrodynamic stress** | | |
| *Chlamydomonas* wild type | Green algae | 40 | Glycoprotein |
| *Methanococcus* | Methane bacteria | 18 | Protein |
| *Chlamydomonas* CW 15 | Green algae | No cell wall | n/a |

n/a = not applicable

## 2.4 THE IMPACT OF STRESS ON ORGANISMS

As a result of the effects of hydrodynamic stress, several changes are observed within the culture in an STR. These include changes in cell viability and cell morphology, as well as a decrease in the overall metabolic rate, an increased requirement for cell maintenance and cell death (Augenstein *et al.*, 1971; Croughan *et al.*, 1987; Abu-Reesh and Kargi, 1991; Chalmers and Bavarian, 1991; Lamaignére, 2002). Depending on the severity of the stress, reduced levels of product formation or transformation may result and thus influence the overall process performance. Basson *et al.* (1997) proposed a scheme (Figure 2.6) highlighting the effects of hydrodynamic and physiological stress on microbial performance in process systems. In this scheme, the effects of differing degrees of hydrodynamic stress on the cell are illustrated, starting with minor damage to the outer cell layers and leading up to cell lysis.

University of Cape Town

Healthy cells exposed to mild mechanical stress experience **minor envelope damage**. Although the extent of this damage may not affect cell growth or metabolism directly, other factors such as the release of certain proteins or wall fragments into solution may be undesired. More severe mechanical stress leads to **membrane damage** in which cells lose their ability to replicate due to weakened membrane function. During this process cells become 'leaky' and are unable to maintain internal cytoplasmic function. Prolonged or extreme mechanical stress may lead to **cell death** and in extreme cases, **cell lysis**. The sensitivity of organisms to hydrodynamic stress depends on the stability and morphology of the cell wall (Märkl *et al.*, 1991). Hence, in the case of organisms with no cell walls, e.g. animal cells, or organisms with cell walls of reduced structural integrity, e.g. Gram-negative Archaea, this effect is seen on exposure to less extreme hydrodynamic stress.

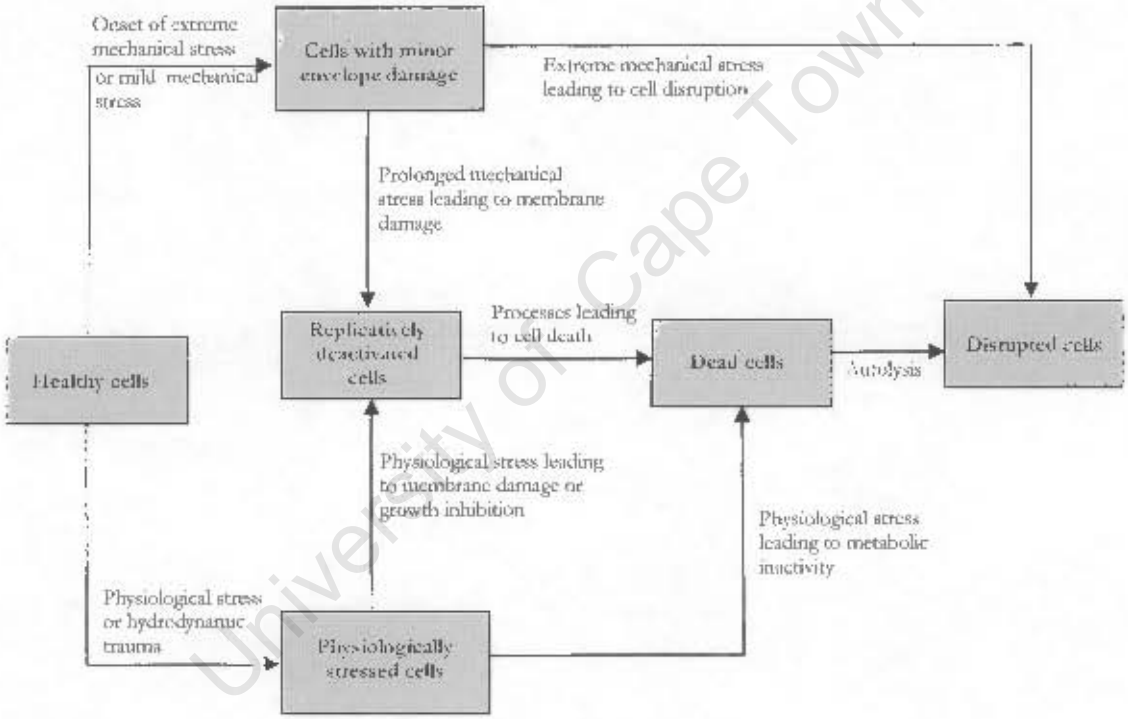


Figure 2.6 Scheme for the loss of cell quality due to the effect of physiological and hydrodynamic stress (adapted from Basson *et al.*, 1997).

### 2.4.1 CELL WALL DAMAGE

The lack of a cell wall or the presence of a cell wall of reduced structural strength has been proposed to increase the susceptibility of organisms to mechanical stress. Loss of cell wall integrity has been linked to hydrodynamic stress as well as to stress induced by changes in temperature and pH (Abu-Reesh and Kargi, 1991; Han *et al.*, 1997; Lamaignére, 2002). A cell with

University of Cape Town

a damaged wall may retain its ability to grow and metabolise. However, extreme or prolonged mechanical stress may lead to rupture of the cell wall and consequently the cell membrane. For example, Lamaignére (2002) investigated the effect of mechanical stress on *S. cerevisiae* and found that on exposure to 1 % v/v quartzite and an agitation rate of 850 rpm, rupture of the cell wall was observed. Figure 2.7 shows a yeast cell with a disrupted cell envelope releasing intracellular compounds into the growth medium.

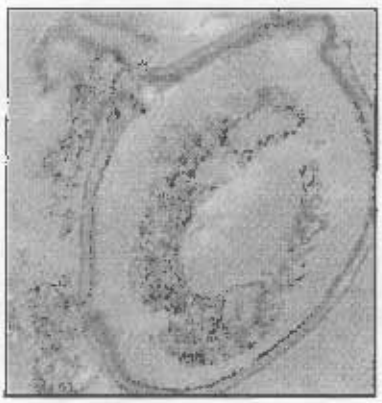

**Figure 2.7:** Transmission electron micrograph of a lysed yeast cell exposed to 1 % v/v quartzite and an impeller speed of 850 rpm (sourced from Lamaignére 2002).

University of Cape Town

### 2.4.2 CELL MEMBRANE DAMAGE

When mechanical stress leads to damage of the cell membrane, the growth and metabolism of the cell becomes compromised. The cell membrane is vital for separating the biological function of the cell from its environment. If membrane integrity is lost, the cell integrity is destroyed (Brock and Madigan, 1991). Three main metabolic processes are affected by damage to the cell membrane: the 'reproductive capability' (viability) of the cells, the functioning of the electron transport system and, for acidophilic micro-organisms in particular, chemiosmosis and maintenance of a near neutral internal pH. The viability of a cell is dependent on the presence of a functional plasma membrane (Jones, 1987). If the membrane is damaged, the cell loses the ability to divide. In addition to having a reproductive function, the cell membrane also provides a barrier to the low pH environment, regulating a constant internal pH necessary for maintaining microbial growth and metabolism. Permeabilisation of the cell membrane of acidophiles leads to rapid inactivation of biomolecules in the cytoplasm (Peeples and Kelly, 1995). The membrane of acidophilic micro-organisms maintains a pH gradient of 4 or 5 pH units (van de Vossenberg *et al.*, 1998). Thermoacidophiles such as *S. acidocaldarius* accomplish this task by proton pumping (Anemüller *et al.*, 1985). When *Metallosphaera sedula*, growing at 74°C, was transferred to temperatures above 80°C, the micro-organism appeared to lose its capability to maintain the equivalent near neutral internal pH levels measured during growth at optimal temperatures.

Han *et al.* (1997) proposed this to result in part from damaged membrane integrity at non-optimal temperatures. In addition to maintaining a near neutral intracellular pH, the large pH gradient is linked to cellular respiration. The extracytoplasmic oxidation of sulphur and metal sulphides has been linked to the generation of energy through chemiosmotic coupling in chemolithotrophic acidophiles (Peeples and Kelly, 1995). Thus, permeabilisation of the membrane could cause acidification of the cytoplasm and affect the cell energetics.

### 2.4.3 THE IMPACT OF HYDRODYNAMIC STRESS IN SOLIDS-FREE AND SOLIDS-CONTAINING SYSTEMS

As discussed in Section 2.2.2, in well mixed biological reactors in the absence of particulate solids, hydrodynamic stress may be attributed to the interaction between cells and turbulent eddies, shear stress generated through fluid flow, shear stress generated by rising bubbles and those associated with bubble rupture. In the slurry bioreactor, where particulate solids are present, hydrodynamic stress arises primarily from particle-cell-particle collisions, particle-cell-reactor internal collisions and attrition in the expanded bed of solids should incomplete suspension result (Section 2.2.2). In this section, literature studies on microbial cell damage in solids-free and solids-containing reactor systems are reviewed.

#### 2.4.3.1 The impact of hydrodynamic stress in solids-free systems

The effect of hydrodynamic stress on growth and death in unicellular systems has been extensively studied. Table 2.3 lists relevant studies carried out on human, animal, plant, yeast and microbial cells in the presence of hydrodynamic shear conditions in the absence of solids. Experiments were carried out in a variety of reactors ranging from stirred tank reactors to capillary systems. The negative effects induced by hydrodynamic shear included loss of viability, decreased product formation, physical damage and cell death while in mass transfer limited systems, improved mixing of the reactor contents led to an increase in biomass production. In general, cell-turbulent eddy as well as cell-bubble interactions have been identified as the primary causes of hydrodynamic stress. The extent of damage was also linked to the cell type, more specifically the cell wall structure and cell size.

University of Cape Town

Table 2.3: The effect of hydrodynamic shear in solids-free systems.

| Organism | Proper cell wall present? | Reactor | Experiment | Cause of stress | Effect | Reference |
|---|---|---|---|---|---|---|
| Human HeLa S3 and mouse L929 | No | Capillaries | Effect of pumping cells through capillaries | Wall shear | Loss of viable cell count and cell death | Augenstein *et al.*, 1971 |
| *Methanococcus thermalithotrophicus* | No | STR | Effect of agitation Rate | - | Increase in agitation rate increased biomass production | Pellex *et al.*, 1988 |
| Hybridoma cells | No | Stirred vessel | Effect of agitation rate | Fluid shear | Inhibition of DNA synthesis; increased metabolic activity; decrease in growth rate | Al-Rubeai *et al.*, 1990 |
| Hybridoma cells | No | STR | Effect of agitation rate | Fluid shear | Decrease in cell concentration and respiration; increased lactate dehydrogenase release; increase in specific glucose consumption rate | Abu-Reesh and Kargi, 1991 |
| Insect cells | No | n/a | Effect of insect-bubble interactions | Bubble shear | Cell death | Chalmers and Bavarian, 1991 |
| *Brevibacterium flavum*, *Trichoderma reesei* and *Saccharomyces cerevisiae* | Yes | STR | Effect of agitation rate | Fluid shear | Inhibition of microbial growth and metabolism | Toma *et al.*, 1991 |
| Plant cells | Yes | STR | Effect of fluid forces | Fluid shear | Physical damage to cells as well as loss of viability | Dunlop and Namdev, 1994 |
| Insect cells | No | n/a | Effect of bubble rupture | Bubble shear | Cell death due to cell adhesion on bubble surface; protective additives decreased the damage effect | Chattopadhyay *et al.*, 1995 |
| *Pyrococcus furiosis* and *Methanococcus vanbellii* | No | Stirred membrane reactor | Effect of agitation rate | Fluid shear | *P. furiosis* low cell yields above 1800 rpm; *M.vanbellii* low cell yield above 1000 rpm | Krahe *et al.*, 1996 |
| *Methanococcus jannaschii* | No | STR | Effect of agitation rate | - | Increase in cell density with increase in tip speed up to 2.35 m $s^{-1}$ | Mukhopadhyay *et al.*, 1999 |
| *Corynebacterium glutamicum* | Yes | STR and Air lift reactor | Effect of agitation rate | -Fluid shear: -Bubble shear: | Cell aggregate breakup | Illing and Harrison, 1999 |

n/a = not applicable

University of Cape Town

*2.4.3.1.1 The effect of fluid shear*

Increasing the agitation and aeration rate in a system may increase microbial activity by enhancing mass transfer and mixing. However, beyond a certain limit, turbulent flows inhibit microbial growth and activity (Toma *et al.*, 1991). In most studies where agitation and aeration rates were increased up to a critical point, there was an initial increase in growth rate and metabolic activity of the culture (Mukhopadhyay *et al.*, 1999; Abu-Reesh and Kargi, 1991). Abu-Reesh and Kargi (1991) studied the effect of impeller speed on cell viability, glucose consumption, lactate dehydrogenase (LDH) release and monoclonal antibody (MAb) production of hybridoma cells in an STR. They determined that increasing the agitation rate from 60 to 137 rpm in a STR resulted in an increase in the hybridoma cell concentration as the oxygen-transfer limitation found at low agitation rates was overcome. Increasing the agitation rate from 100 to 191 rpm did not enhance growth further and led to a loss of culture activity, a decrease of 15 % in the cell concentration, a decreased MAb production and a release of 20 % of LDH into the culture medium. Increasing the speed from 191 to 350 rpm caused approximately 75 % of the LDH to be released into the medium.

Toma *et al.* (1991) found that the microbial growth rate and lysine biosynthesis of the Gram-positive bacterium *B. flavum* decreased when the impeller tip speed of the STR was increased above 3.11 m $s^{-1}$ (900 rpm). Lysine production was affected due to a decrease in aconitase production, the key enzyme in lysine biosynthesis. In addition, the high agitation rates induced the production of the stress indicator, histadine. The growth rates of the fungus *T. reesei* and the yeast *S. cerevisiae* were also shown to decline above impeller tip speeds of 0.52 m $s^{-1}$ (150 rpm) and 2.76 m $s^{-1}$ (800 rpm) respectively. The authors also showed that shear effects caused decreased adenosine triphosphate (ATP) generation. Shear stress damaged cell membranes regulating ATP regenerating systems and led to alterations in cell morphology and metabolism. The term turbohypobiosis was introduced to describe this inhibition. Turbohypobiosis was characterised by a stress factor expressing the interaction of medium flow with microbial cells in local turbulent zones, dependent on the energy distribution of the agitation regime.

The extent to which fluid shear affects cells is a function of the cell morphology and the cell wall structure. In the study of Toma *et al.* (1991), results indicated that although the shear stress caused by increasing agitation rate had an effect on all three cell types (bacterial, fungal and yeast) tested, the resistance to shear varied between the micro-organisms. The bacterium, *B. flavum*, showed the highest resistance to increased agitation rates. Bronnenmeier and Märkl (1982) showed cells devoid of cell walls are more prone to shear effects. The authors investigated the effect of impeller speed on the cyanobacterium, *Spirulina platensis* and a cell-wall-defective mutant strain of the green alga,

University of Cape Town

*Chlamydomonas reinhardii* in a STR. *S. platensis* was found to be sensitive to shear stress but still less sensitive than the cell-wall-defective mutant strain of *C. reinhardii*. The specific growth rate of the cyanobacterium remained at 0.105 $h^{-1}$ on increasing the impeller speed to 2400 rpm while the specific growth rate of the cell-wall-defective green alga declined from 0.085 $h^{-1}$ at 300 rpm to 0.04 $h^{-1}$ at 900 rpm. The authors continued this study and Märkl *et al.* (1991) reported the effect of shear stress again on *C. reinhardii* and *S. platensis* and also studied a *Synechococcus* sp., a *Methanobacterium thermoautotrophicum* culture and a *Methanococcus vanielli* culture. The susceptibility of the cells to hydrodynamic stress was dependent firstly on the absence or presence of a cell wall as reported by Bronnenmeier and Märkl (1982), and secondly on the cell wall structure. Of all the organisms studied, the cell-wall-defective mutant strain of *C. reinhardii* was the most sensitive to the effects of shear stress, indicating that the lack of a cell wall was the overriding factor in determining the hydrodynamic stress capacity of an organism. The resistance to damage of the murein-containing cyanobacterium *Synechococcus* and the pseudomurein-containing *M thermoautotrophicum* was higher than *M vanielli* cells whose walls consisted of only protein or glycoprotein S-layers.

*2.4.3.1.2 The effect of cell-bubble interactions*

In Section 2.2.2.2, the mechanism of cell injury induced by the presence of bubbles was discussed. Rupture of bubbles at the liquid surface was determined to be the primary mechanism of cell damage. Chalmers and Bavarian (1991) subjected two strains of insect cells to bubble shear. The authors found that cell death occurred when cells were either attached to or found near rupturing bubbles. Chattopadhyay *et al.* (1995) reported a similar effect. Insect cells were killed when exposed to bubbles which, when ejected from a hypodermic needle ruptured at the liquid surface. The number of disrupted cells decreased on addition of protective agents such as pluronic acid into the medium. Illing (1996) investigated the effects of both liquid shear and bubble rupture at the liquid surface on the bacterium *C. glutamicum*. No effect on the viability, rate of growth, rate of metabolism and cell lysis was observed, however fragmentation of cell aggregates occurred. Further experiments using the same micro-organism were conducted to determine the contribution of collapsing bubbles to cell aggregate break-up. The cells were grown in continuous culture in a STR and an airlift reactor. Aggregate break-up in the airlift reactor was exclusively due to collapsing air bubbles whereas in the STR both agitation and collapsing air bubbles contributed. The particle count in the STR increased by 15 % compared to 7 % in the airlift. The increase in particle count was indicative of an increase in aggregate break-up, illustrating a contribution from both agitation and collapsing air bubbles (Illing and Harrison, 1999)

University of Cape Town

### 2.4.3.2 The effect of hydrodynamic stress in solids-containing systems

In Section 2.2.2.3 it was shown that when solids are present in a reactor, the cell disruption occurs primarily due to solid-cell interactions and that fluid shear and bubble shear effects are negligible (Pearce 1993; Scholtz-Brown, 1998).

#### *2.4.3.2.1 Solids loading*

The concentration of solids in a reactor can affect the extent of cell damage owing to its effect on the collision frequency. Increasing the solids loading increases the frequency of collisions between cells and solids and thus increases the hydrodynamic stress. Croughan *et al.* (1988) studied the effect of increasing microcarrier concentration on animal cells in an STR. At high concentrations of microcarriers, the cells showed very long lag phases and decreased rates and extents of growth. Whereas a 2.3 fold increase in cell concentration was observed at a 0.05 g $l^{-1}$ loading, a 1.2 fold increase was observed over the same time period at a loading of 15 g $l^{-1}$ (Figure 2.8a). Furthermore, the growth rate decreased from 5.51 to 1.53 $h^{-1}$ on increasing the microcarrier concentration from 0.0 to 30 g $l^{-1}$ (Figure 2.8b).

In a quartzite slurry system, Scholtz *et al.* (1997) and Scholtz-Brown (1998) investigated the effects of solids concentration on **non-growing** cells of *Saccharomyces cerevisiae*. They reported increased soluble protein release with increasing solids loading. The disruption rate of *S. cerevisiae* at a tip speed of 2.91 m $s^{-1}$, and a particle size distribution in the range 600 to 850 μm, varied from 7.08 x $10^{-5}$ $s^{-1}$ at 5 % (v/v) inert solids, to 4.05 x $10^{-3}$ $s^{-1}$ at 40 % (v/v) inert solids. The study by Scholtz-Brown (1998) was extended by Lamaignére (2002) to investigate the effect of solids loading (0 to 5 % v/v) on **growing** cells of *S. cerevisiae*. An increase in the lag phase from 3.0 through to 6.5 h was observed on increasing the solids loading from 0 to 2 %. Furthermore the specific death rate increased from 0.00 through to 0.142 $h^{-1}$ on increasing the quartzite concentration form 0 to 2 %. At a 5 % quartzite loading, no cell growth, substrate consumption or product formation was observed, indicating a complete loss of metabolic activity. At this solids concentration the specific death rate was 0.275 $h^{-1}$.

University of Cape Town

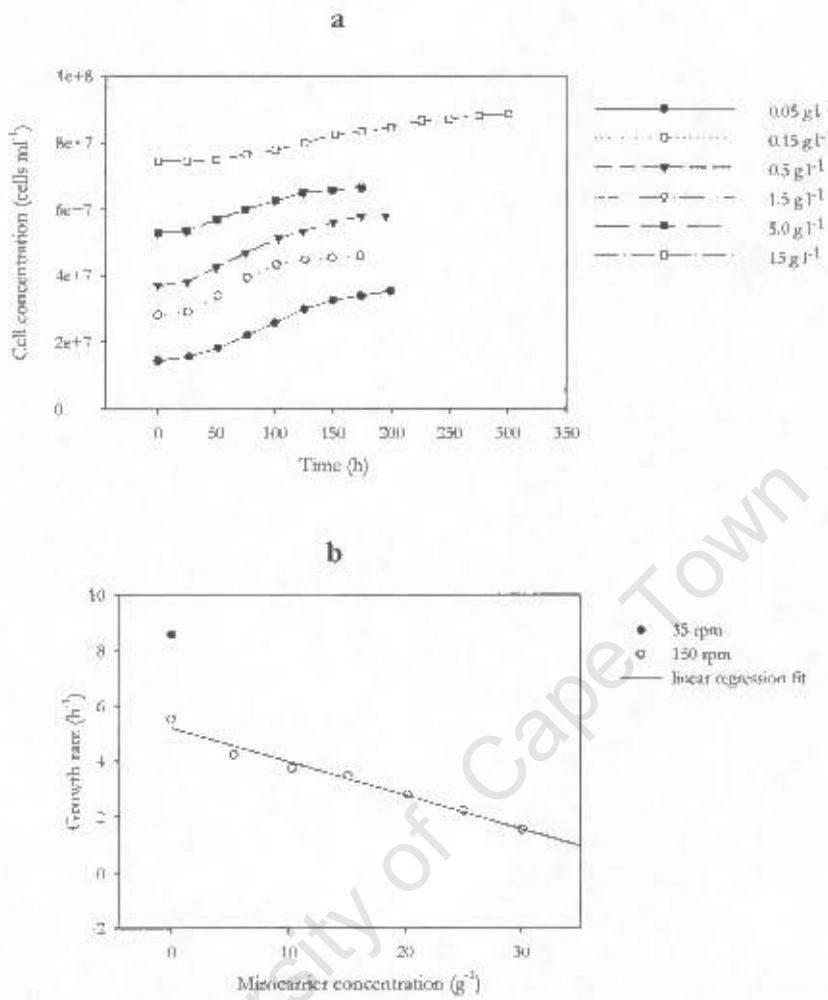


**Figure 2.8:** Change in (a) cell concentration and (b) growth rate of HS-4 cells at increasing microcarrier concentrations (adapted from Croughan *et al.*, 1988).

University of Cape Town

*2.4.3.2.2 Impeller speed and type*

Croughan *et al.* (1987) investigated the effect of agitation speed in a magnetically stirred vessel at a solids loading of 0.3 % w/v on the growth of human diploid fibroblasts cells attached to micro-carriers. They reported a decrease in the growth rate and an increase in the specific death rate (Table 2.4) with increasing impeller speed. The specific death rate increased as a power law function of impeller speed. A similar relationship between the specific death rate constant and impeller speed was observed by Lamaignére (2002). The author studied the influence of agitation intensity at a solids loading of 1 % v/v on growing cells of *S. cerevisiae*. The cell death rate was found to increase as a power law function of increasing impeller speed (Table 2.4). Below an impeller speed of 565 rpm, the cell growth rate and the extent of growth was low. This effect was attributed to nutrient limitation

owing to inadequate mass transfer. At speeds above 600 rpm, a decrease in cell viability and activity was observed.

**Table 2.4:** Specific death rates calculated for various impeller speeds and cell types.

| Croughan *et al.* (1987) | | Lamaignére (2002) | |
|---|---|---|---|
| Human diploid fibroblasts immobilised on micro-carriers ; magnetically stirred vessel | | *S. cerevisiae* grown in the presence of quartzite; STR | |
| **Impeller speed (rpm)** | **Specific death rate ($h^{-1}$)** | **Impeller speed (rpm)** | **Specific death rate ($h^{-1}$)** |
| 60 | 0 | 565 | 0.118 |
| 140 | 0.011 | 600 | 0.128 |
| 180 | 0.018 | 800 | 0.140 |
| 220 | 0.027 | | |

The type of agitator used in a STR critically affects solids suspension, mass transfer and the intensity of hydrodynamic stress. Scholtz-Brown (1998) found that at a given impeller speed, either below or above the critical impeller speed required for complete suspension of the solids, cell disruption was lower on agitation with the pitched blade turbine than the Rushton turbine. She attributed this difference to the lower power input of the pitched blade turbine compared to the Rushton turbine and successfully modelled the disruption rate as a function of power input per unit volume across both impellers. Lamaignére confirmed these observations for the growing yeast system (Table 2.5). At a 0 % v/v solids concentration the maximum specific growth rate ($\mu_{max\ exp}$) of the culture was higher using a Rushton impeller than a pitched blade impeller. This difference in $\mu_{max\ exp}$ was attributed to improved mass transfer provided by the Rushton impeller. On increasing the solids loading to 1 % v/v, a sharp decline in $\mu_{max\ exp}$ was observed with the Rushton impeller. Increasing the solids concentration to 1 % had a less significant influence on $\mu_{max\ exp}$ and $\mu_{viable\ cells}$ (specific growth rate based on the viable cell concentration) using the pitched blade impeller compared to the Rushton impeller. The increased turbulence caused by the Rushton turbine improved the maximum specific growth rate compared to the pitched blade turbine when there were no solids present in the reactors. However, the increased turbulence combined with increased solids concentration at 1 % compounded the hydrodynamic stress effect leading to a decrease in the maximum specific growth rate.

University of Cape Town

**Table 2.5:** Influence of impeller type on the maximum specific growth rate and the specific growth rate based on the viable cell concentration of *S. cerevisiae* in the presence or absence of quartzite solids (650-800 µm) (Lamaignére, 2002).

| Solids loading (%; v/v) | Impeller type | $\mu_{max\ exp}$ ($h^{-1}$) | $\mu_{viable\ cells}$ ($h^{-1}$) |
|---|---|---|---|
| 0 % | Rushton turbine | 0.254 | 0.253 |
| 0 % | pitched blade turbine | 0.164 | 0.155 |
| 1 % | Rushton turbine | 0.135 | 0.138 |
| 1 % | pitched blade turbine | 0.141 | 0.144 |

*2.4.3.2.3 Particle size*

Harrison *et al.* (2003) investigated the effect of varying quartzite particle size (mean diameters ranging from 114 to 1245 µm) on stationary phase *S. cerevisiae* in a STR. At a solids concentration of 20 % v/v, the disruption rate constant (k) increased from 0.00013 to 0.00037 $s^{-1}$ on increasing the mean particle diameter from 114 to 304 µm. The rate constant reached a plateau at a mean diameter of 703 µm. The maximum extent of disruption, given by the ratio of the maximum disrupted soluble protein to the maximum available soluble protein, increased from 30.8 to 74.3 % with increasing the mean particle diameter from 114 to 304 µm. A 96.0 % disruption was observed at a particle size of mean diameter of 1245 µm. Lamaignére (2002) found that increasing the mean quartzite particle diameter from 693 to 1021 µm even at a solids loading of 1 % v/v, caused a decrease in the specific growth rate and biomass yield *of S. cerevisiae* culture on glucose. The specific growth rate declined from 0.135 to 0.109 $h^{-1}$ while the yield of cells on glucose decreased from 7.15 to 2.09 x $10^9$ cells $g^{-1}$ on increasing the mean particle diameter from 693 to 1021 µm. No difference in terms of specific growth rate and biomass yield was observed at particle sizes below 693 µm.

*2.4.3.2.4 Solids shape and type*

In a study conducted in shake flask cultures, Deveci (2004) showed that spherically shaped glass beads induced a greater loss of cell viability of a mixed mesophilic culture of acidophilic bacteria (*At. ferrooxidans* and *Leptosprillum ferriphilum*) than the irregular and angular quartzite particles. It was found that after a 3 h exposure to glass beads particles, 92 % of viable cells were deactivated while 84 % were deactivated with the irregular quartzite particles. This effect was ascribed to the more efficient grinding action of the spherical glass beads. In agreement with results of Deveci (2004), Dispirito *et al.* (1981) who studied the effect of glass beads on ferrous iron oxidation by *At. ferrooxidans* in shake flask culture at 160 rpm, found that the smooth, spherical glass beads caused significant inhibition. The rates of iron oxidation declined with increasing solids loading from 1 to 4 % and almost complete

University of Cape Town

inhibition was observed at a 5 % concentration of solids. In contrast, Pearce (1993) who studied the effect of particle shape in a yeast-quartzite slurry reactor, showed that irregular quartzite particles (mean size of 364 μm) with jagged edges caused a higher maximum extent of disruption of yeast cells when compared to smooth quartzite particles (mean size of 304 μm). The ratios of the maximum soluble protein released on disruption to the maximum available soluble protein was 74 and 88 % for the smooth and jagged particles respectively.

In addition to glass beads, Dispirito *et al.* (1981) also studied the effect of flowers of sulphur, fluorapatite, glass beads and pyrite on ferrous iron oxidation by *At. ferrooxidans*. Pyrite and flowers of sulphur had the greatest effect on ferrous iron oxidation. At a 0.1 % solids loading both particle types caused inhibition of the bacteria. Above a 1 % pyrite concentration, bacterial oxidation was completely inhibited. In contrast, 5 % fluorapatite had little influence on iron oxidation but at lower concentrations (0.1 to 4 %) these particles completely inhibited bacterial activity (Dispirito *et al*, 1981).

## 2.5 THE EFFECT OF COMPOUNDING STRESSES

Stresses to micro-organisms in bioreactors are rarely singular. Hydrodynamic stress in itself can be termed a compound stress resulting from the combination of stresses induced by aeration, mixing and the presence of solids resulting in shear stress, attrition and pressure fluctuations. Frequently, hydrodynamic stress is accompanied by one or more of the physicochemical stresses listed in Section 2.2. According to Al-Rubeai *et al.* (1990), it is recognised that the sensitivity of cells such as hybridomas to hydrodynamic stress is elevated by physicochemical factors such as ammonia accumulation and pH changes, decrease in culture medium viscosity, decrease in sera concentration and the absence of surface-active agents. Furthermore, in processes such as high temperature tank bioleaching, the solubility of oxygen and carbon dioxide is reduced and thus nutrient limitation may occur and compound the already intensive hydrodynamic stress that is prevalent in these slurry reactors.

On investigating shear effects on animal cells, Grima *et al.* (1997) observed that conditions (e.g. temperature) that yield higher membrane fluidity produce more fragile cells. Furthermore, Al-Rubeai (1990) identified membrane integrity as well as metabolic state, as having an influence on shear sensitivity. The authors found that the sensitivity of the cells to hydrodynamic stress increased with decreasing incubation temperatures from 34 to 28°C. At lower temperatures the viability declined more rapidly at high agitation rates. Reduced temperatures not only affect cell physiology and

University of Cape Town

metabolism but also alter membrane fluidity with potential to cause increased permeability. Nutrient starvation also influenced the cell activity on subsequent exposure to high agitation rate. Similar results were found by Märkl *et al.* (1991) who also found that nutrient stress affected the sensitivity of cells to hydrodynamic stress. The authors found that cells of *Methanococcus vanielii* cultured in a STR showed increased sensitivity to mechanical stress when a trace element (selenium) was absent from the growth medium.

Thus, it is integral in the design of bioprocesses that mechanical and physicochemical stresses are not treated as separate factors but as having combined and compounding effects.

## 2.6 THE BIOLOGICAL STRESS RESPONSE

In nature all organisms are subjected to a changing environment and have developed a variety of response mechanisms to help them survive these changes. Unicellular micro-organisms are particularly vulnerable to the changing environment due to their large surface area to volume ratio. The stress response seen in nature is also found, possibly to a greater extent, in bioprocess systems where conditions are optimised to maximise productivity rather than enhance the physiological state of the cells. A fundamental understanding of the stress response of micro-organisms is thus useful to further optimise biosystems. Unlike physicochemical stresses, the response to hydrodynamic stress is not well documented. However, preliminary studies have led to the hypothesis that many of the stress responses may be similar. In addition, once a micro-organism has survived the effect of one form of stress, tolerance to other forms of stress may be induced, for example cells exposed to substrate limitations have increased resistance to heat shock, osmotic stress or disinfecting agents (Schlegel, 1993).

In nature, micro-organisms such as the thermoacidophilic Archaea are found in hostile, low pH, high temperature habitats. However, in their commercial application as bioleaching micro-organisms in high temperature tank leaching processes, they are required to tolerate and thrive under more severe sub-optimal conditions. For example, interactions with high concentrations of metal ions, increased energy inputs and, in some cases, interactions with finely milled mineral are required in conventional leach environments. Furthermore, occasional disruption of culture conditions in terms of temperature or reduction potential may occur. Consequently, the capacity of the thermoacidophiles to respond to various stresses is of interest (Burton *et al.*, 1995; Peeples and Kelly, 1995).

University of Cape Town

Micro-organisms display several responses to stress effects. Most micro-organisms possess defence mechanisms that are initiated once the stress has been "sensed". The response to physicochemical stresses, especially thermal stress, has been studied to a greater extent in mesophilic bacteria and eukaryotes than Archaea. The generalised understanding of this stress response is shown in Figure 2.9 (López-García and Forterre, 2000b). The response to stress appears to be transitory. A shift in an environmental parameter such as temperature is first detected (1) by the cell which subsequently adjusts gene expression (2) to counteract the physical effects of the external change on its molecular components, finally recovering a steady state (3). In this section a short review on sensing mechanisms is presented followed by a discussion on selected stress responses of micro-organisms to physicochemical and mechanical stress.

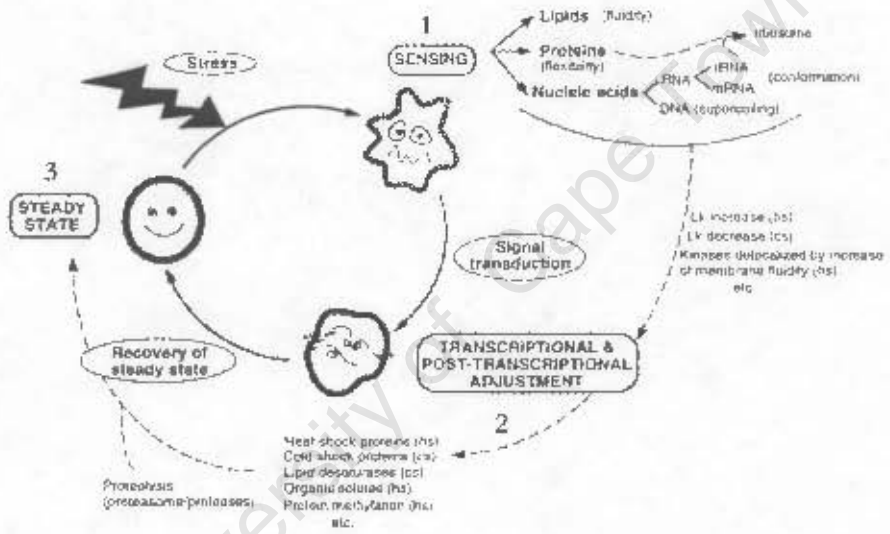


**Figure 2.9:** General mechanisms involved in the transient response to thermal stress (sourced from López-García and Forterre, 2000b).

Lk = linking number (the number of times two closed strands are linked or, the number of times that one DNA strand winds around another)

hs = heat shock;

cs = cold shock

Sensing mechanisms are not well understood; however, several theories exist. According to a classical model, the major trigger of stress protein formation is accumulation of denatured proteins in the cytoplasm. A second model implicates the cell membrane as an ideal location for a stress sensor.

University of Cape Town

The physical state of the membrane is known to be a very sensitive monitor of the most diverse environmental changes. The fluidity properties of cell membranes permit the cell to sense changes in, for example, temperature, pH, osmotic and atmospheric pressure (Vigh *et al.* 1998). Data show that the expression of several genes, particularly those that respond to changes in temperature, is influenced and controlled by the membrane's physical state (Horváth *et al.* 1998). The micro-organism responds to the changes in its environment by means of signal transduction across its membrane. A major mechanism of signal transduction is the so-called two-component sensory system (Bourret *et al.*, 1991; Stock *et al.*, 1989). The first component of the sensor includes histidine kinase that autophosphorylates a histidine residue in response to an environmental stimulus. The phosphate group is then transferred to an aspartate residue on the second component, the response regulator, which effects a cellular response. Limited studies exist on the archaeal signal transduction systems but evidence suggests that a sensory system in the archaeon *Halobacterium halobium* may be similar to those of bacteria (Osorio and Jerez 1996). Osorio and Jerez (1996) studied the adaptive responses in *Sulfolobus acidocaldarius* BC65 to phosphate starvation. They found preliminary evidence for the existence of a two-component sensory system in the archaeal micro-organism.

Changes in the physical state of macromolecules may also function as a sensory mechanism. For example, a shift in temperature acts on the physical state of macromolecules. Alterations in the fluidity of membrane lipids, changes in supercoiling of DNA and mRNA, protein conformation and the state of the ribosome may be involved in this step. It has been proposed that DNA supercoiling could also be used as a sensor for environmental changes (Wang and Syvanen, 1992; López-García and Forterre 2000a). Changes in temperature or ion concentration have been found to induce changes of the linking number of DNA in *E. coli* (Dinnbier *et al.*, 1988). Increasing the linking of DNA causes the molecule to become more compact which may also serve as a protection mechanism. A transcriptional response follows the change in the physical state of the macromolecules. A set of specific proteins is synthesized. For example during heat shock most proteins synthesized are molecular chaperons involved in protein folding, proteases involved in degradation of partially denatured proteins, proline and disulfide isomerases or specific regulators.

Possible sensory and response mechanisms to mechanical stimuli have been found in the Archaea. Mechanosenstive (MS) ion channels are proposed to play a significant role in the responses of Archaea to a variety of mechanical stimuli. A distortion of cellular membranes is converted into electrical or biochemical signals or both. The MS channels function as mechanoelectrical transducers of the mechanical force exerted on cellular membranes and coordinate numerous cellular processes associated with mechanosensory transduction (Hamil and Martinac, 2001). Among the prokaryotes,

University of Cape Town

the MS channels of *Escherichia coli* have been rigorously investigated while recently MS channels in *Haloferax volcanii*, *Thermoplasma acidophilum* and *Methanococcus jannaschii* have been found (Martinac and Kloda, 2003).

### 2.6.1 THE HEAT-SHOCK PROTEINS

Stress proteins are commonly termed heat shock proteins (HSPs) because they derive their name from early studies on the effect of changes in temperature on the protein content of various organisms. Heat shock proteins represent the most highly conserved genetic system known and have been found in all organisms in which they have been sought (Lindquist and Craig, 1988). In general, a short exposure of cells to elevated temperatures or other stress agents reduces the synthesis of normal cellular proteins and induces a transient overproduction of a specific group of proteins, the HSPs (Jerez, 1988). The HSPs are divided into sub-groups based on their molecular weights (Table 2.6) (Laksanalamai *et al.*, 2001; López-García and Forterre, 2000b). Large numbers of HSPs can be induced by stress. When *Escherichia coli* is starved for phosphate, over 80 different genes are transcribed in response (Brock and Madigan, 1991). Even though they are still termed heat shock proteins, it is now accepted that not all HSPs are exclusively induced by heat (Craig *et al.*, 1993).

**Table 2.6:** Classification of HSPs into families according to their molecular weights (adapted from Macario *et al.*, 1999).

| Name | Mass (kDa) |
|---|---|
| Heavy (high mol wt, Hsp100) | 100 or higher |
| HSP90 | 81-99 |
| HSP70 | 65-80 |
| HSP60 | 55-64 |
| HSP40 | 35-54 |
| Small HSPs | < 35 |

#### 2.6.1.1 The function of HSPs

The very nature of the heat-shock response is that of an emergency reaction where cells respond rapidly to the onset of stress (Lindquist and Craig, 1988). The mechanism by which HSPs protect cells at high temperatures still remains unclear (Trent *et al.*, 1990). Several authors have hypothesised the function of these HSPs. Finley *et al.* (1984) suggested that heat-shock proteins might bind to denatured or abnormal proteins after a heat shock to prevent their aggregation and thus prevent cellular damage. Pelham (1986) extended this hypothesis to include the assembly and disassembly of

University of Cape Town

proteins and protein-containing complexes both during normal growth and after heat shock. A second hypothesis suggests that the heat shock proteins need not bind to denatured proteins to have an influence but as heat stable globular proteins themselves, an increase in their concentration after stress can prevent aggregate formation by influencing the diffusion-rate-limited interaction of denatured proteins (Trent *et al.*, 1990).

HSPs may be found in cells under normal growth conditions and play a vital role in cell function (Lindquist and Craig, 1988; Macario *et al.*, 1999). Under normal growth conditions they assist in the folding, translocation and assembly of other proteins and are termed molecular chaperones. However not all stress proteins are chaperones and not every molecular chaperone is a stress protein (Macario *et al.*, 1999, López-García and Forterre, 2000b, Laksanalamai *et al.*, 2001). An alternative hypothesis to the chaperone function of HSPs (during optimal and sub-optimal conditions) is that these proteins mediate membrane permeability (Trent, 2000). In some bacteria the majority of the chaperonins are not present in the cell cytoplasm where most protein folding is believed to occur. Instead, they are associated with the plasma membranes (Garduno *et al.*, 1998; Török *et al.*, 1997). Trent (2000) found that in hyperthermophilic Archaea most of the chaperonin proteins are associated with the plasma membrane and suggested that chaperonin interactions with membranes allow cells to adjust membrane permeability rapidly and respond to short-term fluctuations in their environment. The hypothesis is further substantiated by observations that most of the stresses that induce cells to produce HSPs are suspected or known to damage membranes (Trent, 2000). These stresses include the presence of alcohol, peroxide, and heavy metals. The small HSP from *Leuconostoc oenos* (smHSP Lo18) investigated by Jobin *et al.* (1997) was associated with the cytoplasmic membrane. Based on the expression of Lo18 and its cellular location, the authors concluded that smHsp Lo18 may be involved in the maintenance of membrane integrity. Sales *et al.* (2000) also found a membrane associated HSP in the yeast *Saccharomyces cerevisiae*. The LEA-like protein HSP 12 was identified as having a plasma membrane location in yeasts. The authors proposed that the role of the LEA-like protein HSP 12 is to protect the plasma membrane against desiccation. From the evidence presented, it is proposed that the primary function of HSPs is membrane stabilisation with a secondary chaperone function.

#### 2.6.1.2 The archaeal HSPs

Table 2.7 lists some the HSPs found thus far in several hyperthermophilic Archaea. The archaeal chaperonin (chaperone of the HSP60 family) is the most abundant and the best studied (López-García and Forterre, 2000b). It is also considered the most critical of the HSPs in *Sulfolobus shibatae* (Trent, 2000). One of the chaperonins of the HSP60 family, thermophilic factor 55 (TF55), is referred to as the thermosome (or rosettasome or archeosome). Unlike eubacteria and eukaryotes,

University of Cape Town

which strongly induce 5 to 15 proteins in response to high temperatures, it is reported that *Sulfolobus* produces only TF55 (Parsell and Lindquist, 1993). Given that members of the *Sulfolobales* appear to contain a single, prominent heat shock protein, they represent an interesting model with which the regulation of thermal stress response can be studied (Han *et al.*, 1997).

**Table 2.7:** Some of the HSPs found in hyperthermophilic Archaea in response to temperature or nutrient starvation.

| Micro-organism | Type of stress | Test | Proteins induced | Cross reaction with any known HSPs | Reference |
|---|---|---|---|---|---|
| *Sulfolobus acidocaldarius* | Heat | Shifted from 70 to 85°C | 64-66 kDa; 38, 86, and 22kDa | Not determined | Jerez, 1988 |
| *Sulfolobus shibatae* B12 | Heat | Shifted from 70 to 92°C | 55 kDa (TF55); 28 and 35 kDa | Negative cross reaction with DnaK and GroE from *E. coli* | Trent *et al.*, 1990 |
| *Pyrococcus* strain ES4 | Heat | Shifted from 95 to 105°C | 98 kDa | Not determined | Holden and Baross, 1993 |
| *Metallosphaera sedula* | Heat | Shifted from 70 to 80 or 85°C | 62 kDa | Cross reaction with TF 55 from *Sulfolobus shibatae* | Peeples and Kelly, 1995 |
| | Nutrient | Reduced levels of Casamino acids and ferrous iron | 62 kDa | Cross reaction with TF 55 from *Sulfolobus shibatae* | |
| | Heat | Shifted from 74 to 81°C in continuous culture | 66 kDa (MseHSP60) | Cross reaction with TF 55 from *Sulfolobus shibatae* | Han *et al.*, 1997 |
| *Pyrococcus furiosis* | Heat | Shifted from 95 to 105°C | SHSP (Pfu-sHSP) | Not determined | Laksanalamai *et al.*, 2001 |

### 2.6.2 OTHER PROTEINS

Proteolytic systems, which degrade unfolded proteins, are as essential as heat shock proteins. A large, ubiquitous (2mDa) ATP-dependent proteolytic complex, the 26S proteasome performs these tasks (Ruepp *et al.*, 1998). The proteasome is the major non-lysosomal proteolytic system in eukaryotes. The proteasome of the moderate thermophile *Thermoplasma acidophilum* was found to be expendable under normal growth but not under heat shock (Ruepp *et al.*, 1998). Complete cessation of cell growth was observed under proteasome inhibition.

The peptidyl-prolyl *cis-trans* isomerases (PPI) also play an important role analogous to the HSPs. They are involved in protein folding and are induced by heat shock (López-García and Forterre, 2000b).

University of Cape Town

Substrate deficiency stress has been shown to initiate the production of non-HSP proteins. These catabolic enzymes have higher substrate affinities than the enzymes produced in nutrient rich media allowing them to scavenge nutrients (Schlegel, 1993).

### 2.6.3 ORGANIC SOLUTES

A variety of non-protein molecules play a role in protecting the cell from the effects of stressors. Some of these molecules may play a role similar to that of the chaperone proteins (Macario *et al.*, 1999). Most micro-organisms subjected to osmotic stress accumulate organic solutes to control their internal water activity, maintain appropriate cell volume and turgor, and protect intracellular macromolecules. The compatible organic solutes, also called osmolytes, include sugars, amino acids and their derivatives. Recent investigations of water and temperature stress in thermophilic and hyperthermophilic micro-organisms led to the identification of several new compatible solutes. Some (e.g. mannosylglycerate) accumulate in response to salt stress while others (e.g. di-*myo*-inositol-phosphate) accumulate in response to growth at supraoptimal temperatures (Lamosa *et al.* 1998). Di-glycerol-phosphate was the prominent organic solute accumulated by the archaeon *Archaeoglobus fulgidus*. This solute increased in concentration as the salinity of the medium and the growth temperature were raised, suggesting that this compound serves as a general stress solute (Martins *et al.*, 1997). While di-*myo*-inositol-phosphate (and its derivatives) is particularly characteristic of hyperthermophilic Archaea or bacteria, the type of solutes accumulated varies depending on the micro-organism and the medium composition. The non-methanogenic Archaea and bacteria appear to use the same range of organic solutes as osmoprotectants and thermoprotectants. Solutes commonly found in mesophiles also accumulate in micro-organisms that grow at the highest temperatures (Martins *et al.*, 1997).

Members of the kingdom *Crenarchaeota* belonging to the domain Archaea also appear to accumulate trehalose (Lamosa *et al.*, 1998). The disaccharide has been found in a few archaeal species but its function has not been elucidated (Macario *et al.*, 1999). Trehalose is a well known stress protectant playing a role in protein folding and membrane fluidity in yeast and some bacteria. Heat shock, cold shock, exposure to toxic chemicals and desiccation have all been shown to promote trehalose synthesis (Wiemken, 1990; Quain, 1991). Trehalose may trigger a slowing-down in metabolism prior to entry into a resting state (Quain, 1991). Iwahashi *et al.* (1995) hypothesised that trehalose acts as a protecting agent which stabilises membrane structure while Galinski (1995), Wiemken (1990) and Macario *et al.* (1999) reported that trehalose also serves as a reserve carbohydrate.

University of Cape Town

### 2.6.4 MULTICELLULAR STRUCTURES

As discussed previously, the first line of defence of micro-organisms against mechanical, physical and chemical stressors is the cell wall. The cell wall can be re-enforced by the formation of supracellular structures, which may be flat or globular and termed the biofilm and granule respectively (López-García and Forterre, 2000b). Biofilms and granules are very resistant to disruption by chemical and mechanical means (Macario *et al.*, 1999).

Biofilm formation may be a common stress response mechanism in hyperthermophilic Archaea. LaPaglia and Hartzell (1997) found that *Archaeoglobus fulgidus* formed a biofilm in response to stressors such as non-optimal pH, temperature, high concentrations of metals, antibiotics, xenobiotics or oxygen. The biofilm was composed of proteins, polysaccharides, and metals and enhanced cell survival presumably by creating a protective environment. Cells within the biofilm showed an increased tolerance to otherwise toxic environmental conditions. Metals caught up within the biofilm were found to stimulate the growth of the micro-organism in metal depleted medium. Thus the biofilm may serve as a protective barrier and as a reserve source of nutrients (LaPaglia and Hartzell, 1997). This phenomenon has also been observed in *Archaeoglobus profundus*, *M. jannaschii*, and *Methanobacterium thermoautotrophicum* suggesting a common stress response among the Archaea (López-García and Forterre, 2000b).

### 2.6.5 MORPHOLOGICAL CHANGES AND METABOLIC RESPONSES

Several morphological changes have been observed in response to stress. These include change in cell size and thickening of cell walls (Wase and Patel, 1985; Gormerly and Branion, 1989; Lamaignére, 2002). Lamaignére (2002) found that the cell walls of *Saccharomyces cerevisiae* cultivated in a quartzite slurry bioreactor at a 1 % v/v solids loading increased in cell wall thickness. Increasing the quartzite loading from 0 to 1 % caused an increase in the cell wall thickness from approximately 70 to 110 nm. It is possible that the increase in wall thickness is a repair mechanism in response to damage of the cell wall by the presence of solids in the reactor. Slaninová *et al.* (2000) postulated a similar repair mechanism in *S. cerevisiae* in response to hyperosmotic shock. The authors found that local redistribution of periplasmic and matrix cell wall material occurred with the onset of stress. Portions of the cell wall matrix may have been incorporated into the invaginated areas formed during shrinkage of the plasma membrane caused by hyperosmotic shock.

University of Cape Town

Nemati and Harrison (2000) found that the size of freely suspended cells of *Sulfolobus metallicus* cultivated in a pyrite slurry were smaller in experiments conducted at higher levels of hydrodynamic stress. Smaller cells have a higher surface area to volume ratio and provide increased relative area for the rate of nutrient transport. To maintain this diminished size, non-essential cellular components are not synthesised (Shuler and Tsuchiya, 1975). It is possible that the energy expenditure shifts from growth to maintenance, resistance to mechanical stress and repair of cell injury. Illing (1996) stated that hydrodynamic stress may result in the use of the carbon and energy source normally used for cell division and product formation for maintaining intracellular functioning and repair mechanisms. Potgieter (2002) observed this effect through a metabolic flux analysis of *Corynebacterium glutamicum* on exposure to shear stress in cross-flow filtration for cell retention. Searby and Hansford (2003) found kinetic evidence of an increase in the maintenance requirement of thermoacidophilic Archaea on studying the effect of temperature and nutrient stress on the kinetics of ferrous iron oxidation. When grown at low dilution rates or elevated temperatures there was an increase in the cell maintenance requirements and reduced cell concentrations. This increase in maintenance requirements could point towards higher energy expenditure on repair mechanisms and the maintenance of cellular function instead of growth under the sub-optimal growth conditions. Sissing (2002) and Lamaignére (2002) observed a decrease in the biomass yield coefficient $Y_{x/s}$ on exposure of *S. cerevisiae* and *S. metallicus* respectively, to increasing stress due to solids loading and agitation. This is consistent with an increase in maintenance energy (not measured).

University of Cape Town

## 2.7 SUMMARY: PART A

In Part A of the literature review, Section 2.2.1 covered reactor considerations in the STR that are relevant to the present study. Mixing, gas-liquid mass transfer and the presence of solids were discussed. Mixing is attained through rotation of the impeller. Impellers such as the Rushton turbine require a greater power input per unit volume than pitched blade and hydrofoil impellers, thus providing more energy dissipation dispersion and potential cell damage in the reactor. Gas-liquid mass transfer was shown to be an important consideration in the thermophilic bioleaching STR due to the limited solubility of oxygen and carbon dioxide especially at high temperatures. The limited solubility of these gases requires intensive agitation and aeration of the reactor which leads to increased hydrodynamic stress. The presence of solids in the reactor not only increases the intensity of hydrodynamic stress through interactions of solid particle with the cells but has been shown to reduce gas-liquid mass transfer in the reactor. In Section 2.2.2, the key mechanisms of hydrodynamic

stress within solids-free and solids-containing STR systems were discussed. In solids-free systems, mechanisms included interactions between cells and turbulent eddies and interactions between cells and bursting bubbles. In solids-containing systems, the principle mechanism of cell damage was identified as particle-cell-particle interactions. These mechanisms of cell damage have an effect at the process performance level as well as at the cellular level. At the process performance level, changes in substrate utilisation rates, product formation and growth rates were observed. While at the cellular level, changes in morphology, viability and cell envelope integrity were identified.

In Section 2.3, it was shown that the cell envelopes of the Archaea differed considerably from those of the bacteria and yeasts. The cell envelopes of the Archaea are of reduced structural integrity due to the lack of re-enforcing macromolecules. Furthermore, the sensitivity of micro-organisms to hydrodynamic stress was shown to be determined primarily by the presence of a cell wall or the cell wall composition. Cells with no cell wall or with walls of reduced structural integrity are more susceptible to the effects of hydrodynamic stress.

In Section 2.4, the impact of physiological and, to a greater extent, mechanical stress on micro-organisms was discussed. It was shown that depending on the intensity of stress applied, the effect of stress can lead from minor envelope damage to complete cell disruption. The impact of a disrupted cell wall and cell envelope was also examined. Permeabilisation of the cell membrane leads to a loss of 'reproductive capability' (viability) of the cells, impairs the functioning of the electron transport system and, for acidophilic micro-organisms in particular, impairs chemiosmosis and maintenance of a near neutral internal pH. This section culminated in a review of the impact of hydrodynamic stress in solids-free and solids-containing systems. In essence, increasing hydrodynamic stress by increasing either fluid and bubble shear or by changing solids loading, impeller speed and type, particle size and solids shape and type has an influence on the morphology, viability and metabolic activity of the organisms leading to reduced rates and extents of growth which ultimately result in reduced process performance. Increasing the impeller speed up to a critical rate leads to improved process performance due to improved mass transfer. However, above this critical rate, process performance declines.

In Section 2.5 the effect of the combination of physicochemical and hydrodynamic stress was considered. Investigators have shown that when organisms are physiologically stressed, their sensitivity to mechanical stress increases. Finally, Section 2.6 the various mechanisms micro-organisms possess to counteract the effects of stress were presented. The first step in the response process is sensing the stress. The second step is initiation of the response mechanism and eventually

University of Cape Town

a resumption of steady-state. The response mechanisms identified in this section were (i) the production of stress proteins and non-protein molecules; (ii) the formation of biofilms; (iii) morphological changes such as reduction in cell size and increase in cell wall thickness; and (iv) metabolic changes such as a shift in energy expenditure from growth to maintenance.

Thus, in Part A of this review, an understanding of the mechanisms of cell damage within the STR, the effects of this damage at the reactor performance level and cellular level, and the biological response to stress was attained. This understanding can now be applied to systems directly relevant to the present study.

University of Cape Town

# PART B
# BIOLEACHING SYSTEMS

Bioleaching systems for the extraction of metals have been in existence for many years. Rio Tinto mines in south-western Spain have been exploited since pre-Roman times for their copper, gold and silver values (Brandl, 2001). In Sweden, Germany and China, biooxidation of sulphide ores for copper recovery has been practised for centuries by solution mining techniques. Typically, early leach processes took place as uncontrolled dump leaching. Presently, bioleaching processes use engineered heap bioleaching systems for low-grade ores and tank leaching for flotation concentrates. Because tank leaching operations employ classic STRs, hydrodynamic stress conditions prevail in these systems.

Thus far the focus of this review has been on the stress, particularly hydrodynamic stress, experienced by micro-organisms, particularly the thermophilic Archaea, in slurry reactors. The current section focuses on bioleaching in STRs and provides an overview of the principles and mechanism of bioleaching with an emphasis on chalcopyrite systems. Further to this, the typical bioleaching micro-organisms, particularly those belonging to the genus *Sulfolobus*, are discussed. The section culminates in a detailed review of the literature on hydrodynamic stress in bioleaching systems.

University of Cape Town

## 2.8 THE PRINCIPLES OF BIOLEACHING

### 2.8.1 THE ROLE OF BIOLOGICAL LEACHING

Two primary incentives drive the need for biological leaching. The first is the need for cleaner mineral extraction technologies and the second is the cost effectiveness of the process, especially for the leaching of low-grade ore. Universal metal extraction processes such as roasting or smelting produce sulphur dioxide and other environmentally harmful gases (Rawlings, 2002). For example, in the pyrometallurgical treatment of chalcopyrite, two tonnes of sulphur dioxide gas are produced for every tonne of copper extracted (Rivera-Santillán *et al.*, 1999; Rawlings, 2002). Sulphur dioxide has been implicated in acid precipitation and in several ecological and health problems including crop damage, forest die-back and respiratory complications (Warhurst and Bridge, 1996). Another advantage of bioleaching is that mine tailings from biological leaching operations are also less

chemically active due to the absence of oxidisable iron and sulphur and thus less likely to lead to acid mine drainage (Rawlings, 2002). Process economics are measured by capital and running costs. Depending on the application, bioleaching may be a favourable option due to lower capital costs, lower energy requirements and flexibility of scale. Biological leaching is thus an innovation in the mining industry enabling mining companies to combine gains in productivity with improvements in environmental management.

### 2.8.2 THE BIOLEACHING PROCESS

The bioleaching process involves the oxidation of iron and sulphur moieties contained in mineral complexes by micro-organisms either to expose trapped metal e.g. gold in the case of pyrite or to solubilise commercially important base metals, e.g. copper in the case of chalcopyrite. The process is proposed to occur via chemical attack of the mineral by ferric iron. The main role of the micro-organisms is to re-oxidise the resultant ferrous iron back to ferric iron (Rawlings, 2002; Brandl, 2001).

The process is based upon the microbial utilisation of ferrous iron as an oxidisable energy source. Using pyrite as an example the following equations are proposed:

Ferric iron oxidises the metal sulphide mineral, resulting in the solubilisation of the metal as the metal sulphate (Chong *et al.*, 2002):

$$FeS_2 + Fe_2(SO_4)_3 \rightarrow 3\ FeSO_4 + 2\ S^0 \qquad \ldots \text{Eqn. 2.5}$$

The resultant ferrous iron is oxidised by the micro-organisms to regenerate the ferric iron oxidant according to (Barr *et al.*, 1992):

$$4\ FeSO_4 + O_2 + 2H_2SO_4 \rightarrow 2\ Fe_2(SO_4)_3 + 2\ H_2O \qquad \ldots \text{Eqn. 2.6}$$

Several factors are known to affect the bioleaching process. Some of these are listed in Table 2.8. These factors affect the biological leaching process performance to varying extents. Process optimisation requires an ideal balance between each parameter.

University of Cape Town

**Table 2.8:** Factors and parameters affecting bacterial mineral oxidation and metal mobilisation (adapted from Brandl, 2001).

| Factor | Parameter |
|---|---|
| Physicochemical parameters of a bioleaching environment | Temperature; pH; redox potential; oxygen content and availability; carbon dioxide content; mass transfer; nutrient availability; ferric iron concentration; water potential; light; pressure; surface tension; presence of inhibitors |
| Microbiological parameters of a bioleaching environment | Metal tolerance; microbial diversity; morphology of the micro-organism; population density; microbial activities; spatial distribution of micro-organisms; adaptation abilities of micro-organisms |
| Properties of the minerals to be leached | Mineral type; surface area; mineral composition; mineral dissemination; grain size; porosity; hydrophobicity; galvanic interactions; formation of secondary minerals |
| Processing | Leaching mode (*in situ*, heap, dump, or tank leaching); solids loading, agitation rate (in the case of tank leaching operations); heap geometry (in the case of heap leaching) |

- *Physicochemical parameters*

Temperature of the bioleaching process affects the rate of chemical reactions occurring in the system as well as the activity of the micro-organisms present. In exothermic leaching systems, an increase in temperature above the optimal physiological temperature of the leaching micro-organisms may lead to inactivation of the cells.

In order for leaching to occur, the redox potential of the system is required to be above the rest potential of the mineral. In addition, minerals such as chalcopyrite have a narrow redox potential operating window (estimated between 490 and 590 mV; Ag/AgCl) within which the process operates optimally (Hiroyoshi *et al.*, 2004). Outside this operating window the rate of bioleaching leaching is reduced due to passivation of the mineral surface.

Oxygen is a vital microbial nutrient. The limited solubility of oxygen necessitates intensive mixing of reactor contents in tank leaching systems. Intensity of mixing must be optimised to improve oxygen transfer with minimal loss in microbial activity due to cell damage.

- *Microbiological parameters*

The metal tolerance of micro-organisms involved in the bioleaching process is an important consideration. In chalcopyrite tank bioleaching operations, iron and copper concentrations in the order of 30 to 40 g $l^{-1}$ have been reported. Bioleaching micro-organisms, though resistant to a range of metals, have varied metal tolerances (Rawlings, 2002).

University of Cape Town

In tank bioleaching operations, the resistance of the leaching micro-organisms to hydrodynamic stress plays an important role in determining the efficiency of the leaching process. The thermophilic acidophiles used in high temperature tank leaching processes possess cell walls of reduced structural integrity compared to their mesophilic counterparts. This difference in cell wall structure reduces the concentration of mineral that can be treated by the thermophilic micro-organisms and agitation rate at which the system can be operated.

- *Properties of the mineral*

Some minerals such as chalcopyrite are resistant to conventional bioleaching techniques used in commercial pyrite bioleaching operations while secondary copper sulphide minerals such as chalcocite and covellite are more amenable to leaching.

Increased oxidation rates have been reported with an increase in the surface area of the mineral available for leaching (Nemati *et al.*, 2000; Gericke *et al.*, 2001). However, in some studies where the mineral particle size was reduced to below a critical size, reduced rates of leaching were observed. This reduction was attributed to damage of the leaching micro-organisms by the fine mineral particles (Nemati *et al.*, 2000; Harrison *et al.*, 2003).

- *Processing*

Heap leaching operations are long term operations. Tank leaching operations are faster processes because intensive mixing and aeration to promote mass transfer are attainable. In tank leaching operations, the solids loading determines the agitation rate required to suspend the solids and thus determines the power requirements of the system.

University of Cape Town

#### 2.8.2.1 Pyrite bioleaching

Pyrite is a common metal sulphide of importance in the sulphur cycle. It is of economic interest because uranium and gold are often closely associated with it (Sand *et al.*, 2001). Further, it is frequently found in combination with base metals. The pre-treatment of refractory gold-bearing pyritic minerals is necessary to remove in the interfering metal sulphide in order to facilitate the cyanide leaching process to liberate the gold. Biooxidation presents both an economic and environmentally attractive alternative to conventional pre-treatment methods such as pressure leaching and roasting. Mesophilic, moderately thermophilic and extremely thermophilic micro-organisms have been implicated in pyrite bioleaching.

The pyrite bioleaching system has been studied extensively. The reactions describing pyrite leaching are given in Eqns. 2.5 and 2.6. In Table 2.9, selected mesophilic and thermophilic laboratory-scale pyrite bioleaching systems are presented to illustrate key performance factors. Thermophilic bioleaching is an attractive process due to increased reaction rates at elevated temperatures and the enhanced temperature driving force for cooling of the exothermic process (Konishi *et al.*, 2001a). The data of Konishi *et al.* (1995) and Nemati and Harrison (2000) show that the thermophilic bioleaching process offers a higher extent of iron solubilisation than the mesophilic process. In general, similar extents of pyrite solubilisation were observed for the studies using thermophilic micro-organisms (Table 2.9). At low pulp densities (1 to 3 %) in STRs almost complete solubilisation was observed in 5 to 6 days (Konishi *et al.*, 1995; Nemati and Harrison, 2000; Sissing and Harrison, 2003). The type of bioreactor utilised has also been shown to influence the pyrite leaching process. Norris and Barr (1988) found that the maximum rate of solubilisation of pyrite by *Sulfolobus* BC was 200 mg $l^{-1}$ $h^{-1}$ iron using an airlift reactor at a 5 % w/v solids loading while a rate of 40 mg $l^{-1}$ $h^{-1}$ was obtained at a 1 % w/v solids loading using a STR. Valencia *et al.* (2003) studied the effects of increasing solids loading and particle size on the bioleaching of pyrite using *Sulfolobus metallicus* in shake flask reactors. The authors found lower extents of pyrite solubilisation than Nemati and Harrison (2000) who studied pyrite bioleaching in STRs at various pulp densities using the same micro-organism.

University of Cape Town

**Table 2.9:** Comparison of pyrite bioleaching data obtained by different investigators.

| Reference | Micro-organism | Mode and reactor type | Impeller type | Agitation rate (rpm) | Aeration | Temperature (°C) | Size fraction of pyrite (μm) | Pyrite loading (%) | Extent of Fe leaching (%) or Fe solubilisation rate (mg $l^{-1}h^{-1}$) | Time (days) |
|---|---|---|---|---|---|---|---|---|---|---|
| Norris and Barr, 1988 | Mixed mesophilic pyrite enrichment culture | 1 litre STR | n/g | 100 | 1% $CO_2$ in air at 0.25 l $min^{-1}$ | 30 | < 75 | 10; staged addition | 40 mg $l^{-1}$ $h^{-1}$ | n/a |
| | *Sulfolobus* BC | 1 litre STR | n/g | 100 | 1% $CO_2$ in air at 0.25 l $min^{-1}$ | 70 | < 75 | 10; staged addition | 40 mg $l^{-1}$ $h^{-1}$ | n/a |
| | *Sulfolobus* BC | Airlift reactor | n/a | n/a | 1% $CO_2$ in air at 0.5 l $min^{-1}$ | 70 | < 75 | 10 and 15; staged and single additions | 200 mg $l^{-1}h^{-1}$ | n/a |
| Konishi *et al.*, 1995 | *Acidithiobaclillus ferrooxidans* | 1 litre round-bottomed flask | n/g | 500 | 0.5-2 l $min^{-1}$ | 30 | 25-44 | 0.2-1 | 50 % | 9 |
| | *Acidianus brierleyi* | 1 litre round-bottomed flask | n/g | 500 | 0.5-2 l $min^{-1}$ | 65 | 25-44 | 0.2-1 | 100 % | 5 |
| Nemati and Harrison, 2000 | *Sulfolobus metallicus* | Batch; 1 litre STR | Pitched blade | 550 | 1 l $min^{-1}$ | 68 | 53-75 | 3; 6; 9; 12; 15; 18 | 3 % = 100 %<br>6 % = 92 %<br>9 % = 88 %<br>12 % = 88 %<br>15 % = 70 %<br>18 % = 11 % | 6 days for a 3 % pyrite loading |
| Valencia *et al.*, 2003 | *S. metallicus* | Batch; 1 litre shake flasks | n/a | 220 | n/a | 68 | 38-75 | 2.5; 5; 10; 15 | 2.5 % = 64 %<br>5.0 % = 74 %<br>10 % = 41 %<br>15 % = 22 % | - |
| Sissing and Harrison, 2003 | *S. metallicus* | Batch; 1 litre STR | Pitched blade | 560 | 2 l $min^{-1}$ | 68 | 38-75 | 3 | 91% | 5 |

n/a = not applicable; n/g = not given

University of Cape Town

### 2.8.2.2 Chalcopyrite bioleaching

Copper is the third most widely used metal in terms of tonnage throughout the world, after iron and aluminium. Copper is an excellent conductor of electricity and heat. At present, almost 75 % of copper consumption is centred on its conducting properties. In its natural state, copper is found mixed with numerous minerals. This gives rise to the following classification: native copper; sulphide minerals and oxidised minerals (http://www.escondida.cl/english/copper_uses.htm). The common sulphidic copper minerals are chalcopyrite ($CuFeS_2$), chalcocite ($Cu_2S$), covellite (CuS), and bornite ($Cu_5FeS_4$) (Murr, 1980). Chalcopyrite is the most widely occurring copper-bearing sulphide mineral. It is processed entirely by mineral concentration and smelting to achieve up to 99 % copper recovery. However this process generates sulphur dioxide and in addition, there is a limitation on the grade of chalcopyrite that can be smelted. A cleaner technology with economic advantage is sought (Montealegre and Bustos, 1991).

The bio heap and dump leaching of copper oxide and secondary copper sulphides are proven processes and account for about 20 % of annual copper production. Copper recoveries of 70 to 90 % can be achieved in 150-210 days (Montealagre and Bustos, 1991). Stirred tank bioleaching processes for the extraction of copper from chalcopyrite are not currently being used at a commercial scale, but are at an advanced state of development (Rawlings, 2002).

The main intermediates of chalcopyrite leaching are polysulphides and elemental sulphur (Konishi *et al.*, 1999):

$$CuFeS_2 + 2\,Fe_2(SO_4)_3 \rightarrow CuSO_4 + 2\,S^0 + 5\,FeSO_4 \qquad \ldots \text{Eqn. 2.7}$$

The elemental sulphur is further oxidised microbially to sulphate by the following reaction (Konishi *et al.*, 2001b):

$$2\,S^0 + 3\,O_2 + 2\,H_2O \rightarrow 2\,H_2SO_4 \qquad \ldots \text{Eqn. 2.8}$$

Chalcopyrite ores are notoriously difficult to leach both biologically or abiotically (Mehta and Murr, 1982; Sand *et al.*, 1992; Stott *et al.*, 2003). Leaching is characterised by an initially rapid rate of copper extraction that slows as a function of time owing to a phenomenon often referred to as passivation (Rivera-Santillán *et al.*, 1999; Gericke *et al.*, 2001). Sulphur depositions, polysulfide surface layers and jarosite precipitation have all been proposed as possible causes of passivation (Stott *et al.*, 2003). Thus in a bacterially assisted heap leach, while it may take 50 to 100 days to recover 75 to 80 % of the copper in a chalcocite deposit, the same recovery of the copper in a chalcopyrite deposit would be achieved in 250 to 600 days (www.hatch.ca/Non_Ferrous/ articles/copper_hydrometallurgy.pdf).
Thermophilic bioleaching of chalcopyrite has shown increased rates and extents of leaching compared to mesophilic processes. Several studies with mesophilic micro-organisms such as *Acidithiobacillus*

University of Cape Town

*ferrooxidans* and *Leptospirillum ferriphilum* have shown very slow copper leach rates (Mehta and Murr, 1982; Sand *et al.*, 1992). Typically, *At. ferrooxidans* releases only 10 to 25 % of the available copper via the aerobic oxidation of ferrous iron and sulphur before the copper release slows significantly or ceases (Mehta and Murr, 1982; Le Roux and Wakerley, 1988; Stott *et al.* 2000). Thus the incentive exists to focus current research on processes which increase the bioleaching rate. Thermophilic chalcopyrite bioleaching yields increased leach rates due to high temperatures and higher metal tolerance capacities (Clark and Norris, 1996). Brierley and Brierley (1978) found that, using *Acidianus brierleyi*, a chalcopyrite concentrate (74-210 μm) was efficiently leached with 78 % copper dissolution in 60 days. The high temperature leaching was approximately 10 times faster than leaching at mesophilic temperatures. In the presence of thermophilic micro-organisms at 55°C, Mehta and Murr (1982), found that a chalcopyrite concentrate (< 37 μm) was solubilised appreciably beyond 30 % in 30 days. When *Sulfolobus* BC was used for the leaching of chalcopyrite concentrate (< 90 μm) at 68°C, greater than 80 % leaching was achieved in 28 days (Le Roux and Wakerley, 1988).

For more than two decades, researchers have studied chalcopyrite bioleaching under thermophilic conditions. A précis of their results is given in Table 2.10. High extents of solubilisation have been obtained for temperatures between 65 and 78°C under a wide range of experimental conditions and reactor designs. In general the concentrates used were finely milled (< 90 μm). The finely ground concentrate yielded high extents of copper dissolution. On average, greater than 80 % dissolution was obtained within approximately 10 days. The highest solids loading tested was 12 % w/v. Agitation rates ranged from 250 to 500 rpm in the studies utilising STRs. In almost all investigations, air was enriched with carbon dioxide; however Konishi *et al.* (2001a) obtained complete chalcopyrite dissolution within 10 days using *Acidianus brierleyi* in the absence of carbon dioxide supplementation.

The thermophilic Archaea most studied are those of the genus *Sulfolobus* that oxidise metal sulphides, sulphur or ferrous iron at an optimum temperature of about 68°C. However, the most promising data presented in Table 2.10 is that of Dew *et al.* (1999) who obtained high rates of copper solubilisation in a large-scale continuous system at 78°C. The continuous 1040 l pilot plant housed at the BHP Billiton Research Laboratories in Johannesburg (South Africa) consisted of a two 240 l and four 140 l stirred tank reactors connected in series. Copper dissolution of 66 % was obtained in the first tank in a residence time of 5 days with 95 % copper dissolution attained using all six reactors with a total residence time of 14 days. Because these stirred tank systems are most undoubtedly the future of chalcopyrite flotation concentrate bioleaching, the study of the effect of hydrodynamic stress on the micro-organisms used in these processes is important.

University of Cape Town

**Table 2.10:** Comparison of thermophilic chalcopyrite bioleaching data obtained by different investigators.

| Reference | Micro-organism | Impeller type | Mode and reactor type | Agitation rate (rpm) | Aeration | Size fraction (μm) | Solids loading (%) | Extent of Cu leaching (%) | Time (days) |
|---|---|---|---|---|---|---|---|---|---|
| Le Roux and Wakerley, 1988 | *Sulfolobus* BC | Single blade paddle | Batch, STR | 500 | 1 vvm; enriched with $CO_2$ | < 90 | 5.5 | 83 | ≈ 29 |
| Gómez *et al.*, 1996 | *Sulfolobus rivotincti* | n/a | Batch, shake flask | 150 | - | < 74 | 1 | > 80 | 11 |
| Konishi *et al.*, 2001a | *Acidianus brierleyi* *Sulfolobus* sp. | Paddle | Batch, STR | 500 | 1 vvm | 38-53 | 10 | Complete dissolution | 10 |
| Gericke *et al.*, 2001 | Extreme thermophile | n/a | Batch, STR | 220 | Air enriched with 0.15 % $CO_2$ | $d_{90}$ 10 | 7.5 | > 98 | 11 |
| Gericke *et al.*, 2001 | Extreme thermophile | Dual impeller: 6-blade Rushton turbine and a 6-blade pitched-blade turbine | Continuous, STR | 250 | Air enriched with 0.15 % $CO_2$ | $d_{90}$ 10 and 5 | 7.5 | > 90 for both grind sizes across all residence times | 6.3-8.4 day overall residence time |
| Dew *et al.*, 1999 | 78°C thermophilic culture | Lightnin A315 | Continuous, 6 cascade reactors, STR | n/a | Air enriched with 0.15 % $CO_2$ | $d_{80}$ 38 | 10 | 95 | 14 day overall residence time |
| d'Hugues *et al.*, 2002 | Novel, mixed 78°C thermophilic culture | Mixed axial-radial impeller | Continuous, STR | 350 | Air enriched with $CO_2$ | $d_{80}$ 44 | 12 | > 90 | 5 |
| Plumb *et al.*, 2002 | Thermophilic micro-organisms related to *S. solfataricus* | n/a | Batch, shake flask | n/a | - | $d_{80}$ 85 | 2 | Up to 91 | 4.5 |

n/a = not applicable

University of Cape Town

### 2.8.3 LARGE-SCALE COMMERCIAL TANK BIOLEACHING PROCESSES

Tank bioleaching of sulphide concentrates has undergone substantial development over the last 20 years and has emerged as a serious alternative to the conventional treatment of mineral sulphides (d'Hugues *et al.*, 2002). Industrial scale processes such as the BIOX® process developed by Gencor (BHP Billiton) and currently operated by Goldfields and MINBAC developed by Mintek South Africa (Warhurst and Bridge, 1996; d'Hugues *et al.*, 2002). There are eleven full-scale stirred tank bioleaching plants worldwide employing three different technologies to process sulphidic-refractory precious metal concentrates and concentrates of pyrite, cobalt and chalcopyrite. Table 2.11 presents commercial pyrite (in association with arsenopyrite and pyrrhotite) plants currently in operation. The full-scale BIOX plant at Fairview in South Africa is the longest running pre-treatment plant. It has been in operation since 1986 treating refractory arsenopyrite-pyrite gold-bearing concentrates (Olsen *et al.*, 2003). All commercial tank leaching operations bar two are operated using either mesophilic or moderately thermophilic bacteria. The exceptions are the BHP Billiton BioCOP™ plant in Chile and a Mintek-BacTech three-way joint venture with Peñoles in Mexico. Both plants operate at temperatures in excess of 60°C using thermophilic bioleaching micro-organisms. The BioCOP plant is the only commercial tank leaching operation used for chalcopyrite leaching (Rawlings *et al.*, 2003).

**Table 2.11:** Operational commercial bioleaching processes for gold recovery (adapted from Rawlings *et al.*, 2003).

| Plant | Year commissioned | Tonnage ($d^{-1}$) | Total reactor volume ($m^3$) | Concentrate | Location |
|---|---|---|---|---|---|
| Fairview BIOX® | 1986 | 14 | 440 | Pyrite 28 %; arsenopyrite 10 % | Barberton, SA |
| São Bento BIOX® | 1991 | 150 | 580 | Pyrite 16 %; arsenopyrite 38 %; pyrrhotite 46 % | Brazil |
| Wiluna BIOX® | 1993 | 115 | 2820 | Pyrite 37 %; Arsenopyrite 22 % | Western Australia |
| Ashanti-Sansu BIOX® | 1994 | 720 | 16 200 | Pyrite 6.5 %; arsenopyrite 17 %; pyrrhotite 14 % | Obuasi, Ghana |
| Tamboraque BIOX® | 1998 | 60 | 1 570 | Pyrite 35 %; arsenopyrite 57 % | San Mateo, Peru |
| Laizhou MINBAC | 2001 | 100 | 4 050 | Pyrite 25-49 %; arsenopyrite 7-15 % | Shandong Province, China |

University of Cape Town

## 2.9 MICRO-ORGANISMS IN BIOLEACHING

A diverse range of micro-organisms spanning two domains and with broad temperature and pH ranges are known to be involved in bioleaching processes. Since the first acidophilic, iron- and sulphur-oxidising bacterium *T. ferrooxidans* (renamed *Acidithiobacillus ferrooxidans*) was isolated and described in 1951 by Temple and Colmer, several new genera have emerged as sulphide mineral oxidisers. These micro-organisms have been sourced from environments such as thermal springs (Le Roux *et al.*, 1977; Brierley, 1976), copper leach dumps (Brierley, 1978), gas vents and coal mine effluents (Brierley, 1986). Table 2.12 lists the commercially important micro-organisms known to be prevalent in bioleaching systems. These micro-organisms are usually present as a consortium of two or more species. Depending on the conditions that prevail, a different micro-organism dominates the system (Olsen *et al.*, 2003).

**Table 2.12:** Micro-organisms involved in bioleaching processes.

| Micro-organism | Domain | Nutrient type | Electron donor/s | Growth Temperature | Reference |
|---|---|---|---|---|---|
| *Acidithiobacillus ferrooxidans* | Bacteria | Autotrophic | Ferrous and reduced inorganic sulphur | Mesophilic | Olsen *et al.*, 2003; Rawlings, 2002 |
| *At. thiooxidans* | Bacteria | Autotrophic | Reduced sulphur compounds | Mesophilic | Rawlings, 2002; Rohwerder *et al.*, 2003, |
| *At. caldus* | Bacteria | Mixotrophic | Reduced sulphur compounds | Moderately thermophilic | Olsen *et al.*, 2003; Rohwerder *et al.*, 2003 |
| *Leptospirillum* sp. | Bacteria | Autotrophic | Ferrous iron | Mesophilic | Das *et al.*, 1999; Rawlings, 2002; Rohwerder *et al.*, 2003 |
| *Sulfobacillus* spp. | Bacteria | Autotrophic or heterotrophic | **Autotrophic:** ferrous iron and reduced inorganic sulphur compounds | Moderately thermophilic | Brierley, 1986; Das *et al.*, 1999; Rohwerder *et al.*, 2003 |
| *Sulfolobus* spp. | Archaea | Autotrophic | Ferrous iron and reduced inorganic sulphur compounds | Thermophilic | Brock *et al.*, 1972; Brandl, 2001 |
| *Acidianus* pp. | Archaea | Autotrophic or heterotrophic | Ferrous iron or reduced inorganic sulphur compounds | Thermophilic | Rawlings, 2002; Rohwerder *et al.*, 2003 |
| *Metallosphaera* sp. | Archaea | Autotrophic or heterotrophic | **Autotrophic:** ferrous iron and reduced sulphur compounds | Thermophilic | Rawlings, 2002; Rohwerder *et al.*, 2003 |
| *Sulfurisphaera* sp. | Archaea | Autotrophic | Ferrous iron and reduced sulphur compounds | Thermophilic | Rawlings, 2002; Rohwerder *et al.*, 2003 |
| *Ferroplasma* spp. | Archaea | Autotrophic | Ferrous iron | Mesophilic | Rawlings, 2002; Rohwerder *et al.*, 2003 |

University of Cape Town

As discussed in Sections 2.6.2.1 and 2.6.2.2, the advantages of high temperature leaching have come to the fore in the last two decades. Bioleaching is an exothermic process and reactor cooling is a requirement in mesophilic systems (Konishi *et al.*, 2001a). Leach dump environments have recorded temperatures up to 80°C (Brierley, 1990). The use of thermoacidophilic Archaea not only increases chemical reaction rates but also minimises cooling requirements. The autotrophic thermoacidophiles are useful in biomining due to their ability to oxidise ferrous and sulphide ions and to thrive at low pHs, high temperatures and high metal concentrations.

The currently recognised taxonomic framework of the Archaea is based on 16S rRNA phylogeny (Itoh, 2003). The thermoacidophilic micro-organisms presented in Table 2.12 fall within the domain Archaea, the phylum Crenarchaeota, the class Thermoprotei, the order Sulfolobales and a single family, Sulfolobaceaea which is composed of six genera (Itoh, 2003). The genera of interest in this study are the strictly aerobic *Sulfolobus*, *Metallosphaera* and *Sulfurococcus* and the facultative aerobic *Acidianus* and *Sulfurisphaera*. In the following section, the characteristics of the genus *Sulfolobus*, are discussed.

### 2.9.1 THE GENUS *SULFOLOBUS*

One of the more common groups of extremophiles used in biomining are the micro-organisms belonging to the genus *Sulfolobus*. The isolation of the first *Sulfolobus*–like species was published by J.A. Brierley in 1966. However, characterisation of the species was only carried out by Brock *et al.* in 1972. *Sulfolobus* cells are coccoid, about 0.8 to 2 μm in diameter, highly irregular and usually occurring singly (Figure 2.10). When cells are tumbling through the microscope field, distinct lobes can be seen (Brock *et al.*, 1972).

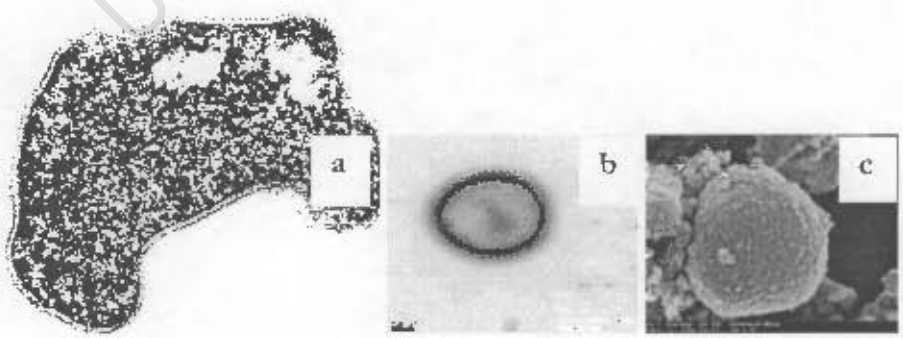


**Figure 2.10:** a) Electron micrograph of a thin section of *Sulfolobus acidocaldarius* (85 000 x). Under the electron microscope the micro-organisms appear as irregular spheres which are often lobed (sourced from Brock and Madigan, 1991). b) *Sulfolobus* cell negative stained with uranyl acetate. c) *S. tokodaii* (sourced from http://web.pdx.edu/~clore/EM%20pics.html).

University of Cape Town

Some members of the genus *Sulfolobus* are aerobic, autotrophic and thermoacidophilic growing above 50°C and at pH 1 to 3. *Sulfolobus* has been isolated from acidic continental solfatara fields including Yellowstone National Park (U.S.A), New Mexico, Solfatara crater (Italy), Birch Coppice (U.K.), Iceland and Japan (Brierley, 1966; Brierley, 1978; Marsh and Norris, 1983). These micro-organisms are able to oxidize sulphidic ores like pyrite, chalcopyrite and sphalerite, forming sulphuric acid and solubilising the heavy metal ions. Many strains are able to oxidise ferrous iron (Brock, 1978; Brierley and Brierley, 1973).

As discussed in Section 2.3.1, the cell walls of the mesophilic (bacteria) and thermophilic (Archaea) bioleaching micro-organisms have differing structural integrities. The cell walls of *Sulfolobus* spp. comprise only protein subunits while the mesophilic bacteria have cell walls re-enforced with peptidoglycan. In bioleaching systems, these structural differences influence optimal system performance i.e. the solids loading utilised in the reactor or energy input into the reactor may govern the system performance rather than the mineral leach rate.

## 2.10 HYDRODYNAMIC STRESS IN TANK BIOLEACHING SYSTEMS

Biohydrometallurgical processes take place in three-phase systems (Rossi, 2001). The solid phase comprises the mineral to be leached (to which micro-organisms may be attached) and precipitates, the liquid phase consists of nutrients, planktonic cells and waste products and the gas phase is usually a combination of air and carbon dioxide. The three phases require mixing at a rate to ensure effective inter-phase contact and transfer. As detailed in Section 2.2.1, these mixing requirements and the presence of solids in the reactor have the potential to cause shear and collision damage of the leaching micro-organisms. These damage events manifest themselves in several ways. In terms of overall process performance: the growth, oxidation rates and cell attachment to the mineral may decrease. At the cellular level: damage to cell walls (if present) and cell membranes can have compounding effects leading to the inability of the cells to maintain internal pH, the shutdown of metabolic pathways and the loss of nuclear activity. In order to improve the efficiency of the bioleaching process it is important to know how hydrodynamic stress affects the rate and extent of leaching (Chong *et al.*, 2002).

The type of the micro-organism used in the bioleaching process plays a role in determining the extent of hydrodynamic cell damage. Mesophilic bacteria possess rigid cell walls while the thermophilic Archaea used in high temperature bioleaching do not possess true cell walls but protein or glycoprotein S-layers. In Sections 2.4.3.1 and 2.4.3.2 cells with no cell wall or cells with

University of Cape Town

walls of reduced structural integrity were shown to be less resilient to the effects of hydrodynamic stress in solids-free reactors and that the presence of solids in the reactor compounded the hydrodynamic stress effect (Scholtz-Brown, 1998; Valencia *et al.*, 2003).

Table 2.13 lists the results of several investigations carried out on the effects of solids in mineral slurries using mesophilic and thermophilic cultures. The investigations highlight the effect of key operating parameters such as solids loading, solids size, agitation rate (power input) and reactor design on bioleaching performance. The investigations are reviewed further in Section 2.10.1 to 2.10.4.

University of Cape Town

**Table 2.13:** The effect of solids loading and agitation intensity on micro-organisms grown in mineral slurry reactors.

| Micro-organism | Peptidoglycan cell wall | Reactor | Impeller type | Batch or Continuous | Solid phase | Experiment | Cause cited for inhibition | Nature of inhibition | Reference |
|---|---|---|---|---|---|---|---|---|---|
| *Acidithiobacillus ferrooxidans* | Yes | Shake flask | n/a | Batch | Flowers of sulphur, fluorapatite, glass beads and pyrite | Effect of particulate materials | Attrition and friction effects; oxygen diffusion; toxic constituents on ore | Declined iron oxidation rates and prolonged lag phases. | Dispirito *et al.*, 1981 |
| *Acidithiobacillus* spp. | Yes | STR | Rushton (RT) and pitched blade (PBT) | Batch | Pyrite and quartzite | Effect of Solids loading (quartzite only) 0-30 % w/v | Attrition effects from solids in the reactor. | Increase in lag phase. Inhibition at 20 % and complete reactor failure at 30 % | Pearce, 1993; Harrison *et al.*, 2003 |
| | | | | | | Effect of impeller speed (400-1090 rpm) | - | No inhibition at the speeds tested | |
| *Sulfolobus* sp. | No | STR | PBT | Batch | Pyrite | Effect of solids loading: 3-9 % (w/v) mineral solids | - | None | Nemati and Harrison, 2000 |
| | | | | | | 12 and 15 % mineral solids | Increased solids loading | Reduced leach rates and cell numbers | |
| | | | | | | 18 % mineral solids | | Process failure | |
| *Sulfolobus* sp. | No | STR | PBT | Batch | Pyrite | Effect of particle size: 37-150 µm | Increased surface area with decreased size | No inhibition observed, rather increased surface area leads to increased oxidation rates | Nemati *et al.*, 2000; Harrison *et al.*, 2003 |
| | | | | | | < 25 µm | -Small particles damaged structure of cells. - Particle size distribution affected the physicochemical properties of the slurry | Reduced leach rates and specific growth rates | |

University of Cape Town

| Micro-organism | Peptidoglycan cell wall | Reactor | Impeller type | Batch or Continuous | Solid phase | Experiment | Cause cited for inhibition | Nature of inhibition | Reference |
|---|---|---|---|---|---|---|---|---|---|
| *At. ferrooxidans* and mixed culture of mesophiles | Yes | STR; Airlift (AL); Modified airlift (MAL) | n/g | Batch | Coal containing pyrite with a particle size < 0.5 mm | Effect of reactor design:<br><br>STR<br>AL<br>MAL | Mechanical stress due to increased solids loading and oxygen limitation | Decreased cell number and pyrite oxidation rate | Beyer *et al.*, 1986 |
| Mixed mesophilic culture | Yes | STR | RT | Batch | Pyrite only and pyrite and quartzite | Effect of solids loading | Oxygen limitation | Decrease in the biooxidation rate | Bailey and Hansford, 1994 |
| *At. ferrooxidans* | Yes | STR | n/g | Batch | Coal containing pyrite | Effect of solids concentration 30 % (w/v) | Oxygen limitation | Decreased leach rates | Loia *et al.*, 1994 |
| *At. ferrooxidans* | Yes | STR and ore-immobilised reactor | | | Pyrite | Comparison between a frictionless reactor and an STR at 12, 20 and 30 % (w/v) solids loading | Shear between sulphide particles; oxygen was not limiting | Decrease in oxidation rate; increase in lag phase | Chong *et al.*, 2002 |
| *At. ferrooxidans*; *Sulfobacillus acidophilus*<br>*Sulfolobus* BC65 | Yes<br>No | STR | RT | Batch | Chalcopyrite | Effect of solids loading: 3, 10, 20, 30 and 40 % (w/v) | Shear stress due to attrition by high solids concentration; toxicity to metal irons (Ag, Cu); formation of precipitates impeding leaching process; oxygen limitation at 30 and 40 % solids | -Rapid decrease in leach rate for *Sulfolobus* BC65 and *S.acidophilus*;<br>-Low redox potential | Witne and Phillips, 2001 |
| *At. ferrooxidans*, *At. thiooxidans* | Yes | STRs | RT and PBT | Continuous | Cobaltiferous pyrite | Effect increasing agitation speed (390 – 550 rpm) at 20 % (w/v) solids loading | Inhibition of bacterial attachment | Limitation of bioleaching efficiency, decrease in bacterial productivity | d'Hugues *et al.*, 1997 |
| *Sulfolobus* B6-2-like micro-organism *Acidianus infernus* | No | STRs | RT- PBT mix | Continuous | Chalcopyrite | Effect of:<br>1. Solids loading: 4, 8, 12, 15 % w/w<br>2. Agitation<br>3. Aeration | - | No significant effect at solids loadings up to 12 % but decrease in oxidation efficiency was noted at 15 % solids loading | d'Hugues *et al.*, 2002 |
| *At. ferrooxidans* | Yes | STR | RT and PBT | Batch | Quartzite | Effect of up to 30 % solids and impeller tip speed range of 2.01-3.35 m $s^{-1}$ | Attrition by solid particles promoted by intense agitation | Loss of viability | Deveci, 2002 |

University of Cape Town

| Micro-organism | Peptidoglycan cell wall | Reactor | Impeller type | Batch or Continuous | Solid phase | Experiment | Cause cited for inhibition | Nature of inhibition | Reference |
|---|---|---|---|---|---|---|---|---|---|
| Mesophile (MES1) | Yes | STR | RT and PBT | Batch | Quartzite, glass beads | Effect of impeller type | - | Greater loss of cell viability with Rushton turbine | Deveci, 2004 |
| Mesophile (MES1) | Yes | STR | RT | Batch | Quartzite, glass beads | Effect of particle size | Attrition | Loss of viability:<br>-45µm 70 %<br>-63+45 µm 63 %<br>-180+125µm 89 % | Deveci, 2004 |
| Mesophile (MES1) | Yes | STR | RT and PBT | Batch | Quartzite, glass beads | Shape of solids | More efficient grinding action of the glass beads | After 3 h, 92 % loss of viability with glass beads and 84 % loss of viability with quartzite | Deveci, 2004 |
| *Sulfolobus metallicus* | No | STR | PBT | Batch | 3 % Pyrite (38 -75 µm) with quartzite loading ranging from 0 to 24 % (38 -75 µm) | Effect of quartzite solids loading: 0-24 % w/v | Increase in the number of particles in solution leading to increased particle attrition | Leach rate decreased significantly with increasing quartzite loading > 15 % | Sissing, 2002; Sissing and Harrison, 2003 |
| | | | | | | Effect of impeller tip speed: 1.67-2.27 m $s^{-1}$ | Increase in the impeller speed leading to increased particle-particle collisions | Cell death and no oxidation at tip speed of 2.27 m $s^{-1}$ and quartzite loading of 15 % | Sissing, 2002 |
| *Sulfolobus acidocaldarius* | No | STR | - | Batch | Pyrite | Effect of particle size: < 70 µm, < 33µm and < 20 µm | - | Leach rate improved on decreasing particle size | Lindström *et al.*, 1993 |
| | | | | | | Effect of solids loading: 1-10 % (w/v) | - | Increase in leach rate up to 6 % and a decline in leach rate from 6 to 10 % | |
| *S. metallicus* | No | Shake flask | - | Batch | Pyrite | Effect of solids loading: 2.5 to 15 % w/v | -Mechanical (attrition) causing metabolic stress<br>-gas transfer limitations | Leach rate declined to 0.58 g Fe $l^{-1}$ $h^{-1}$ at a 15 % pyrite loading using a 38-75 µm size range | Valencia *et al.*, 2003 |
| | | | | | | Effect of particle size: -38, 38-75, 75-106, 106-150 µm | Mechanical (attrition) causing metabolic stress | Increasing particle size at a 15 % pyrite loading decreased the leach rate from 0.62 to 0.08 g Fe $l^{-1}$ $h^{-1}$ | |

n/g = not given

University of Cape Town

### 2.10.1 SOLIDS LOADING

All endeavours to employ STRs for the bioleaching metal sulphide suspensions with oxidisable solids concentrations higher than 20 % have failed (Rossi, 2001). Bailey and Hansford (1994) studied a mesophilic leaching system using both low and high sulphur pyrite and postulated that the determining factor in bioleaching is the proportion of oxidisable solids, i.e. the oxygen–consuming solid fraction in the suspension, not simply the solids concentration. They hypothesised that the solids inert to oxidation only affect the process marginally. This means that the oxygen mass transfer potential of the STRs does not provide enough oxygen for oxidising increased concentrations of metal sulphides. While oxygen availability has been identified by Bailey and Hansford (1994) as a key factor limiting biooxidation at high solids concentration, recently the role of the shear stress and collision forces due to interactions between cells and solid particles in solution has gained more interest in both mesophilic and thermophilic bioleaching systems (Nemati and Harrison, 2000; Sissing 2002; Deveci, 2002). The increase in the aeration rate and agitation rate needed to meet the oxygen transfer rate requirements cause increased turbulence in the reactor thus influence collisions between particles and cells.

#### 2.10.1.1 Mesophilic systems

Dipirito *et al.* (1981), Bailey and Hansford (1994) and Loia (1994) are in agreement that increased oxygen demand was the reason for the failure of their systems at high mineral concentrations. However, the studies of Pearce (1993) and, more recently, Deveci (2002) and Witne and Phillips (2001) were able to show that in the absence of oxygen limitation, reactor failure was caused by the effect of hydrodynamic stress due to increased solids loading.

Dispirito *et al.* (1981) investigated the inhibitory effects of pyrite on growing cultures of *At. ferrooxidans*. The cultures were grown in shake flasks at solids loadings of 0, 0.1, 1, 2, 3, 4, and 5 % w/v on a gyratory shaker at 160 rpm. The authors found inhibition of the bacteria at pyrite concentrations of 1 % and above (Figure 2.11). The inhibition was described by prolonged lag periods with increasing pyrite concentration. At a pyrite concentration of 4 %, the lag period lasted approximately 5 days while at a concentration of 5 % pyrite, iron oxidation was inhibited in excess of 10 days. Increased oxygen demand due to the increased pyrite concentration was cited as the reason for the increased lag phases and complete system failure at a 5 % pyrite concentration.

University of Cape Town

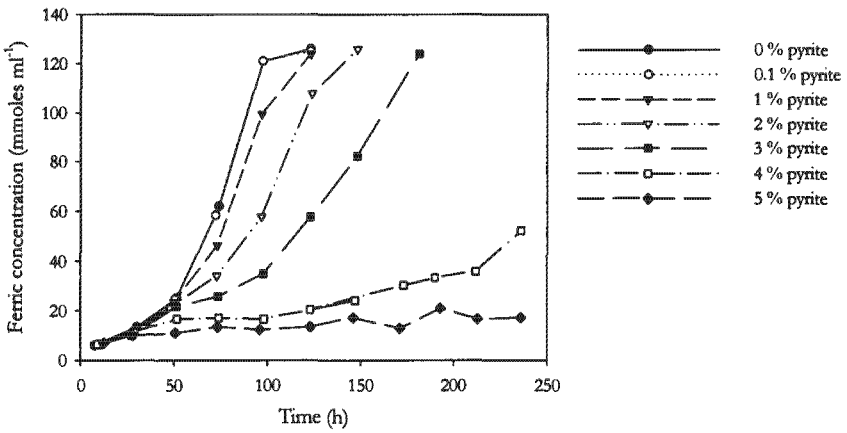


**Figure 2.11:** Effect of particle concentration on bacterial iron oxidation at various pyrite solids loadings (adapted from Dispirito *et al.*, 1981).

Bailey and Hansford (1994) studied the effect of solids loading on a mixed mesophile culture in an STR at an impeller speed of 495 rpm in pyrite and pyrite-quartzite slurries. Using the STR configuration improved mass transfer could be attained compared to the shake flask system of Dispirito *et al.* (1981). In the first study, the effect of solid loading was studied using a mineral with a low sulphide (1.24 % S) content at solids concentrations of 20, 40 and 60 % w/v. The biooxidation rate was found to be proportional to the solids concentration (Figure 2.12a). The maximum solids concentration tested of 60 %, was three times higher than the solids concentration of 20 % where oxygen limitation is commonly encountered with high sulphide content materials in mesophilic systems. The authors observed that the pyrite oxidation rate was directly proportional to the surface area of the mineral, which is affected by the concentration of solids in the reactor. The slope of the oxygen demand line was dependent on the sulphide content of the mineral. By using a low sulphide containing mineral, the authors showed that if sufficient oxygen was available, the biooxidation rate was proportional to the solids concentration, even at high solid loadings. In a second study, a high pyrite content mineral was diluted with inert quartzite. In this way the results of the first study could be confirmed (Figure 2.12b). The specific biooxidation rate remained constant at approximately 0.035 kg pyrite oxidised kg pyrite$^{-1}$ d$^{-1}$ with increasing total solids concentration from 10 to 30 %. This experiment confirmed the authors' previous results that the increasing oxygen demand with increasing pyrite loading was responsible for the decrease in biooxidation using a mesophilic culture over the range tested.

University of Cape Town

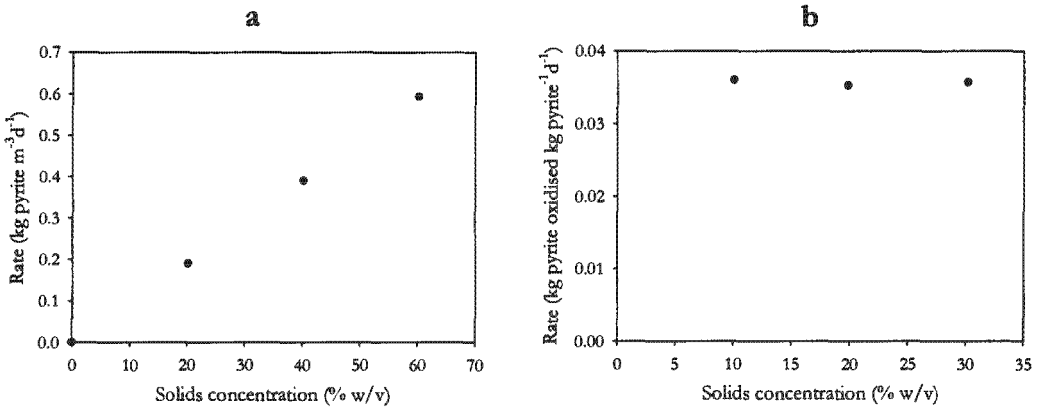


**Figure 2.12:** (a) biooxidation rate vs. solids concentration for low sulphur pyrite and (b) specific biooxidation rate based on amount of high sulphur pyrite present in mixtures of quartz and pyrite in an STR operated at an impeller speed of 495 rpm (adapted from Bailey and Hansford, 1994).

The results obtained by Loia *et al.* (1994) substantiated the inhibition mechanism of Bailey and Hansford (1994). The author studied low sulphur coal depyritisation by mesophiles in a STR. The performance of the bioreactors was relatively unchanged in the solids concentration range of 5 to 40 % whereas failure of pure pyrite bioleach system at 30 % solids concentration was observed in the same reactors. This result supports the finding that the influence of solids concentration on bioleaching performance is related to the proportion of oxidisable mineral present in the solid phase. Conversely, in a study by Pearce (1993) a negative effect of high concentrations of low sulphur pyrite solids (0, 10, 20, 30 % w/v) on mesophilic acidithiobacilli growing in an STR was observed. The mechanism of inhibition was attributed to attrition via solid particles. The redox potential time profiles at 0 and 10 % solids loadings, were similar (Figure 2.13) while at 20 % solids, there was a very slow increase in redox potential indicating the bacteria were still viable. At 30 % solids no change in redox potential was observed. Pearce (1993) used a very similar system to Bailey and Hansford (1994), using low sulphur (1.5 % S) pyrite in order to minimise oxygen limitation. The studies were characterised by different reactor configurations and may have used micro-organisms of differing activity or inoculum size. In both studies the taxonomy of the micro-organisms present in the mixed cultures were not elucidated.

University of Cape Town

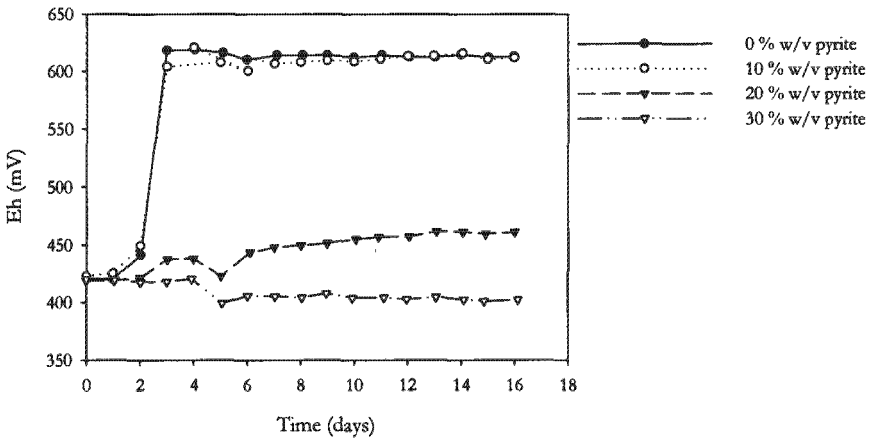


**Figure 2.13:** The effect of low sulphur pyrite on the biooxidation of acidithiobacilli in an STR operated at an impeller speed of 350 rpm (adapted from Pearce, 1993).

Pearce (1993) confirmed the results of the low sulphur pyrite experiments by studying the effect of increasing solids loading of quartzite on the biooxidation of ferrous iron by acidithiobacilli in a one litre STR. The mixed culture of acidithiobacilli was agitated using a Rushton turbine in an STR for two hours at a speed of 770 rpm and quartzite volume fractions of 5, 10, 20 (equivalent to mass fractions of 24, 48, 96 %) and a mean quartzite diameter of 53 μm. The activity of the cells was then determined. The presence of solids caused an increase in the lag phase for the 5 and 10 % volume fractions. No growth was observed using a volume fraction of 20 % (Figure 2.14). These results confirmed that hydrodynamic stress due to the presence of solids negatively affected the cells.

University of Cape Town

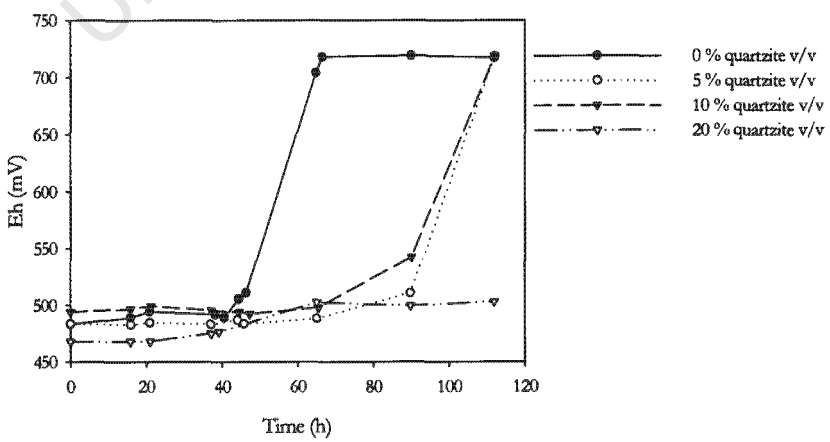


**Figure 2.14:** The effect of quartzite loading on the biooxidation of ferrous iron by acidithiobacilli at an impeller speed of 770 rpm (adapted from Pearce, 1993).

The results obtained by Deveci (2002) on investigating the effect of inert quartzite particles on the viability of mesophiles corroborated the results of Pearce (1993). The choice of quartzite as the solids fraction ensured that there was no oxygen limitation. The effect of increasing solids concentration using a pitched-blade turbine at an impeller speed of 2.51 m $s^{-1}$ resulted in a decrease in the viability of the cells. The extent of decrease in viability depended on the exposure time, the concentration of solids and the impeller speed. At 10 % w/w solids there was a limited effect on the viability of the cells (derived from the oxygen utilisation rate on 100 mM $Fe^{2+}$) over a 4 h period. The extent of the decrease in viability rose significantly with increasing the concentration of solids to 30 % w/w (Figure 2.15). The percent decrease in the cell numbers was lower than the decrease in viability, which suggests that a portion of the cells remained intact despite losing their ability to divide.

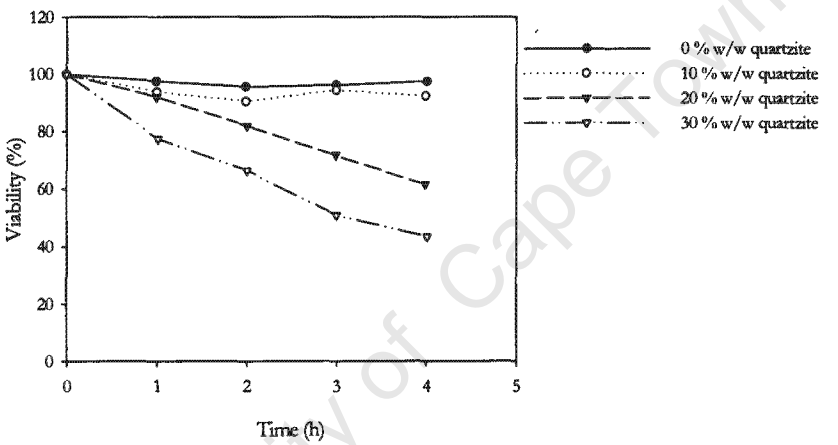


**Figure 2.15:** Effect of quartzite concentration on the viability of a mesophilic bacterial population using a pitched blade impeller at 2.51 m $s^{-1}$ (adapted from Deveci, 2002).

In an applied system using a copper mineral instead of inert quartzite, Witne and Phillips (2001) studied the effect of solids concentration on *At. ferrooxidans*. They used a mixed copper concentrate in which the main minerals were chalcopyrite, bornite, chalcocite and covellite. The concentrate contained 18.4 % sulphur and a size fraction characterised by a $d_{90}$ of 112 µm. Solids loadings of 3, 10, 20, 30, and 40 % w/v were investigated in a STR at 200 rpm. The experiments were conducted under optimal gas (oxygen and carbon dioxide) enrichment conditions determined in previous experiments. At solids loadings of 3, 10 and 20 % almost 100 % mineral solubilisation was achieved (Figure 2.16). The recovery of copper at higher pulp densities decreased with increasing solids concentration. At a solids loading of 40 %, a moderate decrease in copper extraction to 75 % was observed. The authors were able to firmly conclude that since the oxygen and carbon dioxide availability could be excluded as having a negative impact on the

University of Cape Town

leaching process, the low extents of leaching at the higher solids loadings were due to hydrodynamic stress.

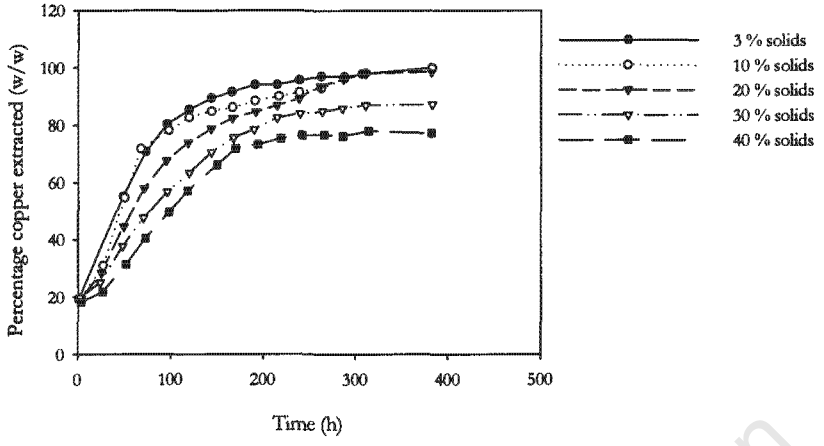


**Figure 2.16:** Copper extraction by *At. ferrooxidans* from a copper concentrate as a function of solids loading (adapted from Witne and Phillips, 2001).

University of Cape Town

### 2.10.1.2 Thermophilic systems

As observed with mesophilic bioleaching systems, investigators have shown that increasing solids loading either by increasing the inert particle concentration or the mineral concentration has a detrimental effect on the leaching micro-organisms and thus on the process performance. Nemati and Harrison (2000) and Sissing and Harrison (2002) reported the effects of solids loading on the growth rate and oxidation of pyrite by a *Sulfolobus* sp.. Nemati and Harrison (2000) investigated the effect of a 53-75 μm size fraction of pyrite up to a solids loading of 18 % w/v and an impeller speed of 550 rpm. They found reduced performance of bioleaching above a 12 % solids loading and complete inhibition at 18 % (Figure 2.17). At a solids loading of 12 %, the mechanism of inhibition was postulated to be due to a low cell to solid ratio and thus the microbial ferric iron regeneration step may have been rate limiting. At solids loadings of 15 and 18 % the dominant mechanism of inhibition was proposed to be attrition of cells by the pyrite particles imposing severe hydrodynamic stress on the cells.

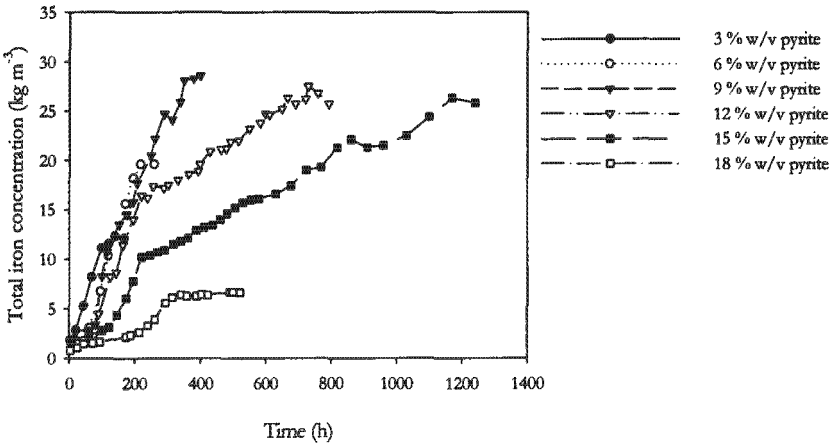


**Figure 2.17:** Effect of solids loading on the bioleaching of pyrite by *S. metallicus* (adapted from Nemati and Harrison, 2000).

Sissing and Harrison (2003) carried out similar studies to those of Nemati and Harrison (2000). They studied the effect of solids loading on *S. metallicus* using inert quartzite particles (38-75 μm) to increase the solids loading above the 3 % pyrite. In this way they eliminated all effects except those of the solids phase. On addition of the inert particulates, no effect on bioleaching or microbial growth was observed on increasing the inert solids concentration from 0 to 15 %. However bioleaching rates were progressively reduced with increasing quartzite loading above 15 %. The specific growth rate increased to 0.020 $h^{-1}$ at a 15 % quartzite loading and decreased to 0.011 $h^{-1}$ at a 21 % quartzite loading. No growth was observed in the presence of 24 % quartzite. The biomass yield decreased with increasing quartzite loading above 15 %. The decreased pyrite oxidation was attributed to both decreased microbial concentration and decreased specific activity.

Valencia *et al.* (2003) ascertained the effect of solids loading on the biooxidation of pyrite by *S. metallicus* grown in shake flasks (220 rpm). Pyrite loadings of 2.5, 5, 10, and 15 % w/v were investigated. Using a size fraction of 38-75 μm pyrite the extent of iron solubilisation increased from 64.0 to 73.7 % using pyrite concentrations of 2.5 and 5 % respectively (Table 2.14). However, increasing the pyrite concentration above 5 % to 10 and 15 % caused a decline in the extent of solubilisation to 40.9 and 21.5 % respectively.

The extents of solubilisation obtained by Nemati and Harrison (2000) and Sissing and Harrison (2003) are similar at the low particle loadings (up to 12 %) (Table 2.14). Nemati and Harrison (2000) showed that increasing the solids loading beyond 12 % caused a sharp decrease in the extent of pyrite solubilisation while Sissing and Harrison (2003) only showed this effect above

University of Cape Town

21 % total solids. It is likely that phenomena such as oxygen limitation, the difference in the densities of the pyrite and quartzite particles and to a lesser extent, metal inhibition and low pH were responsible for the observed difference. Comparing the results obtained by Nemati and Harrison to those of Valencia *et al.* (2003) show much lower extents of solubilisation in the latter. Valencia *et al.* (2003) employed shake flasks hence oxygen limitation may have occurred. Furthermore, incomplete suspension of the pyrite could have led to cellular stress caused by the grinding effects of the incompletely suspended particles (Scholtz *et al.*, 1997).

**Table 2.14:** Comparison of iron solubilisation at varying solids loadings and a particle size fraction of 38-75 μm reported in the literature.

| **Nemati and Harrison (2000) Pyrite only** | | **Sissing (2002) 3 % pyrite with varying quartzite loading** | | **Valencia *et al.* (2003) Pyrite only** | |
|---|---|---|---|---|---|
| Total solids loading (%; w/v) | Extent of solubilisation (%; w/w) | Total solids loading (%; w/v) | Extent of solubilisation (%; w/w) | Total solids loading (%; w/v) | Extent of solubilisation (%; w/w) |
| 3 | 100 | 3 | 91 | 2.5 | 64.0 |
| 6 | 92 | 9 | 86 | 5.0 | 73.7 |
| 9 | 88 | 15 | 80 | 10 | 40.9 |
| 12 | 88 | 18 | 86 | 15 | 21.5 |
| 15 | 70 | 21 | 86 | | |
| 18 | 11 | 24 | 62 | | |
| | | 27 | 46 | | |

Witne and Phillips (2001) studied the effects of a copper concentrate at solids loadings of 3, 10, 20, 30 and 40 % w/v on acidophilic micro-organisms including a *Sulfolobus* sp.. For the *Sulfolobus* sp., the leaching rate decreased with increasing solids loading in the range 30 to 40 %. The decrease in leaching rate observed at high solids loadings under optimum gas enrichment (i.e. oxygen and carbon dioxide availability were not limiting) was accompanied by low metal dissolution and low redox potential. These effects were postulated to be due to shear stress caused by attrition of the cells at high solids concentration. d'Hugues *et al.* (2002) identified potential limiting factors in an STR with a *Sulfolobus*-like micro-organism and *Acidianus infernus* used for bioleaching chalcopyrite. These factors were the sensitivity of the micro-organisms to hydrodynamic stress, nutrient concentrations, and oxygen transfer efficiency. The authors investigated the effects of increased chalcopyrite loading on the oxygen and carbon dioxide utilisation rates (OUR and CUR respectively). At a 15 % (w/v) solids loading they observed a decrease in the OUR from 820 mg $l^{-1}$ $h^{-1}$ to 450 mg $l^{-1}$ $h^{-1}$ in 4 days. A comparable decrease was also observed with microbial growth (CUR). Although the study did not conclusively show disruption of the thermophilic cells due to mechanical shearing, the authors proposed that hydrodynamic turbulence caused by agitation (and aeration) could potentially be a limiting factor if they are combined with relatively high solids concentrations.

University of Cape Town

### 2.10.2 SOLIDS SIZE

It is recognised that increasing solids loading and decreasing particle size across a limited operating window have positive effects on the volumetric rate of biooxidation of refractory gold concentrates. Decreasing particle size increases the surface area of mineral available for oxidation (Bailey and Hansford, 1994, Nemati *et al.*, 2000). However, below a critical particle size, this positive effect can be negated by decreased attachment of cells to the particles as well as increased collision events associated with increased loading, leading to reduced leach rates. Deveci (2004) and Valencia *et al.* (2003) postulated that cell attachment is impaired when the diameters of the particles and cells are of similar magnitude. Deveci (2004) found that the first order death rate of a mixed mesophilic culture growing on ferrous iron in an STR, increased from 0.23 to 0.58 $h^{-1}$ with decreasing particle size from the 125-180 μm range to the 45–63 μm range, below which a reverse trend was noted. Nemati *et al.* (2000) studied the effect of particle size on a thermophilic *Sulfolobus* sp.. A change in particle size from the 150-180 μm range to the 25-45 μm range enhanced the bioleaching rate from 0.05 kg $m^{-3}$ $h^{-1}$ to 0.098 kg $m^{-3}$ $h^{-1}$. This increase in rate was attributed to an increase in the surface area available for leaching and was consistent with the findings of Bailey and Hansford (1994). No influence on morphology or growth kinetics was seen at these size fractions. However, decreasing the particle size to less than 25 μm had a negative effect on the activity of the cells. The presence of fine particles appeared to damage the structure of the cells, resulting in their inability to oxidise pyrite. Using particle size fractions with nominal mean diameters varying from 25 to 5 μm, a reduction in both iron leach rate (from 0.065 kg $m^{-3}h^{-1}$ at 20 μm to 0.020 kg $m^{-3}$ $h^{-1}$ at 5 μm) and specific growth rate (from 0.040 $h^{-1}$ at 25 μm to 0.025 $h^{-1}$ at 5 μm) were observed on decreasing particle size. The authors postulated that below a critical size fraction, the increase in the number of particle-particle collisions increased the hydrodynamic stress factor. Further, the fine particulate phase affected physiochemical properties of the suspension such as viscosity and oxygen transfer potential.

In a system where the influence of improved leaching due to increased surface area was not a factor, Pearce (1993) was able to elucidate clearly the effect of particle size on acidithiobacilli. The rate of oxidation of ferrous iron was monitored at quartzite particle sizes ranging from 53 to 255 μm, at a solids loading of 5 % v/v and an impeller speed of 770 rpm (Figure 2.18). Lag periods of 98 hours were observed for the 53, 114 and 161 μm size fractions. A shorter lag period of 74 hours was found in the presence of the 255 μm size fraction. It is probable that a similar effect is seen here as observed by Nemati *et al.* (2000) where the reduced size fractions damage the cells more easily. Furthermore, Pearce (1993) proposed, as postulated by Deveci (2004) and Valencia *et al.* (2003), that since acidithiobacilli are known to attach to solid particles, the shorter lag period observed with the larger particles may be related to the reduced surface area

University of Cape Town

available for attachment allowing equilibrium concentrations of planktonic cells to be achieved more rapidly.

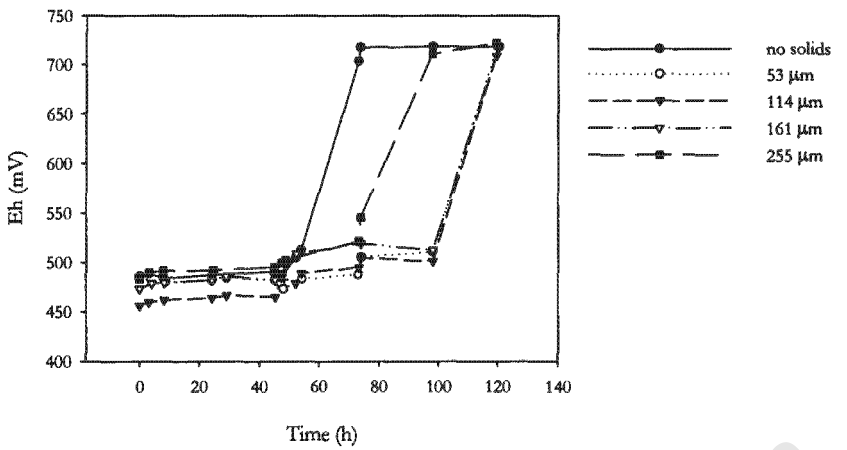


**Figure 2.18**: The effect of quartzite particle size on the oxidation of ferrous iron by acidithiobacilli at a solids loading of 5 % v/v and an impeller speed of 770 rpm (adapted from Pearce, 1993).

University of Cape Town

### 2.10.3 IMPELLER DESIGN AND IMPELLER SPEED

As with other solids-containing and solids-free systems discussed in Section 2.2.2, the impeller plays an important role as regards the intensity of hydrodynamic stress within the bioleaching STR. The extent of the adverse effect depends on the impeller design and speed. The power input per unit volume is higher for radial (Rushton) turbines compared to axial (pitched blade) turbines. This increased power input for the Rushton turbine causes more damage to micro-organisms as was shown in the studies of Pearce (1993) and Deveci (2002). Pearce (1993) investigated the effect of impeller type on the bioleaching of 10 % w/v pyrite by acidithiobacilli. The axial and radial turbines showed no inhibition and similar redox potential profiles at 350 rpm (Figure 2.19). Increasing the impeller speed to 630 rpm caused a lag period of approximately 14 days using the axial flow impeller. The redox potential for the system agitated by the radial turbine at 630 rpm did not increase during the course of the experiment (20 days). These results illustrate clearly the increased hydrodynamic stress induced by the radial turbine compared to axial turbine.

Deveci (2002) also found similar effects to those observed by Pearce (1993). The author reported that the loss of viability of mesophilic bioleaching micro-organisms growing on ferrous iron was more extensive with the Rushton turbine than the pitched blade turbine at impeller tip speeds in the range 2.01 to 3.35 m $s^{-1}$. With the pitched blade turbine, there was no effect on cell viability at

a 10 % solids loading on increasing tip speed from 2.51 to 3.35 m $s^{-1}$ while the viability of the cells decreased by 15 % under the same conditions using the Rushton turbine. The higher power input per unit volume generated by the Rushton turbine resulted in an elevated intensity of hydrodynamic stress to the micro-organisms.

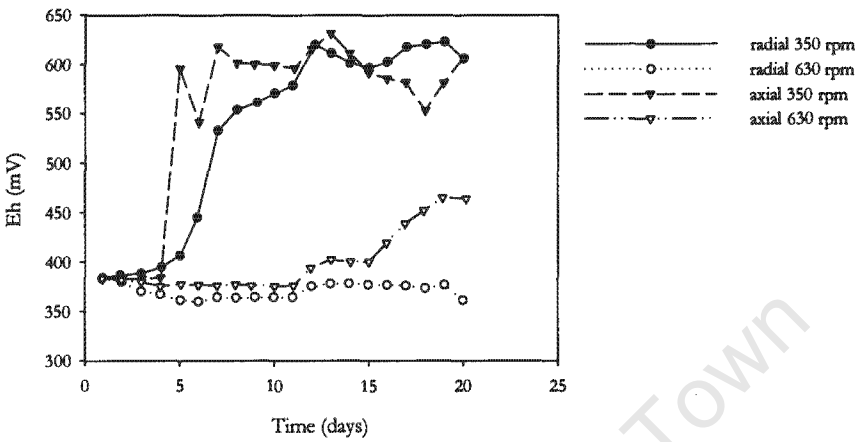


**Figure 2.19:** The effect of impeller speed and impeller type on the biooxidation of high sulphur pyrite by acidithiobacilli at a 10 % w/v pyrite loading (adapted from Pearce, 1993).

Sissing (2002) investigated the effect of agitation speed (1.67, 1.97 and 2.27 m $s^{-1}$) on pyrite oxidation by the archaeon *Sulfolobus* sp. in a STR in the presence of 18 % w/v total solids (3 % pyrite and 15 % quartzite). The iron leach rate and extent of pyrite solubilisation was higher at a tip speed of 1.97 m $s^{-1}$ (650 rpm) than at 1.67 m $s^{-1}$ (560 rpm). Leach rates of 0.091 and 0.096 kg $m^{-3}$ $h^{-1}$ were obtained at tip speeds of 1.67 and 1.97 m $s^{-1}$ respectively. The extent of leaching was 86 % at a tip speed of 1.67 m $s^{-1}$ and 90 % at a tip speed of 1.97 m $s^{-1}$. This effect was attributed to increased mass transfer at the higher tip speed. However, the specific growth rate and culture activity were higher at a tip speed of 1.67 m $s^{-1}$. Improved mass transfer at the higher impeller speed may have increased the metabolic activity of the micro-organisms through an increase in the rate of ferrous iron and sulphur oxidation; however the increased hydrodynamic stress at the increased impeller speed may have affected the viability of the organisms. At a tip speed of 2.27 m $s^{-1}$ (760 rpm) there was no pyrite solubilisation and cell death occurred. At this impeller speed, the negative effects of increased hydrodynamic stress outweighed the positive effects of improved mass transfer. The results obtained by Sissing (2002) suggest a greater resilience of the Archaea than the acidithiobacilli studied by Pearce (1993) even though Sissing utilised a higher size fraction and a micro-organism without a true cell wall. This comparison is however invalid as a rigorous comparison of reactor geometry, microbial activity, inoculum size and mass transfer achieved has not been included.

University of Cape Town

### 2.10.4 REACTOR DESIGN

In an effort to reduce the detrimental effects of interactions between particles and bioleaching organisms, Beyer *et al.* (1986) and Karamanev *et al.* (2001) proposed two new reactor designs. Beyer *et al.* (1986) showed that modification of an air lift reactor could improve the rate of pyrite biooxidation by *At. ferrooxidans*. The author studied three reactor configurations, namely a conventional airlift (AL) a STR and a modified airlift (MAL). At a pyritic coal (1.7 % sulphur) concentration of 20 %, both the STR and conventional airlift reactors failed. In contrast, the redox potential and the cell concentration of the modified airlift reactor increased. The redox potential in the STR and AL reactors did not increase during the course of the experiment (16 days) and remained at approximately 425 mV (Figure 2.20). The redox potential in the MAL increased from 465 to 669 mV over the 16 day period. The cell concentration in the MAL increased from 6.25 x $10^7$ to 9.13 x $10^7$ cells $ml^{-1}$. No growth was observed in both the AL reactor and STR. In the conventional airlift reactor, rigorous mixing was required to achieve forced recycle of the coal slurry. Modification of the air lift reactor through replacing the round bottom of the airlift with a conical bottom reduced the intensity of mixing required to circulate the coal without sedimentation and thus reduced the degree of detachment of micro-organisms from the surface of the coal as well as the frequency and intensity of particle-cell-particle collisions.

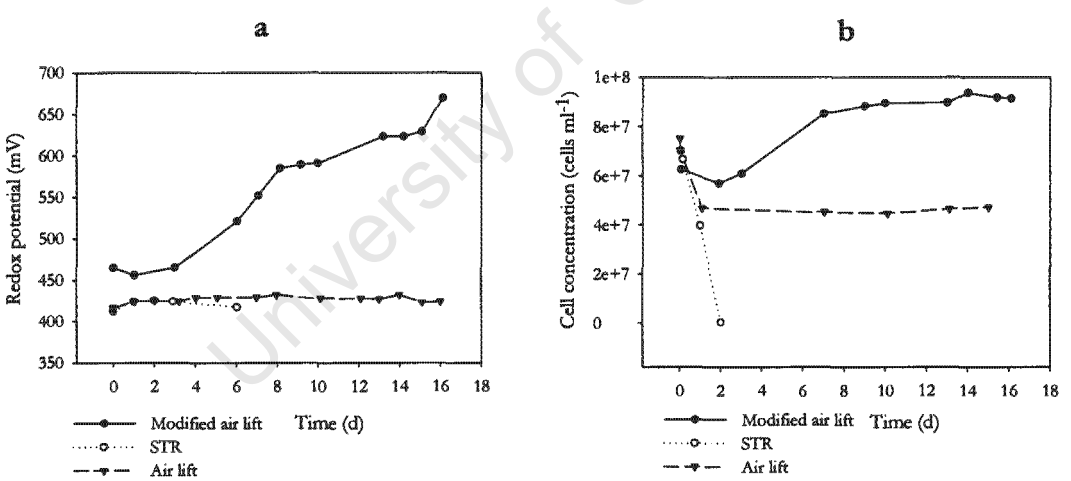


**Figure 2.20:** Influence of bioreactor design on (a) pyrite oxidation and (b) microbial growth at a 20 % w/v solids loading (adapted from Beyer *et al.*, 1986).

Karamanev *et al.* (2001) proposed a new type of bioreactor, named the immobilised ore bioreactor, to reduce particle-cell-particle interactions within the leaching system. The reactor, based on the airlift principle utilises a porous matrix (geotextile fibre) within which the mineral particles are trapped. Nutrients are supplied to the micro-organisms by circulation of the nutrients through the immobilised structure. The assumption made is that the majority of the leaching organisms are attached to the surface of the mineral. Under frictionless conditions there

University of Cape Town

was fast adsorption of *At. ferrooxidans* cells onto pyrite whereas in the slurry reactor it was difficult for the cells to adsorb to the surface of the particles due to the great amount of shearing. The reactor was shown to handle solids loading up to 40 % w/v pyrite, two fold that reported by Bailey and Hansford, 1994 for classic mesophilic stirred tank operations. The volumetric rate of pyrite oxidation by *At. ferrooxidans* in the immobilised ore reactor was found to be 2.5 times higher than in a STR. Changing reactor configuration reduced the intensity of hydrodynamic stress and promoted cell attachment and this in turn influenced the extent and rate of solubilisation.

## 2.11 SUMMARY: PART B

In Part B of the literature review, a slurry STR system of industrial importance and directly relevant to the current study was considered. Sections 2.8 to 2.10 detailed the relevance of bioleaching in the mining industry, the bioleaching process, the extremophilic micro-organisms involved in commercial bioleaching processes and finally the role of hydrodynamic and to a lesser extent chemical stress in tank bioleaching were discussed. The bioleaching of chalcopyrite was shown to present a particular challenge to the bioleaching industry because of the recalcitrance of this mineral to chemical and biological leaching. Passivation of the mineral causes reduced rates of mineral leaching and hence nutrient limitation of the micro-organisms.

Section 2.9 reviewed the diverse range of micro-organisms involved in bioleaching process with an emphasis on the characteristics of the genus *Sulfolobus*. Section 2.10 reviewed studies from the literature investigating hydrodynamic stress of bioleaching micro-organisms in STRs using quartzite-only, quartzite-mineral and mineral-only slurries. Hydrodynamic stress was shown to be a function of the solids loading, particle size the impeller design and speed, and the reactor design.

In solids loading studies, in the absence of oxygen limitation, increasing solids loading reduced the productivity of the tank bioleaching process under both mesophilic and to a greater extent, thermophilic conditions. Deceasing particle size within a limited window increased the rate and extent of leaching. However, below a critical particle size, the process performance was adversely affected due to increased hydrodynamic stress to the cells at the reduced particle size. The Rushton turbine was shown to cause a greater decline in microbial viability and system performance than the pitched blade turbine. This difference in effect was attributed to the higher power input per unit volume generated when using the Rushton turbine causing increased hydrodynamic stress conditions. Increasing the impeller speed up to a critical level improved mass transfer which improved the metabolic activity of the cells and resulted in an increased extent of leaching. However, beyond a critical speed the negative effects of hydrodynamic stress

University of Cape Town

outweighed the positive effects of improved mass transfer. By changing reactor design investigators were able to minimise the effect of hydrodynamic stress in the bioleaching reactor. Modifying an airlift reactor (i) through changing the shape of the reactor base from round to conical and thus reducing the intensity of mixing required to circulate solids, and (ii) through immobilisation of the mineral in a matrix, the detachment of micro-organisms and the frequency and intensity of particle-cell interactions were reduced. These changes in reactor design resulted in improved rates and extents of leaching.

Although physiological stresses such as reduced mass transfer, increased metal concentrations and increased acidity have been identified as contributing to loss in the rate and extent of leaching, hydrodynamic stress has been shown to be one of the primary reasons for reduced metal recoveries in mesophilic and thermophilic bioleaching systems.

## 2.12 CONCLUDING REMARKS: LITERATURE REVIEW

This literature review has shown that hydrodynamic stress is an important consideration in the slurry STR, in particular the bioleaching STR. It has been shown that increasing solids loading and impeller tip speed causes (i) a decline in the overall process performance of the bioleaching system and (ii) influences the micro-organisms at a cellular level by changing for example their viability, metabolic activity and morphology. Furthermore, it was also shown that micro-organisms possess response mechanisms to stress. In this way they are able to sense and react to the effects of stress and regain a steady state.

The present study aims to determine the effect of and the biological response to increasing solids loading and impeller tip speed, separately and in combination, on the bioleaching of a chalcopyrite mineral by an acidothermophilic archeaon. This would provide improved understanding of the effects of hydrodynamic stress on a micro-organism devoid of a proper cell wall, growing in a nutrient limited environment under increased levels of hydrodynamic stress.

University of Cape Town

# Chapter 3: Materials and Methods

In this chapter, the experimental protocols utilised in this study are discussed with emphasis on the reactor set-up and configuration, reactor start-up, experimental protocol and the analytical methods employed. In addition to these, a description of the micro-organism as well as the solids fractions is provided.

## 3.1 REACTOR CONFIGURATION

A stirred tank reactor was used as this configuration is ideal for the study of slurry systems. A pitched blade (axial) impeller was chosen to provide good solids suspension and generate low shear. Currently, commercial stirred tank bioleach processes utilise axial hydrofoil impellers such as the Lightnin A315. Owing to the high solidity of the Lightnin A315, this impeller type could not be scaled-down for use in a 1 litre stirred tank and thus a conventional pitched blade impeller was chosen. A standard reactor configuration was not utilised because complete solids suspension was not possible under standard reactor set up conditions. A decreased off-base impeller height was utilised. Decreasing this height enabled complete solids suspension at the lowest power input to maximise the range of impeller speeds attainable with the overhead stirrer motor used.

The experimental setup consisted of a one litre jacketed glass, stirred tank reactor equipped with a 4-blade pitched blade impeller, a condenser, a 4-blade ring baffle and an L-shaped sparger through which 2 vvm air supplemented with 1% v/v $CO_2$ was supplied. The L-shaped sparger contained 6 holes, 1 mm in diameter, on the surface of the arm of the sparger tube. The temperature of the reactor was maintained between 66 and 68°C using a circulating water bath. The speed of the impeller was controlled with a Heidolf overhead stirrer. In order to minimise evaporation, the condenser water was cooled to 4°C using a Lauda thermocirculator. A schematic representation of the reactor system is illustrated in Figure 3.1. The dimensions of the reactor components are given in Figure 3.2.

University of Cape Town

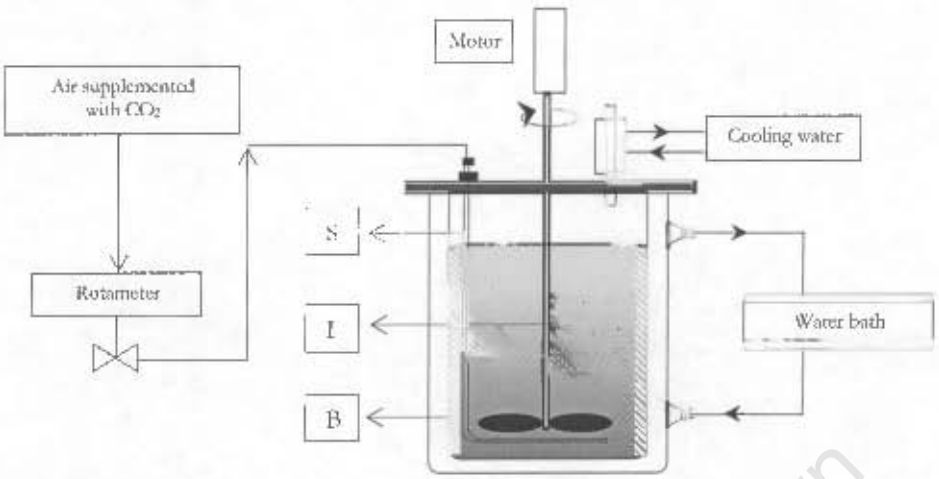


**Figure 3.1:** Schematic representation of the stirred tank system. B = baffle; I= impeller; S = sparger tube

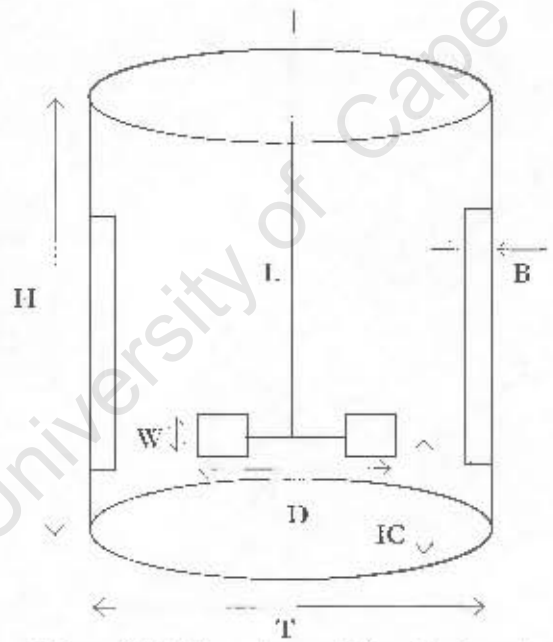


**Figure 3.2:** Dimensions of stirred tank reactor.

| | | | | | |
|---|---|---|---|---|---|
| T | Internal diameter of reactor | = 115 mm | D | Diameter of impeller | = 53 mm |
| H | Height of working volume | = 145 mm | W | Width of impeller | = 20 mm |
| B | Baffle width | = 10 mm | | Blade thickness | = 2 mm |
| L | Length of impeller shaft | = 470 mm | | Angle of twist | = 45° |
| IC | Impeller clearance | = 10 mm | | | |

University of Cape Town

## 3.2 SOLIDS FRACTION

Two types of particulates were used for the experiments. A chalcopyrite concentrate comprised the reactive mineral particulates releasing microbial substrate while quartzite particles comprised the inert solids fraction. The properties and size fractions of the solids are described below.

### 3.2.1 CHALCOPYRITE MINERAL

A chalcopyrite concentrate (Andina) milled and sieved to a size fraction between 38 and 75 μm was provided by BHP Billiton, South Africa. The density of the chalcopyrite concentrate was determined to be 4.53 g $cm^{-3}$. Density measurements were carried out using an AccuPyc 1330 V1.02 pycnometer. The major elemental composition and mineralogy of the concentrate are presented in Tables 3.1 and 3.2.

**Table 3.1:** Major element composition of the Andina chalcopyrite concentrate.

| Copper (%) | Iron (%) | Total sulphur (%) |
|---|---|---|
| 29.8 | 25.9 | 31.7 |

**Table 3.2:** Mineralogy of the Andina chalcopyrite concentrate.

| Mineral | Formula | Wt % |
|---|---|---|
| **Sulphides** | | |
| Chalcopyrite | $CuFeS_2$ | 79.52 |
| Bornite | $Cu_5FeS_4$ | 4.14 |
| Chalcocite | $Cu_2S$ | 0.01 |
| Covellite | $CuS$ | 0.33 |
| Pyrite | $FeS_2$ | **8.05** |
| Other sulphides | | 1.23 |
| Gypsum | $CaSO_4.2H_2O$ | 0.50 |
| **Silicates** | | |
| Quartz | $SiO_2$ | 1.45 |
| Feldspar | $CaAl_2Si_2O_8$ | 1.83 |
| Mica | $K_2Al_4(Si_6Al_2O_{20})(OH)$ | 1.88 |
| Altered silicates | | 0.10 |
| Other silicates | | 0.29 |
| **Other** | | |
| Iron-oxides | $Fe_2O_3$ / $Fe_3O_4$ | 0.32 |
| Carbonates (calcite) | $CaCO_3$ | 0.09 |
| Accessories | | 0.17 |
| Other | | 0.08 |
| **Total** | | 100 |

University of Cape Town

The particle size distribution (Figure 3.3) of the chalcopyrite sample used in this study was determined by laser diffraction using a Malvern Mastersizer (Malvern Instruments) particle size analyser. For the chemical control experiments, the mineral was irradiated to destroy any organisms that were present on the surface of the particles. The material was treated by exposing the particles to gamma radiation (Atomic Energy Corporation, South Africa).

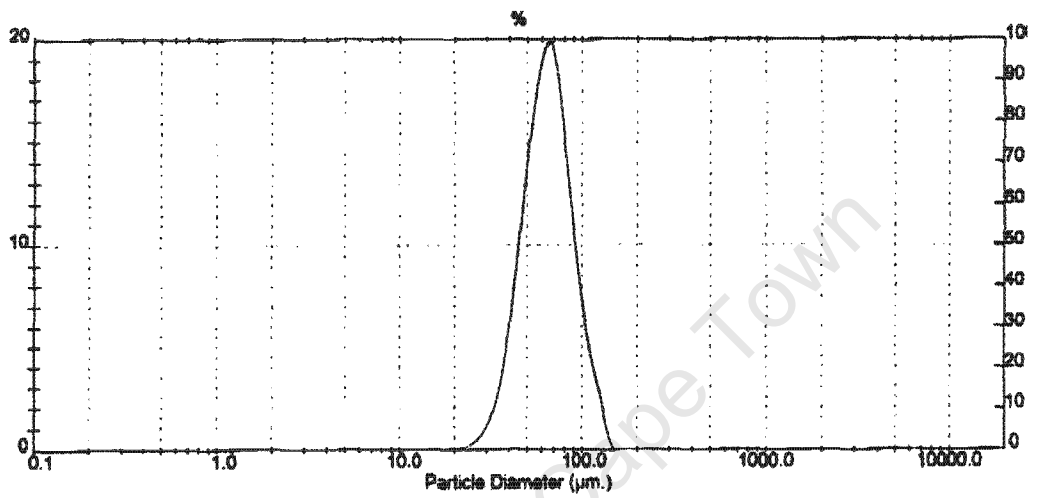


**Figure 3.3:** Size distribution of chalcopyrite particles sieved in the 38 to75 µm size range.

$d_{10}$ = 48 µm, $d_{50}$ = 66 µm, $d_{90}$ = 89 µm.

### 3.2.2 QUARTZITE

Quartzite particles of the 38 to 75 µm size fraction were obtained by milling and wet sieving quartzite provided by CONSOL Glass (Cape Town). The quartzite required pre-treatment to remove organic and inorganic impurities. To remove inorganic contaminants, the solids were washed in 30 % v/v nitric acid at 40°C for 4 h and subsequently rinsed with distilled water at least 8 times until the supernatant appeared colourless and the pH stabilised. To remove organic contaminants, the quartzite was calcined in a furnace at 400°C for 6 h. The density of the quartzite was determined to be 2.6 g $cm^{-3}$. The size distribution of the washed and calcined quartzite sample is presented in Figure 3.4.

University of Cape Town

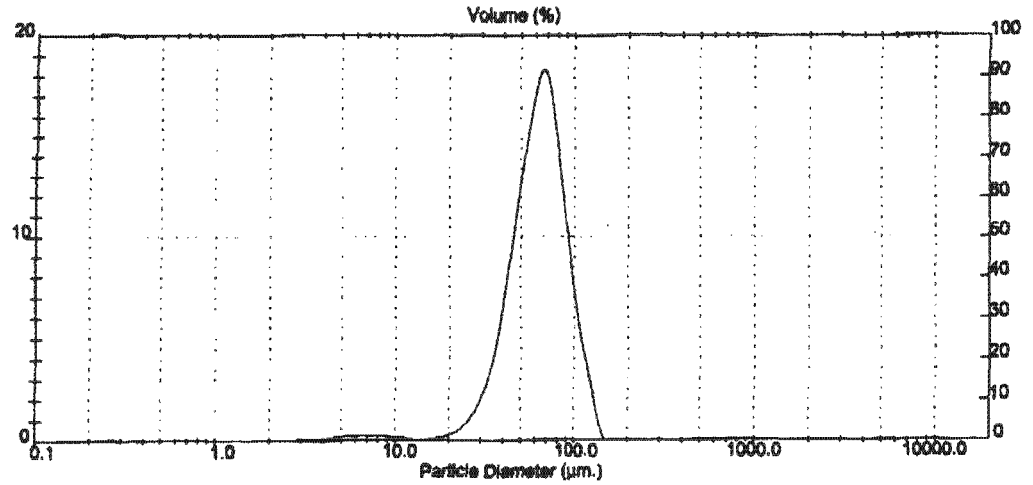


**Figure 3.4:** Size distribution of quartzite particles sieved in the 38 to75 µm size range.

$d_{10}$ = 41 µm, $d_{50}$ = 65 µm, $d_{90}$ = 104 µm

## 3.3 CULTURE

The experimental work was initiated using a *Sulfolobus metallicus* culture, provided by BHP Billiton (South Africa), was maintained in a one litre stirred tank reactor at 68°C on Norris 0K mineral salts medium at pH 1.6 (Norris and Barr, 1988) and 30 g $l^{-1}$ of a < 22 µm size fraction of Andina chalcopyrite (Section 3.2.1). The reactor setup was as described in Section 3.1. The stock culture was sub-cultured daily by removing 150 ml of slurry from the reactor and replacing it with 150 ml of fresh Norris 0K mineral salts medium and 4 g of chalcopyrite. The Norris 0K mineral salts medium consisted of (per litre of distilled water):

| | |
|---|---|
| $(NH_4)_2SO_4$ | = 0.40 g |
| $MgSO_4$ | = 0.25 g |
| $KH_2PO_4$ | = 0.20 g |
| KCl | = 0.10 g |

University of Cape Town

# 3.4 REACTOR OPERATION AND EXPERIMENTAL PROCEDURE

## 3.4.1 REACTOR START-UP

The first step in the start-up procedure was pH stabilisation of the chalcopyrite concentrate. pH stabilisation was carried out in the reactor prior to inoculation. This stabilisation procedure was necessary to prevent fluctuations in the solution pH causing stress to the micro-organisms on inoculation of the reactor. A 21 g sample of the 38-75 μm fraction of the concentrate was added to 550 ml of Norris medium at 68°C in the STR. The solution pH was measured (Section 3.5.1) every hour and adjusted to pH 1.6 with sulphuric acid until a stable pH of 1.6 was obtained.

After pH stabilisation the reactors were inoculated. For each reactor, the inoculum was prepared by removing a 200 ml sample from the stock reactor sub-cultured 24 h earlier. The sample was allowed to settle for 30 min to remove as much precipitate and mineral phase as possible. A 150 ml aliquot of the supernatant containing cells and residual precipitate was added to the equilibrated medium and pH stabilised chalcopyrite and allowed to mix in the reactor for 10 min before sampling for the 0 h sample. The gas flow rate was maintained at 2 vvm. The tip speed of the stirrer was set to 0.76 $ms^{-1}$. The culture was allowed to grow under the minimal hydrodynamic stress conditions for 24 h. After 24 h, the impeller speed was increased and the inert particulate fraction was added to the reactors where required to achieve the conditions specified for the experiment.

The critical impeller speed at which the solid particles were completely suspended was determined using the method of Scholtz-Brown (1998). The reactor vessel was raised and a mirror placed under the base of the vessel. The impeller speed at which the particles did not remain on the vessel base for greater than 1 or 2 seconds was determined to be the critical impeller speed (1.67 m $s^{-1}$). Impeller speed was measured using a Veeder-Root 6611 tachometer.

## 3.4.2 REACTOR MONITORING AND SAMPLING PROCEDURE

The reactor temperature, gas flow rates and impeller speed were checked on a daily basis. In addition, the reactor volume was compensated for evaporation, with distilled water, every 12 h. Samples were removed from the reactors daily using a 50 ml syringe with a silicone tubing attachment. Samples were removed from midway down the reactor approximately 2 cm away from

University of Cape Town

the impeller shaft. Upon extraction of the sample, the syringe was inverted for 30 seconds to retain the concentrate at the base of the syringe. After 30 seconds, a 20 ml sample devoid of mineral and quartzite particles and containing precipitate and cells was expelled from the syringe. The sample and concentrate remaining in the syringe were mixed thoroughly and returned to the reactor. The 20 ml suspension sample was used for all analyses described in Section 3.5.

## 3.5 ANALYTICAL PROCEDURES

When using an analytical technique, it is important to consider the reliability of equipment, reproducibility and the robustness of the procedure in order to ensure accurate data retrieval. In the current study, the reproducibility of the analytical methods was tested by conducting analyses in triplicate and calculating the standard deviation between the replicates. Equipment used for the analyses was tested and calibrated on a regular basis to ensure proper functioning and reliability. Analytical methods were chosen from procedures widely used by researchers in the field of bioleaching and those working with extremophilic micro-organisms. Some techniques utilised were modified for application to the specific requirements of this study. The analytical error was calculated where possible according to the calculation presented in Appendix A.6.

Bioleaching performance was determined by measuring the suspension pH, redox potential, cell concentration and iron and copper concentration. The response of the micro-organisms to hydrodynamic stress was determined by observing changes in (i) cell morphology using phase contrast microscopy, particle size analysis (CellFacts) and scanning electron microscopy (SEM), (ii) viability using differential fluorescence staining, (iii) metabolic activity by measuring the oxygen utilisation rate of the culture using respirometry methods, and (iv) protein expression by conducting SDS PAGE analysis.

### 3.5.1 pH

pH measurements were taken *in situ* using a hand-held Metrohm 704 pH meter and probe. The analytical error was calculated to be 0.71 %.

University of Cape Town

### 3.5.2 REDOX POTENTIAL

Redox potential measurements were taken *in situ* using a hand-held Metrohm 704 pH meter equipped with a combined Pt|Ag/AgCl electrode redox probe. The redox electrodes were tested weekly by measuring a Crison standard redox solution of 468 mV (25°C). The analytical error was calculated to be 0.09 %.

### 3.5.3 CELL CONCENTRATION IN TERMS OF CELL NUMBER

Cell concentration was determined by either direct microscopic counting using a Thoma counting chamber with well dimensions of 0.02 mm in depth and a 1/400 $mm^2$ area and phase contrast optics at a magnification of 1000 x or by using a CellFacts particle analyzer (Microbial Systems, U.K.). Direct microscope counting has been successfully employed by several researchers (Konishi *et al.*, 1995; Nemati and Harrison, 2000; Lamaignére, 2002; Sissing, 2002). However, Konishi *et al.* (1995) reported that the inherent error of this method could be as high as 11 %. Although the inherent error of direct cell counting is high, the reproducibility of the method was found to be acceptable. Only the planktonic cell concentration was measured. The free cell count was postulated to be representative of the total cell count in the reactor based on the bioleaching studies by Nemati and Harrison (2000), Nemati *et al.* (2000) and Sissing (2002). Sissing (2002) completed adsorption studies on the partitioning of *Sulfolobus* cells between the pyrite mineral phase and the liquid phase in a pyrite bioleaching system. These experiments were conducted to confirm the applicability of the proposed method of biomass determination i.e. microscopic counting of planktonic cells. The results of these studies showed that the *Sulfolobus* cells remained predominantly in the liquid phase, thus confirming the applicability of free cell counting as a method for biomass determination in the bioleach slurry reactor.

The CellFacts particle size analyser system (Cellfacts I, Cellfacts Instruments Limited) can be used for the detection of planktonic cells and the generation of a cell size distribution curve. The system is based on the Coulter principle, employing electrical sensing flow impedance to enumerate and size particles by volume displacement. Integration of the area under the peak of cell number as a function of cell size yields a cell concentration. Error is minimised by dynamic procedures for self-check, calibration and a wash routine to eliminate cross contamination between samples. Several researchers have successfully utilised flow cytometry methods including the CellFacts system to enumerate and size micro-organisms (Kubek and Shuler, 1978; Illing, 1996; Lu Chau *et al.*, 2001; Schwarzentruber, 2002).

University of Cape Town

### 3.5.3.1 Direct microscopic counting method

A 1 ml aliquot of sample was allowed to settle for 30 min in a 2 ml Eppendorf microfuge tube to remove residual precipitate particles. For direct counting, the top 0.5 ml of the settled sample was removed and mixed thoroughly. A 40 µl aliquot of the settled sample was diluted as required. A 10 µl aliquot was ejected into the well of the counting chamber under a coverslip. Direct counts were made at a 1000 x magnification using phase contrast microscopy. The concentration of micro-organisms (cells $ml^{-1}$) in the sample was calculated using the following equation:

$$C_N = \frac{c * \left(\frac{N_T}{N_L}\right)}{D * A} * \frac{1}{d_r} * 10^3 \qquad \text{...Eqn. 3.1}$$

where: $C_N$ = cell concentration (cells $ml^{-1}$)

$c$ = number of cells counted in the large squares

$N_T$ = total number of large squares = 16

$N_L$ = number of large squares where cell were counted

$D$ = depth of the chamber (0.02 mm)

$A$ = total area of the chamber (1 $mm^2$)

$d_r$ = dilution ratio

The analytical error was calculated to be 6.33 %.

### 3.5.3.2 Cell counting based on the Coulter technique

To determine cell concentration using the CellFacts analyser, a 100 µl sample was removed from the upper region of the 1 ml sample using the CellFacts sample wand and diluted 100 fold with the electrolyte solution (Cell lyte, Microbial systems, U.K.). In order to confirm the absence of cell debris, precipitate and fine quartzite and chalcopyrite particulates the sample was viewed under 1000 x magnification using phase contrast microscopy before CellFacts analysis. All samples analysed were free of particulates and only cells remained in solution. The CellFacts was set to perform two dilutions per sample. The cell diameter limits were set between 0 and 2 µm and 0 and 5 µm where applicable. The analytical error of this method was calculated to be 1.32 %.

University of Cape Town

### 3.5.4 FERROUS IRON ANALYSIS

Ferrous iron analyses were carried out using a standard potassium dichromate titration (Vogel, 1989). This procedure has been used by several investigators in the field of bioleaching for ferrous iron determinations (Bailey and Hansford, 1993; Nemati and Harrison, 2000; Third *et al.*, 2000; Sissing, 2002).

#### 3.5.4.1 Procedure

The bulk 20 ml suspension sample was mixed thoroughly. A 2 ml suspension sample devoid of mineral or inert solid particulates and containing iron precipitates was removed for ferrous iron determinations. Acid digestion of the precipitate in the suspension samples was necessary in order to solubilise any ferrous iron present in the precipitate. A 2 ml aliquot of concentrated hydrochloric acid was added to each sample prior to heating at 100°C until complete dissolution of the precipitate was attained. Three drops of a barium diphenylamine sulphonate indicator (Appendix A.3.2) were then added to the samples which were titrated against 0.0149 M potassium dichromate (Appendix A.3.1). The redox reaction is based on the oxidation of the ferrous ion to ferric ion (Eqn. 3.2). The endpoint of the reaction is characterised by a purple colour mediated by the indicator.

$$6\,Fe^{2+} + Cr_2O_7^{2-} + 14\,H^+ \rightarrow 2\,Cr^{3+} + 6\,Fe^{3+} + 7\,H_2O \qquad \ldots\text{Eqn. 3.2}$$

The moles of potassium dichromate added in the titre required to convert all ferrous iron is proportional to the number of moles of ferrous iron in the sample. The concentration of ferrous iron in solution was determined using Eqn. 3.3.

$$C_1 = \frac{C_2 * V_2 * M * N_{Fe}}{V_{sol}} \qquad \ldots\text{Eqn 3.3}$$

where: $C_1$ = concentration of $Fe^{2+}$ (g $l^{-1}$)
$C_2$ = concentration of $K_2Cr_2O_7$ (g $l^{-1}$)
$V_2$ = titre volume (l)
$V_{sol}$ = sample volume (l)
M = molar mass of iron (g $mol^{-1}$)
$N_{Fe}$ = number of moles of iron (mol)

The analytical error was calculated to be 1.37 %.

University of Cape Town

### 3.5.5 COPPER AND TOTAL IRON ANALYSIS

Atomic absorption spectroscopy (AAS) was used to determine copper and total iron concentrations in solution. A Varian Spectra AA-200 Atomic absorption spectrophotometer, incorporating Spectra AA 100/200 version 1.1 software, was utilised. The analytical error was calculated to be 2.86 and 0.62 % for iron and copper respectively.

#### 3.5.5.1 Procedure

A 2 ml aliquot devoid of mineral and inert quartzite solids was removed from the bulk 20 ml suspension sample (Section 3.4.2). The sample was acidified with 2 ml of concentrated hydrochloric acid, heated at 100°C to just below boiling point and diluted to the required concentration range. Standards were prepared by diluting 1000 mg $l^{-1}$ acidified copper and iron standard solutions (Merck) to 500, 250, and 50 mg $l^{-1}$ for copper and 250, 100 and 10 mg $l^{-1}$ for iron. Examples of iron and copper standard curves are given in Appendix A.4. The detection limit of the analysis was 0.03 and 0.06 mg $l^{-1}$ for copper and iron respectively. The concentration of iron and copper in all suspension samples was above the detection limit of the AAS. The operational parameters were as follows:

| | |
|---|---|
| Slit width | = 0.2 nm; |
| Flame | = air/acetylene; |
| Lamp current | = 4 mA; |
| Wavelength | = 217.9 nm. |

### 3.5.6 PROTEIN ANALYSIS

Protein profiles of the cells were obtained by extracting total intracellular protein from samples taken at mid-growth phase and separating the proteins on sodium dodecyl sulphate polyacrylamide gels (SDS PAGE). The concentration of protein in the bulk solution was determined using the Bradford assay (Appendix A.2).

#### 3.5.6.1 SDS PAGE

Protein separation by SDS-PAGE is commonly used to determine the relative abundance of proteins in a sample, their approximate molecular weights, and in what fractions or under what conditions they are found. Sodium dodecyl sulphate (SDS) denatures proteins enhancing the separation process by ensuring reproducibility of the technique. SDS is an anionic detergent, its molecules having a net negative charge. It binds to most soluble protein molecules in aqueous solutions over a wide pH

University of Cape Town

range. The negative charge destroys most of the complex (secondary and tertiary) structure of proteins, and is strongly attracted toward an anode (positively-charged electrode) in an electric field. The samples treated with SDS are run on a vertical gel bed composed of a porous acrylamide gel. The relative amount of acrylamide in the gel determines the rate at which protein molecules move through the matrix. Larger proteins migrate more slowly than smaller proteins. Because the charge-to-mass ratio is similar among SDS-denatured polypeptides, the final separation of proteins is dependent on the differences in molecular weight of polypeptides. In a gel of uniform density the relative migration distance of a protein ($R_f$) is negatively proportional to the log of its molecular weight. If proteins of known molecular weight are run simultaneously with the unknowns, the relationship between $R_f$ and molecular weight can be plotted, and the molecular weights of unknown proteins determined.

*3.5.6.1.1 Procedure*

One 100 ml sample was removed from each reactor during mid growth phase and centrifuged at 500 g in a Hettich Universal centrifuge for 6 min to remove mineral concentrate and ferric precipitate. The supernatant was decanted into a beaker and 12 x 1.5 ml samples were transferred to Eppendorf tubes and centrifuged for 3 mines in a Heraeus Biofuge centrifuge at 16 000 g. The supernatant was discarded and the pellets combined in 1 ml saline solution (pH 1.6). The sample was then centrifuged for 3 min at 16 000 g. The supernatant containing soluble metals was discarded. Although the initial centrifugation step was included to remove precipitates from the sample, some precipitate particles were found associated with the washed pellet. The washed pellet consisted of two layers. Microbial cells have a lower density than the precipitate particles and thus comprised the top layer. The top layer was used for protein extractions. The pellet was resuspended in 200 µl of Tris-HCl pH 8 (Appendix A.1.1.11). A 200 µl aliquot of 2 x SDS sample buffer (Appendix A.1.1.6) was added to the sample and incubated at 60°C for 20 min. The protein markers (Appendix A.1.1.12) were prepared by removing 10 µl of marker protein solution from the vial and adding equal volumes of 2 x SDS sample buffer. After heat treatment, the samples were centrifuged for 3 min at 16 000 g. The supernatant was decanted into a clean Eppendorf tube.

A 100 µl aliquot of samples and standards was loaded into each well. The gel was run at 15 mA for 18h (overnight) and then removed and stained for 2 h on a gel shaker with Coomassie blue stain (Appendix A.1.1.8). After 2 h, the gel was destained by removing the stain solution and adding destain I (Appendix A.1.1.9) for 1 h. This process was repeated with destain 1 for 30 min and then

University of Cape Town

with destain 2 (Appendix A.1.1.10) until the background of the gel was totally destained. The gel was then stored in an airtight container in 5 % acetic acid.

#### 3.5.6.2 Bulk solution protein measurements

A bulk sample of 300 ml was removed from each reactor and was centrifuged at 500 g for 6 min to remove all precipitates. After centrifugation, the sample was concentrated through a polyethersulfone Pellicon Biomax 5 membrane filter (Millipore) retaining molecules larger than 5 kDa. The samples were circulated through the filter until only 2.5 ml remained (80-fold concentration). Soluble protein was measured using the Bradford assay (Appendix A.2). The analytical error of the Bradford assay was calculated to be 8.9 %.

### 3.5.7 ANALYSIS OF CELL MORPHOLOGY

Cell morphology was determined using phase contrast microscopy, particle size analysis and scanning electron microscopy (SEM).

#### 3.5.7.1 Phase contrast microscopy

Changes in cell size, shape and density were determined with phase contrast microscopy. This method has been utilised successfully by Illing (1996) and Nemati and Harrison (2000). Samples were prepared as described in Section 3.5.3.1. Micrographs were taken using an Olympus BX40 microscope equipped with a ColorView Soft Imaging System camera which was controlled using analySIS 5 Image Processing software.

#### 3.5.7.2 Particle size analysis

Quantitative analysis of cell size was performed by using data generated by the CellFacts particle analyser. The sampling procedure was the same as discussed in Section 3.5.3.2. The change in cell size was determined by fitting a Weibull 4 parameter peak curve (Section 5.1.3) to the size distribution curves generated by the CellFacts analyser. Three of the 4 parameters, $X_0$, $a$ and $b$, describing the curve were utilised. Parameter $X_0$ represented the mode of the peak. Using these mode data, the change in cell size was determined as a function of time and intensity of hydrodynamic stress.

University of Cape Town

### 3.5.7.3 SEM

Scanning electron microscopy was used as a tool to magnify and enable a 3-dimensional observation of the archaeal cells which approached the detection limit of light microscopy at 1000 x magnification. A 20 ml sample was removed from the experimental reactor and centrifuged in a Hettich Universal centrifuge at 500 g for 4 min to remove particluates. The supernatant was carefully removed. A 1 ml sample was centrifuged in a Heraeus Biofuge at 13 000 g for 3 min. The resultant pellet was washed with saline solution of pH 1.6. The pellet was re-suspended in 3 % gluteraldehyde in 0.1 M sodium cacodylate buffer (pH 7.4) and then filtered through a 1 cm, Nucleopore (Millipore) filter with a pore size of 0.22 μm. The sample was kept in contact with the glutaraldehyde solution for 30 min and then washed three times with 0.1 M sodium cacodylate buffer. A 30 % solution of ethanol in water was then passed through the filter. The filter was left for 15 min in contact with the ethanol solution. This procedure was repeated for 50, 70, 90 and 100 % ethanol. The 100 % ethanol step was repeated three times. The filter was taken through a critical point drying (CPD) process. Samples were subsequently coated with a gold/palladium plasma and viewed using a JEOL JSM-840 scanning electron microscope. On average a 5 kV beam and a working distance of 13 cm were utilised.

Initially, residual precipitate embedded the cells and obscured the view of the cells on SEM analysis. Subsequent samples were centrifuged at 500 g for 6 min and washed three times with saline solution to separate the cells from the fine precipitate prior to sample preparation for SEM. The disadvantage of increasing the centrifugation time and increasing the number wash steps is that a higher percentage of cells were lost compared with the previous centrifugation and wash regime.

University of Cape Town

## 3.5.8 CULTURE VIABILITY USING DUAL FLUORESCENCE STAINING

Dual fluorochrome staining is often used to determine the viability of micro-organisms (Beck and Huber, 1997). The stains differentiate between viable and non-viable cells based on the ability of one of the dyes to penetrate permeabilised cell membranes. In the current study, membrane integrity was determined using a dual fluorescence staining method. SYTO 13 green (Molecular Probes) which has a green fluorescence emission at 520 nm and propidium iodide (Molecular Probes) which has a red fluorescence emission at 610 nm were the fluorochromes of choice. Dual staining using propidium iodide and SYTO dyes is commonly used to distinguish between dead and live bacterial cells such as *Staphyloccous aureus*, *Pseudomonas fluorescens* and *Escherichia coli* (Comas and Vives-Rego, 1998; Gunasekera *et al.*, 2003). Propidium iodide can only penetrate cells with damaged membranes. SYTO 13 green can permeate through most cell membranes. The dye is non fluorescent until it

binds to nucleic acids. When combined with propidium iodide, simultaneous staining of live- and dead-cell populations is possible. In membrane compromised and dead cells, the SYTO 13 green is replaced by the red fluorescent dye, resulting in yellow-, orange- or red-fluorescence depending on the extent to which the membrane is compromised.

To date the methodology reported with these fluorochromes has been developed to function optimally at neutral pHs. The pH of the suspending medium utilised in this study was approximately pH 1.6. This presented a particular problem since increasing the pH caused the archaeal cells to rupture. A range of pHs (pH 1 to pH 6) were tested to determine at which pH optimal staining without cell lysis could be attained, resulting in selection of pH 2. The relative concentrations of the fluorochromes and staining times required for optimal dual staining without severe background effects were provided by Norris (2001).

#### 3.5.8.1 Sample preparation and viewing

A 5 ml sample was removed from the reactor using a syringe. The sample was settled for 30 min before centrifuging at 500 g for 6 min to remove precipitates. The supernatant was centrifuged at 16 000 g for 5 min to separate the cells from the suspending medium. The cells were resuspended in 0.85 ml Norris medium adjusted to pH 2.0. A 5 µl aliquot of SYTO 13 green (5 mM) and a 10 µl aliquot of propidium iodide (1 mg $ml^{-1}$) were added to the sample and allowed to stain for 5 min. The sample was viewed using a Nikon Eclipse E600 microscope fitted with a B-2A (EX 450-490, DM 505, BA 520) filter set. Images were captured using a Nikon DXM1200F digital CCD camera.

### 3.5.9 OXYGEN UTILISATION RATE (OUR) MEASUREMENTS

Respirometry methods provide a well recognised approach to assess the microbial activity of micro-organisms (Illing, 1996; Basson *et al.*, 1997; Sampson and Blake, 1999; Harahuc *et al.*, 2000). This technique can also be applied to autotrophic organisms present in bioleaching systems. The processes of carbon dioxide catabolism and energy generation via the oxidation of ferrous and sulphide ions result in the consumption of oxygen. Thus, by measuring the oxygen utilisation rate, the activity of the micro-organisms can be elucidated. OUR measurements were taken using a Micro Oxymax V6.03 Respirometer. The Micro Oxymax is an indirect "closed circuit" respirometer, designed to detect extremely low levels of oxygen consumption. In a closed circuit system, the air in the headspace above the sample is circulated through the sensors, measured and then returned back to the headspace. The operation of the instrument is based on the principle that the consumption or production of a gas may be calculated by multiplying the change in the gas concentration on two

University of Cape Town

consecutive readings by the volume of the gas. The rate of gas consumption or production may be obtained by dividing the result by the time interval between the readings according to Eqn. 3.4.

$$r_{O_2} = \frac{([O_2]_1 - [O_2]_2) * V}{t_2 - t_1} \qquad \text{...Eqn. 3.4}$$

where: $r_{O_2}$ = OUR (µl min$^{-1}$)
$V$ = volume of gas (l)
$[O_2]_1$ = oxygen concentration at time $t_1$ (µl l$^{-1}$)
$[O_2]_2$ = oxygen concentration at time $t_2$ (µl l$^{-1}$)
$t_2$ = time 2 (min)
$t_1$ = time 1 (min)

### 3.5.9.1 Procedure

A 5 ml sample was removed from each reactor at intermittent intervals during growth, stationary and death phases of the culture during the experimental runs and allowed to settle for 2 min. The sample was added to a 100 ml Schott bottle (sample chamber) containing 20 ml of Norris medium at pH 1.6 equilibrated to 68°C and 3 % w/v chalcopyrite concentrate (size fraction < 22 µm). The bottles were connected with tubing to the respirometer channels using modified lids that provided a tight seal. The bottles were placed in an incubator set to 68°C (Figure 3.5). The gas blends used for the respirometer calibration are given in Appendix A.5. The OUR was measured at specified time intervals over a 5h period. The analytical error was calculated to be 2.89 %.

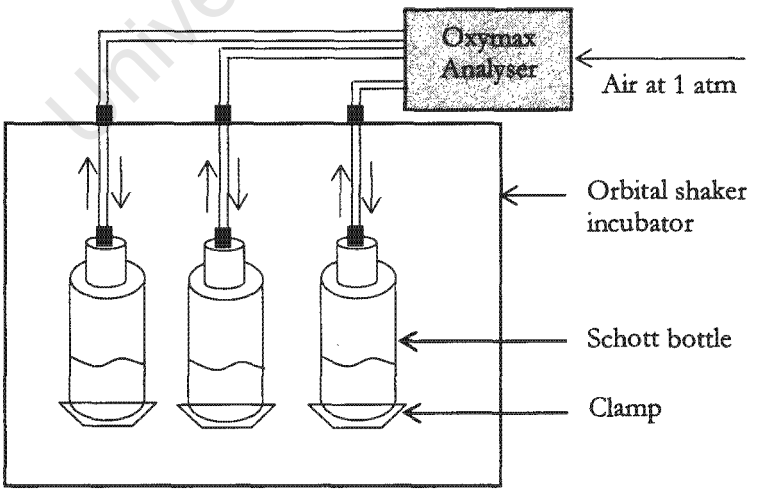


**Figure 3.5:** Schematic representation of the setup used for OUR determinations.

University of Cape Town

### 3.5.10 POWER MEASUREMENTS

Power measurements were made by fixing a one litre glass reactor to a frictionless torque table, which was fitted with a torque arm. Rotation of the impeller in the vessel resulted in the torque arm exerting a force on a load cell. Various solids loadings and impeller speeds were tested. The load cell reading was converted to a global power input using the following equation:

$$P = \frac{mgLN2\pi}{60} \qquad \ldots \text{Eqn 3.5}$$

where: m = the mass reading on the load cell (kg)

g = gravitational acceleration (9.81 m $s^{-2}$)

L = distance from the tip of the torque arm to the centre of the torque table (0.1 m)

N = impeller speed (rpm)

## 3.6 EXPERIMENTAL APPROACH

The one litre STR set up described in Section 3.1 was used to conduct all solids loading and impeller speed experiments (Table 3.3). For all experiments each reactor contained 3 % chalcopyrite as the source of nutrients. The solids loading experiments were conducted in two sets. The first experimental set consisted of 4 reactors with a chalcopyrite loading of 3 % by mass and quartzite loadings of 0, 6, 9 and 12 % w/v operated at 1.97 m $s^{-1}$ while the second experimental set consisted of 3 reactors with quartzite loadings of 0, 15 and 18 % operated at 1.97 m $s^{-1}$. The impeller tip speed experiment was conducted in one experimental set comprising 4 reactors. Two reactors were operated at 1.67 m $s^{-1}$ (0 and 9 % quartzite) while the remaining two reactors were operated at 1.97 m $s^{-1}$ (9 % quartzite) and 2.13 m $s^{-1}$ (9 % quartzite). While the experimental sets described in Table 3.3 formed the central focus of the study, repeat experiments (not shown) were performed which provided confirmation of results reported. A sample of these data is presented in Section 4.3 to illustrate the reproducibility of the experiments.

University of Cape Town

**Table 3.3**: Quartzite loadings and impeller tip speeds employed for each experimental set. 3 % (w/v) chalcopyrite was present in all reactors.

| Experiment | Quartzite solids loading (%; w/v) | Impeller tip speed ($m\ s^{-1}$) |
|---|---|---|
| Solids loading experiment 1 | 0, 6, 9, 12 | 1.97 (650 rpm) |
| Solids loading experiment 2 | 0, 15, 18 | 1.97 |
| Impeller speed experiment | 0 | 1.67 (550 rpm) |
| | 9 | 1.67, 1.97, 2.13 (700 rpm) |

The reactors in each experimental set were run simultaneously to prevent variation in process conditions. All sampling and analyses for each reactor were conducted in an identical manner to minimise experimental and analytical error. The range of impeller tip speeds utilised were chosen based on those used in previous studies conducted by Nemati and Harrison (2000) and Sissing (2002). The authors used impeller tip speeds straddling those utilised by BHP Billtion in the stirred tank reactors operated at the laboratories in Johannesburg (South Africa). The three impeller speeds chosen are above the critical impeller speed required for suspension of up to 27 % (w/v) solids. The solids loading and impeller speed experiments were conducted 24 months apart in different laboratories and using differing analytical approaches, hence direct comparison across these experimental sets is not made. For the impeller speed experiments, a 48 h inoculum build-up phase was required because the cell concentration did not increase appreciably between 0 and 24 h.

It is recognised in the setup of an experimental study that extrapolation from a one litre reactor for scale-up is inappropriate and specific scale-up studies would be required. Scale-up was not considered the focus of this study; hence experiments were not expanded to include it.

The initial redox potential in the reactors was high (500-550 mV). This high redox potential resulted because a sufficiently high cell concentration was required to resist the effects of hydrodynamic stress induced at 24 h. Due to the high initial redox potential, passivation of the chalcopyrite mineral occurred, resulting in nutrient limitation and experiments being complete in 10 days.

In the following two chapters the results of the solids loading, impeller tip speed and combined experiments are presented and discussed. An analysis of the change in process performance and the bioresponse as a function of increasing hydrodynamic stress is reported.

University of Cape Town

# Chapter 4: Results and Discussion I

# The effect of solids loading and impeller tip speed on the bioleaching of chalcopyrite by a *Sulfolobus* sp.

## 4.1 INTRODUCTION

In the present study several process parameters were investigated in order to assess the effect of increased hydrodynamic stress on the bioleaching of chalcopyrite by a *Sulfolobus* sp.. Solution pH, redox potential, the rate and extent of growth, and iron and copper solubilisation were the performance criteria utilised. The effect of hydrodynamic stress was determined by (i) varying quartzite loading at a constant impeller tip speed and (ii) varying impeller tip speed at two solids loadings. In addition to these experiments, repeat experiments (selected randomly) were also conducted for each experimental set. In this way the reproducibly of the results was ensured. Chalcopyrite and quartzite particles in the size range 38 to 75 μm comprised the solids fraction. The temperature was maintained at 68°C and the pH at the start of each run was approximately 1.6 pH units.

University of Cape Town

To study the effect of solids loading, a constant chalcopyrite loading of 3 % was used in all reactors and the solids concentration was varied by the addition of quartzite in increasing quantities of 3 % by mass. Quartzite loadings of 6, 9, 12, 15 and 18 % were used and reactors were operated at a constant impeller tip speed of 1.97 m $s^{-1}$.

To study the effect of impeller tip speed, reactors were run at tip speeds of 1.67, 1.97, and 2.13 m $s^{-1}$, corresponding to averaged liquid shear rates of 91.7, 108 and 117 $s^{-1}$ respectively. Liquid shear rates were calculated using the following equation:

$$\gamma = 10 \times N \qquad \text{...Eqn 4.1}$$

where: $\gamma$ = liquid shear rate ($s^{-1}$)

$N$ = rotational speed of the impeller (rpm)

The solids loadings utilised were 0 and 9 % w/v quartzite in the presence of 3 % chalcopyrite.

For each sub-set of experiments (2 for solids loading, 2 for impeller speed and 3 for the combined study), a reactor containing no quartzite and 3 % chalcopyrite was run concurrently. The impeller

tip speed in the reactor was 1.97 m $s^{-1}$ for the solids loading experiments and 1.67 m $s^{-1}$ for the impeller speed and combined experiments. This reactor was designated as the baseline control reactor operated under conditions of negligible hydrodynamic stress.

## 4.2 CULTURE VARIABILITY

Microbial cultures maintained over long periods are known to show changes in activity. A 3 % chalcopyrite run was repeated after a two-month period in order to determine if the activity of the culture was variable. The results from a set of repeat runs are presented in Figure 4.1. Both redox potential and copper solubilisation data showed good reproducibility. The highest standard deviation for redox potential was determined to be 6.36 mV and variation in the percentage copper solubilised was 2.14 %. These results indicate that there was limited variability in the culture after a two month period.

University of Cape Town

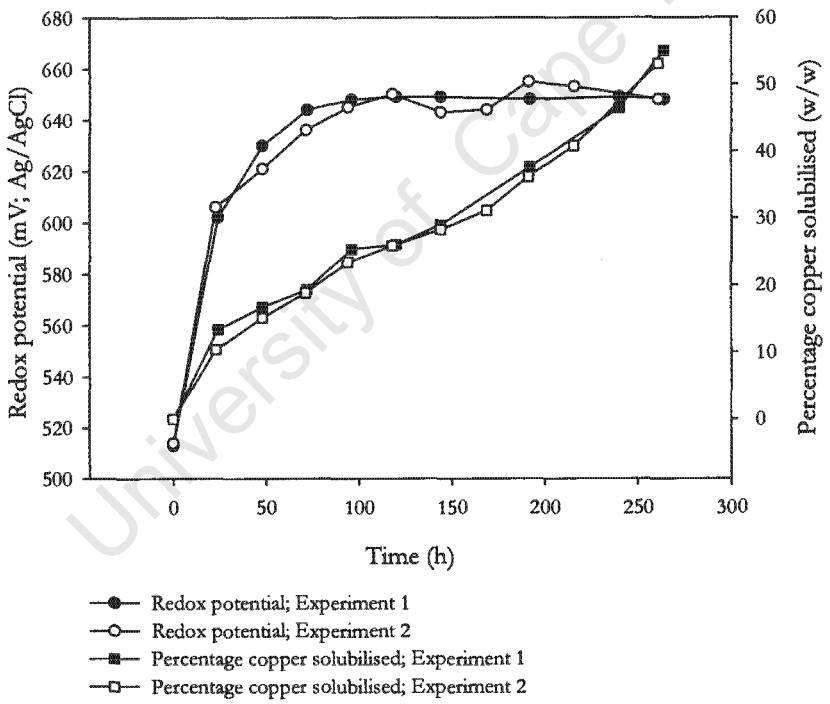


**Figure 4.1:** Chalcopyrite bioleaching at a 3 % w/v chalcopyrite (38-75 µm) loading and an impeller tip speed of 1.67 m $s^{-1}$. Experiments 1 and 2 were conducted two months apart.

## 4.3 REPRODUCIBILITY OF EXPERIMENTS

In an effort to determine whether the experimental data was reproducible within sets of experiments, tests were duplicated for selected experiments. The results of one such repeat experiment for a 6 % quartzite run are presented in Figure 4.2. The highest standard deviations for redox potential and percentage copper solubilised were 3.54 mV and 1.08 % yielding a coefficient of variance of 0.56 and 4.58 % respectively. These results show that the data were reproducible within experimental sets.

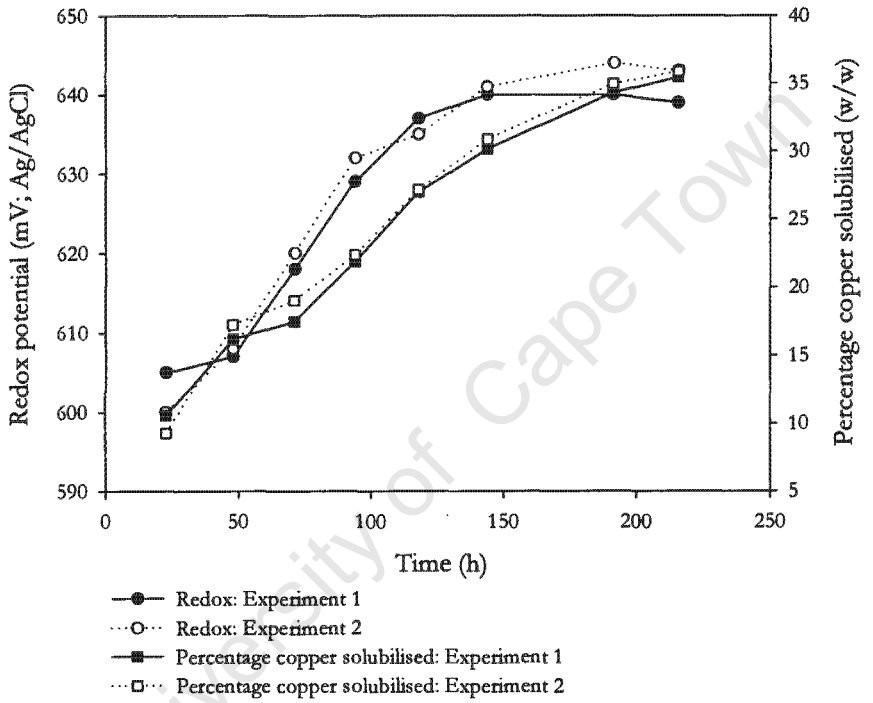


University of Cape Town

**Figure 4.2:** Reproducibility data for chalcopyrite bioleaching at a solids loading of 6 % w/v quartzite (38-75 μm) and 3 % w/v chalcopyrite (38-75 μm) and an impeller tip speed of 1.67 m $s^{-1}$.

## 4.4 ABIOTIC CONTROL

In order to ensure that the leaching of chalcopyrite was primarily as a result of biological activity, control leaching experiments were conducted in the absence of micro-organisms. The experiments were carried out in a similar manner to the bioleaching experiments except that micro-organisms were excluded. The mineral samples were irradiated to ensure no contamination of the solution with micro-organisms from the mineral. The mineral sample, 550 ml Norris 0K medium (pH 1.6) and 150 ml of a one day old 'inoculum', from which the micro-organisms had been removed by centrifugation at 16 000 g for 20 min, were added to the one litre STR. The 150 ml aqueous solution excluding micro-organisms served as the ferric iron oxidant. Compressed air supplemented with 1 % carbon dioxide was supplied at 2 vvm through an L-shaped sparger. The experiments were conducted at 68°C over a 74 h period. The pH, redox potential, cell concentration and ferric and ferrous iron concentrations were monitored.

The data obtained for duplicate chemical leach experiments were averaged and are presented in Figures 4.3 and 4.4. The solution pH increased from pH 1.57 to 1.68 from 0 to 6 h concomitantly with the initial ferric iron leaching. Thereafter it increased gradually to pH 1.82. Stott *et al.* (2000) found a similar result for the abiotic control reactor where the iron concentration did not increase above 0.18 g $l^{-1}$ and the pH increased from pH 2 to 2.4. In the present study, no cells were observed during the course of the experiment (74 h) in the three replicates per sample viewed using phase contrast microscopy. The detection limit for the microscope counting method is approximately 7.8 x $10^4$ cells $ml^{-1}$. The ferrous and ferric iron concentrations in solution increased to 0.43 and 0.24 g $l^{-1}$ respectively. There was an initial sharp decrease in redox potential from 500 to 390 mV due to ferrous iron leaching from the mineral by the ferric iron introduced with the sterile 'inoculum'.

The biological oxidation of chalcopyrite under identical conditions of temperature, aeration and solids loading used in the chemical leach experiments yielded 2.91 g Fe $l^{-1}$ in solution while chemical leaching yielded 0.67 g Fe $l^{-1}$. Chemical leaching of the chalcopyrite, via oxidation of the mineral by ferric iron introduced into the reactor, liberated ferrous iron. The ferric iron concentration in solution decreased while the ferrous iron concentration increased. In order for chemical leaching to be sustainable, regeneration of the leaching agent (ferric iron) is required. In chemical leaching, regeneration of the ferric iron occurs via the oxidation of ferrous iron by oxygen introduced into the system through sparging. This oxidation rate is slower than the biological oxidation of the ferrous iron and thus ferric iron regeneration in the chemical system was slower than in the biological system, leading to reduced mineral solubilisation. The extent of leaching after approximately 74 h was determined to be 25.8 and 7.9 % w/w for the biotic and

University of Cape Town

abiotic systems respectively. However, in the chemical oxidation experiment, the redox potential in solution remained below 400 mV from 4 h to 74 h which is not representative of the bioleaching system where the redox potential remained above 550 mV throughout the course of the experiment. An investigation of chemical oxidation of ferrous iron at high redox potentials and temperature was thus sought. Searby (2005) studied the chemical and biological oxidation of ferrous iron in an STR at 70°C and aeration rate of 400 ml $min^{-1}$ at controlled redox potentials. The rate of chemical oxidation of ferrous iron at 70°C and a redox potential of 606 mV was found to be 1200 fold lower than the biological oxidation rate at the same temperature and redox potential. These data confirm that the contribution of chemical oxidation to the overall oxidation of ferrous iron to ferric iron, for the process conditions utilised in the present study, is negligible compared to the biological oxidation rate.

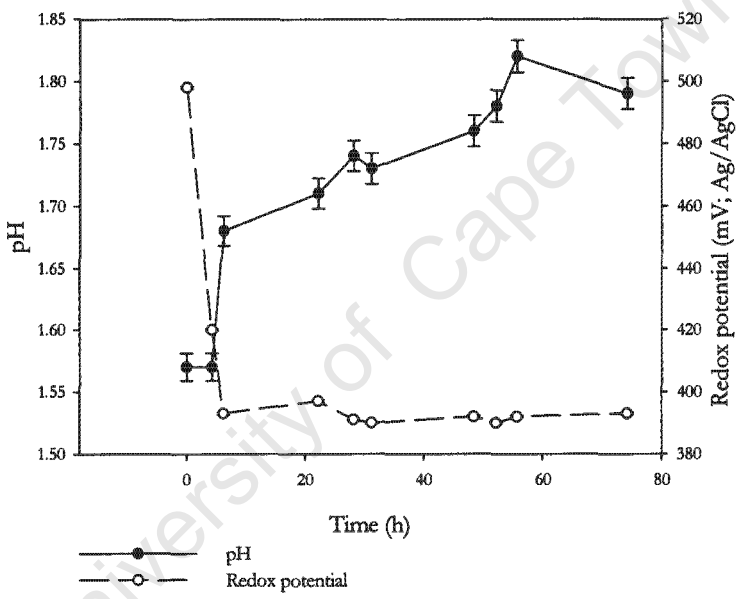


University of Cape Town

**Figure 4.3:** Time profiles of pH and redox potential for a 3 % w/v chalcopyrite solids loading in the absence of micro-organisms. Experiments were run at a pH of 1.6, temperature of 68°C, aeration rate of 2 vvm and an impeller tip speed of 1.97 m $s^{-1}$.

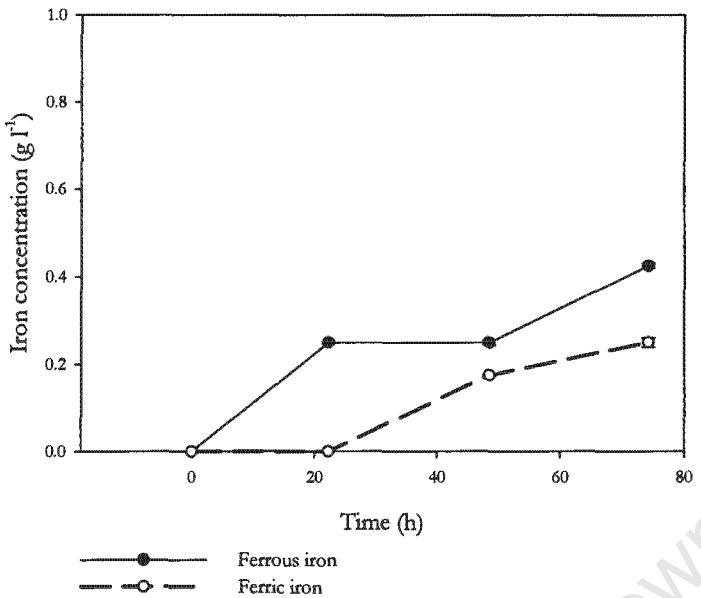


**Figure 4.4:** Time profiles of ferric and ferrous iron concentrations for a 3 % w/v chalcopyrite solids loading in the absence of micro-organisms. Experiments were run at a pH of 1.6, temperature of 68°C, aeration rate of 2 vvm and an impeller tip speed of 1.97 m $s^{-1}$.

University of Cape Town

## 4.5 THE BASELINE EXPERIMENT

The baseline reactor, operating under conditions of negligible hydrodynamic stress, provided a data set to which results from each experimental reactor could be compared. For each set of solids loading, impeller tip speed and combined experiments, a baseline was attained using a reactor in which the solids fraction consisted of 3 % chalcopyrite concentrate and no quartzite. The impeller tip speed was maintained at either 1.67 m $s^{-1}$ or 1.97 m $s^{-1}$. Figure 4.5 illustrates a set of results obtained during one such baseline experiment. Variations in the pH, redox potential, cell concentration and iron and copper concentrations in the system under optimal conditions are shown as a function of time and discussed in Sections 4.5.1 to 4.5.5.

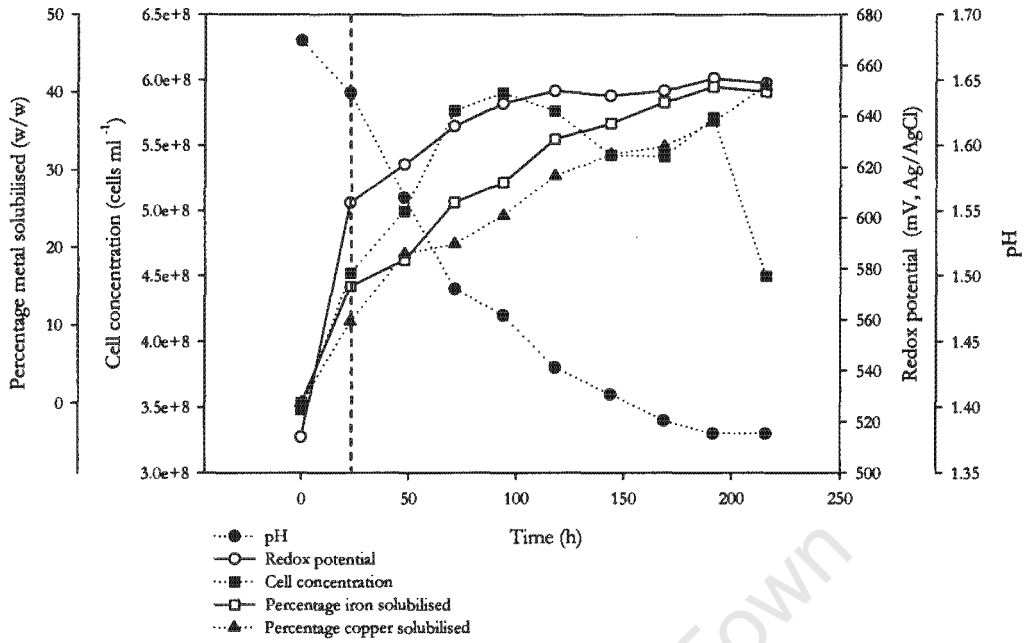


**Figure 4.5:** Chalcopyrite leaching in the baseline reactor characterised by a solids loading of 3 % chalcopyrite and an impeller tip speed of 1.97 m $s^{-1}$. Changes in pH, redox potential, cell concentration and iron and copper solubilisation are shown. Dashed line indicates the time at which the impeller tip speed was increased from 0.76 to 1.67 m $s^{-1}$.

University of Cape Town

### 4.5.1 REDOX POTENTIAL

In sulphide mineral leaching systems, the primary redox couple is the $Fe^{3+}/Fe^{2+}$ couple. Changes in this ratio have a significant influence on the solution redox potential. Therefore the solution potential can be monitored to indicate the relative rates of the various chemical reactions in the bioleaching mechanism. The change in redox potential with time in Figure 4.5 comprised three phases: (i) a sharp increase in redox potential from 520 to 610 mV over the first 24 h, (ii) a slower increase to 650 mV at 120h, and (iii) stabilisation around 650 mV after 120 h.

In phase one, all available ferrous iron in solution, resulting from the initial 24 h acid pH stabilisation (Section 3.4.1) and from leaching of the mineral by the ferric iron introduced with the inoculum, was oxidised to ferric iron by the microbial population according to Eqn. 4.2 (Jordan *et al.*, 1993):

$$2\,FeSO_4 + 0.5\,O_2 + H_2SO_4 \rightarrow Fe_2(SO_4)_3 + H_2O \qquad \ldots \text{Eqn 4.2}$$

The rapid increase in the ferric ion concentration caused the redox potential to rise sharply. Accumulation of ferric ion occurred because the chemical leach step in the two stage leaching process was inhibited i.e. ferric ions were unable to leach the mineral and release additional

ferrous ions into solution while undergoing concomitant reduction to ferrous ion (Eqn 4.3) (Jordan *et al.*, 1993):

$$CuFeS_2 + 2\,Fe_2(SO_4)_3 \rightarrow CuSO_4 + 5\,FeSO_4 + 2\,S^0 \qquad \ldots \text{Eqn 4.3}$$

This inhibition, termed "passivation", has been observed by several researchers (Rivera-Santillán *et al.*, 1999; Gericke *et al*, 2001; Stott *et al.*, 2000) and is cited as the primary cause of the recalcitrance of chalcopyrite to chemical and biological leaching. Passivation of the chalcopyrite leach process is thought to be caused by the coating of the mineral with one or more leach reaction products. Investigators have speculated that the surface of the mineral could be coated with elemental sulphur, jarosite or a copper-rich polysulfide. It is likely that passivation is caused by the combined effects of these products. The presence of these inhibitory compounds creates a diffusional barrier on the surface of the mineral and as a consequence restricts the rate of ferric leaching with concomitant release of ferrous iron and elemental sulphur into solution. Where these rates are lower than the microbial oxidation rates of ferrous iron and elemental sulphur, their concentrations in solution decrease. In the present study, jarosite precipitation was visible in all reactors throughout the run but significant amounts appeared after approximately 30 h (Figure 4.6). These observations are similar to those of Stott *et al.* (2003) who found jarosite precipitation after approximately 50 h. In the present study the inoculum was settled for 30 min prior to inoculation in an effort to reduce the amount of jarosite added to the system. Even so, a significant amount of jarosite was introduced into the reactor and may have provided nucleation sites for further precipitation, speeding up the passivation process. This could explain why passivation occurred earlier in this study. In essence, the microbial cells were substrate- (ferrous iron) limited quite early in the experiment (approximately 48 h after the inoculum build-up phase). This limitation affected the growth rate of the cells and decreased the rate at which ferrous iron was oxidised to ferric iron. Eventually both electron donors (ferrous iron and sulphide) required for microbial growth were limiting.

**Figure 4.6:** Chalcopyrite bioleaching STR showing extensive jarosite present in the reactor after 30 h. STR operated at a 3 % mineral loading and an impeller tip speed of 1.97 m $s^{-1}$.



University of Cape Town

In phase two of the redox potential curve, the chemical leaching process at the mineral surface occurred at a lower rate due to mineral passivation. This led to a decline in the rate of ferric iron generation by the micro-organisms and thus the redox potential increased at a slower rate compared to phase one. In phase three the rate at which the ferric iron leached the mineral (Eqn. 4.3) was equal to the rate at which the micro-organisms regenerated the ferric iron (Eqn. 4.2), thus maintaining a constant redox potential. Stott *et al.* (2003) reported comparable data using *Sulfobacillus thermosulfidooxidans* where the ferrous iron concentration in solution remained low throughout the experiment and the redox potential increased from 435 mV (Ag/AgCl) to 570 mV (Ag/AgCl) in approximately 33 h. Thereafter, the redox potential increased gradually to approximately 600 mV (Ag/AgCl) and stabilised around this value for the remainder of the experiment.

Gericke *et al.* (2001) found that when leaching chalcopyrite with an extreme thermophile, the redox potential increased by 35 mV from 313 to 348 mV after 24 h and then remained at the same value for a further 24 h after which the potential increased at a slower rate to 450 mV after 7 days. During the 7 to 10 day period this rate increased again and finally stabilised to approximately 620 mV. At this time almost complete oxidation of the mineral was realised. The initial redox potential data of Gericke *et al.* (2001) follow a similar trend to the data presented in Figure 4.5, but the overall increase in redox potential was slower than observed in this study. There are two possible reasons for this observation. Firstly, in the present study, the initial redox potential of approximately 514 mV (Ag/AgCl) was high, i.e. the initial ferric ion concentration was high. Investigators have shown that high initial redox potentials (high ferric iron concentration) hamper chalcopyrite leaching possibly owing to passivation of the mineral (Howard and Crundwell, 1999). Third *et al.* (2000) found that even a redox potential of approximately 450 mV was too high to sustain a consistently high chalcopyrite leach rate. Reduced chalcopyrite leach rates at high redox potentials is explained more clearly by the profiles presented in Figure 4.7 which illustrate the ferric iron demand of chalcopyrite and pyrite as a function of the ferric to ferrous iron ratio and hence the redox potential. Region (a) outlines the redox potential window (approximately 450 to 560 mV) wherein the ferric iron demand of chalcopyrite is greatest. Much debate surrounds the exact location of region (a). The data presented in Figure 4.7 is that of Hiroyoshi *et al.* (2004). In the present study the redox potential from 48 h to the end of the experiment lay within the window outlined by region (b) where, at the increased redox potential the ferric iron demand of chalcopyrite was diminished and thus the rate of mineral dissolution was reduced.

University of Cape Town

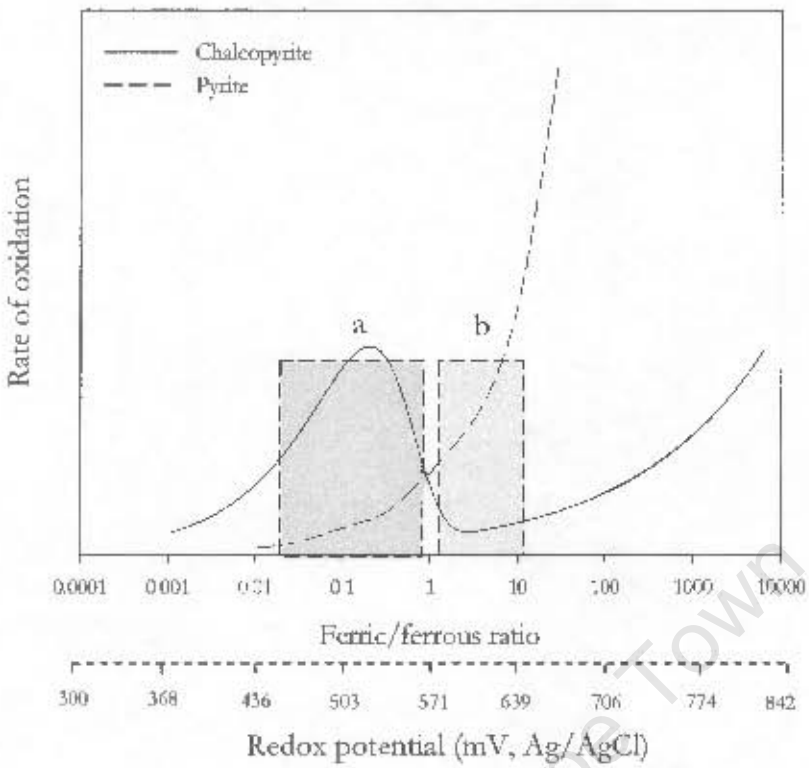


**Figure 4.7:** The rate of oxidation of chalcopyrite and pyrite at 70°C as a function of redox potential (Ag/AgCl) (adapted from Hiroyoshi *et al.*, 2004). Region (a) optimal redox potential window for chalcopyrite leaching, region (b) sub-optimal redox potential window for chalcopyrite leaching. Dashed secondary '*x* axis' shows the corresponding redox potential at each ferric/ferrous iron ratio presented in the primary *x* axis.

In non-recalcitrant bioleaching systems, such as the pyrite system studied by Sissing and Harrison (2003), no reports of mineral passivation have been published and complete dissolution of the concentrate occurs readily. In the study by Sissing and Harrison (2003), the redox potential decreased from 548 to 505 mV over the first 24 h due to the rapid rate of ferric leaching of the mineral exceeding the microbial ferrous oxidation rate and resulting in the accumulation of ferrous iron. Thereafter the redox potential increased gradually before stabilising around 630 mV after approximately 5 days (Figure 4.8). Although Sissing and Harrison (2003) worked in a very high redox potential regime, these redox potentials were ideal for pyrite oxidation as is illustrated in Figure 4.7 where the rate of pyrite oxidation increases exponentially at redox potentials above 500 mV. A second reason for the improved leaching observed by Gericke *et al.* (2001) is postulated to be the very fine size fraction of concentrate ($d_{80}$ 10 µm) used. Ultra-fine grinding has been shown to improve chalcopyrite bioleaching (Lawrence and Poulin, 1996 cited by Gericke *et al.*, 2001).

University of Cape Town

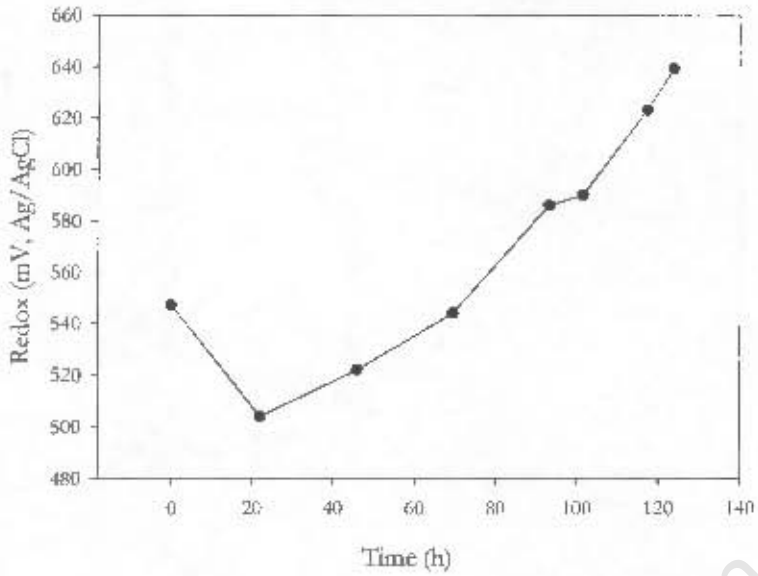


**Figure 4.8:** Redox potential as a function of time for the dissolution of pyrite by *Sulfolobus metallicus* (adapted from Sissing and Harrison, 2003).

University of Cape Town

### 4.5.2 pH

Several processes govern the variation in solution pH in the chalcopyrite bioleaching system. The reactions expected to occur in the thermophilic bioleaching of the Andina chalcopyrite concentrate, which contains a pyrite fraction, are summarised as Eqns. 4.4 to 4.8. These are either acid-consuming or acid-producing reactions and occur simultaneously, at varying rates depending on conditions prevailing in the reactor.

**Ferrous iron oxidation by micro-organisms**: Ferrous iron leached from the mineral during the chemical leach step was re-oxidised to ferric ion, regenerating the ferric leaching agent through an acid consuming reaction (Jordan *et al.*, 1993):

$$2\ FeSO_4 + 0.5\ O_2 + H_2SO_4 \rightarrow Fe_2(SO_4)_3 + H_2O \quad \textit{acid consuming} \qquad \ldots \text{Eqn.4.4}$$

**Precipitation of jarosite**: Significant jarosite precipitation commenced between 25 and 50 h into the leach process. In addition, precipitation increased with a rise in solution pH. Ferric ions precipitated with monovalent cations (especially $K^+$) present in solution, with the concomitant generation of acid as illustrated in Eqn. 4.5 (Gomez *et al.*, 1996):

$$3\ Fe^{3+} + X^+ + 2\ H_2SO_4 + 6\ H_2O \leftrightarrow XFe_3(SO_4)_2(OH)_6 + 10\ H^+ \quad \textit{acid generating} \qquad \ldots \text{Eqn 4.5}$$

**X=** $K^+$, $Na^+$, $NH_4^+$, $H^+$

**Elemental sulphur oxidation by micro-organisms**: The sulphide oxidised to elemental sulphur in the chemical leach step was further oxidised by the micro-organisms to sulphate with concomitant acid generation according to Eqn. 4.6 (Stott *et al.*, 2000):

$$2\,S^0 + 2\,H_2O + 3\,O_2 \rightarrow 2\,SO_4^{2-} + 4\,H^+ \quad \textit{acid generating} \qquad \ldots \text{Eqn. 4.6}$$

**Pyrite dissolution**: The Andina chalcopyrite concentrate used in this study contained approximately 9 % w/w pyrite. The pyrite dissolution is acid generating as illustrated by Eqn. 4.7 (Stott *et al.*, 2003):

$$4\,FeS_2 + 15\,O_2 + 2\,H_2O \rightarrow 4\,Fe^{3+} + 8\,SO_4^{2-} + 4\,H^+ \quad \textit{acid generating} \qquad \ldots \text{Eqn. 4.7}$$

**Acid-induced chalcopyrite dissolution**: The acid-induced partial dissolution of chalcopyrite can be represented by Eqn. 4.8 (Stott *et al.*, 2003):

$$CuFeS_2 + 4\,H^+ \rightarrow Cu^{2+} + Fe^{2+} + 2\,H_2S \quad \textit{acid consuming} \qquad \ldots \text{Eqn. 4.8}$$

During the baseline experiments the pH decreased steadily from pH 1.68 to 1.49 over the first 70 h after which the rate of $H^+$ production decreased causing a more gradual decline in the pH. The pH stabilised around pH 1.4 at approximately 200 h. In some baseline experiments an initial increase in pH was observed for the first 24 h whereafter it decreased over the ensuing 100 h. This initial rise in pH was consistent with the oxidation of ferrous ions present in solution at the start of the run. When ferrous iron availability decreased due to mineral passivation, the oxidation of elemental sulphur was the predominant reaction and the solution pH decreased i.e. the decrease in pH is indicative of a change in the metabolic activity of the bacteria from a dominant dependence on ferrous oxidation, an acid consuming reaction to sulphur oxidation, an acid generating reaction (Stott *et al.*, 2000). The decline in the rate at which the solution pH decreased and the stabilisation of the pH around 1.4 correlates with an increase in the culture death rate. The profile of cell concentration, shown in Figure 4.5, indicates that at the onset of the stationary phase, the rate of pH decrease declined. When the cells entered the death phase, the pH remained around pH 1.4. Stott *et al.* (2003) observed a similar pH profile, an initial sharp decrease in pH with stabilisation around pH 1.4 during leaching of chalcopyrite using *Acidianus brierleyi*.

University of Cape Town

### 4.5.3 CELL CONCENTRATION

In batch culture, the microbial growth curve consists of lag, exponential growth, stationary and death phases. The growth curve for the thermophilic acidophiles used in this study showed a growth phase, a stationary phase and a death phase (Figure 4.5). The 24h inoculum build-up period exhibited rapid growth. As a result of substrate limitation due to passivation of the mineral and because large inocula were used in the experiments, the growth phase of the culture on commencing the experiment at 24 h was not exponential but rather in the late growth phase. Hence a limited number of generations resulted before the chalcopyrite mineral became passivated. However, as discussed in Section 3.6., a sufficiently high inoculum size was required in all experiments to resist the effects of hydrodynamic stress induced at 24 h. From 24 to 71 h, the cell concentration increased from 4.52 x $10^8$ to 5.76 x $10^8$ cells $ml^{-1}$ after which the culture reached the stationary phase. The culture remained in the stationary phase till 121 h and the cell concentration started to decline appreciably after 192 h. As mentioned earlier, the chemical leach step is the rate-limiting step in the biological leaching of chalcopyrite under the conditions utilised in this study. If chemical leaching is inhibited, the concentration of ferrous ion and elemental sulphur available for biological oxidation is affected and the growth rate will decrease more rapidly owing to limitation of nutrient and energy sources. In practice, under the conditions studied, leaching reactions continued at a reduced rate following initial passivation (Figure 4.5). Hence the percentage of total iron and copper in solution continued to increase, but at a slower rate. This continued leaching indicates that the micro-organisms, though substrate-limited, were still metabolically active. Another factor that could hamper microbial growth, to a more limited extent, was the precipitation of jarosite removing nutrients form solution. According to Eqn. 4.5, ammonium and potassium ions may co-precipitate with jarosite.

### 4.5.4 IRON SOLUBILISATION

Iron solubilisation followed in three distinct phases (Figure 4.5). Over the first 24 h there was a rapid increase in amount of iron solubilised with an iron solubilisation rate of 0.055 $g\,l^{-1}h^{-1}$. At 24 h when the impeller tip speed was increased to 1.97 m $s^{-1}$ to attain complete solids suspension, the iron solubilisation rate declined to 0.017 $g\,l^{-1}h^{-1}$ during the 24 to 118 h period. After 118 h the rate declined further to 0.0079 $g\,l^{-1}h^{-1}$. From 191 to 216 h no further iron solubilisation was observed.

University of Cape Town

### 4.5.5 COPPER SOLUBILISATION

Copper solubilisation followed the same trend as iron dissolution up to 191 h (Figure 4.5). There was a rapid increase in solubilised copper over the first 48 h with a solubilisation rate of 0.035 g $l^{-1}h^{-1}$. Thereafter the rate of solubilisation decreased to 0.013 g $l^{-1}h^{-1}$ during the 48 to 118 h period. A further decrease in the copper solubilisation rate to 0.0099 g $l^{-1}h^{-1}$ was observed from 118 to 191 h. Sadowski *et al.* (2003) found a similar trend when leaching a copper sulphide flotation concentrate with *Acidithiobacillus ferrooxidans*. Two similar phases of biooxidation were observed. Stott *et al.* (2000) also found that copper release was initially rapid (over the first 50 h) but slowed over time. This reduction in the copper solubilisation rate coincided with significant precipitation of jarosite on the mineral surface.

Care must be used in comparing results obtained in this study with those of other researchers due to the diverse microbial species, mineral types, solids loadings, particle sizes, reactor types and reaction conditions used. These variations in process conditions are expected to lead to variation in the leach results. Despite the differences in process conditions, normalisation of the copper data presented in Table 4.1 to the mass of copper leached per volume corrected to 10 days, showed very similar extents of copper solubilisation for all studies detailed, except those of Gericke *et al.* (2001) and Konishi *et al.* (1999). The higher extents reported by Gericke *et al.* (2001) and Konishi *et al.* (1999) may be attributed to the use of ultra-fine chalcopyrite particles and a low solids loading respectively. Literature reports (Gericke *et al.*, 2001; Stott *et al.* 2000; Konishi *et al.*, 1999) indicate that improved chalcopyrite bioleaching rates and extents may be achieved by fine grinding mineral concentrates (e.g. $d_{90}$ 10 μm), decreasing solids loadings, controlling redox potential or using different microbial cultures.

In this section it has been established that chalcopyrite leaching does not follow the conventional sulphide mineral leaching process. It is a complex system controlled by several inter-linked processes. An understanding of these processes occurring under conditions of negligible hydrodynamic stress provides a basis for comparison to conditions of increased hydrodynamic stress mediated either by the addition of quartzite to the reactors or by increasing the tip speed of the impeller. In the sections that follow, the effects of increasing solids loading and impeller tip speed on the processes discussed in this section are determined. It is hypothesised that the hydrodynamic environment caused by the solid phase results in stress or stresses on the microbial cells and, as a result, impact chalcopyrite leaching via inhibition of two biological oxidation reactions, namely the oxidation of ferrous iron to ferric iron, and the oxidation of sulphur to sulphate.

University of Cape Town

**Table 4.1:** Percentage total iron and copper leached from chalcopyrite using thermophilic Archaea for the present study and studies from literature.

| Reference | Concentrate | Organism | Size fraction (µm) | Solids loading (%, w/v) | Initial redox potential (mV; Ag/AgCl) | Time of run (days) | Agitation rate (rpm), Reactor type | Total Fe released (%, w/w) | Total Cu released (%, w/w) | Mass of Cu leached per unit volume, corrected to 10 days (g Cu $l^{-1}$ $day^{-1}$) |
|---|---|---|---|---|---|---|---|---|---|---|
| Present study | Chalcopyrite | *Sulfolobus* -like | 38-75 | 3 | 514 | 10 | 550; STR | 40.03 | 40.8 | 1.22 |
| Rivera-Santillán *et al.*, 1999 | Predominantly chalcopyrite | *Sulfolobus* sp. | Not available | 5 | 285 | 10 | 150; shake flask | ≈8 | ≈25 | 1.25 |
| Plumb *et al.*, 2002 | Chalcopyrite | *Sulfolobus metallicus* | $d_{80}$ 85 | 2 | n/g | 10 | Airlift | n/g | ≈58 | 1.16 |
| Gericke *et al.*, 2001 | Chalcopyrite | Extreme thermophile | $d_{90}$ 10 | 7.5 | 320 | 11 | 220; STR | 98.4 | 95.9 | 6.5 |
| Le Roux and Wakerley, 1988 | Chalcopyrite | *Sulfolobus* sp. | < 90 | 5 | n/g | 29 | 500; STR | n/g | ≈83 | 1.43 |
| Konishi *et al.*, 1999 | Chalcopyrite | *A. brierleyi* | 38-53 | 0.5 | n/g | 9 | 500; STR | 70 | ≈95 | 2.1 |
| Stott *et al.*, 2003 | Chalcopyrite | *A. brierleyi* | $d_{80}$ 66 | 3.2 | 415 | ≈24 | 160; shake flask | n/g | 72 | 0.96 |

n/g = not given

University of Cape Town

# 4.6 THE EFFECT OF SOLIDS LOADING ON THE BIOLEACHING OF CHALCOPYRITE BY A SULFOLOBUS sp.

The effect of solids loading was investigated at quartzite loadings in the range 0 to 18 % w/v. Reactors were operated over a 9 day period at an impeller tip speed of 1.97 m $s^{-1}$ and maintained at approximately 68°C. Solution pH, redox potential, and cell, iron and copper concentrations were measured on a daily basis.

Quartzite was chosen to replace chalcopyrite because a number of investigators have shown that studying the effects of increased solids loading in bioleaching systems by increasing the mineral concentration caused changes in the physicochemical process conditions, typified by an increase in oxygen demand and increased iron and copper concentrations in solution (Bailey and Hansford, 1994; Nemati and Harrison, 2000). Experiments were standardised to contain 3 % chalcopyrite concentrate while the balance of the solids comprised inert quartzite particles of the same size fraction. By using this experimental protocol, the combined effects of increasing chalcopyrite mineral concentration on the physicochemical environment with increasing solids loading were reduced.

Earlier investigations by Nemati and Harrison (2000), where the authors studied the effect of solids loading on *Sulfolobus metallicus* using a pyrite concentrate, concluded that a 3 % pyrite loading caused negligible mechanical damage to the culture and provided sufficient nutrients for the duration of the experiment. However, in the present study, using chalcopyrite, initial experiments showed that when using 3 % chalcopyrite concentration, nutrient limitation occurred approximately 48 h after the inoculum build-up phase. This limitation was not due to complete dissolution of the mineral, but due to mineral passivation. Thus increasing the chalcopyrite concentration above 3 % would not have improved the nutrient supply and hence a 3 % concentrate loading was maintained.

University of Cape Town

## 4.6.1 SAMPLE DATA

In the analysis of the effect of solids loading and impeller tip speed on thermophilic bioleaching performance, direct comparison between results across experimental sets was not possible. Thus the experimental data was normalised against a baseline experiment conducted concurrently. Through this, simplified data was readily integrated and inter-batch variation in operating procedures overcome. In this section, a set of results (Figures 4.9-4.11) representing typical baseline (0 % quartzite) and experimental (12 % quartzite) results is presented to enable

comparison between the typical time profiles (prior to normalisation) obtained when quartzite particles were added to a growing *Sulfolobus* culture. In each experiment, a 23 h inoculum build-up phase (0 to 23 h) was conducted in the reactor before the quartzite fraction was added. On addition of quartzite, the impeller tip speed was increased in both reactors from 0.76 m $s^{-1}$ to 1.97 m $s^{-1}$ to ensure complete suspension of the solids. Figure 4.9 provides a comparison of solution pH and redox potential between the baseline and the experimental reactor at a 12 % quartzite loading. In Figure 4.10 the cell concentration results are compared while Figure 4.11 presents a comparison between the extent of iron and copper solubilisation in the two reactors.

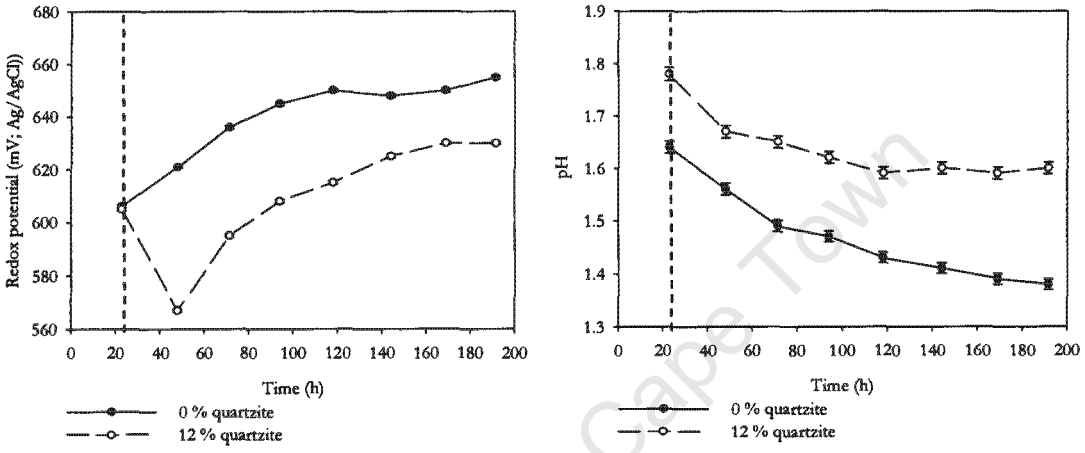


**Figure 4.9:** Effect of solids loading on redox potential and pH at 0 and 12 % w/v quartzite and an impeller tip speed of 1.97m $s^{-1}$. Dashed line indicates the time at which the impeller tip speed was increased from 0.76 to 1.97 m $s^{-1}$.

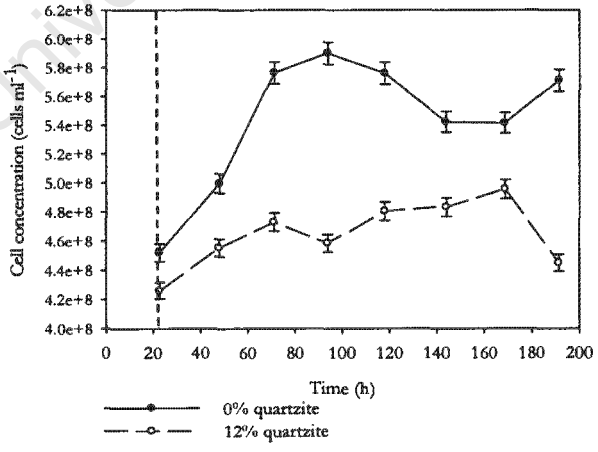


**Figure 4.10:** Effect of solids loading on cell concentration at 0 and 12 % w/v quartzite and an impeller tip speed of 1.97 m $s^{-1}$. Dashed line indicates the time at which the impeller tip speed was increased from 0.76 to 1.97 m $s^{-1}$.

University of Cape Town

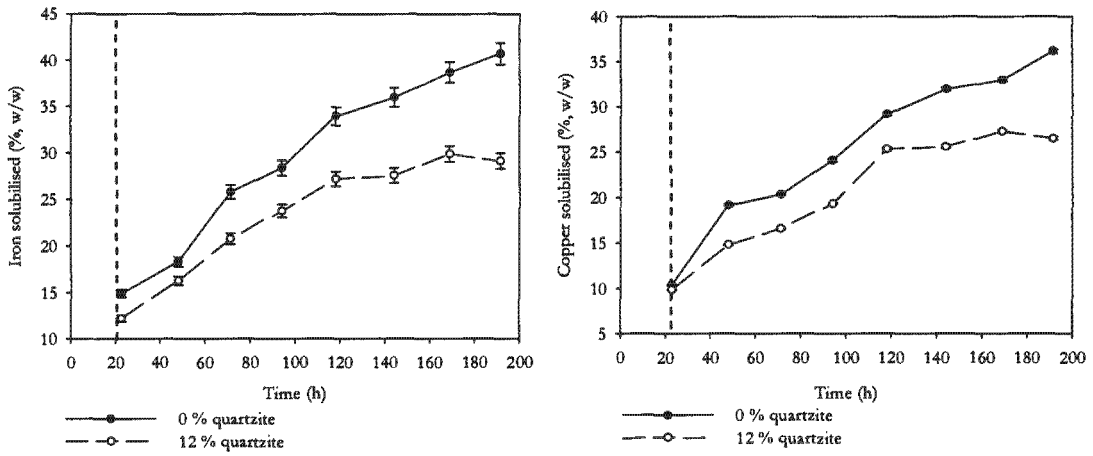


**Figure 4.11:** Effect of solids loading on the percentage of iron and copper solubilised at 0 and 12 % w/v quartzite and an impeller tip speed of 1.97 m $s^{-1}$. Dashed line indicates the time at which the impeller tip speed was increased from 0.76 to 1.97 m $s^{-1}$.

As the primary redox couple in the chalcopyrite leaching system is the $Fe^{3+}/Fe^{2+}$ couple, an increase in the redox potential is indicative of an increasing ferric iron concentration with an associated diminishing or unchanging ferrous iron concentration. In Figure 4.9 the reactor containing 0 % quartzite showed an increase in redox potential from 606 to 650 mV from 23 to 118 h after which the ferrous iron oxidation rate decreased possibly due to continued mineral passivation. The increasing solution redox potential is representative of the microbial oxidation of ferrous ion to ferric iron. Almost no ferrous iron remained in solution (< 0.12 g $l^{-1}$), indicating that the microbial oxidation may be limited by availability of ferrous iron as substrate. At this point the chemical leach reaction is the rate-limiting step in the process.

In the reactor containing 12 % quartzite, the redox potential decreased from 605 to 567 mV over the first 25 h following quartzite addition, after which a similar trend to the baseline reactor was observed. The initial decrease in redox potential could be due to two processes. Firstly, the introduction of solids into the experimental reactor may have caused the micro-organisms present to become stressed, hence the cells may have oxidised ferrous iron in solution at a reduced rate. This in turn decreased the amount of ferric iron in solution, causing a decrease in the chemical leach rate of the mineral. In this case the microbial ferrous oxidation reaction was the rate limiting step in the process. Secondly, a reduction in the solution ferric iron concentration may have occurred due to the precipitation of ferric iron as jarosite. The stressed micro-organisms were unable to regenerate the ferric iron in solution and this contributed toward an overall decrease in the solution redox potential. After 71 h, the ferrous oxidation rate increased to almost

University of Cape Town

the same rate as the control. The redox potential stabilised around 630 mV and did not reach the redox potential of the baseline during the time period of the experiment.

Over the first 24 h after quartzite addition, the same extent of decrease in pH was seen in both reactors (Figure 4.9). From 48 to 118 h the solution pH in the reactor containing 12 % quartzite decreased at a slower rate than the baseline reactor and plateaued to around pH 1.6 at 192 h. During this time the pH of the baseline reactor continued to decrease to pH 1.4 at 192 h.

Growth parameters are presented in Table 4.2. The culture growth rate was adversely affected by the addition of inert solids at 23 h (Figure 4.10). In the reactor to which 12 % quartzite was added, the cell concentration remained lower than the baseline reactor throughout the course of the experiment. The apparent specific growth rate (calculated using method outlined in Appendix B.2) and maximum cell concentration were higher in the baseline reactor, indicating the negative influence of the addition of 12 % quartzite. In contrast the length of the growth phase was longer in the reactor containing 12 % quartzite.

**Table 4.2:** Growth parameters for 0 and 12 % quartzite loadings operated at an impeller tip speed of 1.97 m $s^{-1}$.

| Quartzite loading (%, w/v) | $\mu_{app}$ ($h^{-1}$) (23-71 h) | $X_{max}$ (x$10^8$ cells $ml^{-1}$) | Time at $X_{max}$ (h) | Length of growth phase (h) |
|---|---|---|---|---|
| 0 | 0.005 | 5.90 | 94 | 48 |
| 12 | 0.002 | 4.96 | 168 | 144 |

The rate of iron oxidation is not directly growth linked but linked indirectly through the chemical leach rate of the mineral. Over the first 118 h of the run, the iron oxidation rate in both reactors was similar (Figure 4.11). After 118 h, the rate of iron release in both reactors decreased. This decrease occurred to a greater extent in the reactor containing 12 % quartzite. At this stage the rate of the chemical leach step was significantly reduced due to passivation of the mineral and this led to a decline in the amount of iron solubilised. The specific iron oxidation rates for the two phases of leaching at both solids loadings are presented in Table 4.3. The specific iron leach rate in phase one was higher than in phase two. Thus the specific iron oxidation rate was not only a function of solids concentration but also a function of time.

University of Cape Town

**Table 4.3:** Specific iron oxidation rates for 0 and 12 % quartzite operated at an impeller tip speed of 1.97 m $s^{-1}$.

| Quartzite loading (%, w/v) | Specific iron oxidation rate (x$10^{-11}$ g Fe $cell^{-1}$ $h^{-1}$) (23-118 h) | Specific iron oxidation rate (x$10^{-11}$ g Fe $cell^{-1}$ $h^{-1}$) (118-192 h) |
|---|---|---|
| 0 | 3.12 | 1.40 |
| 12 | 2.88 | 0.46 |

Over the first 25 h after the addition of solids, there was a sharp increase in the copper concentration in solution for both the 0 and 12 % quartzite loadings (Figure 4.11). This rise in concentration was greater for the baseline reactor than for the quartzite reactor; however, the copper solubilisation curves follow each other more closely than their respective iron release curves. Following the initial sharp increase in copper concentration, there were two phases of copper release. The specific copper oxidation rates for the two phases of leaching are presented in Table 4.4. As observed with iron dissolution, the rate of copper solubilisation was higher in the first phase of leaching than in the second and thus copper solubilisation was a function of solids loading and time. However, in phase 1 (48-118 h) the specific rate was higher at the 12 % quartzite loading than at the 0 % quartzite loading. This effect is discussed further in Sections 4.6.2 and 4.6.3.

**Table 4.4:** Specific copper solubilisation rates for 0 and 12 % quartzite operated at an impeller tip speed of 1.97 m $s^{-1}$.

| Quartzite loading (%, w/v) | Specific copper solubilisation rate (x$10^{-11}$ g Cu $cell^{-1}$ $h^{-1}$) (48-118 h) | Specific copper solubilisation rate (x$10^{-11}$ g Cu $cell^{-1}$ $h^{-1}$) (118-192 h) |
|---|---|---|
| 0 | 2.27 | 1.51 |
| 12 | 2.85 | 0.29 |

From Figures 4.9-4.11 it is clear that the overall effect of adding 12 % quartzite to the experimental reactor is a decrease in the extent of leaching effected primarily by a decrease in cell concentration. This decrease in cell concentration may be due to a decrease in the culture growth rate or an increase in the culture death rate or both. Further, the decrease in redox potential, prior to acclimatisation to increased solids loading, resulted from a reduced rate of ferrous iron oxidation by the microbial phase.

University of Cape Town

### 4.6.2 THE EFFECT OF INCREASING QUARTZITE LOADING ACROSS THE RANGE 0 TO 18 % w/v AT AN IMPELLER TIP SPEED OF 1.97 m $s^{-1}$

Two sets of experimental runs were carried out to determine the effect of increasing solids loading at an impeller tip speed of 1.97 m $s^{-1}$ (agitation rate of 650 rpm and shear rate of 108 $s^{-1}$). The total solids loadings used were 3, 9, 12, 15, 18 and 21 % w/v containing 3 % w/v chalcopyrite and 0, 6, 9, 12, 15 and 18 % quartzite respectively. The quartzite and the chalcopyrite concentrate were of the 38-75 μm size fraction (Section 3.2). Table 4.5 summarises the experimental conditions utilised.

**Table 4.5:** Test regime for solids loading experiments.

| Reactor conditions | All Reactors |
|---|---|
| Impeller speed (m $s^{-1}$): | |
| 0-23 h | 0.76 |
| 23 h-192 h | 1.97 |
| Working volume (ml) | 700 |
| Temperature (°C) | 68 |
| Initial pH | ≈1.6 |
| Inoculum size (%, v/v) | 21 |

University of Cape Town

The time profiles for these experiments are presented in Figures 4.12, 4.14, 4.16, 4.19 and 4.22. The two sets of experiments were conducted at different times. In order to facilitate comparison between the two experimental sets, the data obtained from these runs were normalised. Each experimental run consisted of a baseline reactor (0 % quartzite) containing only 3 % chalcopyrite and two or three experimental quartzite-supplemented reactors. Operating conditions were held consistent between reactors, hence the difference in process performance between the baseline and experimental reactors was attributed only to the presence of the inert quartzite. Normalisation of the data was achieved in two ways. Firstly, all 24 h readings were set to 1 (reference point). Secondly, the data was normalised by dividing the result obtained for the experimental reactor at each time point by the corresponding result for the baseline reactor. Using an example to illustrate, the normalised pH value for the baseline reactor at 48 h was calculated using Eqn. 4.9:

$$\text{Normalised pH}_{\text{baseline}} = \frac{pHBase_{48h}}{pHBase_{48h}} \qquad \ldots\text{Eqn 4.9}$$

Similarly, the normalised pH values for experimental reactors at 48 h were calculated using Eqn. 4.10:

$$\text{Normalised pH}_{\text{experimental}} = \frac{pHExp_{48h}}{pHBase_{48h}} \qquad \ldots \text{Eqn 4.10}$$

where: $pHBase_{48h}$ = the pH value for the baseline reactor at 48 h

$pHExp_{48h}$ = the pH value for the experimental reactor at 48 h

Normalised pH, redox potential, cell concentration, iron and copper data are presented in Figures 4.13, 4.15, 4.17, 4.20 and 4.23. The significance of the data has been shown using a t-Test: paired two sample for means (Appendix E).

The calculations for growth and metal solubilisation rates are detailed in Appendix B.1. The calculations were performed over the same time period for each solids loading. These results were subsequently normalised against the baseline data (Figures 4.18, 4.21 and 4.24).

In Section 2.2.1.4, it was reported that van Weert *et al.* (1995) and Derksen *et al.* (2000) determined that the presence of particles impaired oxygen mass transfer in quartzite slurries. In order to determine whether the presence of quartzite in the experimental reactors caused oxygen limitation, dissolved oxygen concentrations were measured at the various solids loadings and impeller tip speeds tested. Using an aeration rate of 2 vvm, the dissolved oxygen concentration was maintained in the range 2.1 to 2.3 mg $l^{-1}$ for all experiments. This result is greater than the critical dissolved oxygen concentration and within the acceptable limits of 1.5 and 4.1 mg $l^{-1}$ published by Dew *et al.* (1999).

University of Cape Town

#### 4.6.2.1 The effect of solids loading on slurry pH

The solution pH in all reactors, except the reactor containing 18 % quartzite, decreased over time (Figure 4.12). The rate of decrease in pH was faster in the reactor containing 0 % quartzite than in the experimental reactors. In the baseline reactor, the magnitude of the decrease was about 0.3 pH units while the magnitude of decrease the experimental reactors ranged from 0.10 to 0.18 pH units. The pH in the reactor containing 18 % quartzite continued to rise for the duration of the experiment from a pH of 1.77 at 23 h to a pH of 2.03 at 216 h. Analysis of the data normalised against the baseline reactor (Figure 4.13) clearly shows that the pH in the experimental reactors remained higher than the baseline reactor throughout the experimental runs. In addition, the difference in pH values between the experimental reactor and the baseline reactor increased with time. The reactors containing 6, 9 and 12 % quartzite behaved similarly with respect to the baseline reactor while the pH in the reactor containing 15 % quartzite was unexpectedly more similar to the baseline reactor than the 6, 9 and 12 % quartzite cluster.

Several reactions are responsible for changes in pH during chalcopyrite leaching (Section 4.5). The most pertinent processes that could contribute towards a slower rate in the decrease of pH observed for the 6 to 15 % quartzite loading and the continuous increase in pH observed for the 18 % quartzite reactor are the suppression of the oxidation of elemental sulphur to sulphate (especially post 50 h) and the suppression of pyrite dissolution due to hydrodynamic stress experienced by the micro-organisms. The extent of the suppression was proportional to the solids loading hence resulting in a proportional decrease in the rate of pH decline and an increase in pH at an 18 % quartzite loading. When a critical quartzite loading was exceeded, the pH increased instead of decreasing. It is clearly seen that in the reactor containing 18 % quartzite different chemical reactions were dominating in the system. It is possible that at an 18 % quartzite loading, in addition to suppression of elemental sulphur oxidation and pyrite leaching, physicochemical conditions favoured the leaching of chalcopyrite. It is postulated that the shift in the leaching bias is controlled by the redox potential and will be discussed further in Section 4.6.2.5. It is concluded that with respect to the pH data presented, the critical solids loading at which the leaching process was affected significantly due to hydrodynamic stress lay between 15 and 18 % quartzite.

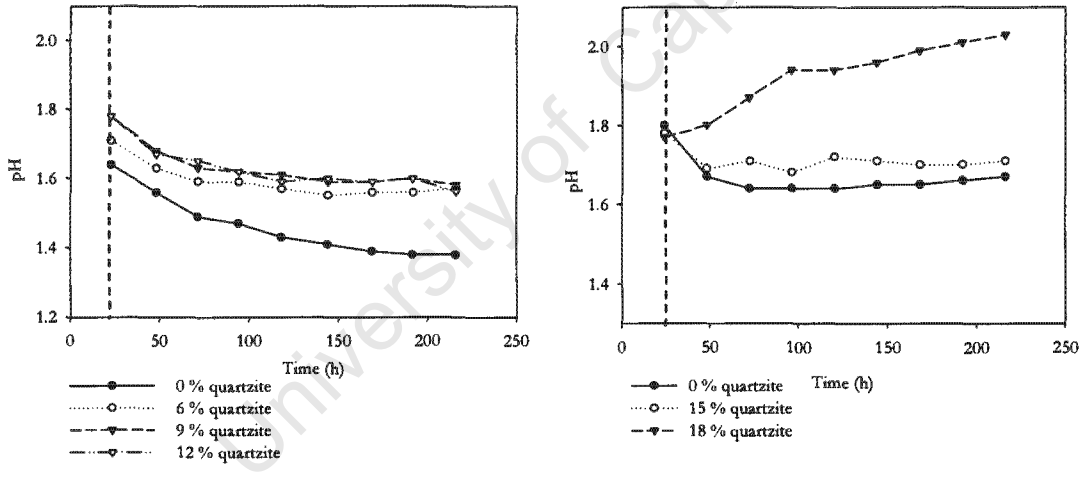


**Figure 4.12:** Effect of solids loading on solution pH for two experimental sets with solids loadings of 0, 6, 9, 12 and 0, 15 and 18 % w/v quartzite and operated at an impeller tip speed of 1.97 m $s^{-1}$. Dashed line indicates the time at which the impeller tip speed was increased from 0.76 to 1.97 m $s^{-1}$.

University of Cape Town

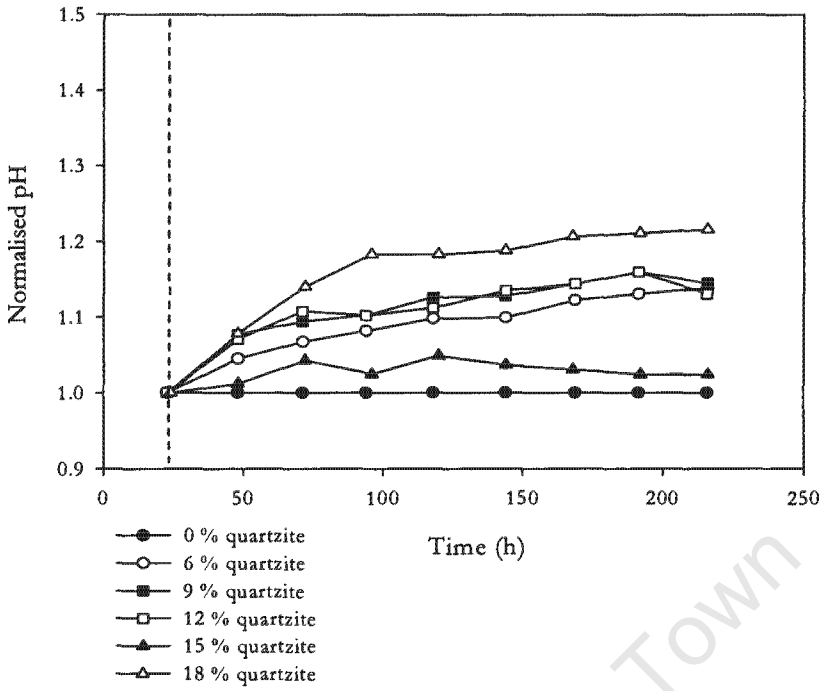


**Figure 4.13:** Change in pH relative to the baseline as a function of time for 0 to 18 % w/v quartzite loadings operated at an impeller tip speed of 1.97 m $s^{-1}$. Dashed line indicates the time at which the impeller tip speed was increased from 0.76 to 1.97 m $s^{-1}$.

University of Cape Town

#### 4.6.2.2 The effect of solids loading on slurry redox potential

There was an initial decrease in redox potential for the reactors containing 6 to 15 % quartzite with an apparent recovery after 48 h (Figure 4.14). The magnitude of this decrease was proportional to the solids loading used. The extent of recovery was inversely proportional to the solids loading. At the end of the run the redox potential in the experimental reactors approached that of the baseline reactor. The redox potential profile for the reactor containing 18 % quartzite differed from the reactors with lower quartzite loadings. While a large decrease in redox potential was observed on addition of 18 % quartzite, the redox potential in this reactor continued decreasing throughout experiment even after the redox potential in all the other reactors had stabilised above 600 mV. This decline in redox potential of approximately 140 mV was due to an increase in the solution ferrous iron concentration. This correlated to reduced microbial activity resulting in limited or no ferrous iron oxidation. Normalised redox potential profiles are presented in Figure 4.15. In the reactors containing 6 to 15 % quartzite there was an initial decrease in redox potential with respect to the baseline reactor whereafter the redox potential increased at a higher rate than the baseline. This increase, post 71 h, is attributed to earlier passivation of the chalcopyrite in the baseline reactor causing a stabilisation of the redox potential around 650 mV. The profiles for the reactors containing 6 and 9 % quartzite followed a similar

trend while the profiles for the reactors containing 12 and 15 % quartzite were similar. It is concluded that with respect to the redox potential data presented, the critical solids loading at which the leaching process became significantly affected due to hydrodynamic stress was 9 % quartzite.

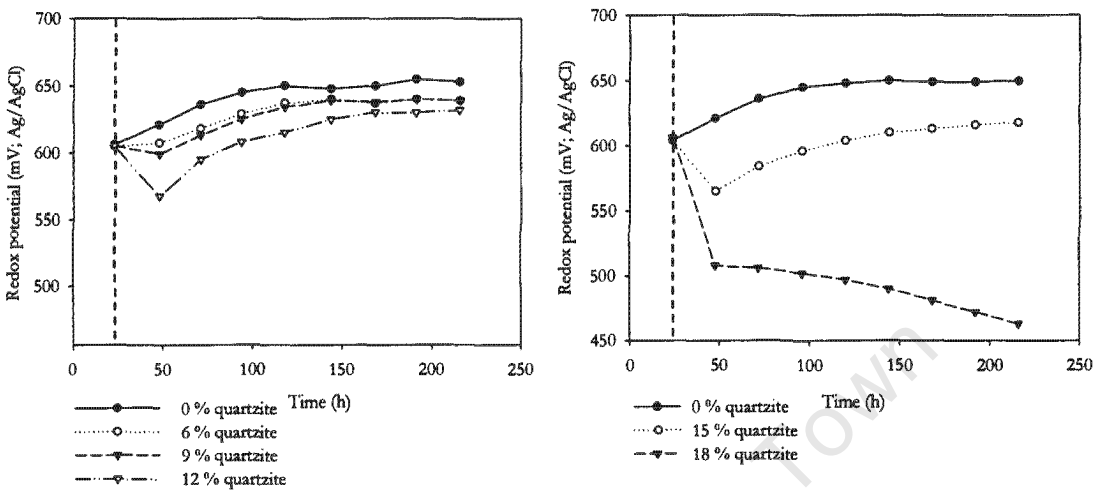


**Figure 4.14:** Effect of solids loading on redox potential for two experimental sets with solids loadings of 0, 6, 9, 12 and 0, 15 and 18 % w/v quartzite and operated at an impeller tip speed of 1.97 m $s^{-1}$. Dashed line indicates the time at which the impeller tip speed was increased from 0.76 to 1.97 m $s^{-1}$.

University of Cape Town

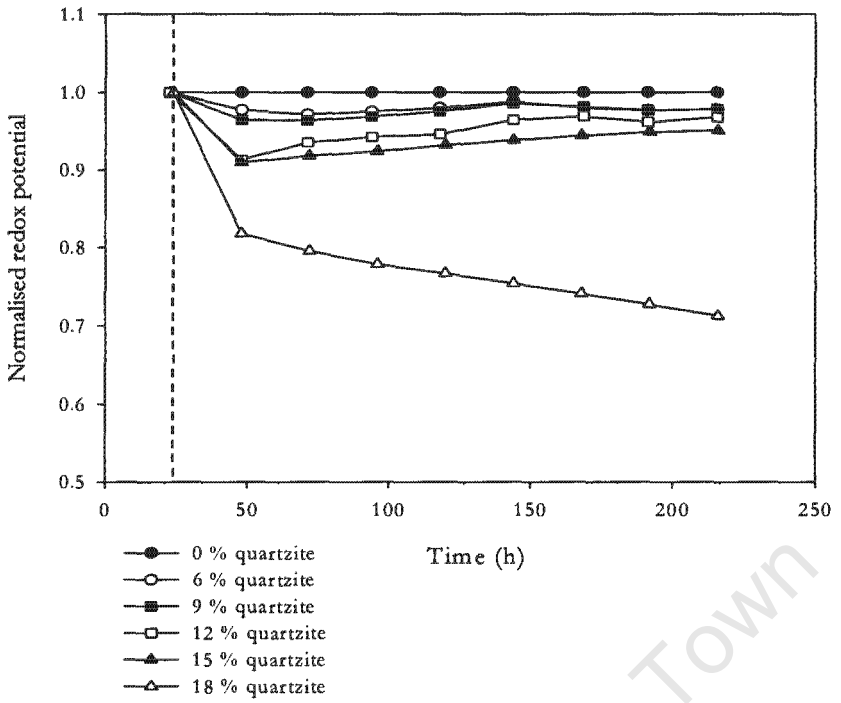


**Figure 4.15:** Change in redox potential relative to the baseline as a function of time for 0 to 18 % w/v quartzite loadings operated at an impeller tip speed of 1.97 m $s^{-1}$. Dashed line indicates the time at which the impeller tip speed was increased from 0.76 to 1.97 m $s^{-1}$.

University of Cape Town

#### 4.6.2.3 The effect of solids loading on the planktonic cell concentration

Several authors have reported increased lag periods on increasing solids loading in the minerals slurry reactor (Liu *et al.* 1987; Pearce, 1993; Nemati and Harrison, 2000; Sissing and Harrison, 2003). No distinct lag periods were observed in the current study. A lag period was not observed because of the 24 h inoculum build-up phase where only 3 % chalcopyrite was present in the reactors and agitation was restricted to a tip speed of 0.76 m $s^{-1}$ (250 rpm). The high cell concentration, sufficient nutrients and conditions of negligible hydrodynamic stress ensured no lag period. The inert quartzite was added after this 24 h inoculum build-up period. Nemati and Harrison (2000) and Sissing and Harrison (2003) used similar reactor configurations and experimental protocols to this study however they added all solids at the beginning of their experiments exposing the inoculum to the grinding effects of partially suspended solids prior to complete suspension. This caused stress to the culture and thus when the agitation rate was increased at 24 h after the inoculum build-up phase, a lag phase was induced.

Over the 23 to 94 h period, at the 0, 6, 9, 12 and 15 % quartzite loadings, the cell concentration increased in all reactors (Figure 4.16). After 94 h the reactors containing 0 and 6 % quartzite reached stationary phase, while the reactors containing 9, 12 and 15 % quartzite reached the

stationary phase after 118, 168 and 118 h respectively. At an 18 % quartzite loading, no growth phase was observed; instead cell death occurred over the 23 to 71 h period. This phase was followed by a lag phase that extended to the end of the experiment. Although no growth was observed, mineral dissolution continued (Section 4.6.2.4 and 4.6.2.5). Kelly and Jones (1978), Mandl (1984) and Nemati and Harrison (2000) have reported ferrous iron oxidation in the presence of non-growing micro-organisms.

A comparison of cell concentration in all reactors using the normalised data, presented in Figure 4.17 showed that over the 23 to 94 h period the cell concentration in reactors containing 6, 9, 12 and 15 % quartzite was lower, between 0.7 and 0.9 fold that of the baseline reactor. Thereafter an increase in the normalised cell concentration from 94 to 168 h was observed for the 6, 9 and 12 % quartzite loadings. This increase coincided with the baseline reactor shifting from growth to the stationary phase with a concomitant increase in cell concentration in the experimental reactors. As observed with the redox potential and pH profiles, the reactor containing 18 % quartzite showed the greatest difference with respect to the baseline reactor with a cell concentration of 0.3 fold that of the baseline reactor for most of the experiment.

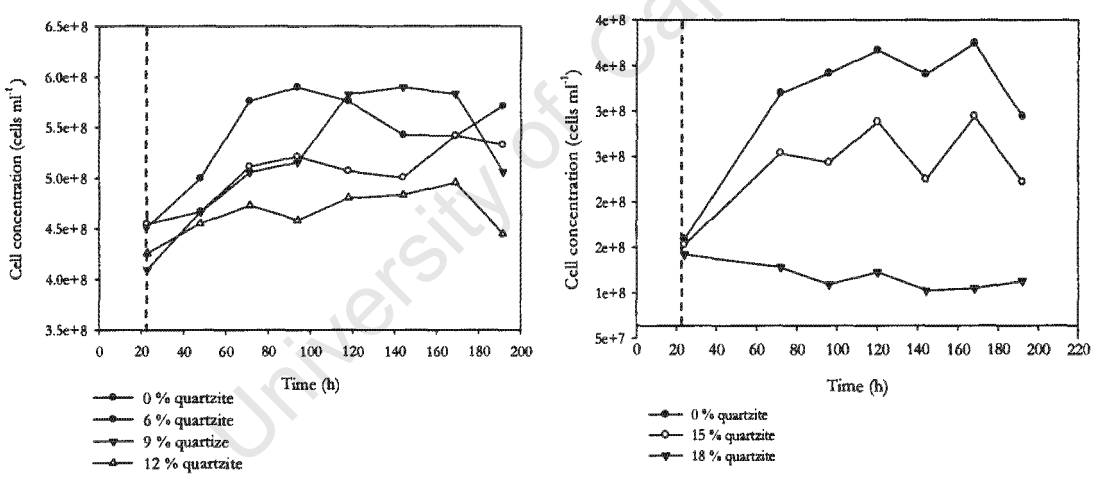


**Figure 4.16:** Effect of solids loading on cell concentration for two experimental sets with solids loadings of 0, 6, 9, 12 and 0, 15 and 18 % w/v quartzite and operated at an impeller tip speed of 1.97 m $s^{-1}$. Dashed line indicates the time at which the impeller tip speed was increased from 0.76 to 1.97 m $s^{-1}$.

University of Cape Town

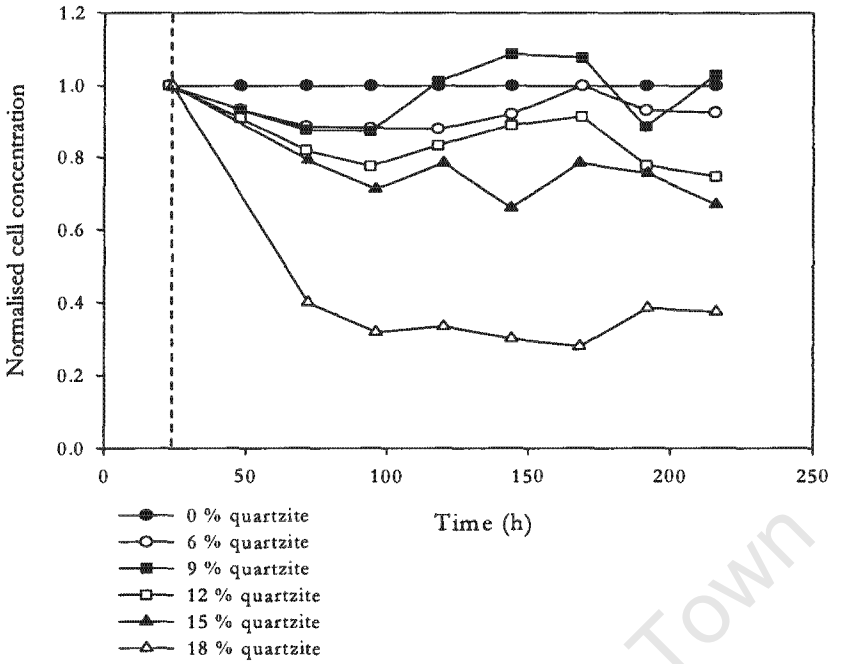


**Figure 4.17:** Change in cell concentration relative to the baseline as a function of time for 0 to 18 % w/v quartzite loadings operated at an impeller tip speed of 1.97 m $s^{-1}$. Dashed line indicates the time at which the impeller tip speed was increased from 0.76 to 1.97 m $s^{-1}$.

Both the apparent specific growth rate and the extent of growth were influenced by the addition of quartzite to the experimental reactors. Apparent specific growth rates, calculated using the method detailed in Appendix B.1, are shown as a function of solids loading in Figure 4.18. The addition of quartzite to the experimental reactors caused the apparent specific growth rate to decrease from 0.005 $h^{-1}$ at a 0 % quartzite loading to 0.004, 0.003, 0.002 and 0.001 $h^{-1}$ at 6, 9, 12 and 15 % quartzite respectively. At an 18 % quartzite loading cell death occurred and the specific death rate was 0.002 $h^{-1}$.

The extent of growth defined as the stationary phase cell concentration (71 h) was lower in all reactors containing quartzite compared to the baseline reactor (Figure 4.18). The maximum cell concentration in suspension was highest at a 0 % quartzite loading and decreased with increasing solids loading. Several processes resulting from increased hydrodynamic stress due to the addition of solids may contribute towards a reduced extent of growth. These processes include (i) the loss of cell viability; (ii) damage to cell structure leading to cell death and thus causing a reduction the extent of growth and (iii) an increase in the maintenance energy requirement for cell repair mechanisms (Chapter 5). The reduced extent of growth may be linked to an increase in the death rate with increased solids concentration and can be related to the specific growth rate by

University of Cape Town

Eqn 4.11. Further analysis of the specific death rate constant as a function of solids concentration is given in Section 4.9.

$$\mu_{app} = \mu - k_d \quad \text{...Eqn. 4.11}$$

where $\mu_{app}$ = the apparent specific growth rate ($h^{-1}$)

$\mu$ = the specific growth rate ($h^{-1}$) and is a function of physiological factors such as temperature, pH, nutrient availability, and ferrous and ferric iron concentration

$k_d$ = the specific cell death rate ($h^{-1}$)

Using the cell concentration data presented in this section the critical solids loading at which the leaching process became significantly affected due to hydrodynamic stress was 9 % quartzite. Process failure in terms of absence of culture growth was observed at 18 % quartzite.

University of Cape Town

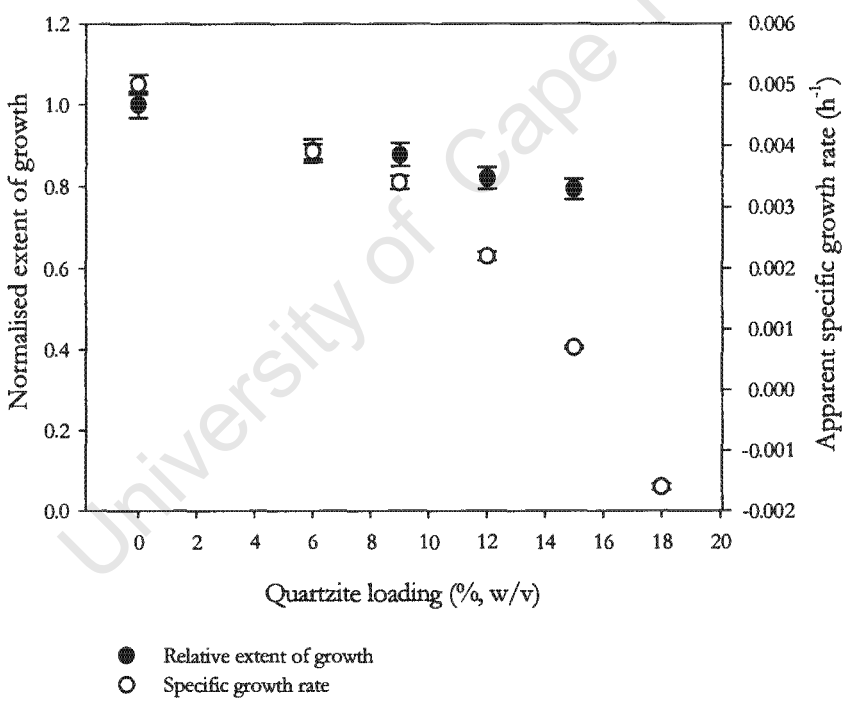


**Figure 4.18:** Apparent specific growth rate and normalised extent of growth and as a function of quartzite loading and an impeller tip speed of 1.97 m $s^{-1}$.

#### 4.6.2.4 The effect of solids loading on iron solubilisation

Figure 4.19 reflects the change in soluble iron concentration with time and quartzite concentration while Figure 4.20 illustrates the change in iron concentration in the quartzite-containing reactors relative to the baseline reactor. The concentration of solubilised iron was lower in the quartzite-containing reactors than in the baseline reactor over the course of the

experiments. Over the 24 to 96 h period, the percentage iron solubilised increased in all reactors; however the rate of increase was higher in the baseline line reactor compared to the experimental reactors (Figure 4.19). This effect is more clearly seen when comparing the normalised data (Figure 4.20). The normalised percentage iron solubilised in the experimental reactors decreases with respect to the baseline reactor over the 23 to 94 h time period. Clusters of solids loading showing similar extents of solubilisation were identified. At 216 h, the 6 and 9 % solids loading showed similar extents of solubilisation of approximately 0.9 fold that of the baseline reactor while the 12 and 15 % quartzite loadings resulted in extents of solubilisation of 0.7 to 0.75 fold that of the baseline reactor. Iron solubilisation remained very low in the reactor containing 18 % quartzite and decreased to 0.2 fold that of the baseline value even after passivation had occurred in the baseline reactor.

As illustrated in Figure 4.19, the iron solubilisation followed two phases. The first phase (23 to 118 h) was characterised by a high solubilisation rate followed by a slower rate over the second phase (118 to 216 h). The first phase of solubilisation coincided with the growth phase of the culture while the second phase corresponded to the stationary phase of the micro-organisms. The rate of iron solubilisation decreased in phase 2 due to increasing passivation of the chalcopyrite mineral surface with time. Further analysis of this data is presented in Section 4.6.2.5.

University of Cape Town

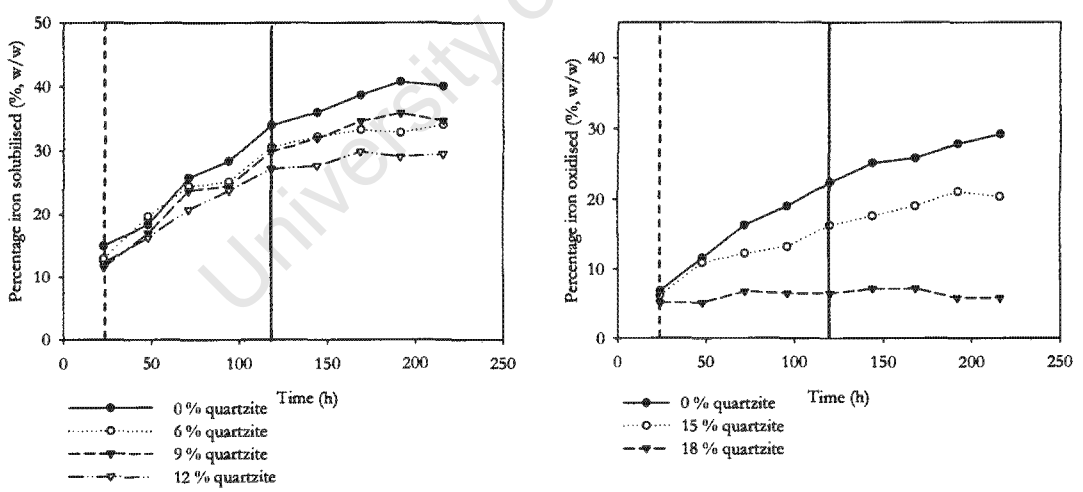


**Figure 4.19:** Effect of solids loading on the percentage iron solubilised for two experimental sets with solids loadings of 0, 6, 9, 12 and 0, 15 and 18 % w/v quartzite and operated at an impeller tip speed of 1.97 m $s^{-1}$. Dashed line indicates the time at which the impeller tip speed was increased from 0.76 to 1.97 m $s^{-1}$. Solid line indicates the start of phase 2 of iron solubilisation.

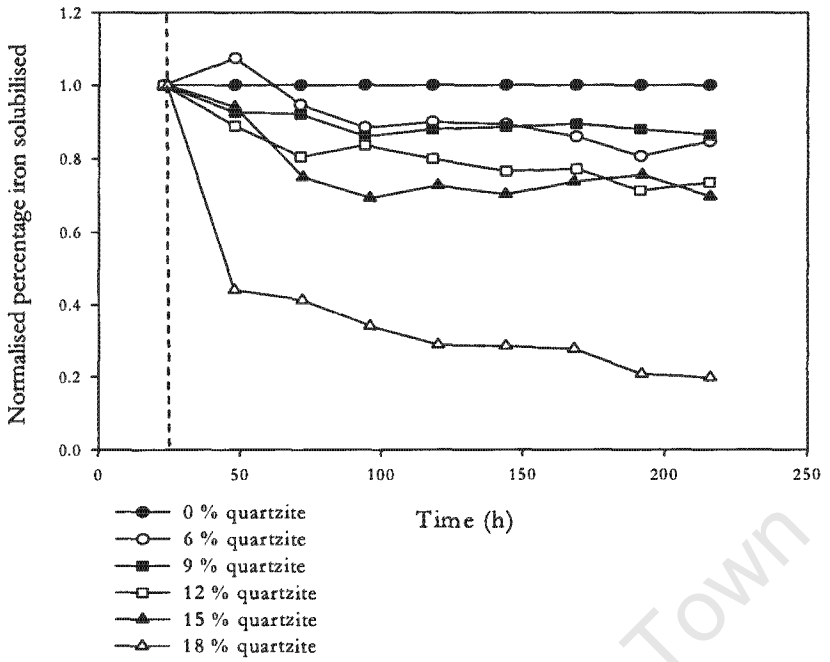


**Figure 4.20:** Change in iron solubilisation relative to the baseline as a function of time for 0 to 18 % w/v quartzite loadings operated at an impeller tip speed of 1.97 m $s^{-1}$. Dashed line indicates the time at which the impeller tip speed was increased from 0.76 to 1.97 m $s^{-1}$.

The normalised, overall iron solubilisation rate data (23 to 192 h) and extent of iron solubilisation (192 h) are presented in Figure 4.21. The solubilisation rates were calculated as detailed in Appendix B.1. The rate at which iron was released into solution decreased with increasing pulp density. At 6 and 9 % quartzite loadings, the iron release rate was approximately 0.85 fold that of the baseline while at 12 and 15 % quartzite concentrations, the iron solubilisation rate was 0.7 fold that of the baseline reactor. The iron solubilisation rate for the reactor containing 18 % quartzite was approximately 10 fold lower than the baseline reactor. The extent of iron solubilisation from 0 to 192 h was calculated as the percentage of the iron content of the mineral present in the reactor (5.9 g) released into solution during this period. The extent of iron solubilisation decreased with increasing hydrodynamic stress. With respect to the iron data presented, the critical solids loading at which the leaching process became significantly affected due to hydrodynamic stress was 9 % quartzite.

University of Cape Town

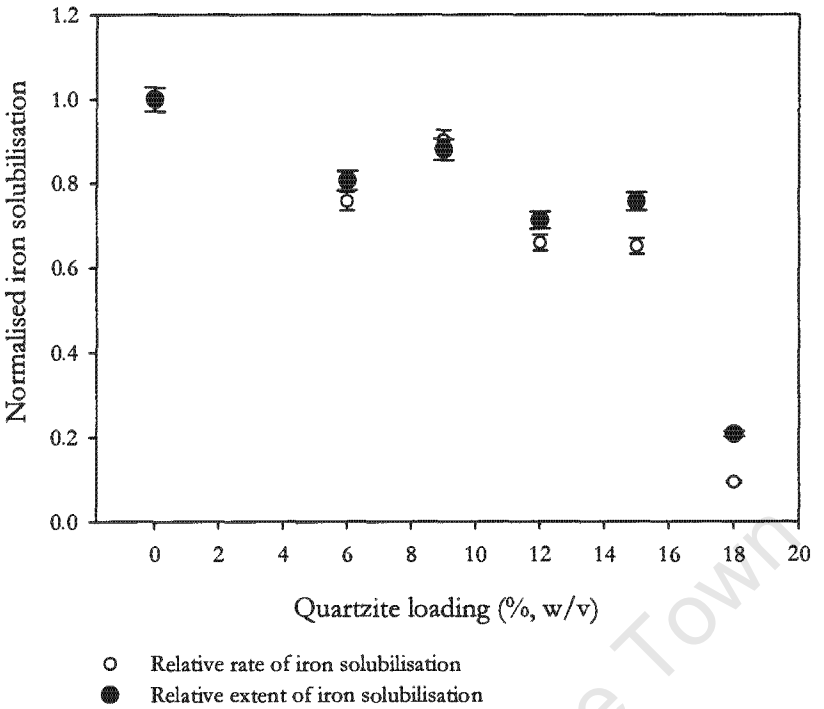


**Figure 4.21:** Normalised rate and extent of iron solubilisation as a function of quartzite loading and an impeller tip speed of 1.97 m $s^{-1}$.

#### 4.6.2.5 The effect of solids loading on copper solubilisation

The concentration of copper in solution as a function of time is shown, across the range of solids loadings studied, in Figure 4.22 and is normalised with respect to the baseline in Figure 4.23. Copper solubilisation followed a similar trend to iron solubilisation except that there was an initial sharp increase in copper in solution over 23 to 48 h. Thereafter the solubilisation followed two distinct phases. As observed with iron solubilisation, the first phase of leaching was characterised by a higher solubilisation rate than the second.

University of Cape Town

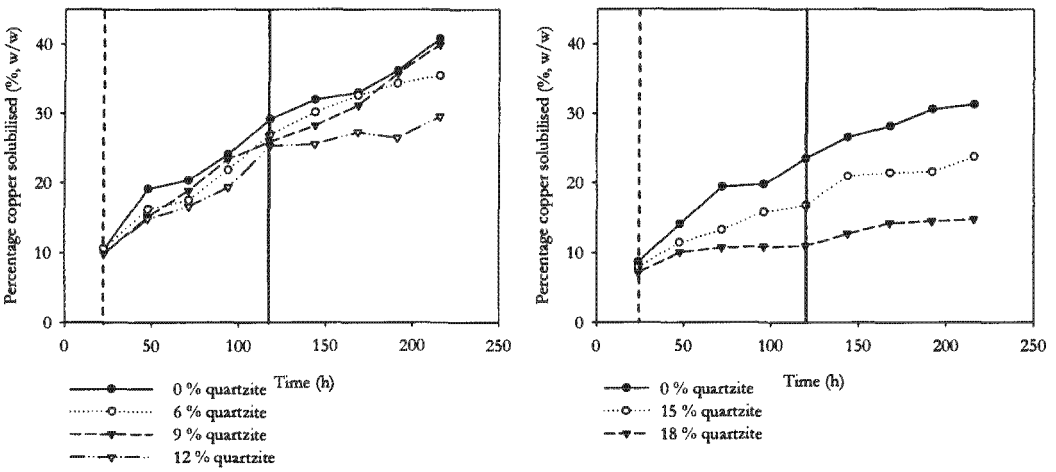


**Figure 4.22:** Effect of solids loading on the percentage copper solubilised for two experimental sets with solids loadings of 0, 6, 9, 12 and 0, 15 and 18 % w/v quartzite and operated at an impeller tip speed of 1.97 m $s^{-1}$. Dashed line indicates the time at which the impeller tip speed was increased from 0.76 to 1.97 m $s^{-1}$. Solid line indicates the start of phase 2 of iron solubilisation.

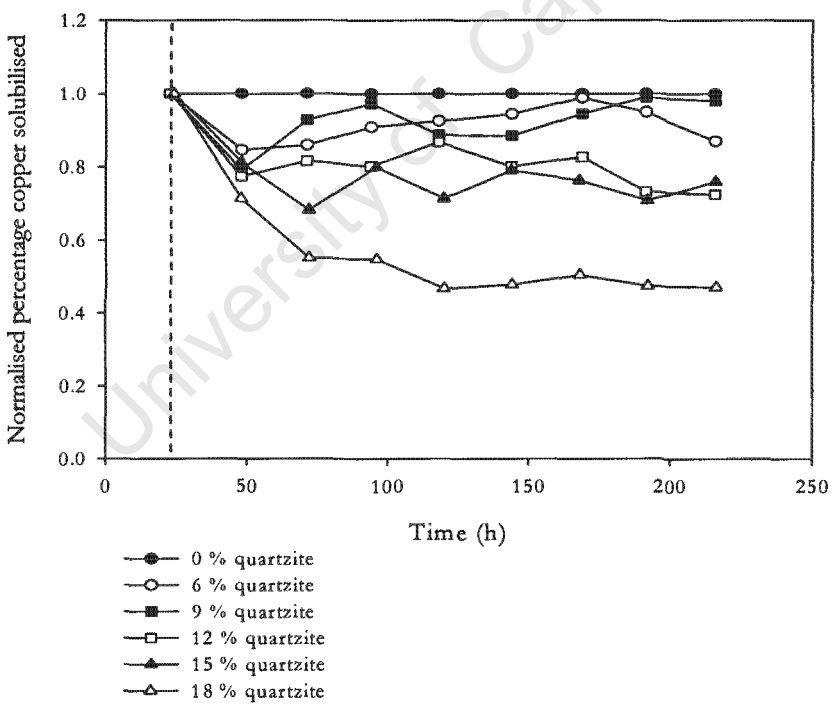


**Figure 4.23:** Change in copper solubilisation relative to the baseline as a function of time for 0 to 18 % w/v quartzite loadings operated at an impeller tip speed of 1.97 m $s^{-1}$. Dashed line indicates the time at which the impeller tip speed was increased from 0.76 to 1.97 m $s^{-1}$.

Copper solubilisation rates (0 to 192 h) were calculated as detailed in Appendix B.1. The extent of copper solubilisation from 0 to 192 h was calculated as the percentage of the copper content of

University of Cape Town

the mineral present in the reactor (6.2 g) released into solution during this period. A decrease in both the copper solubilisation rate as well as the extent of copper leaching with increasing solids loading was observed. The rate of copper solubilisation was similar at 0, 6 and 9 % quartzite loadings and decreased to approximately 0.7 fold that if the baseline reactor at 12 and 15 % quartzite loadings. At an 18 % quartzite loading the normalised copper solubilisation rate was 0.32.

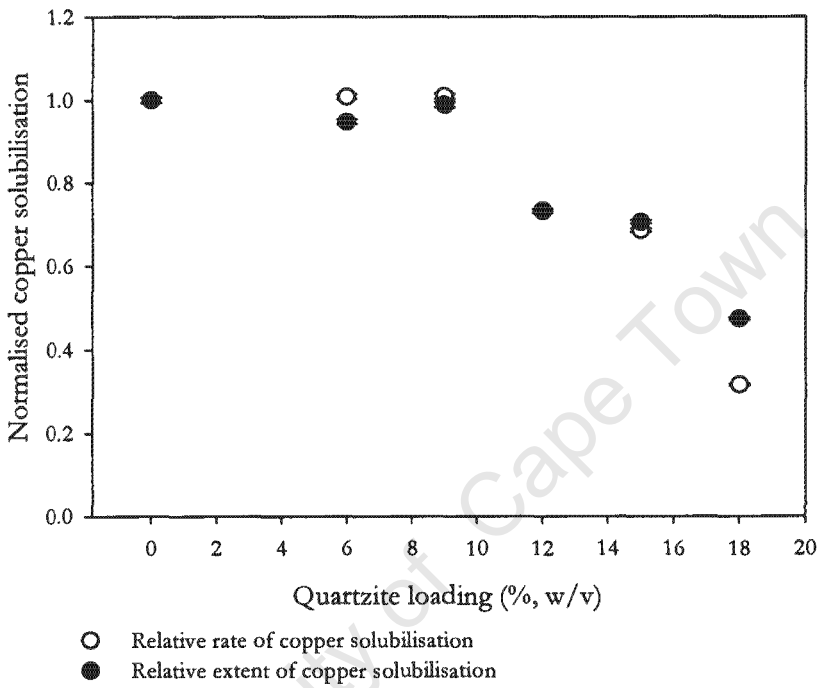


**Figure 4.24:** Normalised rate and extent of copper solubilisation as a function of quartzite loading and an impeller tip speed of 1.97 m $s^{-1}$.

The ratio of the extents iron to copper solubilised at the end of leach phases 1 and 2 are compared in Table 4.6. The ratio at the end of phase 1 varied between 0.62 and 1.10 while in phase 2 the ratio varied between 0.50 and 0.94. There is 29.8 % copper and 25.9 % iron in the Andina concentrate which comprises predominantly chalcopyrite with 8.1 % pyrite and 4.1 % bornite (Section 3.2.1). If all minerals leached at equivalent rates, the iron to copper ratio would be 0.87. Instead, during the first leach phase, the ratio was greater than 1.00 at solids loadings ranging from 0 to 12 % quartzite and lay between 0.82 and 0.94 in phase 2 for these quartzite concentrations. Investigators have linked several processes to the change in the iron to copper ratio. These processes include (i) complete dissolution of pyrite leading to predominantly chalcopyrite leaching, (ii) increased precipitation of iron as jarosite on the surface of the mineral (Konishi *et al.*, 1999), (iii) galvanic interactions between pyrite and chalcopyrite minerals present in the concentrate leading to the preferential leaching of chalcopyrite (Natarajan, 1990) and (iv) the

University of Cape Town

selective leaching of non-ferrous copper sulphide minerals such as chalcocite, covellite or bornite (Witne and Phillips, 2001; Arce and González, 2002). In the present study, several theories may be proposed. Firstly, if the iron to copper ratio is higher, as observed in phase one, then a mineral devoid of copper (e.g. pyrite) was leaching at a higher rate leading to a higher iron concentration in solution. The complete dissolution of pyrite (1.32 g Fe $l^{-1}$) in phase one may have led to predominantly chalcopyrite leaching in phase two and thus a decrease in the ratio. Secondly, the selective leaching of bornite in phase 2 may have resulted in higher concentrations of copper in solution than iron. Thirdly, jarosite precipitation is greater at higher pH. It can be seen from Figure 4.12 that the pH increased in the reactors with increasing solids loading. If the jarosite precipitated from solution coated the mineral surface, it would not have been taken into account during iron analysis (Sections 3.5.4 and 3.5.5). Stott *et al.* (2000) found extensive jarosite precipitation on the surface of chalcopyrite particles during bioleaching while Konishi *et al.* (1999) found that when leaching a chalcopyrite concentrate with *Acidianus brierleyi*, all the metals in the concentrate were equally released into solution. However, after nine days, there was a decrease in the iron concentration in solution. The substantial decline in the percentage of iron leached observed after nine days was attributed by the authors to the formation of iron precipitates such as jarosite.

At 15 and 18 % quartzite loadings, the iron to copper ratio remained below 1.00 in both phases 1 and 2 of leaching. This effect was more significant at the 18 % quartzite loading. In this reactor it is proposed that chalcopyrite leaching dominated throughout the experiment, more so in phase 2 than in phase 1 where the ratio decreased further to 0.50. Chalcopyrite leaching dominated because the redox potential in this reactor lay between 460 and 510 mV from 48 to 216 h (Figure 4.14). As discussed in Section 4.5.1, these redox potentials lie within the redox potential window for optimal chalcopyrite leaching. In addition, the higher pHs (Figure 4.12) measured at this quartzite loading could have led to greater jarosite precipitation than at the other quartzite loadings. Despite the phenomena discussed here and considering the copper and iron solubilisation in conjunction, the important observation is that the reactor containing 18 % quartzite had the lowest final copper concentration in solution indicating the lowest extent of copper leaching. With respect to the copper data presented, the critical solids loading at which the leaching process became significantly affected due to hydrodynamic stress was 9 % quartzite. This adverse effect increased in magnitude as the quartzite loading increased from 9 to 18 %.

University of Cape Town

**Table 4.6a:** Iron to copper concentration ratios at 118 h (end of phase 1) for all reactors. Total suspension iron and copper concentrations measured after acid solubilisation of precipitate.

| Quartzite loading (%; w/v) | Redox potential (mV; Ag/AgCl) | Iron concentration (g $l^{-1}$) | Copper concentration (g $l^{-1}$) | Fe/Cu ratio |
|---|---|---|---|---|
| 0 | 650 | 2.85 | 2.58 | 1.10 |
| 6 | 637 | 2.56 | 2.39 | 1.07 |
| 9 | 634 | 2.51 | 2.29 | 1.10 |
| 12 | 615 | 2.28 | 2.24 | 1.02 |
| 15 | 604 | 1.37 | 1.49 | 0.92 |
| 18 | 497 | 0.60 | 0.97 | 0.62 |

**Table 4.6b:** Iron to copper concentration ratios at 216 h (end of phase 2) for all reactors.

| Quartzite loading (%; w/v) | Redox potential (mV; Ag/AgCl) | Iron concentration (g $l^{-1}$) | Copper concentration (g $l^{-1}$) | Fe/Cu ratio |
|---|---|---|---|---|
| 0 | 653 | 3.36 | 3.61 | 0.93 |
| 6 | 639 | 2.85 | 3.14 | 0.91 |
| 9 | 639 | 2.91 | 3.53 | 0.82 |
| 12 | 632 | 2.47 | 2.62 | 0.94 |
| 15 | 618 | 1.71 | 2.10 | 0.81 |
| 18 | 463 | 0.66 | 1.30 | 0.50 |

University of Cape Town

The results discussed thus far show clearly the detrimental effect of the addition of inert solids into the stirred tank after the 23 h inoculum build-up period. The reduced performance increased with increasing solids loading and the nature of the inhibition varied from decreased growth rates to decreased metal solubilisation rates. The intensity of the stress appeared to be clustered within three sets of solids loadings. The first cluster comprised the 6 and 9 % quartzite loading which appeared to perform similarly and caused a low intensity of stress to the micro-organisms. The second cluster comprised the 12 and 15 % quartzite loadings which showed significantly reduced reactor performance compared to the first 6 and 9 % solids loading cluster. Finally, at an 18 % quartzite loading a drastic decline in system performance, approaching system failure, was observed.

#### 4.6.2.6 Integration of analysis of microbial growth and mineral leaching

Further analysis of growth data as a function of solids loading are presented in Table 4.7. The duration of the growth phase increased from 48 h at the 0 and 6 % quartzite loadings to 95 and 144 h at the 9 and 12 % quartzite loadings respectively. It is postulated that because the cell concentration was lower in these reactors, the ferrous oxidation rate was slower, thus delaying the

onset of passivation of the mineral. At the 0 % quartzite concentration, a high redox potential of 640 mV was attained more rapidly (at approximately 80 h) and the mineral became passivated earlier in the time course than in the quartzite-containing reactors, resulting in nutrient limitation of the micro-organisms. Nutrient limitation caused the cells to enter the stationary phase of growth at 71 h and further nutrient limitation led to a decline in cell concentration at 118 h. Nemati and Harrison (2000) found a similar effect. Following nutrient exhaustion at the lowest solids loading (conditions of low hydrodynamic stress), they observed a sharp decrease in the biomass concentration. In the current study, the increase in redox potential to above 640 mV was delayed by approximately 72 h at 6 and 9 % quartzite loadings and at quartzite loadings above 9 %, the redox potential did not reach 640 mV during the course of the experiment.

Table 4.7 presents the biomass yield on substrate ($Y_{x/Fe}$). If the assumption is made that all ferrous iron leached from the mineral is oxidised by the cells, then the ferric iron concentration provides an estimation of the amount of ferrous iron substrate consumed by the cells. Because this estimation was used to determine the biomass yield on substrate, the $Y_{x/Fe}$ results are approximations and can only be compared within solids loading experiments in the present study and not to the impeller speed experiments or other studies in literature.

The yield was calculated as detailed in Appendix B.3. The yield of microbial cells on iron was similar across quartzite loadings of 6 to 12 %. The average normalised yield over this range was 0.66 with an error of 4.4 %. At a 15 % quartzite loading the normalised yield was higher than at the lower quartzite loadings. A possible reason for this is as discussed in Section 4.6.2.5, at the higher solids loadings, the measured iron solubilised may have been an underestimate of the true concentration of iron solubilised hence leading to a higher yield value. At a quartzite concentration of 18 %, the normalised yield was significantly lower at 0.49 compared to the other quartzite loadings. Here, even though the amount of iron solubilised may have been underestimated, the yield of cells on substrate was very low resulting in an overall decrease in $Y_{x/s}$.

University of Cape Town

**Table 4.7:** Growth parameters for 0 to 18 % w/v quartzite loading experiments operated at an impeller tip speed of 1.97 m $s^{-1}$.

| Quartzite Solids loading (%, w/v) | Length of initial growth phase (h) | Normalised $Y_{X/Fe}$ (72 h) | Error for normalised $Y_{X/Fe}$ (72 h) |
|---|---|---|---|
| 0 | 48 | 1.00 | 0.04 |
| 6 | 48 | 0.59 | 0.02 |
| 9 | 95 | 0.71 | 0.03 |
| 12 | 144 | 0.67 | 0.03 |
| 15 | 72 | 0.96 | 0.04 |
| 18 | n/a | 0.49 | 0.02 |

n/a = not applicable

The decrease in the estimated yield of cells on iron at 6, 9, 12 and 18 % quartzite compared to the baseline reactor suggest that the micro-organisms were less efficient at utilising the substrate for growth. At a quartzite loading of 0 % quartzite, where the effect of hydrodynamic stress was negligible, the culture was able to utilise the energy source efficiently for the production of biomass. Sissing (2002) reported similar trends when using a *Sulfolobus* sp. to leach 3 % w/v pyrite. The biomass yield with respect to iron solubilised decreased from 1.81 $10^{11}$cells g $Fe^{-1}$ at 0 and 6 % quartzite to 1.6 and 1.1 x $10^{11}$cells g $Fe^{-1}$ at 15 and 21 % quartzite respectively and to 0.22 x $10^{11}$ cells g $Fe^{-1}$ when the solids loading was increased to 24 % quartzite. As proposed in Section 4.6.2.3, increased hydrodynamic stress conditions can result in an increased maintenance energy requirement. Energy derived from the oxidation of iron may be directed to cell repair mechanisms instead of growth, resulting in a reduced biomass yield on iron. van Uden (1969) reported that in the absence of stress, the maintenance energy used for counteracting the stress effect will be zero and the yield will be a maximum. However, as the intensity of stress increases the amount of substrate consumed for maintenance will increase. In extreme cases where all the substrate consumed is used for maintenance, the yield will be zero and no growth will occur.

As discussed in Section 4.4.3.5, iron and copper leaching occurred in two phases (Figures 4.19 and 4.22) at all quartzite loadings. In the pyrite system studied by Nemati and Harrison (2000) dual phase leaching was only observed at pyrite loadings greater than 9 %. The change from single to dual phase leaching may be linked to increased hydrodynamic stress at the higher solids loading in the pyrite system. In the chalcopyrite system, the dual phase leaching for iron and copper observed in all reactors was linked to nutrient limitation as well as to increased solids loading. The effect of nutrient limitation causing a decline in the iron solubilisation rate is illustrated in Figure 4.25. At a 9 % total solids loading, the rate of iron solubilisation remained constant throughout the experiment for the pyrite system (no nutrient limitation) with 88 % of the iron solubilised after 357 h. In contrast, the chalcopyrite system showed a change in the solubilisation

University of Cape Town

rate after approximately 118 h and at this stage only 30.5 % of the iron was solubilised from the mineral.

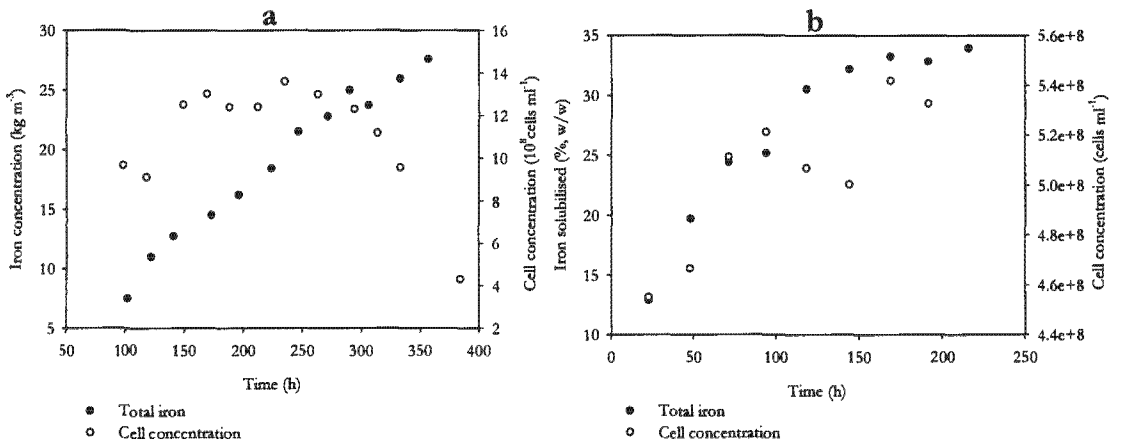


**Figure 4.25:** Iron solubilisation and cell concentration as a function of time for a total solids loading of 9 %. (a) Nemati and Harrison (2000) (b) Present study.

Dual phase leaching due to increased hydrodynamic stress in both systems is observed in Figure 4.26 where at a 15 % total solid loading, the iron solubilisation rate in the pyrite system decreased after 177 h. Only 70 % of the mineral was solubilised at this stage. In the chalcopyrite system, as observed for the 9 % solids loading, the change in solubilisation rate for the 15 % total solids loading occurs after 118 h, however at this stage only 27.5 % the mineral was solubilised compared to 30.5 % at 9 % total solids illustrating the effect of primarily nutrient limitation at 9 % total solids loading and the concomitant effect of nutrient limitation and hydrodynamic stress at a 15 % total solids loading. Rubio and García Frutos (2002) also found dual phase leaching with increasing solids loading when leaching chalcopyrite. Figure 4.27 illustrates the change from single phase leaching at 1 % w/v chalcopyrite to dual phase leaching at 15 and 20 % chalcopyrite.

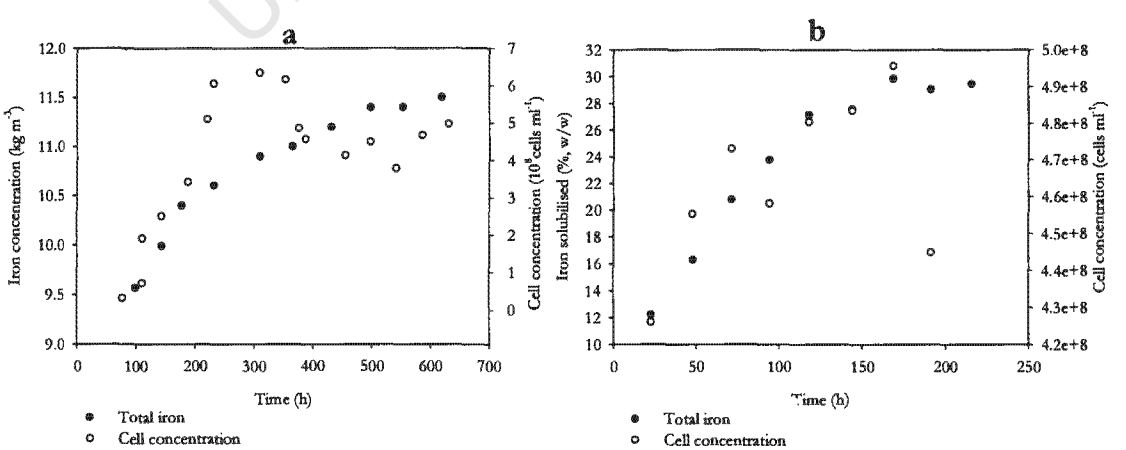


**Figure 4.26:** Iron solubilisation and cell concentration as a function of time for a total solids loading of 15 %. (a) Nemati and Harrison (2000) (b) Present study.

University of Cape Town

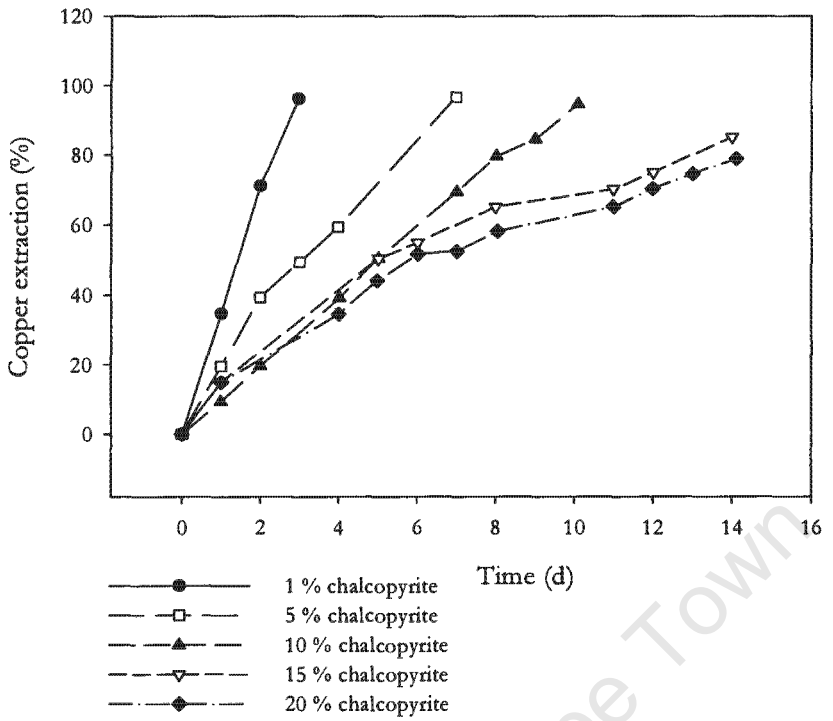


**Figure 4.27:** Copper extraction during chalcopyrite leaching (adapted from Rubio and García Frutos 2002).

University of Cape Town

#### 4.6.2.7 Comparison of results to literature studies

The adverse effects of increased solids loading in slurry reactors have been identified by several researchers (Gómez *et al.*, 1994; Nemati and Harrison, 2000; Chong *et al.*, 2002; Sissing and Harrison, 2003). In most experiments, the effects of increased mineral concentration were investigated. Some authors postulated that, despite the concomitant effects (e.g. oxygen mass transfer limitations and the build-up of toxic leach products) posed by increasing the mineral concentration and not using inert material to bulk up solids, hydrodynamic stress could still be identified as having a profound effect on the mineral leach rate (Torma *et al.*, 1970; Nemati and Harrison, 2000; Brandl, 2001; Valencia *et al.*, 2003). In this section the results obtained in the present study are compared to those in literature where hydrodynamic stress was concluded to have the greatest effect on process performance. The experimental conditions utilised by the different investigators are presented in Table 4.8. It is important to note that although Gómez *et al.*, 1994 conducted experiments in shake flask culture, where oxygen limitation may occur and shear forces may be lower,

**Table 4.8:** Experimental conditions utilised in the various solids loading studies.

| Reference | Reactor | Solids fraction | Size range (μm) | Agitation rate (rpm) | Shear rate ($s^{-1}$) | Solids loading (%; w/v) |
|---|---|---|---|---|---|---|
| Gomez *et al.*, 1994 | Shake flask | Chalcopyrite only | Not given | 100-200 | 16.7-33.3 | 1-7 |
| Nemati and Harrison, 2000 | STR | Pyrite only | 53-75 | 500-550 | 83.3-91.7 | 3-18 |
| Witne and Phillips, 2001 | STR | Chalcopyrite only | $d_{90}$ 112 μm | 200 | 33 | 3-40 |
| Sissing, 2002 | STR | Pyrite and quartzite | 38-75 | 560-760 | 93.3-126.7 | Pyrite : 3<br>Quartzite : 0-24 |
| Rubio and García Frutos, 2002 | STR | Chalcopyrite | $d_{80}$ 20μm | 130 | 21.6 | 1-20 |
| Valencia *et al.*, 2003 | Shake flask | Pyrite only | 38-75 | 220 | 36.7 | 2.5-15 |
| Present study | STR | Chalcopyrite and quartzite | 38-75 | 550-700 | 91.7-116.7 | Chalcopyrite: 3<br>Quartzite: 0-18 |

Gomez *et al.* (1994) studied the effect of solids loading on the bioleaching of chalcopyrite by a *Sulfolobus*-like micro-organism and found similar changes in pH with increased hydrodynamic stress to those obtained in the present study (Figure 4.28). At the higher solids loadings the pH increased, indicating reduced microbial activity. At the lower solids loadings of 1 % chalcopyrite there was initial increase in pH over the first 24 h followed by a decrease in pH from 1.5 to approximately 0.87 at 190 h. At a 3 % solids loading, the pH increased over the first 24 h and then proceeded to decrease from a pH of 1.75 to a pH of 1.4 at 190 h over the remainder of the experiment. At the higher solids loadings of 5 and 7 % chalcopyrite, the pH rose over the first 48 h and then remained constant at a pH of approximately 1.9 until the end of the experiment.

University of Cape Town

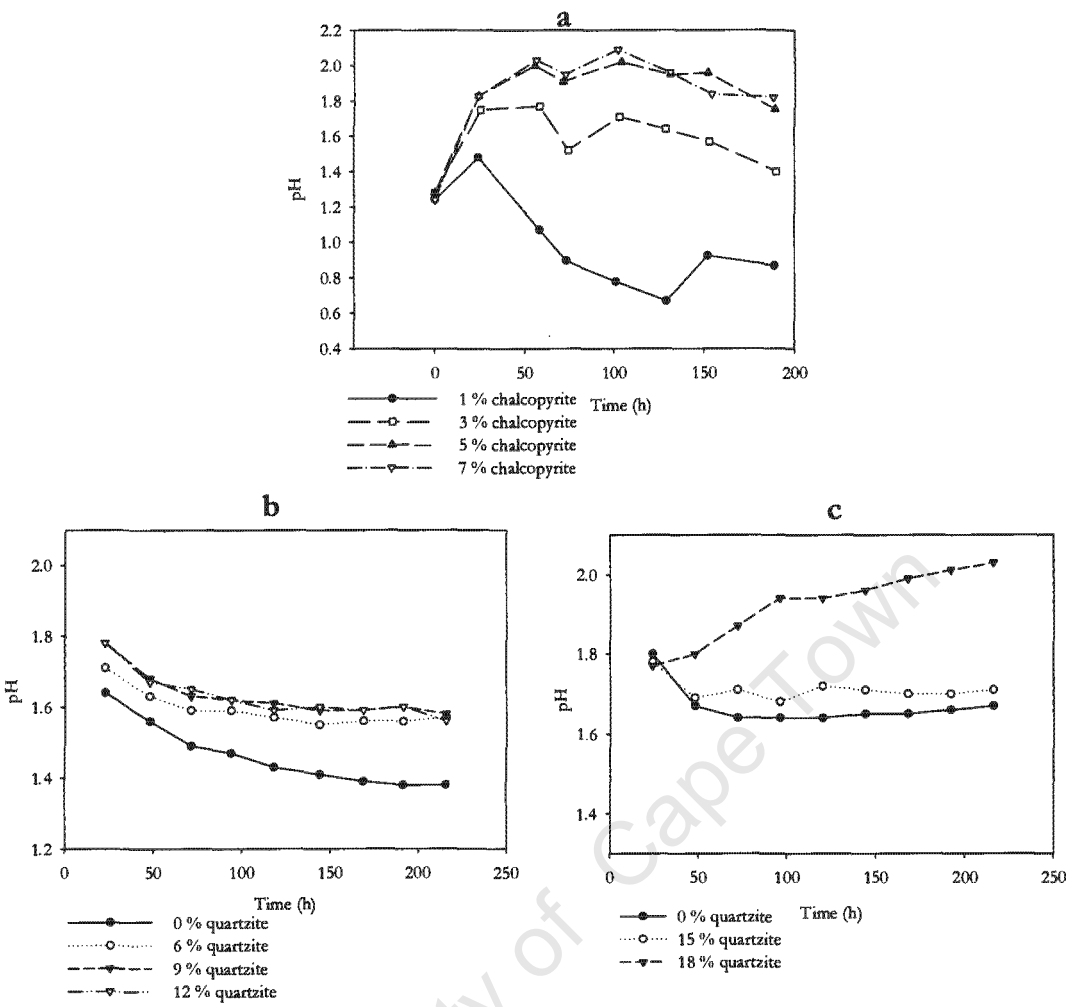


**Figure 4.28:** Effect of solids loading on solution pH for (a) the study of Gomez *et al.* (1994), and (b) 0, 6, 9 and 12 % quartzite for the present study and (c) 0, 15 and 18 % quartzite for the present study.

University of Cape Town

In the present study, increasing solids loading caused a decrease in the solution redox potential. Similar observations were reported by Witne and Phillips (2001) and Nemati and Harrison (2000). Witne and Phillips (2001) investigated the leaching of a primarily chalcopyrite concentrate by a *Sulfolobus* culture in shake flasks. The maximum redox potentials observed, in the absence of oxygen limitation, were 612, 606, 597 mV for 3, 10 and 20 % w/v chalcopyrite loadings respectively. They concluded that one explanation for the low redox potential observed with increased solids concentrations was shear stress to the cell caused by increased solids loading.

Nemati and Harrison (2000) found that at pyrite solids loading of 3 and 6 % w/v, the redox potential increased from 450 to 600 mV during the bioleaching process. At a 9 and 12 % solids loading, the redox potential only increased from 450 to 500mV with a sharp increase during the

final stages of the process. At 15 and 18 % solids loading, the redox potential remained constant between 400 and 450 mV. Although the redox potential is also highly dependent on the quantity of mineral, these data also indicate a decline in the ability of the cells to oxidise ferrous iron as the solids loading increased. This was confirmed by comparison of the ferrous iron and ferric iron concentrations in solution. Two mechanisms were proposed for the lower redox potential values at high solids loadings. Firstly, the low cell to solid ratio may have resulted in limitation of the ferrous oxidation step leading to a decrease in the ferric to ferrous iron ratio and thus low redox potentials. Redox potentials below 500 mV do not support high pyrite dissolution rates. Secondly, intense hydrodynamic stress to the micro-organisms may have caused a decline in the specific microbial ferrous oxidation rate. Severe hydrodynamic stress was proposed as the dominant mechanism for reduced leaching at 15 and 18 % solids loading.

Gomez *et al.* (1994) studied the effects of solids loading on cell concentration. Their results, presented in Figure 4.29, are similar to those obtained in the present study. The authors found a decrease in the rate and extent of growth with increasing chalcopyrite loading across the range 1 to 7 % w/v. The extent of growth declined from 8.5 x $10^8$ to 6.2 x $10^8$ cells $ml^{-1}$ at 1 and 7 % chalcopyrite loadings respectively. At a 7 % chalcopyrite loading, there was growth up to 100 h after which growth ceased and a sharp decline in cell concentration was observed.

University of Cape Town

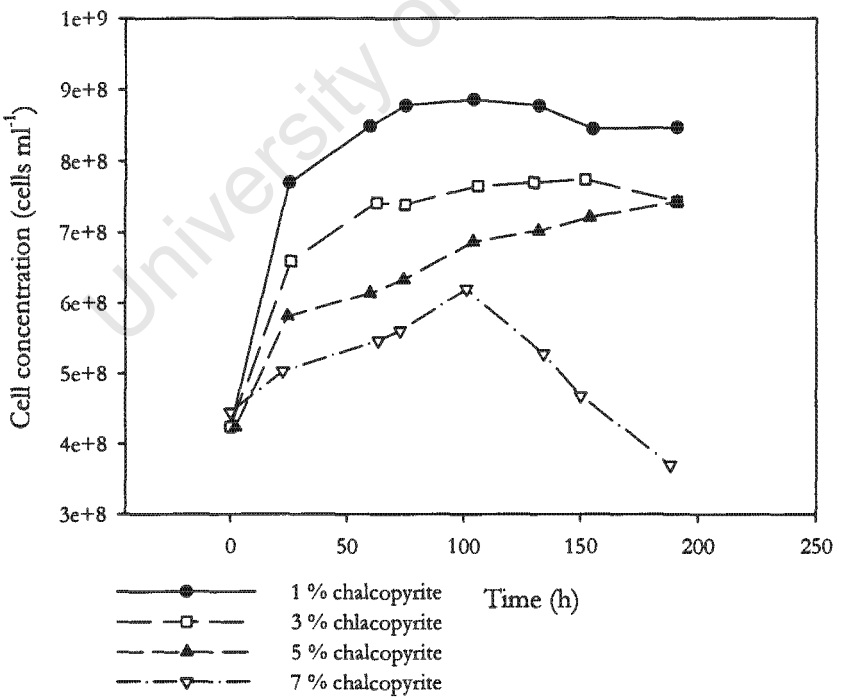


**Figure 4.29:** The effect of chalcopyrite loading on cell concentration (adapted from Gomez *et al.*, 1994).

Sissing and Harrison (2003) investigated the effect of quartzite loading on the leaching of pyrite by *S. metallicus* and found similar apparent specific growth rates over the first 50 h of the experiment for quartzite loadings of 0 to 15 %. The apparent specific growth rates ranged from 0.016 to 0.020 $h^{-1}$ for 0 to 15 % quartzite loadings. No difference in the apparent specific growth rate between the reactor with 0 % quartzite and the reactors containing 12 and 15 % quartzite was observed. This result indicates no influence of solids loading on the growth of the cells over the first 50 h of the experiment. These data differ to those obtained in the present study where on addition of quartzite to the reactors the apparent specific growth rate declined from 0.005 $h^{-1}$ at a 0 % quartzite loading to 0.004 and 0.003 $h^{-1}$ at 6 and 9 % quartzite loadings respectively. Increasing the quartzite loading above 9 % caused a further decline in the apparent specific growth rate to 0.002 and 0.001 $h^{-1}$ at 12 and 15 % quartzite loadings.

Valencia *et al.* (2003) studied the effects of increasing solids loading on pyrite dissolution by *S. metallicus* in shake flasks. A high percentage of iron solubilisation was obtained for the lower pyrite loadings of 2.5 and 5 % w/v while solids loadings above 15 % negatively influenced pyrite oxidation. Although, unlike the present study and the study of Sissing and Harrison (2003), the mineral concentration was not standardised in the experiments, increased mechanical stress was considered as one of the factors contributing to lower leach rates.

Figure 4.30 shows the iron solubilisation results of Gomez *et al.* (1994). As observed in the current study and by other investigators, the authors found a decrease in percentage iron solubilised with increasing solids loading. The rate of iron solubilisation decreased with increasing solids loading and ultimately affected the extent of solubilisation.

University of Cape Town

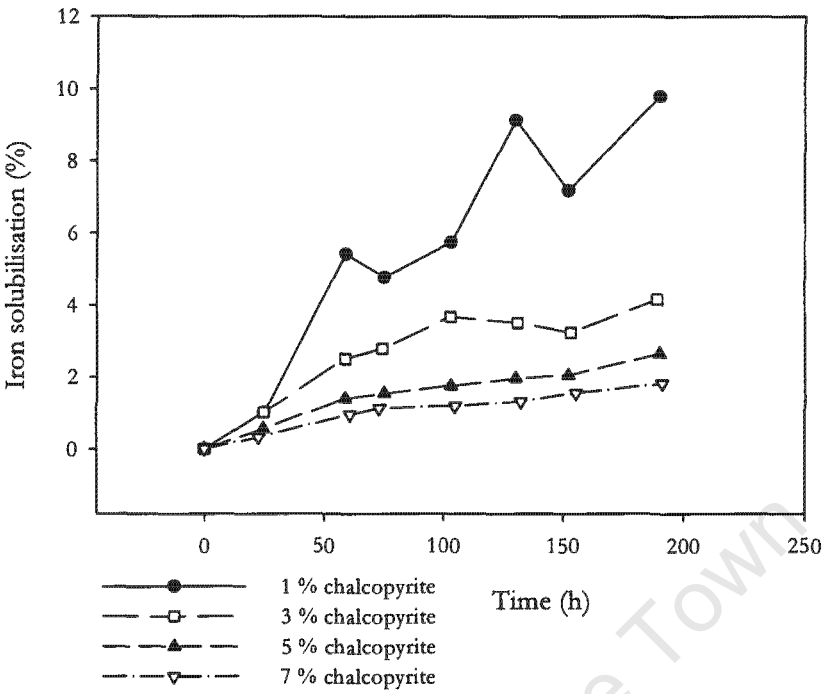


**Figure 4.30:** The effect of chalcopyrite loading on iron solubilisation (adapted from Gomez *et al.*, 1994).

The iron solubilisation results obtained in the present study are compared to results obtained in studies by Gomez *et al.* (1994), Nemati and Harrison (2000), Sissing (2002) and Valencia *et al.* (2003) in Figure 4.31. The solids phases comprised either chalcopyrite only, pyrite only or pyrite and quartzite of the 38-75 μm size fraction. For each study, the data were normalised by dividing results reported for the higher pulp densities by those reported for the lowest pulp density (3, 3, 3, 5, 1 % for Nemati and Harrison, 2000; Sissing, 2002; present study; Valencia *et al.*, 2003 and Gomez *et al.*, 1994 respectively).

University of Cape Town

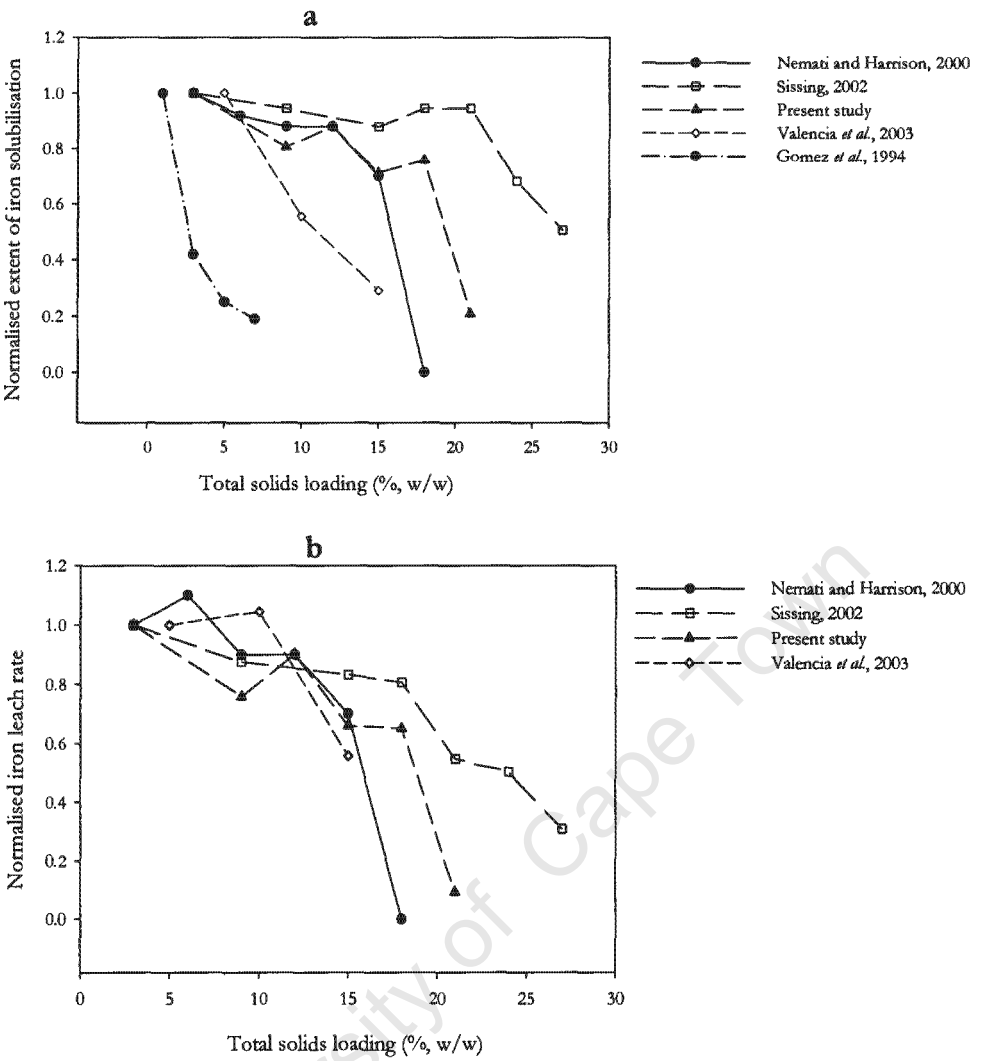


**Figure 4.31:** Comparison of leach parameters determined for pyrite (Nemati and Harrison, 2000, Sissing, 2002 and Valencia *et al.*, 2002) and chalcopyrite (present study and Gómez *et al.*, 1994) at various solids loadings.

University of Cape Town

For both the extent of iron solubilisation as well as the overall iron leach rate, the trends observed by Sissing (2002) and the present study were similar. In both investigations the solids fraction comprised 3 % concentrate (pyrite or chalcopyrite) and the remainder inert quartzite. The overall extent of iron solubilisation was lower for all solids loadings in the chalcopyrite study compared to the pyrite study. This is expected due to the recalcitrance of chalcopyrite to biological leaching. The results also show that the negative impact of hydrodynamic stress was observed at a lower solids loading in the chalcopyrite system compared to the pyrite system. From Figure 4.31, the critical solids loading for the pyrite system was 15 % quartzite (18 % total solids loading) while the critical solids loading for chalcopyrite system was 9 % quartzite (12 % total solids loading). It is postulated that nutrient stress due to passivation in the chalcopyrite system compounded the

effect of hydrodynamic stress causing higher levels of cell trauma at lower solids loadings. The study by Nemati and Harrison (2000) used only pyrite as the solids phase. At solids loadings up to 12 %, where hydrodynamic stress was less significant, the extent of iron solubilisation and the iron leach rate follow the same trend as the present study and the work by Sissing (2002). At 15 % pyrite loading there was a decrease in the normalised extent of iron solubilised and at an 18 % pyrite loading and complete solids suspension, there was complete system failure. The data of Sissing (2002) and the present study show continued leaching up to a total solids loadings of 27 and 21 % indicating that, unlike the study of Nemati and Harrison (2000), complete system failure did not occur.

The solids loadings at which leaching was significantly impaired were lower in the pyrite-only studies than in the studies using a constant mineral concentration and quartzite. Further, some of the experimental conditions employed by Nemati and Harrison (2000) were different to those used in the quartzite-mineral systems. These differences in terms of experimental protocol included a smaller inoculum size while the physicochemical differences intrinsic to increasing the mineral loading are postulated to be (i) decreased oxygen availability due to oxygen scavenging by the mineral; (ii) an increase in the amount of solubilised metal concentration which may be inhibitory; (iii) the adverse effects of increased ionic strength and (iv) a decline in pH to less than pH 1 leading to a decline in microbial activity (Bailey and Hansford, 1993a; Nemati and Harrison, 2000; Witne and Phillips, 2001). In order to assess the effect of these differences, Sissing (2002) repeated the 18 % pyrite loading experiment conducted by Nemati and Harrison (2000). The author used a larger inoculum size and attained improved mass transfer by changing the reactor configuration. Similar results were obtained in the repeat experiment. Inoculum size was discounted as a reason for reactor failure and no decisive conclusion was possible regarding mass transfer. Sissing (2002) compared results obtained for the repeat pyrite-only experiment to her pyrite-quartzite experiment conducted at an 18 % solids loading. The two systems were compared on the basis of iron concentration, solution pH, redox potential, mass transfer coefficient, and particle density (specific gravity). The author concluded that at an 18 % solids loading, the first five effects did not contribute to the reduced pyrite solubilisation observed in the pyrite-only system. Instead, the difference in density of pyrite and quartzite was cited as a contributing factor. The density of a particle affects its momentum. Momentum is a function of particle size, particle density and agitation speed and is a product of the particle mass and the impeller tip speed. Since the particle size and agitation speed of the two systems were similar, the momentum was postulated to vary with particle density. In all experiments conducted by Sissing (2002), the momentum of the $d_{50}$ pyrite and quartzite particles was calculated to be $3.21 \times 10^{-9}$ and $4.20 \times 10^{-10}$ kg m $s^{-1}$ respectively. The pyrite-only system had a higher particle momentum which led to particle-cell-particle collisions with higher momentum. Thus the reduced pyrite

University of Cape Town

solubilisation observed by Sissing (2002) and Nemati and Harrison (2000) at an 18 % pyrite loading may be attributed to increased particle density and possibly mass transfer limitations. Bailey and Hansford (1994) confirmed that mass transfer limitations occur at increased pyrite loadings. The authors investigated oxygen demand in agitated high sulphur pyrite slurries at mesophilic temperatures in an STR. They showed that at a solids concentration less than 13.6 % w/v the system was not oxygen limited. However, increasing the pyrite concentration above 13.6 % was predicted to induce oxygen limitation in the system.

The results of an investigation by Valencia *et al.* (2003) who leached pyrite using *S. metallicus* are also presented in Figure 4.31. The normalised maximum rates and extents of iron solubilisation are presented. There was a sharp decrease in the extent of leaching with increasing pyrite loading from 5 to 15 % w/v. The maximum iron solubilisation rate increased with increasing pyrite loading from 5 to 10 % and decreased at the 15 % pyrite loading. This adverse effect on the extent of leaching observed at a lower solids loading could be because Valencia *et al.* (2003) used shake flask reactors while STRs were employed in the other three studies. Valencia *et al.* (2003) conducted experiments in Erlenmeyer flasks which were rotated at 220 rpm on an orbital shaker. Complete solids suspension and optimal mass transfer are difficult to obtain in shake flask reactors at low shear rates. At the speeds employed in the various studies, the shear rates were lower in shake flasks than in the STRs. If slurry remains at the bottom of the flask, it reduces mixing and oxygen transfer capacities within the flask (Lotter and Büchs, 2004). Scholtz-Brown (1998) showed that when solids are incompletely suspended, the mechanism of cell damage changes from collisions between cells and particles to disruption by grinding of solid particles against each other. This change in mechanism of cell damage as well as reduced mass transfer in the flask reactors could account for the difference observed between data reported by Nemati and Harrison (2000) and Valencia *et al.* (2003). Gomez *et al.* (1994) also studied the effect of increasing solids loading in shake flask culture and found a decrease in the extent of iron solubilisation with increasing solids loading from 1 to 7 %. The extent of leaching at a 3 % chalcopyrite loading decreased sharply to 0.4 fold that at a 1 % chalcopyrite loading. Nutrient limitation, increased hydrodynamic stress as well as oxygen mass transfer are possible reasons for the poor leaching in the flasks containing 3, 5 and 7 % chalcopyrite.

A summary of the critical solids loadings at which the transition between varying intensities of hydrodynamic stress occur for the studies discussed is presented in Table 4.9. The results show clearly that cultures grown in flasks are more sensitive to changes in solids loading than those grown in STRs. In addition, the results of Sissing (2002) compared to those obtained in the present study and Nemati and Harrison (2000) show that the chalcopyrite-quartzite system and pyrite system are more sensitive to increases in solids loading than the pyrite-quartzite system.

University of Cape Town

Furthermore, the system of Gomez *et al.* (1994) failed as a lower solids loading than the system of Vaencia *et al.* (2003). This confirms that in the chalcopyrite systems, nutrient limitation compounds the hydrodynamic stress effect.

**Table 4.9:** Critical solids loadings (total solids) defined by the intensity of hydrodynamic stress for thermophilic bioleaching laboratory studies.

| Reference | Reactor type and scale | Mineral | Critical solids loading (%; w/v) | | | |
|---|---|---|---|---|---|---|
| | | | No Effect or Minor Effect | Moderate Effect | Large Effect | Reactor failure |
| Gomez *et al.*, 1994 | Shake flask; n/g | Chalcopyrite | 1 | 3 | 5, 7 | > 7 |
| Nemati and Harrison, 2000 | STR; 1 litre | Pyrite | 3 to 12 | 15 | n/a | 18 |
| Sissing, 2002 | STR; 1 litre | Pyrite | 3 to 18 | 21-24 | 27 | > 27 |
| Valencia *et al.*, 2003 | Shake flask; 1 litre | Pyrite | 2.5 and 5 | 10 | 15 | > 15 |
| Present study | STR; 1 litre | Chalcopyrite | 3 to 9 | 9-18 | 21 | > 21 |

n/a = not applicable

#### 4.6.2.8 Recovery

In order to determine whether a culture exposed to the effects of hydrodynamic stress can recover or adapt to the stressful conditions, a 456 h experiment was conducted at a 15 % quartzite loading. It is postulated that, on average, there were three phases of leaching in the quartzite experimental runs discussed in Sections 4.6.2.1 to 4.6.2.5. The three phases for a 15 % quartzite experiment are shown in Figure 4.32. In phase 1, the culture required a period of acclimatisation to the addition of quartzite to the reactor. The start of phase 2, depended on the concentration of quartzite added and was delayed as the solids loading increased. In phase 2 the cells acclimatised to the presence of solids and the extent of recovery depended on the percentage solids added. In phase 3 (not visible for all the solids loadings), the process performance started to decline possibly due to prolonged exposure to stress. The decline in system performance was also linked to mineral passivation, which was the primary cause of nutrient limitation.

University of Cape Town

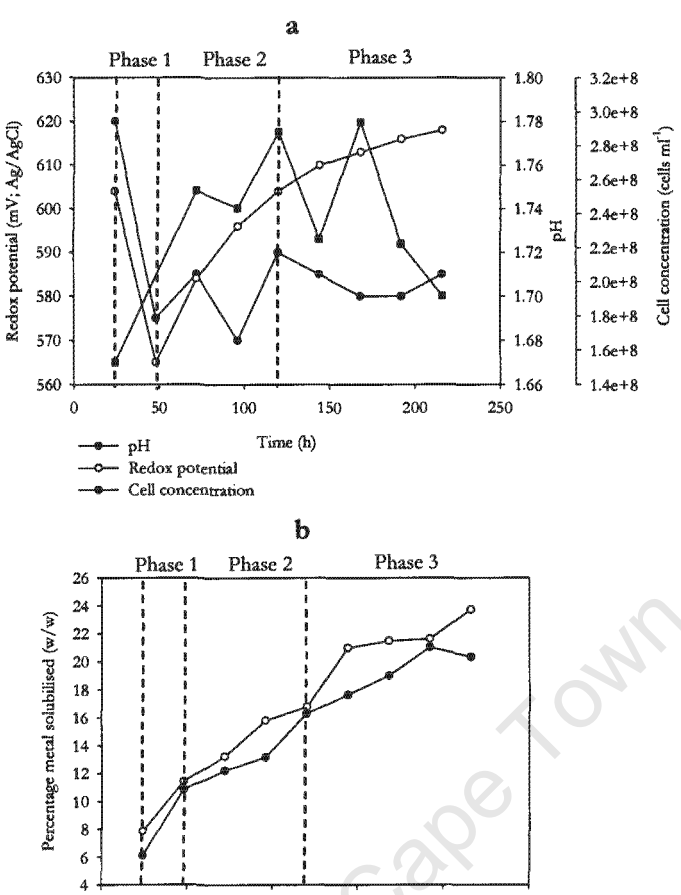


**Figure 4.32:** Time profiles, for (a) redox potential, pH and cell concentration, and (b) metal solubilisation, at a solids loading of 15 % quartzite and 3 % chalcopyrite and an impeller tip speed of 1.97 m $s^{-1}$.

In order for full recovery to occur, the culture must remain viable and consequently the extent of cell damage and the microbial response mechanisms to hydrodynamic stress are important factors. It is clear from the data presented in Sections 4.6.2.1 to 4.6.2.5 that the addition of quartzite adversely affected the rate and extent of bioleaching. Increasing the amount of quartzite added to each reactor also increased the extent of the adverse effect. However, despite these negative effects, complete reactor failure did not occur in the solids loading range investigated. Figure 4.33 shows the change in pH, redox potential, cell concentration and iron and copper solubilisation from 216 to 456 h at a 15 % quartzite loading.

University of Cape Town

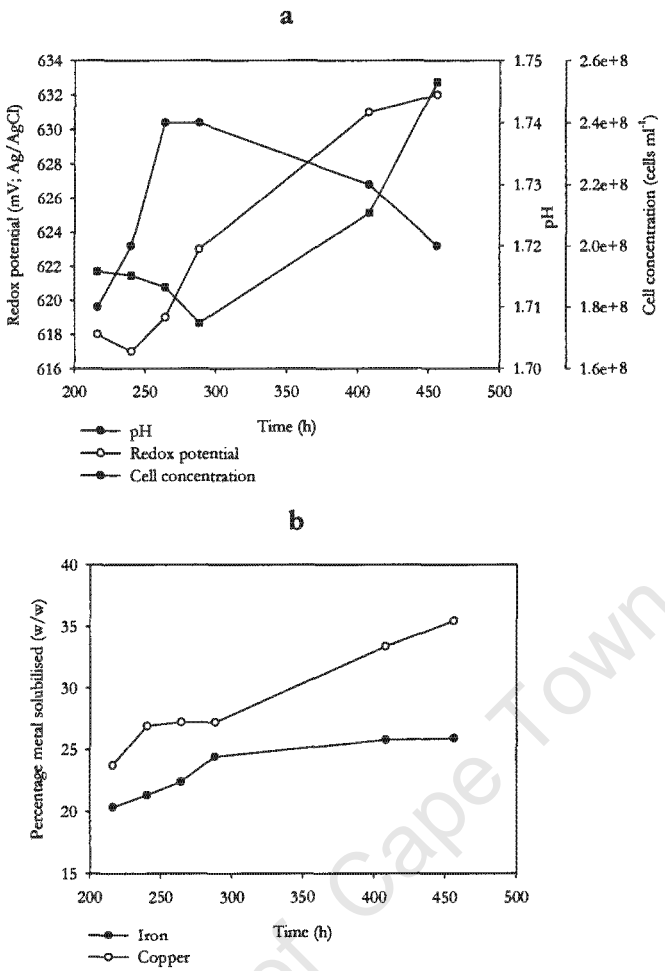


**Figure 4.33:** Extended time profiles for (a) redox potential, pH and cell concentration, and (b) metal solubilisation, at a solids loading 15 % quartzite and 3 % chalcopyrite and an impeller tip speed of 1.97 m $s^{-1}$.

University of Cape Town

The reactor was run for 240 h longer than the average 215 h experiment to determine whether process performance would improve or whether reactor failure would occur. Between 240 and 456 h the reactor performance appeared to improve. The following changes were noted:

(i) An increase in the redox potential from 240 to 456 h indicating the oxidation of ferrous iron

(ii) An increase in the cell concentration from 288 to 456 h indicating cell growth

(iii) An increase in iron and copper solubilisation

The percentage iron solubilised increased from 20.4 % at 216 h to 25.9 % at 456 h. The rate of copper leaching was higher during this time with an increase from 23.7 to 35.5 % in the percentage copper solubilised. Thus, the overall process performance increased showing the ability of the cells to recover from the negative effect of the increased quartzite loading. These

data also suggest the presence of repair and adaptation mechanisms. Other investigators have observed the adaptation of cells to increased hydrodynamic stress. Allan *et al.* (1988) found that over a period of approximately twelve months, *Picrasma quassioides* plant cells were able to develop shear resistance. A suspension culture exposed to an agitation rate of 440 rpm (shear rate of 73 $s^{-1}$) in a STR failed to grow after 2.5 h of exposure to these hydrodynamic conditions. Approximately 12 months later the culture showed improved growth. In addition, no loss of viability was observed when the cells were exposed to a shear rate of 1.67 $s^{-1}$.

## 4.6.3 CONCLUSIONS

In this section, the effect of increasing solids loading on the bioleaching of chalcopyrite by a *Sulfolobus* culture was reported. Increasing solids loading by increasing the inert quartzite concentration caused a decline in process performance as measured by changes in pH, redox potential, cell concentration, and iron and copper solubilisation. The data presented for the 6 and 9 % quartzite loadings show very similar overall process performance when compared to the baseline (0 % quartzite). At the 12 and 15 % quartzite loadings a further decrease in process performance compared to the baseline reactor was observed. The reactor containing 18 % quartzite solubilised the least amount of copper and iron. Even though intensive hydrodynamic stress was applied, complete reactor failure did not occur. Furthermore, results discussed in Section 4.6.2.8 show that, with time, system recovery was possible.

Reviewing the process data presented in this section enables the identification of the critical solids loading at which the leaching process becomes adversely affected due to hydrodynamic stress. This critical solids loading is proposed to be 9 % w/v quartzite in the presence of 3 % chalcopyrite in this laboratory study. The sensitivity of the indicators used to measure the effects of hydrodynamic stress is an important consideration. Some assays, for example cell concentration, are more sensitive indicators of the effects of hydrodynamic stress than pH or redox potential measurements. Copper dissolution was a more accurate indicator of the process performance than iron dissolution due to the precipitation of iron causing underestimation of the iron concentration. Lamaignére (2002) studied the influence of solids loading on the growth of *Saccharomyces cerevisiae*. She reported that the critical solids loading for cell damage varied between 0.5 and 1 % depending on the parameter used as an indicator. Using $\mu_{max}$ as an indicator showed that solids loading exhibited a negative effect on growth at a loading greater than 1 % w/v; however indicators such as the yield of cells on glucose and the length of the lag phase yielded a critical solids loading of 0.5 %. Similar observations apply in the current study.

University of Cape Town

The primary mechanism of cell damage in the present study reactor is proposed to be solid-cell-solid interactions. This conclusion is supported by the literature study (Section 2.2.2.3) where it was shown that the dominant mechanism of cell damage in slurry systems is proposed by several researchers to be solid-cell-solid interactions. In the present study, it was not possible to conduct experiments in the absence of solids to confirm the contribution of other mechanisms to cell damage because chalcopyrite was required as the microbial energy source. However, previous studies conducted with yeast cells in the presence and absence of particles have shown that negligible cell disruption occurs in the absence of solids (Pearce, 1993; Scholtz-Brown, 1998; Lamaignére, 2002) and the primary mechanism of damage is contact between cells and particulates.

As mentioned in Section 4.6.2.7, the rate at which cells contact with solids particles in the reactor is dictated by the particle momentum which in turn is influenced by the impeller tip speed. Increasing impeller tip speed would increase both the rate frequency at which particles collide with each other and with cells in the reactor as well as the momentum transfer of the collision. In Section 4.7 the influence of impeller tip speed on process performance is examined.

University of Cape Town

## 4.7 THE EFFECT OF IMPELLER TIP SPEED ON THE BIOLEACHING OF CHALCOPYRITE BY A SULFOLOBUS sp.

The effect of three impeller tip speeds namely, 1.67, 1.97, and 2.13 m $s^{-1}$, on the bioleaching of chalcopyrite by a *Sulfolobus* culture was determined at quartzite loadings of 0 and 9 % w/v. Two sets of experiments were conducted. In the first set, the solids loading was maintained at 3 % chalcopyrite with no quartzite and the impeller tip speed was varied in the range 1.67 through to 2.13 $ms^{-1}$. In the second set, the solids loading was maintained at 3 % chalcopyrite with 9 % quartzite and the impeller tip speed was varied in the range 1.67 through to 2.13 m $s^{-1}$. For both sets of experiments, the baseline reactor contained 3 % w/v chalcopyrite and no quartzite and was operated at an impeller tip speed of 1.67 m $s^{-1}$.

The impeller tip speeds used exceeded the critical impeller speed required for complete solids suspension at the highest solids loading. Experiments were run under the same conditions as those discussed in Section 4.6 except that the impeller speed was increased after 48 h as opposed to 23 h. Detailed experimental methodology is given in Sections 3.4 and 3.6. Reactors were operated over an 8 day period and maintained at approximately 68°C. Solution pH, redox potential, and cell, iron and copper concentrations were measured on a daily basis. In this section

it was not necessary to normalise the process data since all experiments were run simultaneously. Selected data are presented in Figure 4.41 for the first set of experiments while detailed results for the second set of experiments are presented in Figures 4.34 to 4.40. The data pertaining to the power input per unit volume corresponding to each impeller tip speed and solids loadings utilised in these experiments are detailed in Appendix D.

### 4.7.1 THE EFFECT OF AGITATION RATE ON SLURRY pH

Figure 4.34 illustrates the change in solution pH as a function of time for a 0 % quartzite loading operated at an impeller tip speed of 1.67 m $s^{-1}$ and a 9 % quartzite loading operated at impeller tip speeds of 1.67, 1.97 and 2.13 m $s^{-1}$. During the inoculum build-up phase (0 to 48 h), the pH in all reactors increased to the same extent of approximately 0.2 pH units. The addition of solids and increasing the agitation intensity at 48 h to cause complete suspension of the particulate phase resulted in a sharp decrease in solution pH by approximately 0.3 to 0.4 pH units between 48 and 72 h. At a solids loading of 0 % quartzite, the pH remained constant at approximately pH 1.45 from 72 h to the end of the run. After 72 h the pH in the reactors containing 9 % quartzite increased and subsequently remained constant from 120 h to 192 h. The rate and extent of increase in pH was indirectly proportional to the impeller tip speed applied. At a 9 % quartzite loading, the pH reached a maximum of pH 1.67, 1.69 and 1.80 at tip speeds of 1.67, 1.97 and 2.13 m $s^{-1}$ respectively.

The increase in solution pH in the reactors containing 9 % quartzite coincided with increased hydrodynamic stress imposed by increasing the impeller tip speed and solids loading. As discussed in Section 4.6, this increased hydrodynamic stress combined with ferrous iron limitation (especially post 96 h) owing to passivation of the chalcopyrite caused an increase in pH due to limited elemental sulphur oxidation.

University of Cape Town

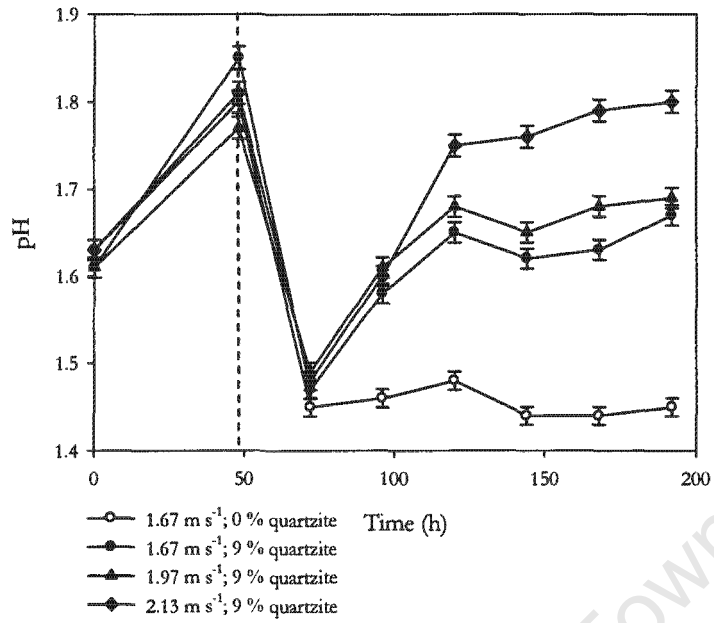


**Figure 4.34:** Change in solution pH in the presence of 3 % chalcopyrite and 0 and 9 % w/v quartzite and impeller tip speeds of 1.67, 1.97 and 2.13 m $s^{-1}$. Dotted line indicates the onset of the specified experimental conditions.

University of Cape Town

### 4.7.2 THE EFFECT OF AGITATION RATE ON SLURRY REDOX POTENTIAL

The change in the ferric to ferrous iron ratio, illustrated by the change in the solution redox potential, is presented in Figure 4.35. The final redox potential attained in the experimental reactors at 192 h was inversely proportional to the intensity of hydrodynamic stress applied. Redox potential increased similarly in all reactors during the inoculum build-up phase prior to the increase in impeller tip speed and the addition of quartzite. An increase from approximately 460 mV to approximately 540 mV was observed. For the reactors containing 0 and 9 % quartzite operated at an impeller tip speed of 1.67 m $s^{-1}$, the redox potential continued to increase to 615 mV for a 0 % quartzite loading and 588 mV for 9 % quartzite loading at 144 h.

At a 9 % quartzite loading and an impeller tip speed of 1.97 m $s^{-1}$, the redox potential decreased for the first 24 h after the inoculum build-up phase. Thereafter, it remained constant for 48 h at approximately 528 mV and increased gradually until the end of the run reaching 540 mV at 192 h. The decrease in redox potential may be attributed to an increase in the ferrous iron concentration due to a decline in the biological ferrous iron oxidation rate as a consequence of the increased solids loading and agitation rate corresponding to increased energy dissipation in the reactor. The culture appeared to recover after 120 h, at which point the redox potential proceeded to increase

with a concomitant decrease in the solution pH. Complete system recovery was not observed within the time frame of the experiment (192 h).

The redox potential in the reactor containing 9 % quartzite operated at 2.13 m $s^{-1}$ decreased from 532 mV at 48 h to 470 mV at the end of the run. The ferrous iron concentration in solution increased to approximately 0.12 g $l^{-1}$ and remained at this concentration for the duration of the experiment. As observed at a 9 % quartzite loading and an impeller tip speed of 1.97 m $s^{-1}$, increasing the impeller tip speed caused a reduction in the biological ferrous iron oxidation rate, indicating impaired microbial function and leading to an increase in ferrous iron concentration and a decrease in the solution redox potential. No apparent recovery was observed at a 9 % quartzite concentration and an impeller tip speed of 2.13 m $s^{-1}$.

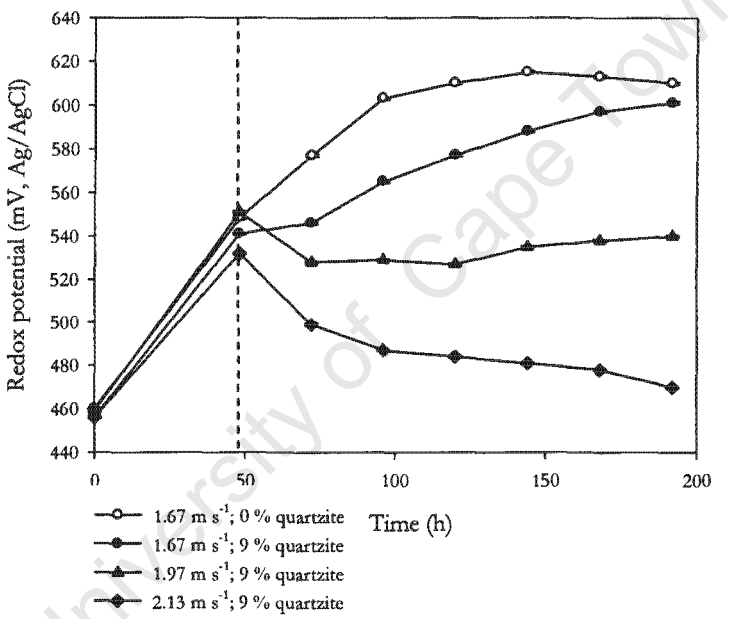


University of Cape Town

**Figure 4.35:** Change in redox potential in the presence of 3 % chalcopyrite and 0 and 9 % w/v quartzite and impeller tip speeds of 1.67, 1.97 and 2.13 m $s^{-1}$. Dotted line indicates the onset of the specified experimental conditions.

### 4.7.3 THE EFFECT OF AGITATION RATE ON THE PLANKTONIC CELL CONCENTRATION

The planktonic cell concentration was also adversely affected by the increase in solids loading and agitation intensity (Figure 4.36). During the inoculum build-up phase, the cell concentration increased similarly in all reactors from approximately 7.5 x $10^7$ to approximately 1.8 x $10^8$ cells $ml^{-1}$. The rate and extent of growth declined on addition of quartzite to the experimental reactors and increasing the impeller speed after the inoculum build-up phase.

In the reactor containing 0 % quartzite and operated at an impeller tip speed of 1.67 m $s^{-1}$, the cell concentration increased to 4.4 x $10^8$ cells $ml^{-1}$ at 120 h. Increasing the solids loading and impeller tip speed caused a reduction in cell growth. From 48 to 72 h no growth was observed at a tip speed of 1.67 m $s^{-1}$ and cell death occurred at a tip speed of 1.97 m $s^{-1}$. Subsequent to this, a growth phase was observed in both reactors. This growth phase was followed by stationary and death phases. For the reactor containing 9 % quartzite and operated at 2.13 m $s^{-1}$, no growth phase was observed. Cell death occurred over the first 24 h after the increase in impeller tip speed and the addition of solids. Thereafter the cell concentration remained constant till 140 h. From 140 to 168 h there was a further decrease in the cell concentration.

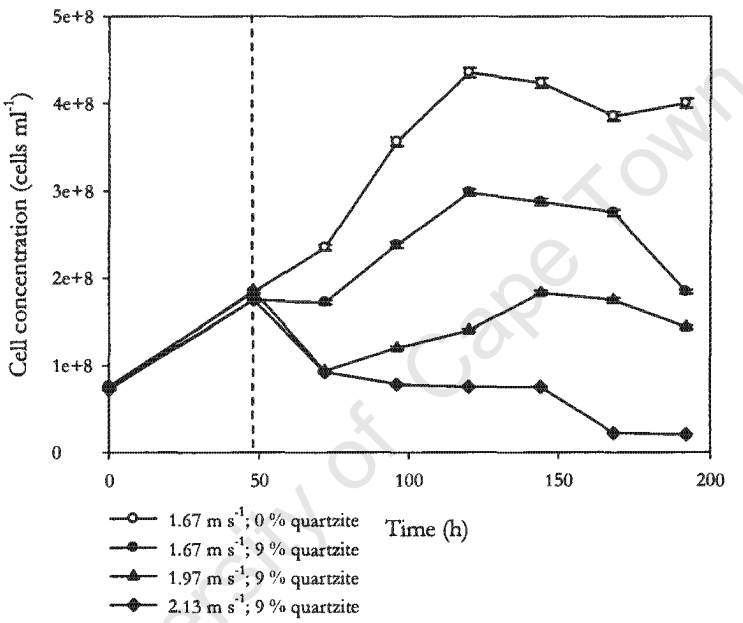


**Figure 4.36:** Change in cell concentration in the presence of 3 % chalcopyrite and 0 and 9 % w/v quartzite and impeller tip speeds of 1.67, 1.97 and 2.13 m $s^{-1}$. Dotted line indicates the onset of the specified experimental conditions.

University of Cape Town

The increase in cell concentration from 72 to 120 h (phase 2) for the 0 and 9 % quartzite loadings operated at 1.67 m $s^{-1}$ and 1.67 and 1.97 m $s^{-1}$ respectively, after the net decline in cell concentrations from 48 to 72 h (phase 1), signifies that the cells adapted or recovered after the increase in hydrodynamic stress applied at 48 h. The extent of recovery was proportional to the intensity of hydrodynamic stress applied. At a 0 % quartzite loading and an impeller tip speed of 1.67 m $s^{-1}$ the growth rate over phase 2 was the highest at 4.17 x $10^6$ cells $ml^{-1}h^{-1}$. At a 9 % quartzite loading at the same impeller tip speed the growth rate over phase 2 was lower at 2.63 x $10^6$ cells $ml^{-1}h^{-1}$. The lowest growth rate of 9.65 x $10^5$ cells $ml^{-1}h^{-1}$ was observed at a tip speed of 1.97 m $s^{-1}$ and a 9 % quartzite loading. The apparent specific growth rate ($\mu_{app}$) was

calculated for the periods 48 to 72 h (phase 1) and 72 to 120 h (phase 2) using the method outlined in Appendix B.2. These data are presented in Table 4.10.

The length of the growth phase, the yield of cells on iron, the maximum cell concentration and the specific death rate presented in Table 4.11 were determined for each impeller speed and solids concentration. The biomass yield on substrate was calculated as described in Appendix B.3 and the specific death rate was calculated as described in Appendix B.2. The length of the growth phase decreased from 72 to 48 h with increasing the solids concentration from 0 to 9 % quartzite at an impeller tip speed of 1.67 m $s^{-1}$ and increased from 48 to 72 h with increasing the impeller tip speed from 1.67 to 1.97 m $s^{-1}$ in the presence of 9 % quartzite. The yield of cells on iron decreased from 2.84 to 1.94 x $10^{11}$ cells $g^{-1}$ Fe due to the presence of 9 % quartzite. Increasing the impeller tip speed from 1.67 to 1.97 m $s^{-1}$ at a constant quartzite loading of 9 %, caused a further decline in the yield from 1.94 to 0.9 x $10^{11}$ cells $g^{-1}$ Fe.

The maximum cell concentration at the initiation of the stationary phase decreased from 4.35 to 2.98 x $10^{8}$ cells $ml^{-1}$ with increasing solids loading from 0 to 9 % quartzite at an impeller tip speed of 1.67 m $s^{-1}$ (Table 4.11). Increasing the impeller tip speed to 1.97 m $s^{-1}$ at a 9 % quartzite loading caused a further decrease in the extent of growth with a maximum cell concentration of 1.83 x $10^{8}$ cells $ml^{-1}$. However, in this reactor the cell concentration did not increase above the initial concentrations of 1.85 x$10^{8}$ cells $ml^{-1}$ observed at 48 h before the increase in impeller speed and the addition of quartzite to the reactors. The extent of growth over a fixed time period is influenced by the growth rate as well as the cell death rate during the growth phase. Increasing the hydrodynamic stress decreased the rate of growth and increased the cell death rate.

In Figure 4.36, a death phase is observed at all solids loadings and impeller tip speeds. The specific death rates shown in Table 4.11 were calculated between 144 and 192 h. The specific death rate increased with increasing intensity of hydrodynamic stress. The specific death rate increased from 0.0012 to 0.0039 $h^{-1}$ with increasing the quartzite loading from 0 to 9 % at an impeller tip speed of 1.67 m $s^{-1}$. Increasing the impeller tip speed from 1.67 to 1.97 m $s^{-1}$ while maintaining a constant 9 % quartzite loading caused the specific death rate to increase approximately two fold from 0.0039 to 0.0082 $h^{-1}$. A further increase in the impeller tip speed from 1.97 to 2.13 m $s^{-1}$ caused an approximately 5 fold increase in the specific death rate to 0.0386 $h^{-1}$.

University of Cape Town

**Table 4.10:** Apparent specific growth rate as a function of impeller tip speed for 0 and 9 % w/v quartzite loadings over phase 1 and phase 2.

| Conditions | $\mu_{app}$ ($h^{-1}$) phase 1 | $\mu_{app}$ ($h^{-1}$) phase 2 | Average $\mu_{app}$ ($h^{-1}$) (48-120 h) |
|---|---|---|---|
| 0 % quartzite; 1.67 m $s^{-1}$ | 0.010 | 0.012 | 0.011 |
| 9 % quartzite; 1.67 m $s^{-1}$ | -0.001 | 0.011 | 0.005 |
| 9 % quartzite; 1.97 m $s^{-1}$ | -0.029 | 0.008 | -0.011 |
| 9 % quartzite; 2.13 m $s^{-1}$ | -0.030 | -0.005 | -0.017 |

**Table 4.11:** Growth parameters for impeller tip speeds of 1.67, 1.97 and 2.13 m $s^{-1}$ at 0 and 9 % w/v quartzite loadings.

| Impeller tip speed (m $s^{-1}$) | Quartzite loading (%; w/v) | Length of growth phase (h) | $Y_{X/Fe}$ ($10^{11}$ cells $g^{-1}$ Fe) (72-120 h) | Maximum cell concentration ($X_{max}$) ($10^{8}$ cells $ml^{-1}$) | Time at $X_{max}$ (h) | Specific death rate ($h^{-1}$) (144-192 h) |
|---|---|---|---|---|---|---|
| 1.67 | 0% | 72 | 2.84 | 4.35 | 120 | 0.0012 |
| 1.67 | 9% | 48 | 1.94 | 2.98 | 120 | 0.0039 |
| 1.97 | 9% | 72 | 0.90 | 1.83 | 144 | 0.0082 |
| 2.13 | 9% | 0 | n/a | n/a | n/a | 0.0386 |

n/a = not applicable

### 4.7.4 THE EFFECT OF AGITATION RATE ON IRON AND COPPER SOLUBILISATION

The percentage iron solubilised as a function of time, solids loading and impeller tip speed is presented in Figure 4.37. At 0 and 9 % quartzite loadings and an impeller tip speed of 1.67 m $s^{-1}$, the iron release curves followed the same trend except that the solubilised iron concentration increased up to 192 h at a 0 % quartzite loading and up to 168 h at a 9 % quartzite loading. At a 9 % quartzite loading and impeller tip speeds of 1.97 and 2.13 m $s^{-1}$, the initial (48 to 96 h) increase in solubilised iron followed the same trend as the reactors run at the lower impeller tip speed, however, the rate of iron solubilisation decreased appreciably from 96 to 148 h with a slight increase from 144 to 192 h. These data show that the increased hydrodynamic stress caused by increasing the impeller tip speed from 1.67 to 1.97 and 2.13 m $s^{-1}$ at a 9 % quartzite loading caused a decline in the concentration of iron solubilised. As the experiment progressed past 96 h this effect was more evident indicating that the reduced concentration of iron solubilised was not only a function of solids loading and impeller tip speed but also time of exposure of the cells to the sub-optimal conditions.

Iron solubilisation followed 3 phases in all reactors. At 0 and 9 % quartzite loadings and an impeller tip speed of 1.67 m $s^{-1}$, there was an increase in the solution iron concentration over the

University of Cape Town

first 48 h after the inoculum build-up phase (phase 1). Phase 1 was followed by a sharper increase in the solution iron concentration over the 96 to 144 h period (phase 2) and a reduced rate of increase from 144 to 192 h. The initial slow increase in the percentage of iron released corresponded to the low apparent specific growth rate of the organisms during the 48 to 72 h time period reported in Table 4.10. The increase in the apparent specific growth rate over the 72 to 120 h period was accompanied by an increase in the iron release rate as observed in phase 2 of the iron release curve.

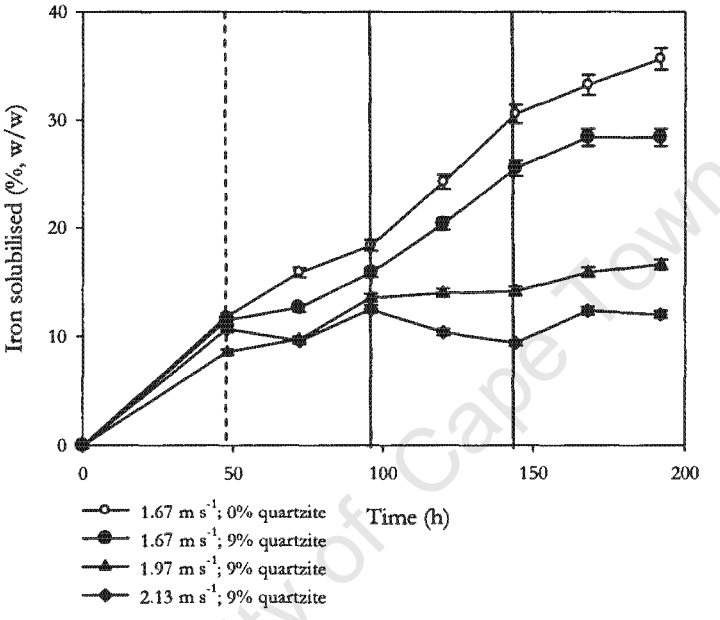


**Figure 4.37:** Change in iron concentration in the presence of 3 % chalcopyrite and 0 and 9 % w/v quartzite and impeller tip speeds of 1.67, 1.97 and 2.13 m $s^{-1}$. Dotted line indicates the onset of the specified experimental conditions. Solid lines indicate the end of phase 1 and phase 2.

The change in the rate and extent of iron solubilisation, as a function of solids loading and impeller tip speed, is more clearly illustrated in Figure 4.38. The specific iron oxidation rate ($q_{Fe}$) was calculated over the phase 1 (Figure 4.38a) and phase 2 (Figure 4.38b) as detailed in Appendix B.2. The specific iron solubilisation rates at 0 and 9 % quartzite loadings and an impeller tip speed of 1.67 m $s^{-1}$ were higher in phase 2 than in phase 1. At a 9 % quartzite loading and an impeller tip speed of 1.97 m $s^{-1}$ the specific iron solubilisation rate was lower in phase 2 than in phase 1. Furthermore, in phase 1 at a 9 % quartzite loading and impeller speed of 1.97 m $s^{-1}$ the specific iron solubilisation rate was 1.7 fold higher than at the lower speed. However, as the experiment proceeded and the culture was exposed to the elevated intensity of hydrodynamic stress for an extended period, the specific iron solubilisation rate at a 9 % quartzite loading and impeller speed of 1.97 m $s^{-1}$ declined significantly from 6.24 x $10^{-4}$ to 7.22 x $10^{-15}$ g Fe $cell^{-1}$ $h^{-1}$ in phase 2.

University of Cape Town

Figure 4.38c presents the average specific iron oxidation rate over phase 1 and phase 2 and the extent of iron solubilisation over the course of the experiment. The extent of iron solubilisation from 48 to 192 h was calculated as the percentage of the iron content of the mineral present in the reactor (5.9 g) released into solution during this period. Increasing the solids concentration from 0 to 9 % quartzite, while maintaining a constant impeller tip speed of 1.67 m $s^{-1}$, resulted in a decline in the average specific rate of iron solubilisation from 5.7 x $10^{-14}$ to 4.9 x $10^{-14}$ g Fe $cell^{-1}$ $h^{-1}$. Increasing the impeller tip speed from 1.67 to 1.97 and 2.13 m $s^{-1}$ while maintaining a constant solids concentration of 9 % quartzite resulted in a further decline in the average specific iron solubilisation rate to 3.5 x $10^{-14}$ and 1.3 x $10^{-14}$ g Fe $cell^{-1}$ respectively. It is important to note that although the specific iron solubilisation rate was higher in phase 1 at an impeller speed of 1.97 m $s^{-1}$ the sharp decline in phase 2 caused a decline in the average specific iron solubilisation rate. The extent of iron solubilisation decreased from 24.0 and 14.0 % at 0 and 9 % quartzite and an impeller tip speed of 1.67 m $s^{-1}$ to 8.0 and 1.8 % at a quartzite loading of 9 % and impeller tip speeds of 1.97 and 2.13 m $s^{-1}$. Further analysis of iron release data was not sought because, as discussed in Section 4.6.2.5, the measured iron concentration may have been an underestimate of the iron concentration in solution. Copper solubilisation data was thus used to represent the status of the system.

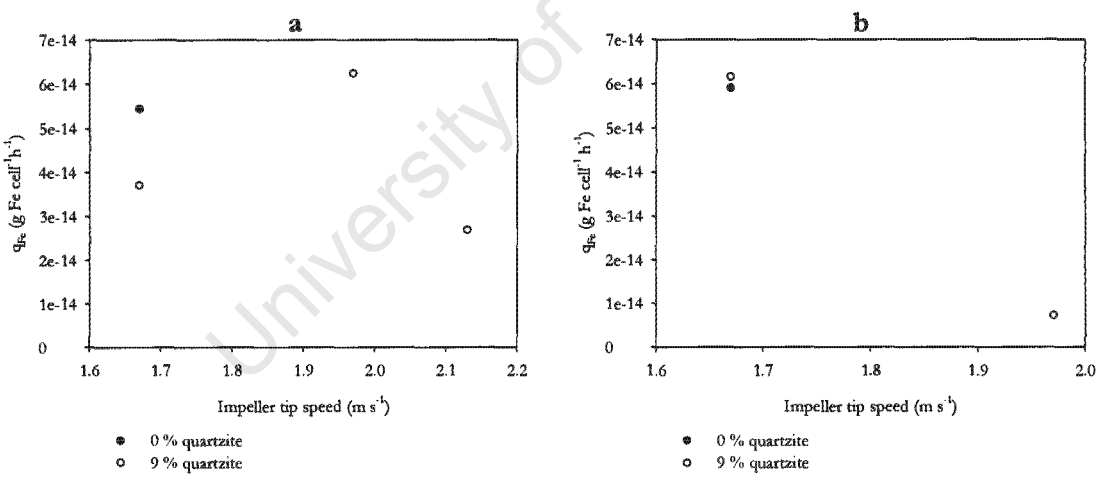


University of Cape Town

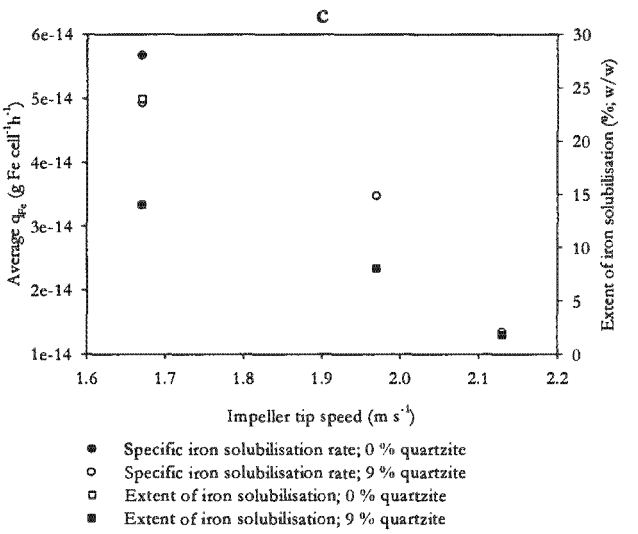


**Figure 4.38:** Specific iron solubilisation rate (a) phase 1 and (b) phase 2, and (c) average iron solubilisation rate and extent of iron solubilisation as a function of impeller tip speed at 0 and 9 % w/v quartzite loadings.

Figure 4.39 illustrates the change in the solubilised copper concentration as a function of time, impeller speed and solids concentration. Copper solubilisation, like iron solubilisation was described by three phases except that the copper solubilisation rate was lower in phase 2 than phase 1 for all reactors. In phase 1 (48 to 96 h) the percentage copper solubilised increased in all reactors. Phase 2 (96 to 144 h) was characterised by a reduced copper release rate, while in phase 3 (144 to 192 h) the rate of solubilisation approached 0 in all reactors. Copper solubilisation was recorded up to 170 h despite the cultures having reached stationary phase at 120 h confirming the continuation of leaching in the presence of non-growing cells. The concentration of copper in solution was inversely proportional to the solids loading and impeller tip speed applied and copper solubilisation ceased earlier in the reactors operated at higher intensities of hydrodynamic stress.

University of Cape Town

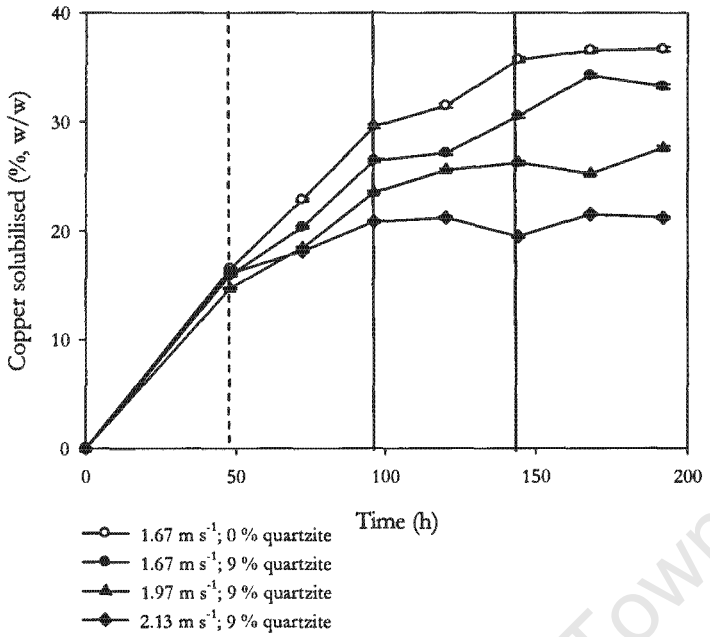


**Figure 4.39:** Change in copper concentration in the presence of 3 % chalcopyrite and 0 and 9 % w/v quartzite and impeller tip speeds of 1.67, 1.97 and 2.13 m $s^{-1}$. Dotted line indicates the onset of the specified experimental conditions. Solid lines indicate the end of phase 1 and phase 2.

University of Cape Town

As discussed in Section 4.6.2.5, if all minerals in the Andina concentrate were leaching at the same rate, the ratio of iron to copper is expected to be 0.87. In the solids loading experiments at the lower solids loadings (lower intensities of hydrodynamic stress), the ratio was higher than 0.87 in both leach phases and higher in phase 1 than in phase 2. The change in ratio of iron to copper was postulated to result from the operating redox potential determining which mineral in the concentrate leached at a higher rate. Using the same argument for the impeller speed experiments, if the ratio was lower than 0.87 in both phases (Tables 4.12a and 4.12b) then this would signify that chalcopyrite leaching dominated both phases. However, at the 0 and 9 % quartzite loadings and an impeller tip speed of 1.67 m $s^{-1}$, the ratio in phase 2 increased approximately 1.4 fold indicating that the pyrite leach rate had increased. This is confirmed by observing the decrease in the solubilisation rate of copper in phase 2 (Table 4.13) and the increase in the solubilisation rate of iron on phase 2 in these reactors. At a 9 % quartzite loading and impeller tip speeds of 1.97 and 2.13 m $s^{-1}$, the ratio was similar in both phases for both reactors. Chalcopyrite leaching is postulated to have dominated in both phases in these reactors because the operating redox potential remained between 480 and 535 mV. These redox potentials are within the redox potential window where the rate of chalcopyrite leaching is elevated. As mentioned previously, care needs to be taken when using iron data because as mentioned in Section 4.7.4, if the measured iron concentration was an underestimate of the true iron

concentration, this would have affected the iron to copper ratio and the ratios presented in Table 4.12a and 4.12b would also be underestimates.

**Table 4.12a:** Iron to copper concentration ratios at 96 h (end of phase 1) for impeller tip speed experiments. Total suspension iron and copper concentrations measured after acid solubilisation of precipitate.

| Quartzite loading (%, w/v) | Impeller tip speed (m $s^{-1}$) | Redox potential (mV) | Iron concentration (g $l^{-1}$) | Copper concentration (g $l^{-1}$) | Fe/Cu ratio |
|---|---|---|---|---|---|
| 0 | 1.67 | 603 | 1.50 | 2.60 | 0.58 |
| 9 | 1.67 | 565 | 1.30 | 2.34 | 0.56 |
| 9 | 1.97 | 529 | 1.14 | 2.10 | 0.54 |
| 9 | 2.13 | 487 | 1.05 | 1.85 | 0.57 |

**Table 4.12b:** Iron to copper concentration ratios at 144 h (end of phase 2) for impeller tip speed experiments.

| Quartzite loading (%, w/v) | Impeller tip speed (m $s^{-1}$) | Redox potential (mV) | Iron concentration (g $l^{-1}$) | Copper concentration (g $l^{-1}$) | Fe/Cu ratio |
|---|---|---|---|---|---|
| 0 | 1.67 | 615 | 2.60 | 3.20 | 0.81 |
| 9 | 1.67 | 588 | 2.15 | 2.70 | 0.80 |
| 9 | 1.97 | 535 | 1.20 | 2.30 | 0.52 |
| 9 | 2.13 | 481 | 1.00 | 1.73 | 0.58 |

**Table 4.13:** Copper leach rates for phase 1 and phase 2 and the ratio of copper release rate for the two phases determined for the impeller speed experiments.

| Impeller tip speed (m $s^{-1}$) and quartzite loading (%; w/v) | Rate of copper release phase 1 (g $l^{-1}h^{-1}$) (48-96 h) | Rate of copper release phase 2 (g $l^{-1}h^{-1}$) (96-144 h) | Ratio of Cu release phase 1/phase2 |
|---|---|---|---|
| 1.67; 0% | 0.0240 | 0.0113 | 2.1 |
| 1.67; 9% | 0.0194 | 0.0075 | 2.6 |
| 1.97; 9% | 0.0163 | 0.0050 | 3.3 |
| 2.13; 9% | 0.0088 | 0.0000 | n/a |

n/a = not applicable

Figures 4.40a and 4.40b present the specific copper solubilisation rates ($q_{Cu}$) over phase 1 and phase 2. The specific copper solubilisation rate was calculated as detailed in Appendix B.2. As observed with iron solubilisation, the specific copper solubilisation rate at a 9 % quartzite loading and an impeller tip speed of 1.97 m $s^{-1}$ was higher than at the 0 and 9 % quartzite loadings operated at 1.67 m $s^{-1}$. During phase 1 (48 to 96 h), the specific copper solubilisation rate at a 9 % quartzite loading and impeller speed of 1.97 m $s^{-1}$ was 1.2 fold higher than at the same solids

University of Cape Town

loading but a lower impeller speed of 1.67 m $s^{-1}$. During this phase the apparent specific growth rate in this reactor was 2.5 fold lower than at the lower impeller speed (Table 4.10). Thus although the apparent specific growth rate is lower at the higher impeller speed, the specific copper solubilisation rate is higher. The specific growth rate is a measure of the formation of biomass. The increased hydrodynamic stress at the higher impeller tip speed may have caused a loss of cell viability and cell lysis due to solid-cell-solid interactions thus causing a decline in the apparent specific growth rate of the culture. The specific copper solubilisation rate is an indirect measure of the metabolic activity of each cell. It is an indirect measure because, as discussed in Section 4.6 the process of copper solubilisation is not directly linked to the metabolism of the micro-organisms but indirectly linked through ferric leaching of the mineral. The increase in specific copper solubilisation rate at the higher impeller speed may be linked to improved mass transfer. Improved mass transfer resulting from the increased agitation rate would have (i) enhanced leach reactions through improved contact between the solid and liquid phase and (ii) improved oxygen transfer would have influenced the microbial ferrous oxidation rate and thus enhanced the rate of leaching. In addition to mass transfer effects, the specific activity of the culture may have been elevated due to the low solution redox potential at the higher impeller tip speed. A similar argument is applicable to the specific iron solubilisation rates, however variation in the measured iron concentrations due to factors such as jarosite precipitation discussed in Section 4.6.2.5 may occur.

At a 9 % quartzite loading and impeller speed of 2.13 m $s^{-1}$, the positive effects of increasing the impeller speed were eclipsed by the negative impact of the increased hydrodynamic stress. This conclusion is validated by data obtained from experiments conducted at a 0 % quartzite loading and impeller tip speeds of 1.67, 1.97 and 2.13 m $s^{-1}$ (Figure 4.41). Increasing the impeller tip speed from 1.67 to 1.97 m $s^{-1}$ while maintaining a constant quartzite loading of 0 % resulted in an increase in the apparent specific growth rate ($\mu_{app}$) from 0.010 to 0.020 $h^{-1}$ and an increase in the specific iron solubilisation rate ($q_{Fe}$) from 6.2 x $10^{-11}$ to 8.2 x $10^{-11}$g Fe $cell^{-1}$ $h^{-1}$ over the 24 to 74 h period. A further increase in the impeller tip speed to 2.13 m $s^{-1}$ caused a decline in the apparent specific growth rate to 0.012 $h^{-1}$; however the specific iron solubilisation rate remained at 8.2 x $10^{-11}$ g Fe $cell^{-1}$ $h^{-1}$. Although the apparent specific growth rate of the cells declined when the impeller tip speed was increased from 1.97 to 2.13 m $s^{-1}$, the apparent specific growth rate remained higher than that at the lowest impeller speed of 1.67 m $s^{-1}$. Furthermore, at an impeller tip speed of 2.13 m $s^{-1}$, the specific iron oxidation rate was equal to that at an impeller tip speed of 1.97 m $s^{-1}$. Thus, the leach rate remained elevated even though the apparent specific growth rate had declined; indicating that the improved mass transfer due to the increased agitation rate was enhancing the leaching process.

University of Cape Town

Figure 4.40c presents the average specific copper release rate and extent of copper release as a function of solids loading and impeller speed. The extent of copper solubilisation from 48 to 192 h was calculated as the percentage of the copper content of the mineral present in the reactor (6.2 g) released into solution during this period. The average specific rate decreased with increasing the quartzite loading from 0 to 9 % while maintaining an impeller speed of 1.67 m $s^{-1}$. However, contrary to the average specific iron solubilisation rate data, the average specific copper release rate increased on increasing the impeller speed to 1.97 m $s^{-1}$ while maintaining a quartzite loading of 9 %. The extent of copper release declined with increasing solids loading and impeller tip speed. Increasing the solids concentration from 0 to 9 % quartzite caused a slight decrease in the average specific copper release rate from 7.15 x $10^{-14}$ to 6.78 x $10^{-14}$ g Cu $cell^{-1}$ and a decrease in the extent of solubilisation from 28.8 to 24.7 %. Increasing the impeller tip speed from 1.67 to 1.97 and 2.13 m $s^{-1}$ caused a significant decline in the average copper release rate to 6.57 x $10^{-14}$ and 4.5 x $10^{-14}$ g Cu $cell^{-1}$ respectively. Although there was no cell growth observed at a 9 % quartzite concentration and an impeller tip speed of 2.13 m $s^{-1}$, the maximum percentage copper leached was 7.7 %. This confirms previous findings indicating that despite the absence of growth in the reactor, the cells still remained metabolically active with iron and sulphur oxidation contributing to the solubilisation of the mineral.

University of Cape Town

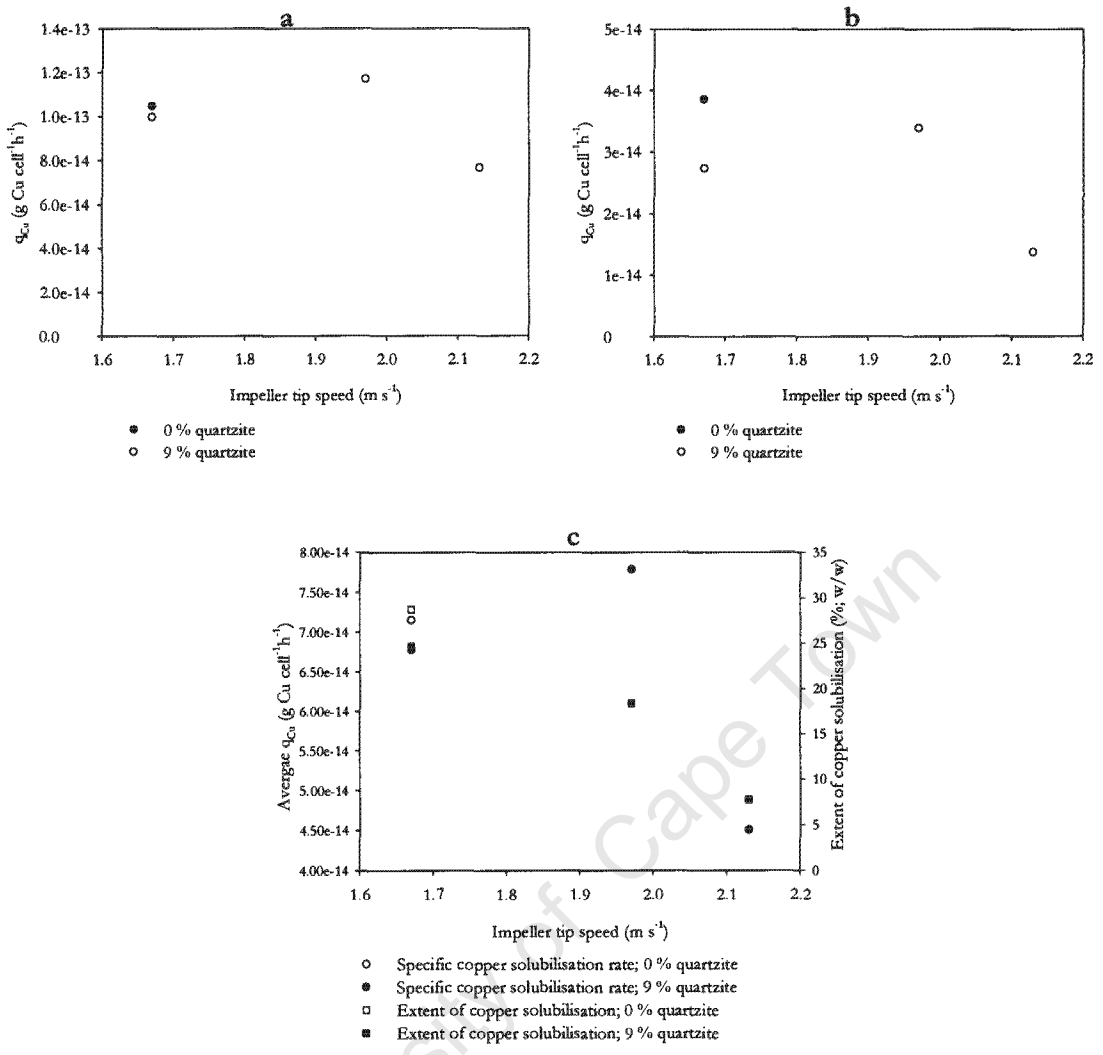


**Figure 4.40:** Specific copper solubilisation rate (a) phase 1 and (b) phase 2, and (c) average copper solubilisation rate and extent of iron solubilisation as a function of impeller tip speed at 0 and 9 % w/v quartzite loadings.

University of Cape Town

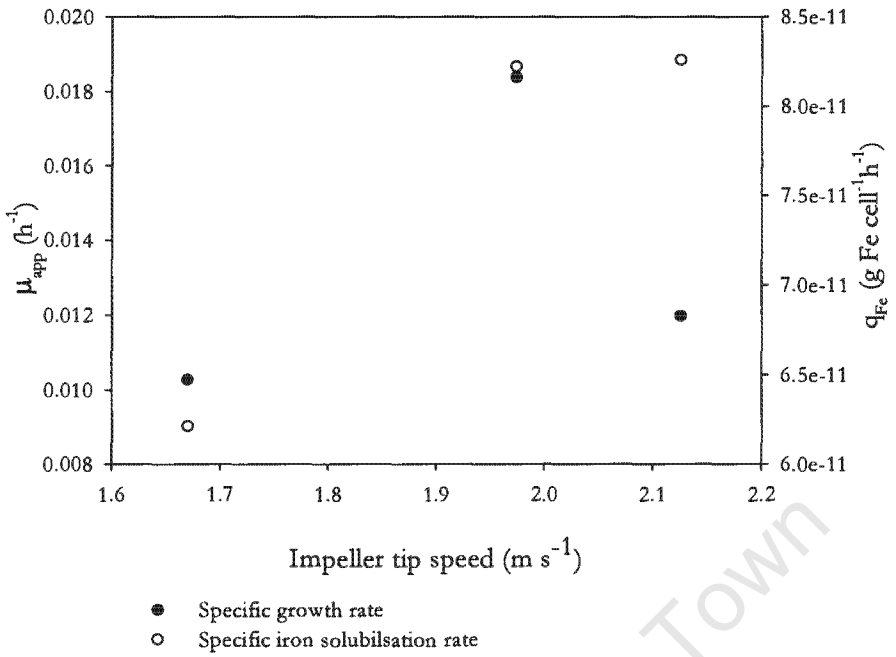


**Figure 4.41:** Apparent specific growth and iron solubilisation rates over the 24 to 74 h period as a function of impeller tip speed at a 0 % w/v quartzite loading.

University of Cape Town

### 4.7.5 COMPARISON OF RESULTS OBTAINED IN THE PRESENT STUDY TO LITERATURE STUDIES

In this section the results from the impeller speed experiments in the present study are compared to related studies on slurry reactors presented in the literature. These studies include mesophilic and thermophilic bioleaching systems as well as yeast systems. The solid phases include pyrite, chalcopyrite and quartzite. Operating conditions are detailed in Table 4.14.

**Table 4.14:** Experimental conditions utilised in the slurry reactor systems reported in literature.

| Reference | Micro-organism | Reactor | Solids loading (%; w/v) | Size range (μm) | Agitation rate (rpm) | Shear rate ($s^{-1}$) |
|---|---|---|---|---|---|---|
| Pearce, 1993 | Thiobacilli | STR | 10 % Pyrite | 55 | 350-630 | 58.3-105 |
| Gomez *et al.*, 1994 | Thermophile | Shake flask | 1-7 % Chalcopyrite | Not given | 100-200 | 16.7-33.3 |
| d'Hugues *et al.*, 1997 | Mesophiles | STR | 20 % Pyrite | $d_{80}$ < 63 | 390-450 | 65.0-75.0 |
| Nemati and Harrison, 2000 | *S. metallicus* | STR | 3-18 % Pyrite | 53-75 | 500-550 | 83.3-91.7 |
| Lamaignére, 2002 | *S. cerevisiae* | STR | 0-1 % Quartzite | 600-850 | 460-850 | 76.7-141.7 |
| Sissing, 2002 | *S. metallicus* | STR | 3% Pyrite 0-24%Quartzite | 38-75 | 560-760 | 93.3-126.7 |
| Present study | *Sulfolobus* sp. | STR | 3 % Chalcopyrite 0-18% Quartzite | 38-75 | 550-700 | 91.7 - 117 |

As discussed in Section 4.7.4, increasing agitation rate up to a critical level can have a positive effect on reactor performance by improving the mass transfer rates of nutrients (e.g. oxygen and carbon dioxide). Typically, gas-liquid mass transfer coefficients are correlated with the agitation rate according to the form:

$$k_L a \propto N^{\alpha} \quad \text{...Eqn 4.12}$$

or

$$k_L a \propto (P/V)^{\beta} \quad \text{...Eqn 4.13}$$

Improved mass transfer rates could lead to increased growth rates, as growth rate is dependent on the carbon dioxide and oxygen concentrations below critical threshold values. In addition, in the chalcopyrite bioleaching system, improved mass transfer could improve iron and copper solubilisation rates as the biological ferrous iron oxidation rate is a function of oxygen concentration. Gomez *et al.* (1994) showed that increasing the mixing rate of flasks from 100 through 150 to 200 rpm improved the growth of *Sulfolobus* sp. on chalcopyrite (Figure 4.42). The growth rate as well as the maximum cell concentration increased with increasing rotational speed. This improvement was attributed to improved oxygen and carbon dioxide mass transfer at higher rotational speeds. The shake flask system utilised by Gomez *et al.* (1994) was mass transfer limited at the low rotational speed. In addition, the energy dissipated in a shake flask system is low compared to the STR at the same agitation rate. Thus increasing rotational speed of the shake flasks over the range of speeds investigated served to improve mass transfer and solids suspension, thus enhancing reactor performance without the negative effects of hydrodynamic stress. For example, it is possible that at 200 rpm, solids suspension was enhanced resulting in improved dissolution kinetics.

University of Cape Town

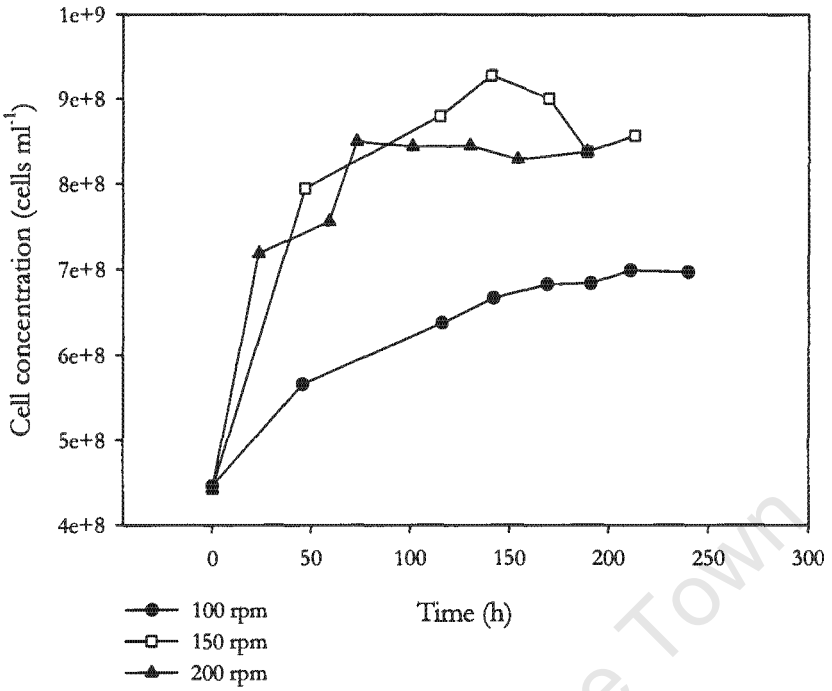


**Figure 4.42:** The influence of agitation rate on cell concentration (adapted from Gomez *et al.*, 1994).

University of Cape Town

However, increasing the impeller tip speed beyond a critical value could lead to a decline in process performance. Pearce (1993) observed the effect of increasing impeller speed on the growth of acidithiobacilli at a quartzite loading of 10 % w/v. The cells were grown in STRs using axial or Rushton turbines (Figure 4.43). Using either impeller, a speed of 350 rpm (1.4 m $s^{-1}$) did not inhibit the metabolic activity of the acidithiobacilli, illustrated through ferrous iron oxidation and thereby the increase in redox potential. However, increasing rotational speed of the axial impeller to 630 rpm (2.6 m $s^{-1}$) induced a lag period of 11 days while no activity was observed using a Rushton impeller at a speed of 630 rpm over 20 days. A similar effect was seen in the present study. At a 0 % quartzite loading, increasing the impeller tip speed from 1.67 to 2.13 m $s^{-1}$ while maintaining a constant quartzite loading of 0 % resulted in an increase in the apparent specific growth rate from 0.010 to 0.018 $h^{-1}$ and an increase in the specific iron solubilisation rate from 6.2 x $10^{-11}$ to 8.2 x $10^{-11}$g Fe $cell^{-1}$ $h^{-1}$ over the 24 to 74 h period. Thus the improved mass transfer improved the metabolic activity of the culture. However, a further increase in the impeller tip speed to 2.13 m $s^{-1}$ in the absence of quartzite caused a decline in the apparent specific growth rate to 0.012 $h^{-1}$ and the specific iron solubilisation rate remained the same at 8.2 x $10^{-11}$ g Fe $cell^{-1}$ $h^{-1}$.

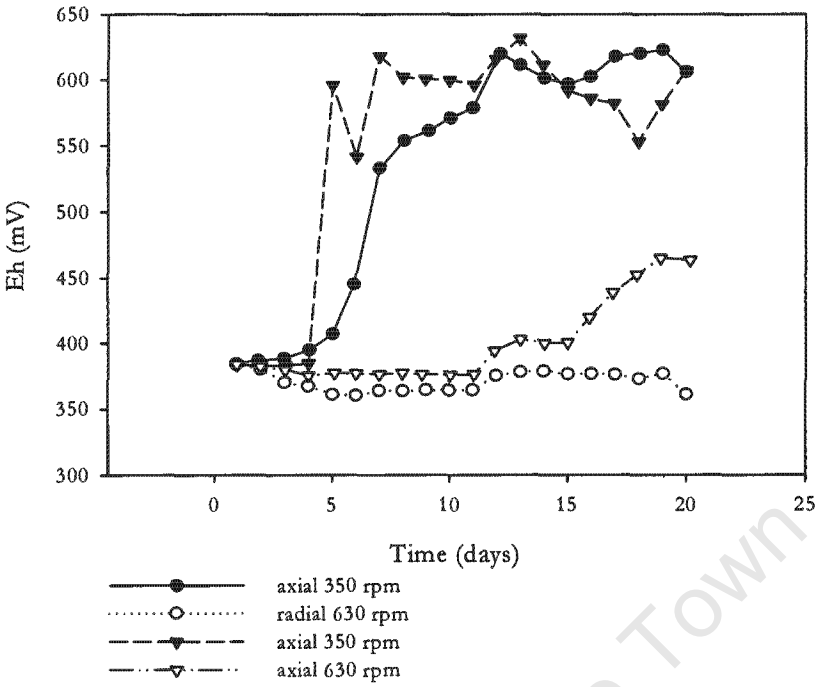


**Figure 4.43:** The influence of agitation rate on metabolic activity of the acidithiobacilli in the presence of 10 % solids loading measured in terms of redox potential (adapted from Pearce, 1993).

University of Cape Town

Lamaignére (2002) carried out similar studies to Pearce (1993), studying the effect of hydrodynamic stress on growing yeast cultures in the presence of 1 % v/v quartzite. The author found similar results to Pearce (1993) and the present study. Increasing the impeller speed from 460 (1.91 m $s^{-1}$) to 565 rpm (2.33 m $s^{-1}$) increased the growth rate of the micro-organisms. However when the agitation rate was raised above a critical speed of 565 rpm, both the rate and extent of growth declined. In addition to a decrease in the growth rate, the author also found a decrease in the biomass yield coefficient with increasing agitation rate. The yield decreased from 7.15 to 4.92 x $10^9$ cells g glucose$^{-1}$ with increasing tip speed from 2.33 to 3.51 m $s^{-1}$. As discussed in Section 4.6, the decreased yield of cells on substrate suggests an increase in the maintenance energy requirement with increased stress. Abu-Reesh and Kargi (1991) found that the specific glucose consumption rate of hybridoma cells increased with increasing agitation rate and postulated the increase to be due to the high cell maintenance requirements at high agitation speeds.

Apparent specific growth rate data obtained in this study are compared to results obtained in previous studies by Sissing (2002) and Lamaignére (2002) in Figure 4.44. Sissing (2002) studied the influence of increasing impeller tip speed on the bioleaching of pyrite by *S. metallicus* in a

pyrite-quartzite system. In these studies the solids loading was kept constant at 15 % quartzite while the impeller tip speed was varied. The results presented in Figure 4.44 were obtained at impeller tip speeds higher than the critical impeller tip speed at which process performance was found to improve. Direct comparison of the *Sulfolobus* systems to the yeast system was difficult because the structure of the cells differ considerably, the solids loading was lower and the impeller speeds were higher in the yeast system compared to the two *Sulfolobus* systems. Despite these differences, the overall results were similar in all three investigations i.e. a decrease in $\mu_{app}$ with increasing impeller tip speed. Both *Sulfolobus* investigations (pyrite and chalcopyrite) showed similar results. Increasing the impeller tip speed from 1.67 to 1.97 m $s^{-1}$ caused a decrease in the apparent specific growth rate. A decline in $\mu_{app}$ from 0.011 to 0.008 $h^{-1}$ was observed in the present study compared to a decline from 0.014 to 0.011 $h^{-1}$ in the study by Sissing (2002). When the impeller tip speed was increased further to approximately 2.20 m $s^{-1}$, no growth was observed in either system, instead cell death occurred. The results of Lamaignére (2002) showed that there was an initial sharp decline in $\mu_{app}$ from 0.135 to 0.125 $h^{-1}$ with marginal increase in the impeller tip speed from 2.33 to 2.48 m $s^{-1}$. A further increase in the impeller tip speed to 3.51 m $s^{-1}$ resulted in a more gradual decline in $\mu_{app}$ to 0.114 $h^{-1}$.

The apparent specific growth rates observed by Sissing (2002) were higher than those observed in the present study. This increased rate may be attributed to the different minerals utilised in the two studies. As discussed in Section 4.5.1, the pyrite-quartzite system utilised by Sissing (2002) was significantly less nutrient limited than the chalcopyrite-quartzite system used in the present study. This nutrient limitation resulted in a lower growth rate and thus a reduced apparent specific growth rate. In addition to the difference between the two *Sulfolobus* systems, the apparent specific growth rates were an order of magnitude higher in the yeast system compared to the *Sulfolobus* systems. In addition, the apparent specific growth rate in the yeast system did not decrease below 0 over the range of impeller tip speeds studied. It is expected that the yeast system would have the highest apparent specific growth rate due to the superior strength of the yeast cell wall comprised of cross-linking mannan and glucan. This cell wall structure would have increased the resistance of these organisms to the effects of hydrodynamic stress.

University of Cape Town

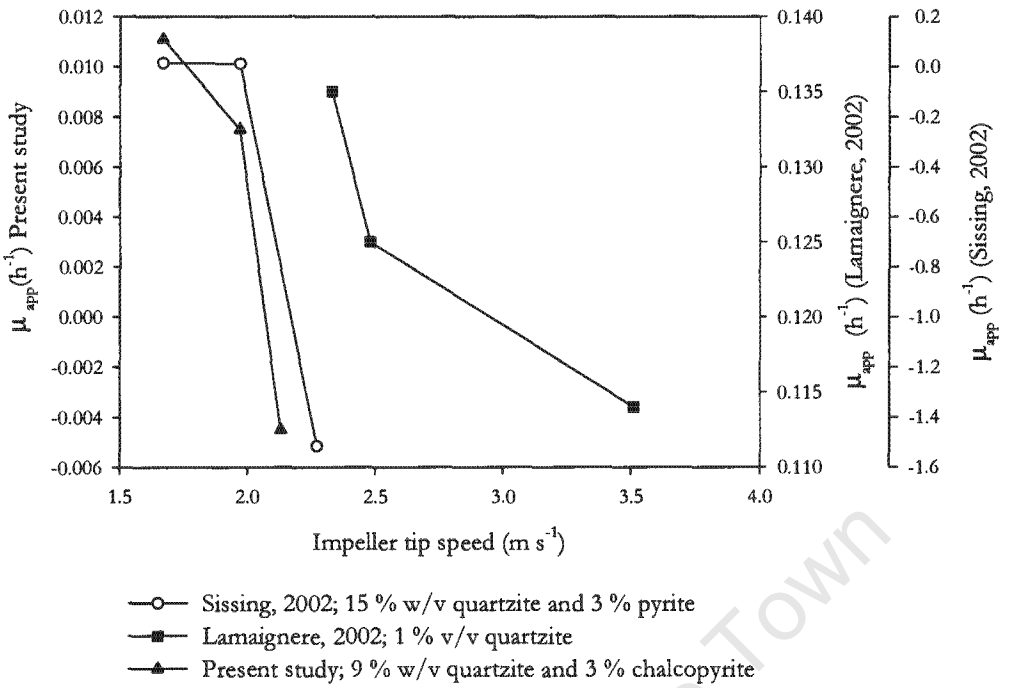


**Figure 4.44:** Comparison of apparent specific growth rates for *S. cerevisiae* (Lamaignére, 2002) and *Sulfolobus* sp. (Sissing, 2002 and present study) at various impeller tip speeds using a pitched blade impeller.

Iron leach data are compared for the chalcopyrite-quartzite system (present study) and the pyrite-quartzite (Sissing, 2002) system in Figure 4.45. At a 9 % quartzite loading, the chalcopyrite system followed the expected trend of a decrease in the iron leach rate with increasing agitation rate. However, in the pyrite system at a 15 % quartzite loading, there was an increase in the leach rate from 0.076 to 0.107 g Fe $l^{-1}$ $h^{-1}$ with an increase in the impeller tip speed from 1.67 to 1.97 m $s^{-1}$. Sissing (2002), like Gomez *et al.* (1994), concluded that this increase in leach rate was possibly due to enhanced mass transfer in the 1.97 m $s^{-1}$ reactor. If the positive effect of improved mass transfer (e.g. oxygen and carbon dioxide) prevailed over the effect of the increased hydrodynamic stress induced by increasing the impeller tip speed, then the result is a higher leaching efficiency. Over the range of impeller tip speeds and solids concentrations tested in the present study, the positive effects of increasing tip speed were observed at a 0 % quartzite loading and to a limited extent at a 9 % quartzite loading. At a 9 % quartzite loading an increase in the initial (48 to 96 h) specific iron and copper solubilisation rates was observed with an increase in the impeller tip speed from 1.67 to 1.97 m $s^{-1}$. However this initial increase in the rate did not improve the overall extent of metal solubilisation due to the decline in the apparent specific growth rate resulting from the increased hydrodynamic stress at the higher impeller tip speed. As discussed in Section 4.6, the sensitivity of the micro-organisms in the chalcopyrite system to lower levels of

University of Cape Town

hydrodynamic stress than the micro-organisms in the pyrite system could stem from nutrient limitation due to passivation of the chalcopyrite i.e. the effects of hydrodynamic stress coupled with nutrient stress outweighed the positive effects of improved mass transfer.

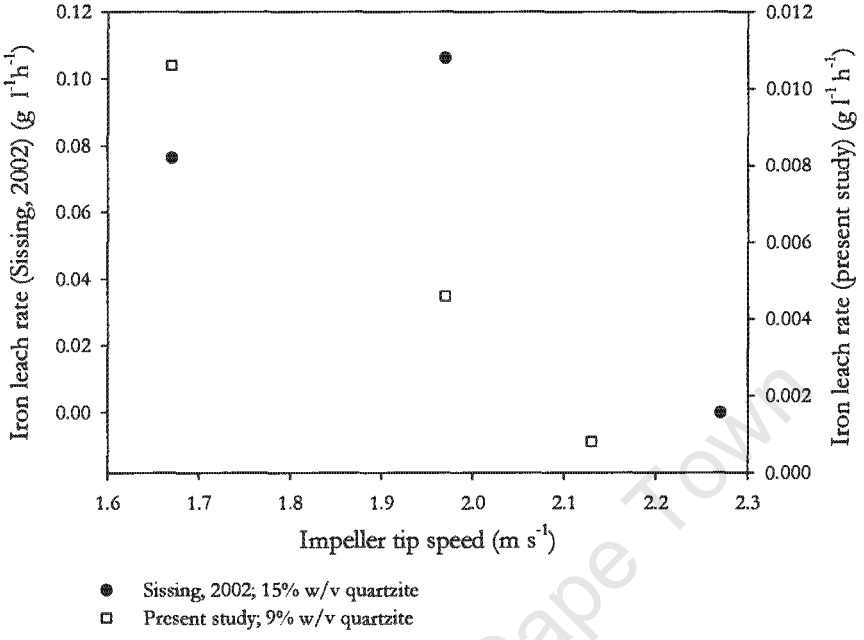


**Figure 4.45:** Comparison of iron leach rates for pyrite (Sissing, 2002) and chalcopyrite (Present study) as a function of impeller tip speeds at quartzite loadings of 15 and 9 % w/v respectively.

Gomez *et al.* (1994) found that the final extractions of copper were similar in tests run at 150 and 200 rpm and greater than those obtained at 100 rpm. At mixing rates of 100, 150 and 200 rpm the extent of solubilisation was 63, 89 and 84 % respectively. Here again mass transfer limitations are cited as the reason for the improved copper solubilisation. The effects of improved mass transfer due to improved mixing conditions need to be accounted for before addressing the effects of hydrodynamic stress. d'Hugues *et al.* (1997) who investigated the bioleaching of pyrite at high solids concentrations using mesophiles were able to conduct experiments in the absence of mass transfer limitations. The authors discovered that, after removing the oxygen limitation in the stirred tank reactors, the decline in bioleaching efficiency was as a consequence of stress induced by increasing the agitation rate from 390 to 450 rpm. Similar results were obtained in the present study where in Table 4.12 it was shown that at a 9 % quartzite loading, increasing the impeller tip speed from 1.67 through to 2.13 m $s^{-1}$ caused a progressive decline in the iron and copper solubilisation.

University of Cape Town

### 4.7.6 CONCLUSIONS

In this section, the effect of increasing quartzite loading from 0 to 9 % and impeller tip speed from 1.67 through to 2.13 m $s^{-1}$ on the bioleaching of chalcopyrite by a *Sulfolobus* culture was investigated. The positive effects of increasing agitation rate on leaching were observed at a 0 % quartzite loading and to a limited extent at a 9 % quartzite concentration and an impeller speed of 1.97 m $s^{-1}$. Increasing impeller tip speed up to a critical level of hydrodynamic stress (determined by the solids loading) resulted in improved mass transfer and hence improved dissolution kinetics. However, above a critical intensity of hydrodynamic stress, the positive effects of improved mass transfer were outweighed by the detrimental effects of increased hydrodynamic stress. The adverse effects were similar to those observed for the solids loading experiments where increasing solids loading caused a decline in the extent of growth, and iron and copper solubilisation. Increasing solids loading increased the number of particles in suspension while increasing agitation rate increased the collision frequencies of the particles in solution as well as the energy dissipated in these events. At a 9 % quartzite loading the critical impeller tip speed above which the effects of hydrodynamic stress on process performance were significant was determined to be 1.67 m $s^{-1}$.

In Section 4.6 and the current section, the effects of solids loading and impeller tip speed have been treated separately. In the following section the combined effect of increasing solids loading as well as impeller speed on the process performance is assessed.

## 4.8 FURTHER ANALYSIS OF GROWTH AND REDOX POTENTIAL DATA

In this section, the analysis of the growth and redox potential results discussed in Sections 4.6.2.3 and 4.6.2.2 is extended. Firstly, growth kinetics data were used to determine the specific death rate. The variation of the specific death rate with the concentration of quartzite was modelled using the power law function. Secondly, the change in redox potential over time observed for the solids loading experiments (Section 4.6) was examined using the kinetics of bioleaching of chalcopyrite by a *Sulfolobus* sp..

### 4.8.1 GROWTH DATA

#### 4.8.1.1 Determining specific growth and death rates

Figure 4.46 illustrates a typical growth profile for the *Sulfolobus* culture used in this study. The profile is described by growth, stationary and death phases. No distinct lag phase is observed

University of Cape Town

owing to the inoculum build-up approach used. Furthermore the growth phase is described by a linear increase rather than an exponential increase in cell concentration. Primary factors that affect the cell concentration and the growth rate in the growth phase include viable cell concentration, maintenance energy and cell lysis. The first factor, cell viability, refers to the ability of cells to grow and reproduce. Viability may be reduced due to damaged cell membranes caused by hydrodynamic stress. The second factor deals with the increase in the cell maintenance energy requirement which may contribute to cell repair mechanisms in response to cell damage due to stress. If the metabolic energy directed to growth is reduced, a decrease in cell concentration is observed. Finally, cell lysis may occur due to high intensity solid-cell-solid collisions causing the cell envelope to rupture.

Primary factors that affect the cell death rate and cell concentration in the death phase include an increase in metal ion concentration and ionic strength of the medium, nutrient limitation and cell lysis. The build-up of toxic concentrations of metals and increased ionic strength of the growth medium may cause cell death. If the substrate becomes limited due to depletion of the nutrient source or passivation of the mineral and no energy is available for cell maintenance, cell death results. Cell lysis may occur due to high intensity solid-cell-solid collisions causing the cell envelope to rupture. Furthermore, cells which remained intact and viable in the growth phase with only minor envelope damage may lyse due to prolonged exposure to hydrodynamic stress during the growth and stationary phases.

University of Cape Town

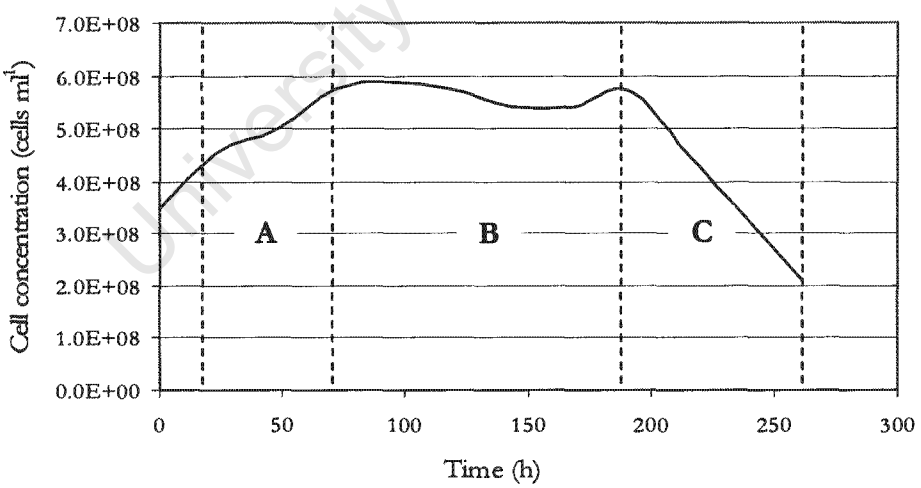


**Figure 4.46:** Growth curve of a *Sulfolobus* culture in the presence of 3 % chalcopyrite. Dashed lines indicate (A) growth, (B) stationary and (C) death phases.

The growth and death phases are represented by regions A and C in Figure 4.46. Under conditions of negligible stress, the growth rate dominates the death rate such that:

$$\mu_{app} \cong \mu \qquad \ldots \text{Eqn. 4.14}$$

where: $\mu_{app}$ = apparent or measured specific growth rate ($h^{-1}$)

$\mu$ = maximum specific growth rate in the absence of stress ($h^{-1}$)

Under conditions of increased hydrodynamic stress it is postulated that the death rate becomes significant hence:

$$\mu_{app} = \mu - k_{d1} \qquad \ldots \text{Eqn 4.15}$$

where: $k_{d1}$ = specific cell death rate in the growth phase ($h^{-1}$)

This death rate is a function of the magnitude of hydrodynamic stress. Lakhotia and Papoutsakis (1992) stated that hydrodynamic forces can reduce $\mu_{app}$ by decreasing $\mu$ or by increasing $k_{d1}$.

In batch culture, the apparent specific growth rate is expressed by the following equation:

$$\mu_{app} = \frac{dC_N}{dt} \Big/ C_N \qquad \ldots \text{Eqn 4.16}$$

In the present study, in the growth phase of the growth curve presented in Figure 4.46, the apparent specific growth rate is controlled by the substrate concentration. As explained in Section 4.5, the system becomes substrate limited due to passivation of the chalcopyrite mineral resulting in reduced ferrous iron in solution. However, although the apparent specific growth rate is controlled by the substrate concentration in the absence of hydrodynamic stress and not by the cell concentration, the rate of change of $\mu_{app}$ on increasing exposure to hydrodynamic stress is significant enough to be used as an indication of the system performance. This is facilitated by the limited change in available ferrous iron following passivation of the mineral.

Integrating Eqn. 4.16:

$$\ln (C_N/C_{N0}) = \mu_{app} t \qquad \ldots \text{Eqn 4.17}$$

where $C_N$ = biomass concentration at time t (cells $ml^{-1}$)

$C_{N0}$ = initial biomass concentration (cells $ml^{-1}$)

t = time (h)

University of Cape Town

Hence $\mu_{app}$ can be determined using the slope of ln $C_N$ as a function of time or differential elements of $C_N$ per unit time and biomass present.

The specific death rate, $k_{d1}$, can be determined by the difference between $\mu_{app}$ and $\mu$, where $\mu$ is defined as the maximum growth rate attainable in the system under the experimental conditions utilised in the absence of the stress factor investigated.

Region C (Figure 4.46) is characterised by a high specific death rate ($k_{d2}$) and a low specific growth rate owing to substrate depletion or reactor product inhibition of metabolic energy generation and the effects of hydrodynamic stress. Where the specific growth rate is very much smaller than the specific death rate, the biomass profile is defined by $k_{d2}$, hence:

$$\mu_{app} = \mu - k_{d2} \quad \cong \quad -k_{d2} \qquad \ldots \text{Eqn 4.18}$$

In this study it was not possible to determine $k_{d2}$ values due to the incomplete growth curves obtained in some experiments and thus only $k_{d1}$ results are presented.

**4.8.1.2 Review of the effect of solids loading and impeller speed on $k_d$ in the slurry reactor**

Pearce (1993) investigated the power law model and the exponential model to describe the correlation between the disruption rate constant ($k$), solids concentration and agitation rate. For solids loading experiments, data were obtained from experiments where non-growing *S. cerevisiae* was exposed to a quartzite volume fraction across the range of 0.00 to 0.40 at an impeller speed of 770 rpm. The extent of disruption was measured by determining the equilibrium release of soluble protein from the cells as a fraction of the maximum soluble protein available for release. The rate of protein released was described by the first order rate constant, $k$. The models were chosen empirically. The exponential model described the experimental data with a correlation coefficient of 0.954 while the power law model described the experimental data with a correlation coefficient of 0.999. An equation of the form:

$$k = 0.00198\ \Phi^{2.33} \qquad \ldots \text{Eqn 4.19}$$

where $\Phi$ = solids loading (w/w or w/v)

was derived for the dependence of $k$ on the solids concentration. The model was validated using the data of Currie *et al.* (1972) collected using a high-speed bead mill cell disrupter.

University of Cape Town

Scholtz-Brown (1998) conducted similar studies and modelled yeast cell disruption in incompletely and completely suspended solids regimes. The author investigated the effect of solids concentration and impeller speed on the disruption rate constant. For the solids loading experiments using a completely suspended solids regime, experiments were performed over a quartzite volume fraction range of 0.00 to 0.40 at an impeller speed of 750 rpm. An equation of the form:

$$k = 0.0202\ \Phi^{1.92} \qquad \ldots \text{Eqn 4.20}$$

with a correlation coefficient of 0.99 was derived.

Pearce (1993) also correlated the impeller speed to cell disruption in the slurry reactor. The author conducted experiments where the impeller tip speed was increased in the range 150 to 1090 rpm at a solids volume fraction of 0.20. The following power law model with a correlation coefficient of 0.95 was obtained:

$$k = 1.278 \times 10^{-9}\ N^{1.91} \qquad \ldots \text{Eqn 4.21}$$

where N = impeller tip speed ($m\ s^{-1}$)

The model derived for impeller speed did not adequately describe all agitation rate data. The disruption rate constant was described by the power law at agitation rates below 600 rpm. Above 600 rpm, the data separated from the model. The impeller speeds used by Pearce (1993) straddled the critical impeller speed of 685 rpm. Scholtz-Brown (1988) observed that the inadequate fit of the power law model above 600 rpm obtained by Pearce (1993) emphasised the need to model the cell disruption for the incompletely and completely suspended solids regimes separately. The appropriateness of the power law model below the critical impeller speed supports the power law dependence of $k$ on the suspended volume fraction of solids, increasing with increasing impeller speed.

Lamaignére (2002) extended the studies of Pearce (1993) and Scholtz-Brown (1998) by using a growing culture of *S. cerevisiae*. The author determined the relationship between the specific death rate constant in the growth phase of the yeast and solids loading and impeller speed using a power law function. For the solids loading experiments, quartzite loading was varied in the range 0 to 5 % v/v at an impeller speed was maintained at 565 rpm. For the impeller speed experiments, the impeller speed was varied between 460 and 850 rpm and the quartzite concentration was maintained at 1 % v/v. The following equations were determined for solids loading and impeller speed respectively:

University of Cape Town

$$k_d = 0.11\ \Phi^{0.50} \qquad R^2 = 0.98 \qquad \ldots \text{Eqn 4.22}$$

$$k_d = 0.014\ N^{0.34} \qquad R^2 = 0.87 \qquad \ldots \text{Eqn 4.23}$$

Good correlation was found using the power law model to describe the solids loading data although the exponent of $\Phi$ was not close to 2 as observed by Pearce (1993) and Scholtz-Brown (1998). Poor correlation was found using the power law model to describe the impeller speed experimental data even though the agitation rates utilised were above the critical impeller speed.

In addition to offering a predictive ability, the power law models derived by Pearce (1993) and Scholtz-Brown (1998) may also serve as mechanistic models. A cell disruption mechanism may be elucidated from the power law model. Abrahamson (1975) indicated that if the exponent of $\Phi$ is close to 2 ($c\Phi^2$), this suggests that solid-cell-solid collisions are the important cell disruption mechanism in the slurry reactor while if the exponent is close to 1 ($c\Phi$), then cell-solid and solid-cell-reactor collision are the dominant disruption mechanisms. The exponents of $\Phi$ in Eqns. 4.19 to 4.21 are all close to 2 confirming that solid-cell-solid collisions were the dominant disruption mechanism in the slurry systems discussed in these studies. However, in the solids loading model derived in the study by Lamaignére (2002) the exponent was close to 1. The author used lower solids loadings (0 to 5 % v/v) than the studies of Pearce (1993) and Scholtz-Brown (1998) (0 to 40 % v/v). Thus in the system of Lamaignére (2002) the results suggest, according to (Eqn. 4.22), that the dominant mechanisms of cell disruption are cell-solid and solid-cell-reactor collisions at lower solids concentrations.

In essence the models derived in the studies by Pearce (1993), Scholtz-Brown (1998) and Lamaignére (2002) have shown that $k_d$ can be related well to solids loading ($\Phi$) and to a lesser extent to agitation intensity (N) through a power law relationship:

$$k_d = c\ \Phi^d \qquad \text{and,} \qquad \ldots \text{Eqn 4.24}$$

$$k_d = c\ N^d \qquad \ldots \text{Eqn 4.25}$$

where c, d = constants

In the present study, the relationship between $k_{d1}$ and solids concentration was investigated. The power law function employed by Pearce (1993), Scholtz-Brown (1998) and Lamaignére (2002)

University of Cape Town

was used. The growth data for impeller speed was not analysed further due to the limited number of impeller speed experiments performed.

#### 4.8.1.3 Effect of solids loading on $k_{di}$

Using the growth data obtained in the solids loading experiments carried out at 0, 6, 9, 12, 15 and 18 % w/w quartzite loadings and an impeller tip speed of 1.97 m $s^{-1}$, $k_{di}$ was determined using the method detailed in Appendix B.2. In this study it was not feasible to determine $\mu$ in the absence of solids because the substrate, chalcopyrite, formed at least part of the solid phase and intensive mixing and aeration was required for solids suspension and oxygen and carbon dioxide mass transfer for microbial growth. The approach of Yang and Wang (1992) was used in which $\mu$ was determined under conditions of mild hydrodynamic stress to minimise the stress effect on cell growth. These data under conditions of minimal cell damage from agitation and sparging served as a control against which $k_{di}$ was determined.

In the present study, $\mu$ for all experiments was defined as the maximum specific growth rate obtained in the absence of quartzite, the presence of 3 % chalcopyrite and an impeller tip speed of 1.97 m $s^{-1}$. The specific growth rate for experiments conducted under these conditions was determined to be 0.007 $h^{-1}$. The apparent specific growth rate ($\mu_{app}$) was defined as the maximum specific growth rate observed at each quartzite loading in the range 6 to 18 %. In Figure 4.47, $k_{di}$, determined by difference between $\mu$ and $\mu_{app}$, is given as a function of solids loading.

As observed by Lamaignére (2002), a power law relationship describes the dependence of $k_{di}$ on solids loading. The modelled data shown in Figure 4.47 was obtained by recalculating the experimental data using the power law equation and minimising the sum of the squares of the difference between the experimental and predicted values. The power law model for the present study was determined to be:

$$k_{di} = 4.61 \times 10^{-5} \Phi^{1.66} \qquad R^2 = 0.98 \qquad \ldots \text{Eqn 4.26}$$

University of Cape Town

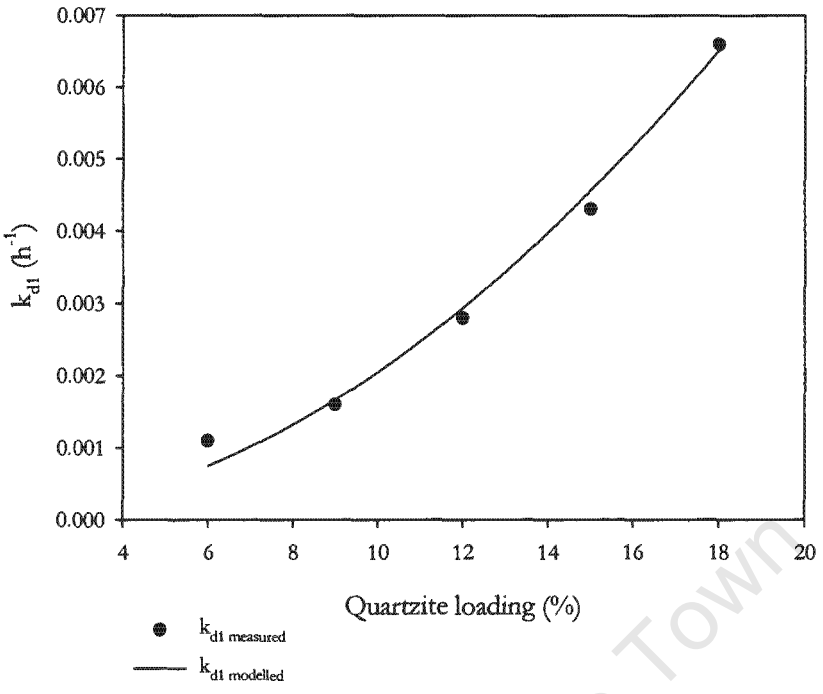


**Figure 4.47:** The specific death rate constant as a function of quartzite loading and an impeller tip speed of 1.97 m $s^{-1}$.

Figure 4.48 shows good correlation between the predicted and measured specific death rate constant. Furthermore, in Figure 4.48, the model is tested against the data obtained by Sissing (2002) using *S. metallicus* cultivated on 3 % pyrite in the presence of quartzite and shows a reasonable predictive ability. This is consistent with the micro-organisms in these studies both being of the genus *Sulfolobus* with similar cell wall structure.

University of Cape Town

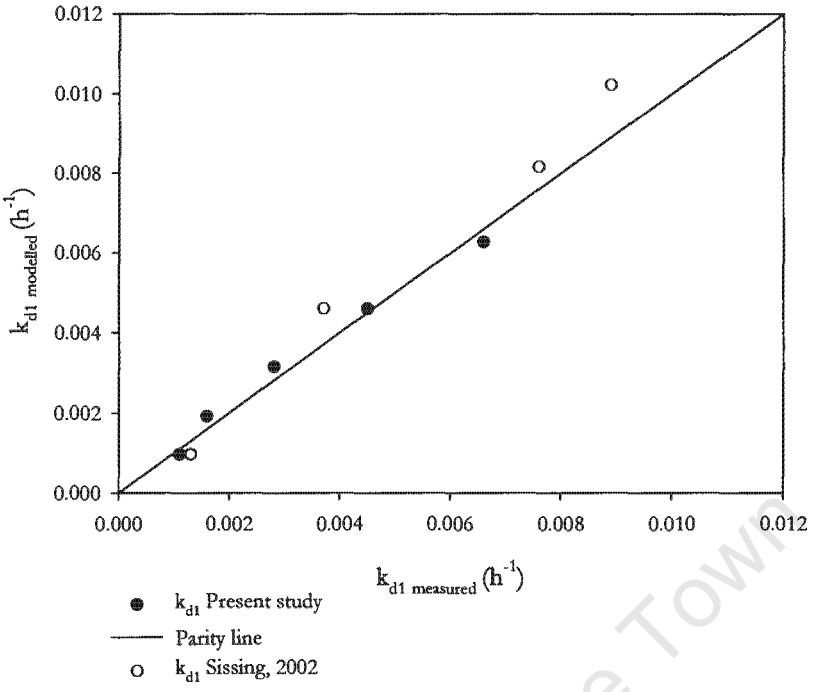


**Figure 4.48:** Comparison between the experimental specific death rate constant, $k_{d1\ measured}$ (data used to generate the model and the data of Sissing (2002)) and the modelled specific death constant ($k_{d1\ modelled}$) for solids loading experiments.

In Table 4.15 the exponent of Φ from Eqn. 4.26 is compared to the values obtained by Pearce (1993), Scholtz-Brown (1998) and Lamaignére (2002). The exponent of 1.66 determined in the present study is similar to those obtained in the investigations of Pearce (1993) and Scholtz-Brown (1998) of 2.33 and 1.92 respectively. The exponent derived in the present study is close to 2 indicating that solid-cell-solid collisions are possibly the cell disruption mechanism in the chalcopyrite-quartzite slurry system.

**Table 4.15:** Comparison between the exponents of Φ obtained in the various studies.

| Parameter | Pearce (1993) | Scholtz-Brown (1998) | Lamaignére (2002) | Present study |
|---|---|---|---|---|
| d | 2.33 | 1.92 | 0.50 | 1.66 |

University of Cape Town

### 4.8.2 REDOX POTENTIAL

The operating redox potential (which can be related directly to the ferric to ferrous iron ratio) of a bioleaching system can be determined by examining the kinetics of bioleaching (Petersen and Dixon, 2005). For this purpose, the rate of oxidation of ferrous iron by the bioleaching micro-organism, and the rate of leaching of the mineral as a function of the ferric to ferrous iron ratio are required. In Section 4.5.1, Figure 4.7 showed the dependence of the rate of chalcopyrite leaching on the ferric to ferrous iron ratio and thus solution redox potential. The mineral leach rate profile was derived using the model of Hiroyoshi *et al.* (2004) and the redox potential window for optimal chalcopyrite leaching was approximated to be between 450 and 560 mV (Ag/AgCl). A profile showing the dependence of the kinetics of microbial ferrous iron oxidation on the ferric to ferrous iron ratio can also be derived for the bioleaching micro-organism. Searby and Hansford (2003) generated a profile for the rate of ferrous iron oxidation by a *Sulfolobus* sp. as a function of the ferric to ferrous iron ratio. Petersen and Dixon (2005) reported that the operating redox potential of a system can be determined from the intersection point between these mineral oxidation rate and microbial oxidation rate curves, plotted as a function of the ferric to ferrous iron ratio. The intersection point between the mineral curve and the microbial curve represents the point at which the system is balanced. In order for balance to be attained, the rate of microbial ferric generation must equal the rate of ferric consumption of the mineral. If these are not balanced then the ferric to ferrous iron ratio will shift until balance is achieved (Petersen and Dixon, 2005).

The relevance of the intersection point between the curves in defining operating conditions within the bioleaching system was first reported by Rawlings *et al.* (1999). The authors determined the intersection points between the ferric demand curve for pyrite and the ferric supply curves for *Leptospirillum ferriphilum* and *Acidithiobacillus ferrooxidans* in an effort to understand why *Leptospirillum*-like species are the dominant iron oxidising bacteria in commercial processes for the bio-oxidation of pyrite and related minerals. The ferric supply and demand curves respectively for the mineral and the bacteria are shown in Figure 4.49. *L. ferriphilum,* unlike *At. ferrooxidans*, has a high affinity for ferrous iron and is not inhibited by ferric iron hence the rate of ferrous oxidation remains high at elevated redox potentials. The curves presented in Figure 4.49 were derived using the kinetic constants for bacterial ferrous iron oxidation obtained by Boon (1996) and van Scherpenzeel (1997) and the kinetic constants for the ferric leaching of pyrite obtained by May *et al.* (1997). Rawlings *et al.* (1999) reported that the intersection point between the mineral and the microbial curves defines the conditions (e.g. redox potential) where the rate of ferric supply and ferric demand is balanced. *L. ferriphilum* has a higher activity at elevated redox potentials compared to *At. ferrooxidans*. The pyrite curve intersects the bacterial oxidation curve

University of Cape Town

for *L. ferriphilum* at a high redox potential. At this elevated redox potential, pyrite leaches at a high rate and *L. ferriphilum* has a high activity. This provided an explanation as to why *L. ferriphilum* out-competes *At. ferrooxidans* in the bioleaching of pyrite.

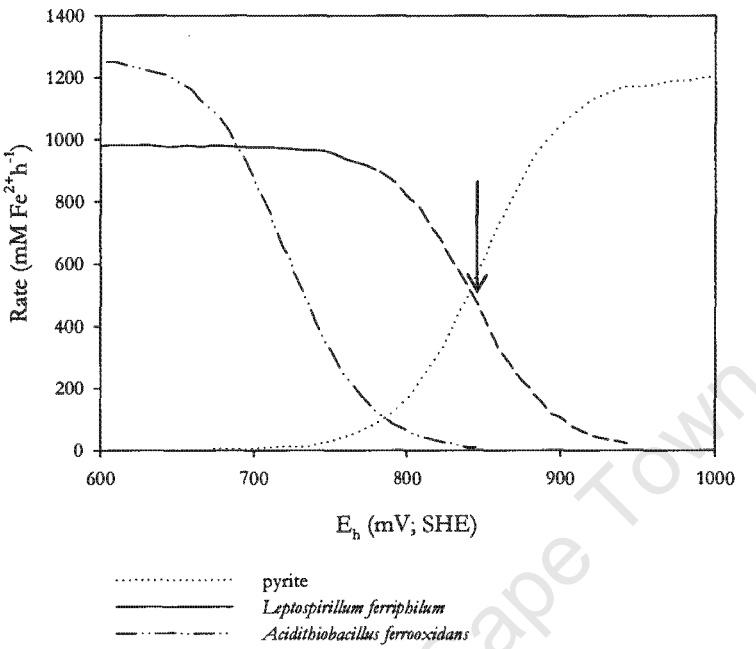


**Figure 4.49:** Rates of ferrous iron production from the chemical ferric leaching of pyrite (64 μm) and the rates of ferrous iron consumption by bacterial oxidation by *L. ferriphilum* and *At. ferrooxidans* (adapted from Rawlings *et al.*, 1999). Arrow indicates the point of intersection between the *L. ferriphilum* and pyrite curves.

In the present study, using the analysis technique of Rawlings *et al.* (1999), adapted by Petersen and Dixon (2005), a further explanation is sought for (i) the high operating redox potential observed in the solids loading experiments and (ii) the change in redox potential observed at each quartzite loading as a function of time in the solids loading experiments. Figure 4.50 illustrates a typical microbial ferrous oxidation rate curve for a *Sulfolobus* sp. (Searby and Hansford, 2003) and mineral oxidation rate curves for chalcopyrite (Hiroyoshi, 2004) and pyrite (May *et al.*, 1997). Arbitrary rate data were chosen since only relative and not absolute values are required for this discussion. The rate of pyrite leaching increases steadily with the ferric to ferrous iron ratio whereas the chalcopyrite curve is raised within a narrow window of low ferric to ferrous iron ratios and the leach rate is significantly reduced at elevated ferric to ferrous iron ratios. This effect is usually associated with passivation of chalcopyrite at high ferric to ferrous iron ratios (redox potentials). As the mineral curves presented in Figure 4.50 represent the rate of oxidation of the two minerals. By stoichiometry, they also represent the rate of ferric iron and hence oxidant demand. The supply to this demand is provided by microbial ferrous oxidation (ferric supply) as

University of Cape Town

represented by the microbial curve in Figure 4.50 (Petersen and Dixon, 2005). The shape of the curves and their position relative to the *x* axis are consistent for each mineral and bioleaching micro-organism under specific conditions. However, the supply and demand curves will shift up with increasing ferric supply by the micro-organisms or ferric demand of mineral and shift down if either the ferric supply by the culture or ferric demand of the mineral decreases. Considering thermophilic chalcopyrite leaching, in Figure 4.50, if the ferrous oxidation capacity of the inoculum is high, then the microbial curve will intersect the mineral curve as shown by arrow *a* and the operating redox potential of the system will increase. In the present study, the redox potential rose sharply during the inoculum build-up period (0-24 h) due to the high cell concentration and activity and hence high ferrous oxidation capacity of the inoculum at 0 h. As shown in Figure 4.50, at the elevated redox potentials, the rate of chalcopyrite dissolution is reduced significantly. Conversely, considering thermophilic pyrite bioleaching, even at high cell concentrations and activity the microbial and mineral curves for the *Sulfolobus* sp. and pyrite intersect (arrow *b*) at an operating redox potential where the mineral ferric demand and the microbial ferric supply are high. Thus pyrite is leached more readily by *Sulfolobus* sp. at the elevated redox potentials. Furthermore, in a system containing both pyrite and chalcopyrite where the activity of the culture is high (elevated ferric supply), pyrite leaching will occur at a faster rate than chalcopyrite leaching.

University of Cape Town

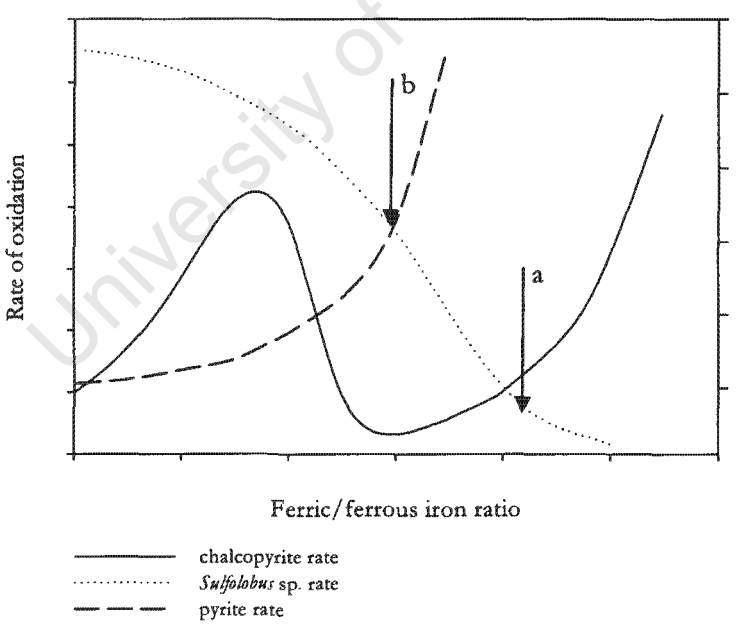


**Figure 4.50:** Proposed supply-demand curves as a function of the ferric/ferrous iron ratio for a chalcopyrite and pyrite mineral bioleach by a *Sulfolobus* sp. (adapted from Hiroyoshi, 2004, May *et al.*, 1997 and Searby and Hansford, 2003).

In Section 4.6 it was shown that increasing quartzite loading in the range 0 to 18 % caused a decline in process performance as shown by changes in pH and redox potential, and a decline in the rate and extent of growth, and iron and copper solubilisation. From 0 to 23 h (inoculum build-up phase) the redox potential increased similarly in all reactors due to identical physiological and hydrodynamic conditions. At 23 h, the addition of quartzite to the experimental reactors caused a decline in their process performance. The change in redox potential over time differed depending on the intensity of hydrodynamic stress applied. Three groups of quartzite loadings were identified within which the change in redox potential over time was similar. The three groups, namely 0 and 6 % quartzite (negligible to mild hydrodynamic stress), 9, 12 and 15 % quartzite (intermediate hydrodynamic stress), and 18 % quartzite (intense hydrodynamics stress) were chosen on the basis of the shape of their redox potential time profiles (Figure 4.14). Table 4.16 shows the change in redox potential observed during the solids loading experiments from 24 to 71 h for the three groups of quartzite loadings. Analysis of Figures 4.51 to 4.56 provides a possible explanation for the change in operating redox potential during the solids loading experiments by considering the shift in the intersection point between the *Sulfolobus* sp. ferric supply and chalcopyrite ferric demand curves. The curves at 23 h represent conditions in the reactor just before quartzite was added and the impeller tip speed was increased.

At 0 and 6 % quartzite loadings, the redox potential increased from 23 to 71 h (Table 4.16). At 9, 12 and 15 % quartzite loadings, the redox potential decreased from 24 to 48 h and subsequently increased but at a reduced rate compared to the reactor containing 0 % quartzite. The reduction in rate was inversely proportional to the quartzite concentration. At an 18 % quartzite loading the redox potential fell sharply over the 24 to 48 h period from 606 to 508 mV with a further decrease to 506 mV at 71 h. Continued mineral leaching was observed during the 23 to 71 h time period in all reactors. Continued mineral leaching would have resulted in a decrease in the mineral ferric demand over time because of the reduced surface area of mineral available for leaching.

University of Cape Town

**Table 4.16:** Change in redox potential from 23 to 71 h for solids loadings in the range 0 to 18 % quartzite operated at an impeller tip speed of 1.97 m $s^{-1}$.

| Reactor conditions | | Redox potential (mV; Ag/AgCl) | | |
|---|---|---|---|---|
| Quartzite loading (%, w/v) | Impeller tip speed (m $s^{-1}$) | 23 h | 48h | 71h |
| | Group 1 (negligible to mild hydrodynamic stress) | | | |
| 0 | 1.97 | 606 | 621 | 636 |
| 6 | 1.97 | 605 | 607 | 618 |
| | Group 2 (mild to intermediate hydrodynamic stress) | | | |
| 9 | 1.97 | 605 | 599 | 613 |
| 12 | 1.97 | 605 | 567 | 595 |
| 15 | 1.97 | 604 | 565 | 584 |
| | Group 3 (intense hydrodynamic stress) | | | |
| 18 | 1.97 | 606 | 508 | 506 |

Figures 4.51 and 4.52 show the proposed ferric supply curves of the *Sulfolobus* culture and the ferric demand curves for the chalcopyrite concentrate over a 71 h period in the presence of 0 and 6 % quartzite (negligible or mild hydrodynamic stress conditions). As bioleaching proceeded under conditions of negligible to mild hydrodynamic stress, the ferric supply capacity of the culture increased causing the microbial curve to shift up. During this time, the mineral curve shifts down because of a reduction in the mineral surface area available for leaching due to (i) leaching of the mineral and (ii) passivation of the mineral surface. Taking into account these changes in the position of the curves relative to the *y* axis, the intersection point (operating point) between the mineral curve and the microbial curve shifts to the right (Figure 4.52) indicating an increase in the operating redox potential in the transition from intersection points *a* to *c*. This analysis explains why the redox potential in the reactors containing 0 and 6 % quartzite increased continuously from 23 to 71 h.

University of Cape Town

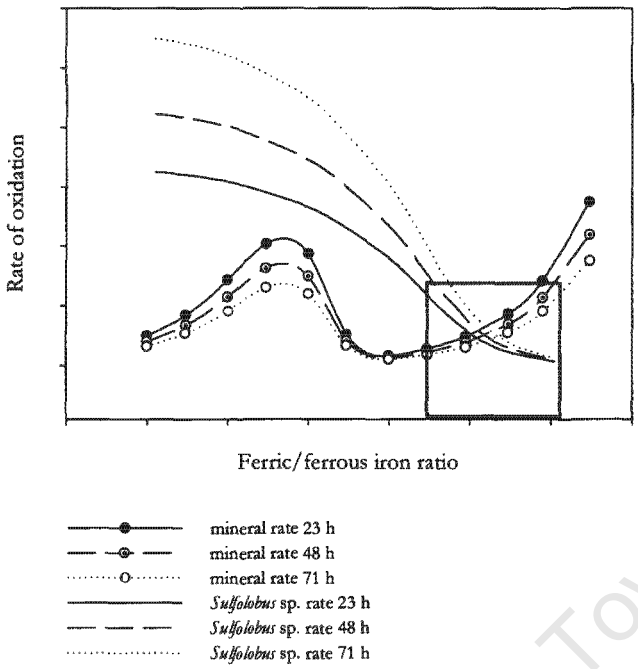


**Figure 4.51:** Proposed supply - demand curves for chalcopyrite and a *Sulfolobus* sp. under conditions of negligible to mild hydrodynamic stress. Open square indicates the intersection points of interest between the mineral curve and the microbial curve.

University of Cape Town

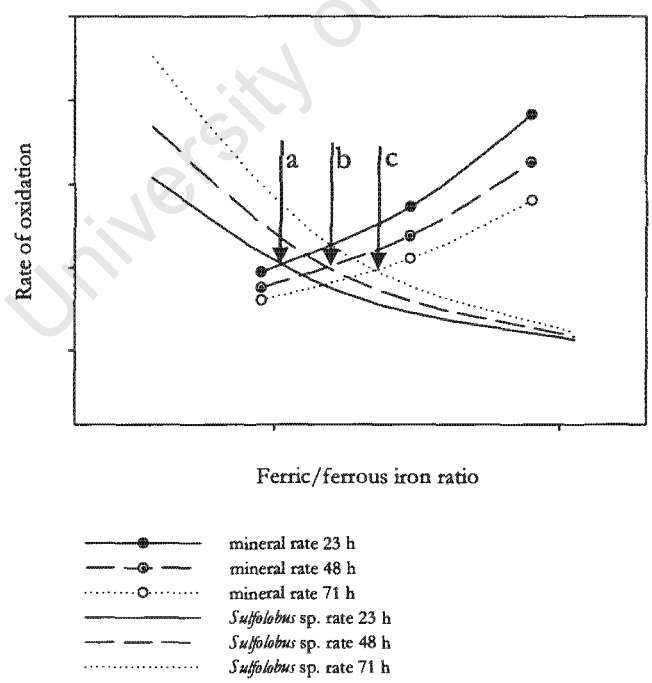


**Figure 4.52:** Magnification of the region represented by the open square in Figure 4.51 showing the intersection points of interest between the mineral curve and the microbial curve. (a) 23 h intersection point; (b) 48 h intersection point; (c) 71 h intersection point.

Figures 4.53 and 4.54 show the proposed ferric supply curves of the *Sulfolobus* culture and the ferric demand curves for the chalcopyrite concentrate over the 23 to 71 h period in the presence of 9, 12 and 15 % quartzite (intermediate hydrodynamics stress conditions). The intersection points between the mineral and microbial curves are shown in Figure 4.54. Increasing hydrodynamic stress conditions after the inoculum build-up phase caused a reduction in metabolic activity, a reduction in cell viability and cell lysis. These effects caused an overall reduction in the ferrous iron oxidising capacity of the culture. The microbial curve shifts down with a concomitant downward shift in the mineral curve due to continued leaching as shown by an increase in the percentage iron and copper solubilised (Figures 4.19 and 4.22). The intersection point shifts to the left (indicated by arrow *b*) indicating a decline in the operating redox potential. Over the 48 to 71 h period the culture began to recover from the effects of the stress conditions. The microbial curve shifts upward with a simultaneous downward shift in the mineral curve due to continued leaching and the intersection point shifts to the right. The extent of this shift is dependent on the quartzite concentration. This analysis explains why the redox potential in the reactor containing 9, 12 and 15 % quartzite decreased from 23 to 48 h and increased from 48 to 71 h. The redox potential indicated by intersection point *c* in Figure 4.54 is representative of the shift observed at a 9 % quartzite loading. Here, at 71 h, the redox potential increased above the 23 h redox potential value. However, at 12 and 15 % quartzite loadings the redox potential increased above the 23 h potential at only 96 and 144 h respectively.

University of Cape Town

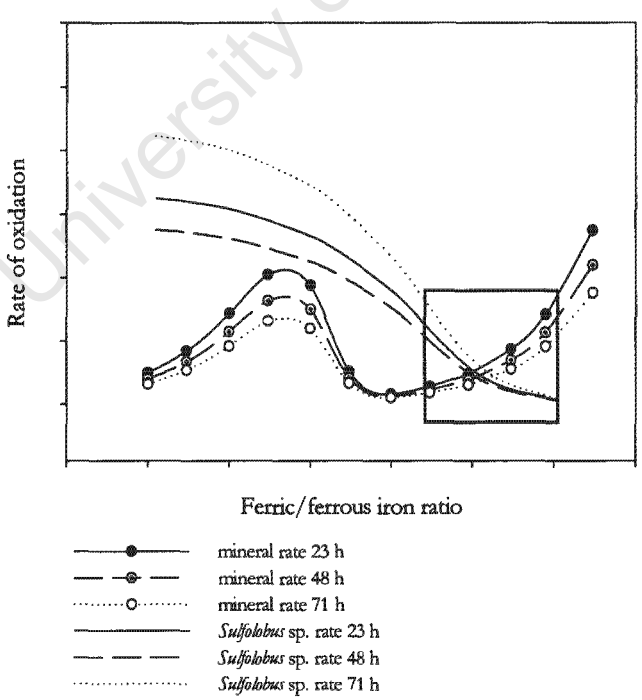


**Figure 4.53:** Proposed supply - demand curves for chalcopyrite and a *Sulfolobus* sp. under conditions of mild to intermediate hydrodynamic stress. Open square indicates the intersection points of interest between the mineral curve and the microbial curve.

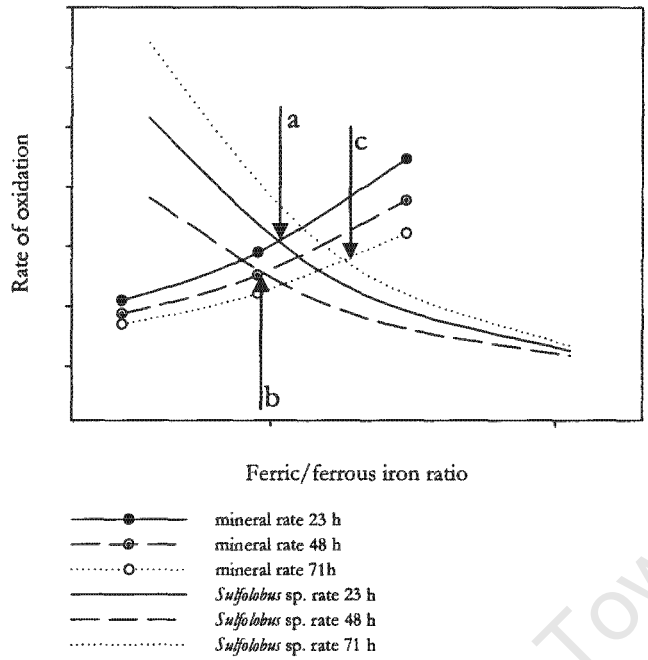


**Figure 4.54:** Magnification of the region represented by the open square in Figure 4.53 showing the intersection points of interest between the mineral curve and the microbial curve. (a) 23 h intersection point; (b) 48 h intersection point; (c) 71 h intersection point.

Figures 4.55 and 4.56 show the proposed ferric supply curves of the *Sulfolobus* culture and the ferric demand curves for the chalcopyrite concentrate over a 71 h period in the presence of 18 % quartzite (intense hydrodynamic stress). Increasing the quartzite concentration above 15 % led to a significant decrease in cell concentration compared to the 0, 6, 9, 12 and 15 % quartzite loadings and hence the overall ferrous oxidation capacity of the culture declined. It is proposed that from 23 to 48 h, on addition of solids to the reactor after the inoculum build-up phase, the microbial ferric supply curve shifts low enough to intersect the mineral ferric demand curve at 3 points (Figure 4.55). Two of the intersection points fall within the redox potential window for increased rates of chalcopyrite leaching (Figure 4.56). The intersection point indicated by arrow *b* is dominant possibly due to the more favourable leaching under these conditions. From 48 to 71 h, the cell concentration did not change and thus the microbial curve remains at the same position. However, the mineral curve shifts downward due to continued leaching (as shown by an increase in the total iron solubilised, Figure 4.19) and the intersection point shifts to the left and the system operated at a lower redox potential. This analysis explains why the redox potential in the reactor containing 15 % quartzite decreased from 23 to 48 h with a further decrease from 48 to 71 h.

University of Cape Town

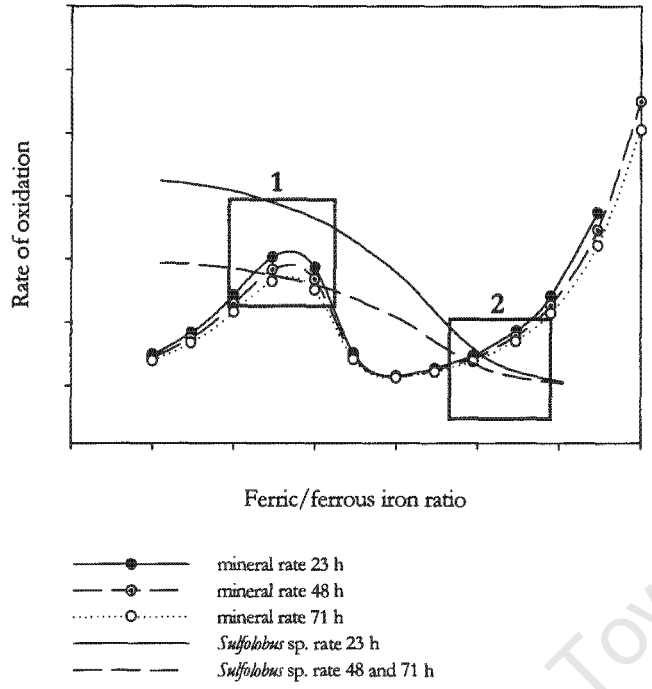


**Figure 4.55:** Proposed supply - demand curves for chalcopyrite and a *Sulfolobus* sp. under conditions of intense hydrodynamic stress. Open squares 1 and 2 indicate the intersection points of interest between the mineral curve and the microbial curve.

University of Cape Town

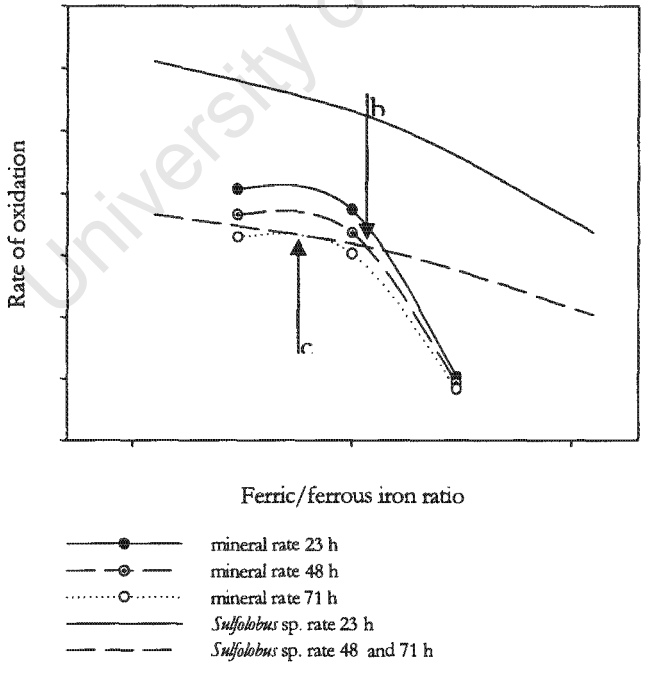


**Figure 4.56:** Magnification of the region represented by open square 1 in Figure 4.55 showing the intersection points of interest between the mineral curve and the microbial curve. (b) 48 h intersection point; (c) 71 h intersection point.

The analysis technique presented here may also be used as a tool to predict the operating redox potential in a system where the ferrous iron oxidation rate of the bioleaching culture and the rate of leaching of the mineral as a function of the redox potential are known. This predictive ability is especially important for the bioleaching of chalcopyrite because, unlike other less recalcitrant minerals, e.g. pyrite, the optimal leaching of chalcopyrite is restricted to a narrow redox potential (ferric to ferrous iron ratio) window.

### 4.8.3 CONCLUSIONS

In this section it was shown that a mathematical model in the form of a power law model can be used for the prediction of the specific death rate constant in the growth phase at various solids loadings other than those used in this investigation. The power law relationship between the specific death rate constant and solids loading proposed by Pearce (1993), Scholtz-Brown (1998) and Lamaignére (2002) showed good correlation with the experimental data from the present study and the study of Sissing (2002).

Further analysis of redox potential data using the approach of Rawlings *et al.* (1999) and Petersen and Dixon (2005) showed that this method of analysis may be used to understand the variation in redox potential with solids loading and time. In addition this method may be used to predict the operating redox potential in a bioleaching system using existing microbial ferric supply curves and mineral ferric demand curves. In the present study, the analysis, based on changes in the ferric supply by the *Sulfolobus* culture and the chalcopyrite ferric demand, explained changes in redox potential observed in the solids loading experiments and showed that at an 18 % quartzite concentration it was possible to improve chalcopyrite leaching by reducing the microbial ferrous iron oxidation capacity of the culture. At lower quartzite concentrations, high microbial activity led to a shift in the operating point to higher redox potentials that were not conducive to chalcopyrite leaching. Although the overall extent of leaching at the lower quartzite loadings was higher than at the 18 % quartzite loading, it is proposed that if the leaching time were extended and leaching in the reactor containing at the 18 % quartzite continued at a low redox potential, a higher extent of leaching would be observed at an 18 % quartzite concentration compared to the lower solids loadings during this extended period.

University of Cape Town

## 4.9 CONCLUSIONS

In this chapter the effects of increasing hydrodynamic stress, through increasing solids loading and impeller tip speed, on the performance of the chalcopyrite bioleaching process were assessed. Increasing solids loading and impeller tip speed had an adverse effect on the bioleaching of chalcopyrite by the *Sulfolobus* culture. The extent of the adverse effect was found to be a function of impeller speed and quartzite concentration. A decline in the rate and extent of growth, and iron and copper solubilisation was observed on increasing solids loading and impeller tip speed. For the solids loading experiments the intensity of the stress appeared to be clustered within three sets of solids loadings. The first cluster comprised the 6 and 9 % quartzite loading which appeared to perform similarly and caused a low intensity of stress to the micro-organisms. The second cluster comprised the 12 and 15 % quartzite loadings which showed significantly reduced reactor performance compared to the first 6 and 9 % solids loading cluster. Finally, at an 18 % quartzite loading a drastic decline in system performance, approaching systems failure, was observed.

The results obtained in this study were compared to mineral-only, mineral-quartzite and quartzite-only slurry reactor systems from literature. A similar trend of a decrease in process performance with increasing hydrodynamic stress was observed in all studies considered. In systems where the effect of solids loading was studied by increasing the mineral concentration, the effects of physiological factors such as oxygen and carbon dioxide availability and build-up of toxic leach products contributed to stress in the system and the effect of hydrodynamic stress could not be elucidated. Using mineral-quartzite systems investigators were able to study the effect of hydrodynamic stress in the absence of physiological stress. The pyrite-quartzite system of Sissing (2002) was found to outperform all other thermophilic STR bioleaching systems investigated. Although the chalcopyrite-quartzite system was not oxygen or carbon dioxide limited, the recalcitrance of chalcopyrite to leaching caused nutrient stress to the micro-organisms. This nutrient stress compounded the effects of hydrodynamic stress.

Further analysis of growth data showed that the specific death rate increased in a power law fashion with increasing hydrodynamic stress. A power law model, describing the relationship between solids loading and the specific death rate constant, was derived. The analysis showed that a power law function may be use to describe the effect of solids loading on the specific death rate constant of *Sulfolobus* spp. in agitated slurries. The power law model derived for solids loading was validated using the data of Sissing (2002). The exponent of the solids loading term in the model was found to be close to 2 in the solids loading study corroborating the results of Pearce

University of Cape Town

(1993) and Scholtz-Brown (1998) and showing that the primary mechanism of damage in the slurry reactor is solid-cell-solid collisions.

Using the data analysis technique of Rawlings *et al.* (1999), adapted by Petersen and Dixon (2005), the change in redox potential time profiles observed in the solids loading experiments in the present study could be explained. It was postulated that if detailed kinetics of a particular bioleaching system under specified conditions are known, then operating redox potential of the system may be predicted. This form of analysis could prove useful in optimising chalcopyrite bioleaching processes, as in recent years investigators have shown that controlling the redox potential of the system within a narrow redox window can lead to higher extents of chalcopyrite leaching.

On analysis of the independent solids loading and impeller tip speed experiments, the critical quartzite loading and critical impeller tip speed, beyond which the effects of hydrodynamic stress were significant, were identified as 9 % and 1.67 m $s^{-1}$ respectively. This conclusion was validated by the results from the combined experiments.

University of Cape Town

# Chapter 5: Results and Discussion II

## The biological response to hydrodynamic stress mediated by increasing solids loading and impeller tip speed

In Chapter 4, process considerations were used as criteria to evaluate the effect of solids loading and impeller tip speed on the thermophilic bioleaching of chalcopyrite. In this chapter the biological response is used to evaluate these effects. The biological response was evaluated by determining cell morphology (Section 5.1), metabolic activity (Section 5.2), membrane integrity (Section 5.3) and the change in intracellular protein composition (Section 5.4). These were measured using the analyses listed in Table 5.1. In this way, the effect of hydrodynamic stress was determined at a cellular level and the results contributed towards an understanding of the mechanism of hydrodynamic cell injury as well as potential mechanisms of stress protection. Samples were selected at different time intervals from the solids loading and speed experiments discussed in Chapter 4. The current chapter is divided on the basis of the effect of hydrodynamic stress at a cellular level and the nature of the biological response to this stress, rather than on solids loading and impeller tip speed.

University of Cape Town

**Table 5.1:** Analyses used to determine the biological response with increasing solids loading and impeller tip speed.

| Biological response | Analysis |
|---|---|
| Change in morphology | Phase contrast microscopy<br>Scanning electron microscopy<br>Cell size distribution |
| Change in metabolic activity of the culture | Specific oxygen utilisation rate ($q_{O2}$) |
| Change in membrane integrity | Dual fluorescence staining |
| Change in intracellular protein composition | SDS PAGE |

# 5.1 THE EFFECT OF HYDRODYNAMIC STRESS ON CULTURE MORPHOLOGY

Morphology is defined as the description of form and structure. In this section the form and structure of *Sulfolobus* cells are investigated after their exposure to hydrodynamic stress incurred by increasing agitation rate and solids loading. Reactors were sampled in mid-growth phase and samples were prepared and analysed immediately. Phase contrast microscopy was used to observe cell morphology for the impeller speed experiments. Although this method was constrained to provide only limited magnification of the cells (1000 x), samples could be viewed as wet preparations without extensive sample preparation. High magnification (6 500 to 40 000 x) morphological analysis of cells from a limited number of samples from the solids loading experiments was performed using a scanning electron microscope (SEM). Quantitative analysis of cell size for the solids loading experiments was achieved using a CellFacts particle analyser that provided a cell-number-based size distribution.

University of Cape Town

## 5.1.1 DIRECT MICROSCOPIC ANALYSIS

Phase contrast microscopy was used to examine the effect of increasing impeller tip speed in the range 1.67 to 2.13 m $s^{-1}$ at 0 and 9 % quartzite loadings on the morphology of planktonic cells. Samples were removed from the reactors and settled for 30 min to remove the majority of the non-biological particulate phase before direct microscopic viewing.

### 5.1.1.1 Description of morphological forms identified

Several cell shapes, sizes and intensities were detected during the growth cycle of the cultures as well as a consequence of increasing hydrodynamic stress. These morphologies are represented diagrammatically in Figure 5.1.

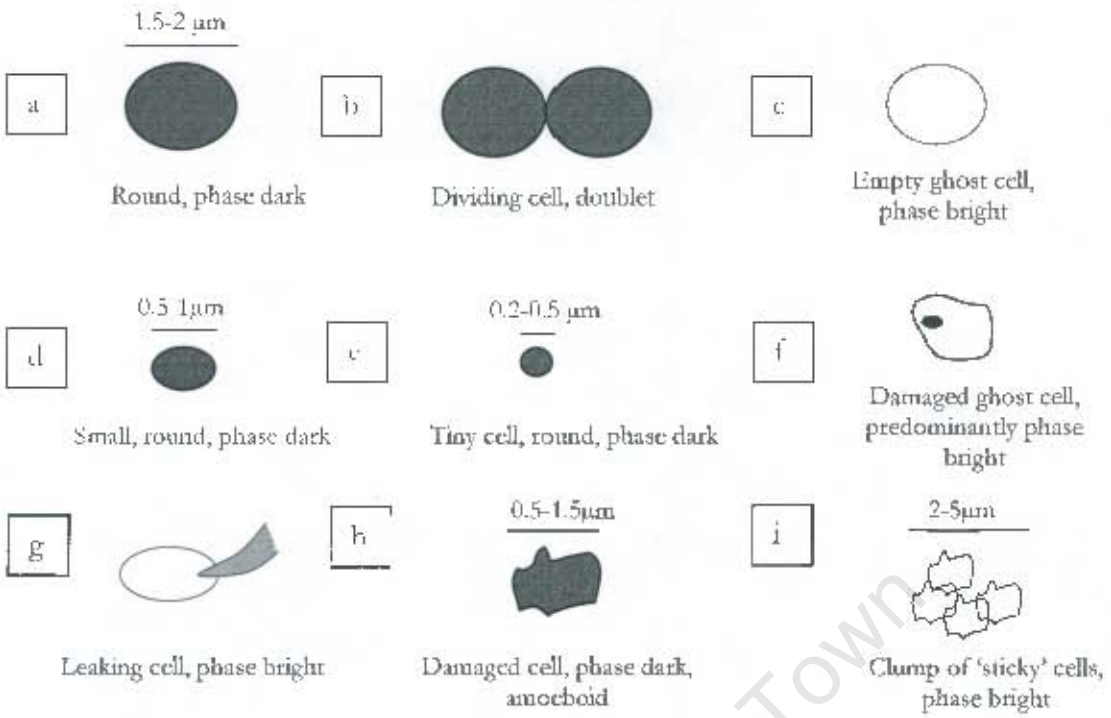


**Figure 5.1:** Schematic representation of cell shapes, intensities and dimensions observed during hydrodynamic stress experiments.

Figures 5.2 to 5.5 present phase contrast images illustrating examples of the different cell morphologies presented in Figure 5.1. Round, phase dark cells (Figure 5.1a; Figure 5.2 arrow *a*) and cell doublets (Figure 5.1b; Figure 5.2 arrow *b1*) were found mostly in the baseline reactor in the absence of quartzite when operated at low impeller tip speeds. Following inoculation, the cells occurred singly and were round and phase dark. In mid exponential phase, several doublets and occasionally chains of cells (Figure 5.2 arrow *b2*) were visible. The stationary phase comprised mostly single, round, phase dark cells.

The reactors supplemented with quartzite and operated at increased impeller tip speeds presented increased variation in cell shapes and sizes depending on the intensity of hydrodynamic stress applied. Cells sometimes appeared phase dark and round ranging from 1.5 to 2µm in size (Figure 5.1a; Figure 5.3 arrow *a*). Other cells remained phase dark and round but were reduced in size, ranging from small (Figure 5.1d; Figure 5.3 arrow *d*) to very tiny cells (Figure 5.1e; Figure 5.3 arrow *e*) with diameters of approximately 0.2 to 0.5µm. Extreme morphological types observed included ghost cells where the micro-organisms displayed round or amoeboid shapes sometimes with dark spots noticeable within the cytoplasm (Figure 5.1c and 5.1f; Figure 5.3 arrows *c* and *f*). In addition to these morphological types, leaking cells were also evident (Figure 5.1g; Figure 5.4). These were classified as cells that had been damaged and from which the cytoplasm was

University of Cape Town

extruding. At the higher solids loadings and impeller tip speeds, clumps of cells were visible (Figure 5.1i; Figure 5.5 arrow *i*). Damaged cells formed large irregular clumps consisting of varying cell sizes. In subsequent sections the various cell morphologies are discussed with respect to operating conditions.

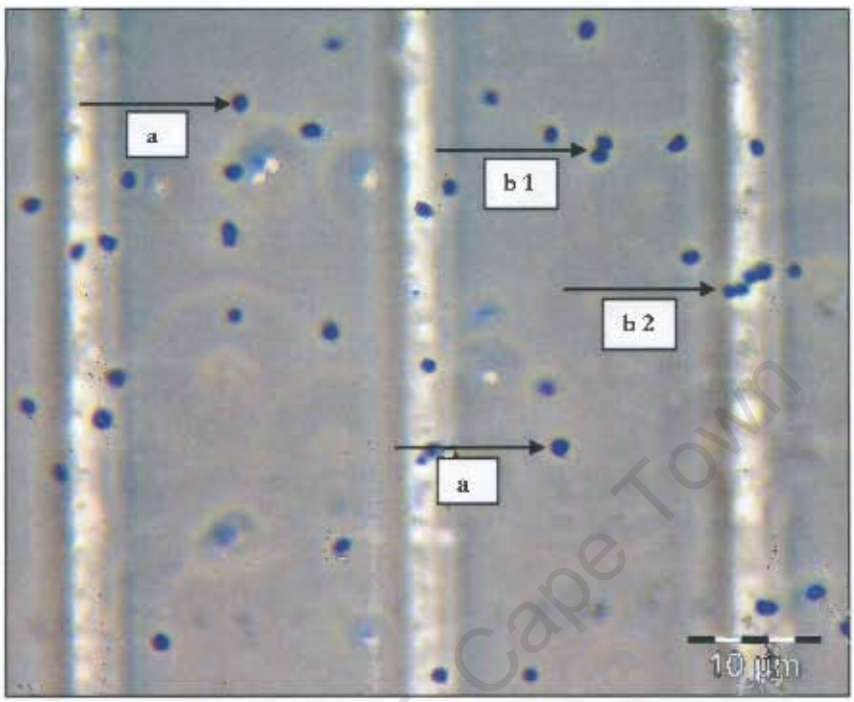


**Figure 5.2:** Image of cells sampled at 72 h from the baseline reactor (0 % quartzite) operated at an impeller tip speed of 1.97 m $s^{-1}$. a = round, phase dark singlets; b1 = doublets; b2 = chain of cells.

University of Cape Town

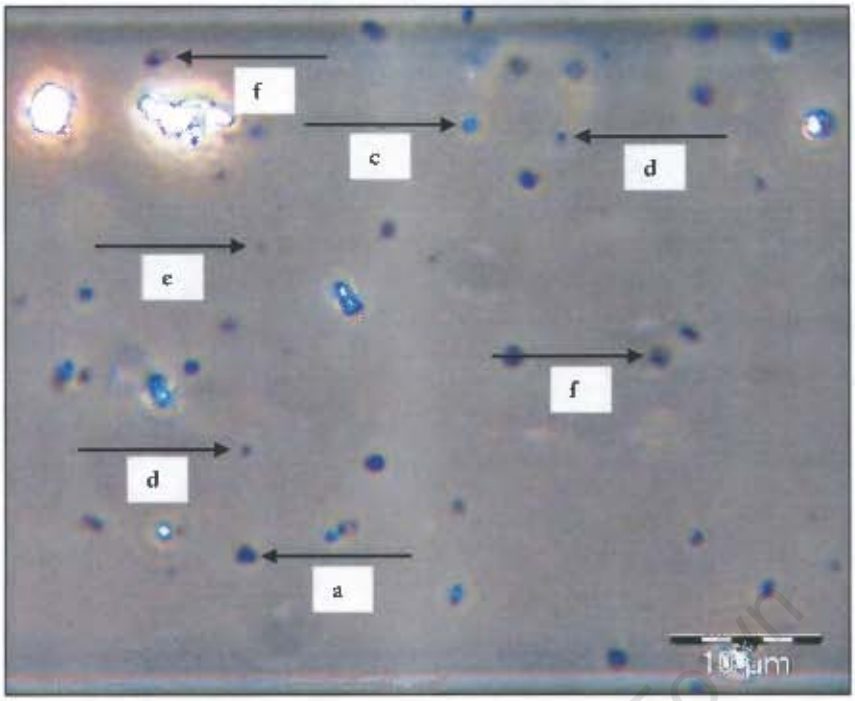


**Figure 5.3:** Image of cells sampled at 72 h from the reactor containing 12 % quartzite operated at an impeller tip speed of 1.97 m s $^{-1}$. a = round, phase dark; c = empty ghost cell; f = damaged ghost cell; d = small cells; e = tiny cells.


**Figure 5.4:** Image of cells sampled at 72 h from the reactor containing 12 % quartzite operated at an impeller tip speed of 1.97 m s $^{-1}$. Arrows indicate leaking cells.

University of Cape Town

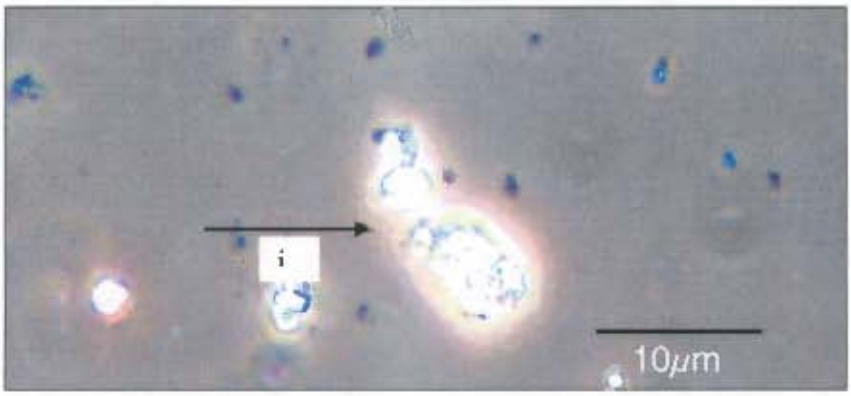


**Figure 5.5:** Image of cells sampled at 72 h from the reactor containing 15 % quartzite operated at an impeller tip speed of 1.97 m $s^{-1}$. i = clump of cells.

### 5.1.1.2 The effect of solids loading and impeller tip speed on cell morphology

The effect of impeller tip speed was determined at 0 and 15 % quartzite loadings. Samples were removed from the reactors during mid-growth phase, settled for 30 min and viewed in a counting chamber under phase contrast at a 1000 x magnification. Owing to the depth of the counting chamber, in some cases it was difficult to obtain images where all cells were in focus but the basic morphology of the cells can still be distinguished.

#### *5.1.1.2.1 0 % quartzite loading*

At a 0 % quartzite loading, no significant difference in cell morphology or cell concentration (Figures 5.6a to 5.6c) was observed between the three impeller tip speeds investigated. The cells were predominantly phase dark and round with a diameter between 1.5 and 2 μm, indicating no visible detrimental effects due to increased hydrodynamic stress. These results validate data presented in Section (4.7), where it was shown that increasing the impeller tip speed at a 0 % quartzite loading only served to improve mass transfer and enhance the metabolic activity of the cells.

University of Cape Town

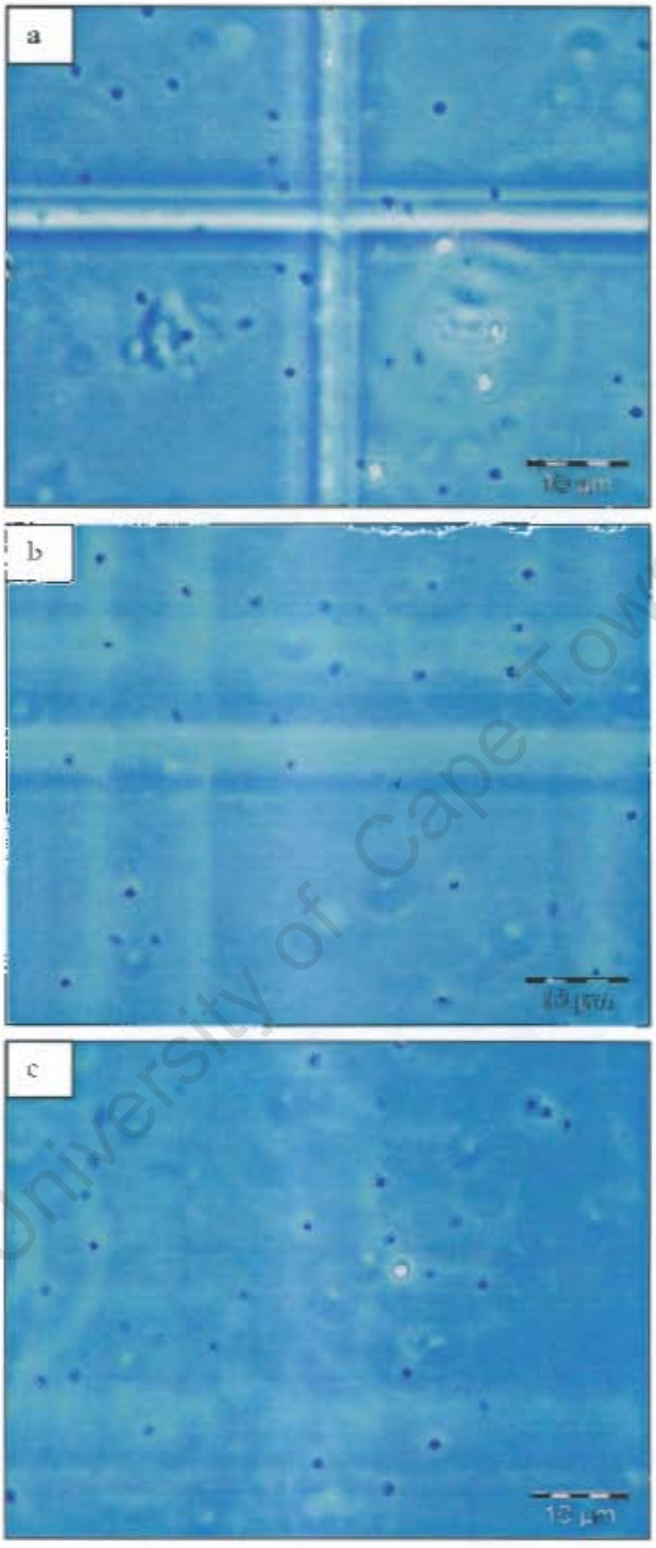


Figure 5.6: Images of cells sampled at 72 h from reactors containing 0 % quartzite and operated at impeller tip speeds of (a) 1.57 m $s^{-1}$; (b) 1.97 m $s^{-1}$ and (c) 2.13 m $s^{-1}$.

University of Cape Town

*5.1.1.2.2 15 % quartzite loading*

The addition of 15 % quartzite to the reactors resulted in extreme changes in the morphology of the cells. The degree of cell damage observed was proportional to the intensity of hydrodynamic stress applied as can be seen by comparison of Figure 5.7a through to 5.7d. At a 0 % quartzite concentration and an impeller tip speed of 1.67 m $s^{-1}$ cells appeared phase dark and round with diameters between 1.5 and 2.0 µm (arrow *a* in Figure 5.7a). Increasing the quartzite concentration to 15 %, while maintaining an impeller speed of 1.67 m $s^{-1}$, resulted in altered cell morphologies. Unfortunately the quality of the image presented in Figure 5.7b is poor but live microscopy analysis showed that some cells remained phase dark and round (arrow *d*) with diameters between 1.5 and 2.0 µm and a few clumps of cells (arrow *i*) were also visible indicating that leaky cells were present. In Figure 5.7c it is seen that increasing the impeller speed to 1.97 m $s^{-1}$ at a constant quartzite loading of 15 % resulted in more pronounced changes in cell morphology. Only small cells (approximately 0.78 µm in diameter), leaking cells and cell clumps (indicated by arrows *d*, *g*, and *i* respectively) were observed. No round, phase dark cells with a diameter between 1.5 and 2 µm remained in suspension. Thus the increased impeller speed caused increased hydrodynamic stress resulting in a decrease in cell size, an increase in the number of leaking cells and hence an increase in the number of cell clumps. When the tip speed was further increased to 2.13 m $s^{-1}$, the number of cells per field of view declined considerably and more cell debris was found in suspension. Several leaking as well as ghost cells, cell clumps and cell debris were also visible (indicated by arrows *g*, *e*, *i* and *f* in Figure 5.7d).

University of Cape Town

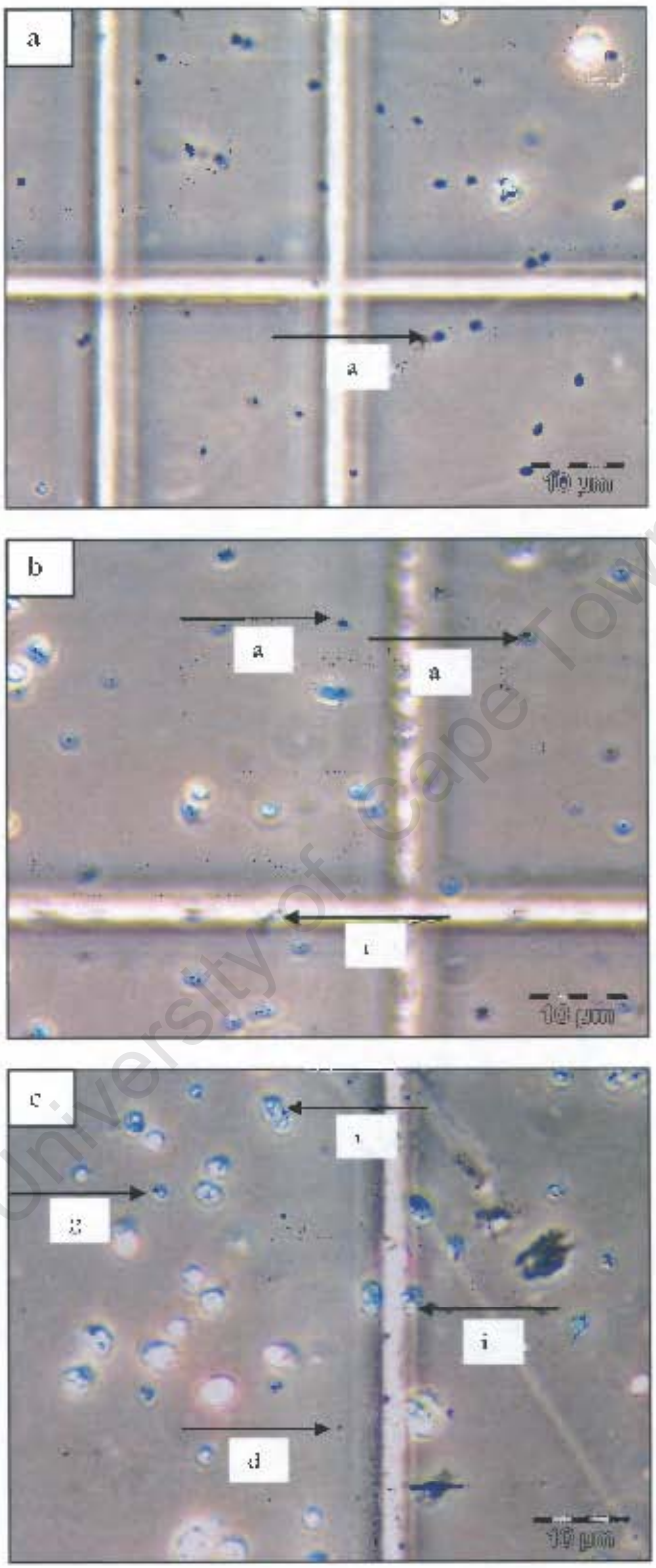


University of Cape Town

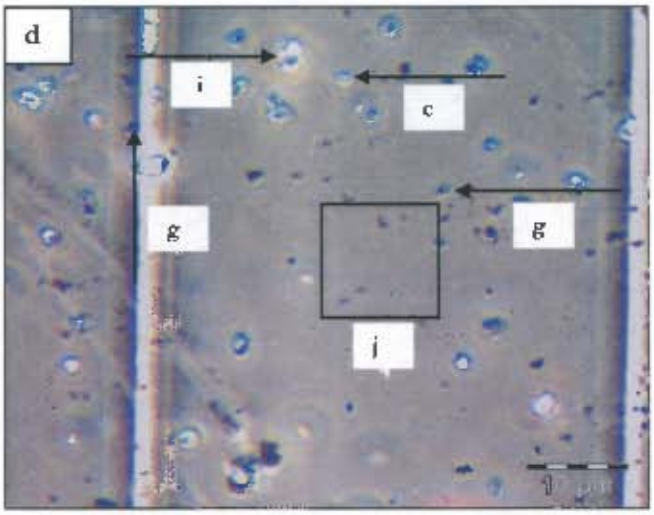


**Figure 5.7:** Images of cells sampled at 72 h from reactors containing 0 and 15 % quartzite and operated at impeller tip speeds of 1.67, 1.97 and 2.13 m $s^{-1}$.

a= Image of cells from a 0 % quartzite reactor run at 1.67 m $s^{-1}$. a = phase dark, round cells

b= Image of cells from a 15 % quartzite reactor run at 1.67 m $s^{-1}$. a = phase dark, round cells; i = small clump of cells

c= Image of cells from a 15 % quartzite reactor run at 1.97 m $s^{-1}$. d = small cells; g = leaking cell; i = cell clumps

d= Image of cells from a 15 % quartzite reactor run at 2.13 m $s^{-1}$. g = leaking cells; c = ghost cell; i = cell clump; j = cell debris

It is evident from the micrographs presented that increasing hydrodynamic stress by increasing agitation intensity at a high solids concentration (15 % quartzite) caused an alteration in cell morphology. Cells were transformed from dense, round structures to smaller cells, leaking cells, ghost cells, sticky cell clumps and cell debris. Increasing impeller speed increases the frequency of solid-cell-solid collisions. The cell morphologies presented here are characteristic of these damage events. Mild hydrodynamic stress results in healthy cells experiencing **minor envelope damage**. As discussed in Section 2.4, although the extent of this damage does not directly affect cell growth or metabolism, other factors such as the release of certain cell wall proteins into solution may be undesired. More severe mechanical stress leads to **membrane damage** which results in the cells losing their ability to replicate due to weakened membrane integrity. In the extreme case, cells rupture and extrude cytoplasm resulting in cell debris.

Lamaignère (2002) investigated the effect of hydrodynamic stress on the growth and morphology of *S. cerevisiae* in slurry reactors. Using transmission electron microscopy, the author obtained images of the cells exposed to quartzite loadings of 0 and 1 % v/v and impeller speeds of 565 and 850 rpm. Exposure to 1 % quartzite and an impeller speed of 850 rpm for 28 h resulted in rupture of the cell envelope. Figure 5.8 shows two points of lysis on a yeast cell indicated by the

University of Cape Town

arrows. The image shows disruption of the cell envelope and the release of cytoplasm into the growth medium. Extrusion of cytoplasm also caused the cells to shrink in size.

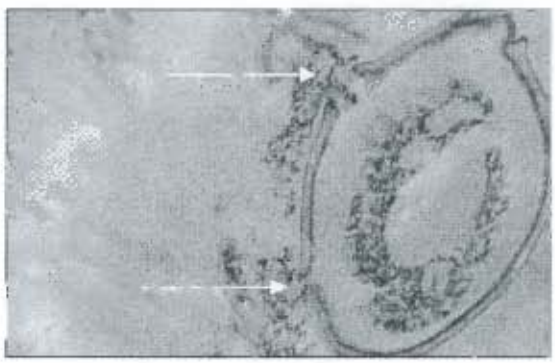

**Figure 5.8:** Illustration of a lysed yeast cell sampled from a STR containing 1 % v/v quartzite and operated at 850 rpm (sourced from Lamaignére 2002).

Comas and Vives-Rego (1998) investigated the effect of temperature on *Staphylococcus aureus*. They found that the cells decreased in size possibly due to seepage of the cytoplasm out of the cell when the cell membrane was damaged by heat. Nkosi (2001) reported similar decreases in cell size due to desiccation of *S. cerevisiae* on cold shock. Reis *et al.* (2004) studied the effects of nutrient stress on *B. licheniformis* and observed the presence of ghost cells. These cells had been permeabilised as seen by the disruption of the cytoplasmic membrane in Figure 5.9, and contained little or no cytoplasmic material inside the cell envelope. The extrusion of cytoplasm causes the cells to become sticky and consequently the cells proceed to clump.

**Figure 5.9:** Transmission electron micrograph of *Bacillus licheniformis* cells starved of nutrients (sourced from Reis *et al.*, 2004).

University of Cape Town

## 5.1.2 SCANNING ELECTRON MICROSCOPY ANALYSIS OF CELL MORPHOLOGY

Scanning electron microscopy (SEM) was used to determine the effect of hydrodynamic stress on cell morphology. The analysis was also used as a tool to magnify and enable a 3-dimensional observation of the tiny cells which approached the detection limit of light microscopy at 1000 x magnification. Figure 5.10 presents a high magnification image of the *Sulfolobus* culture growing under optimal conditions. During the logarithmic phase of growth and under mild conditions of hydrodynamic stress, cells appear large, round and smooth. A similar morphology was observed using phase contrast microscopy.

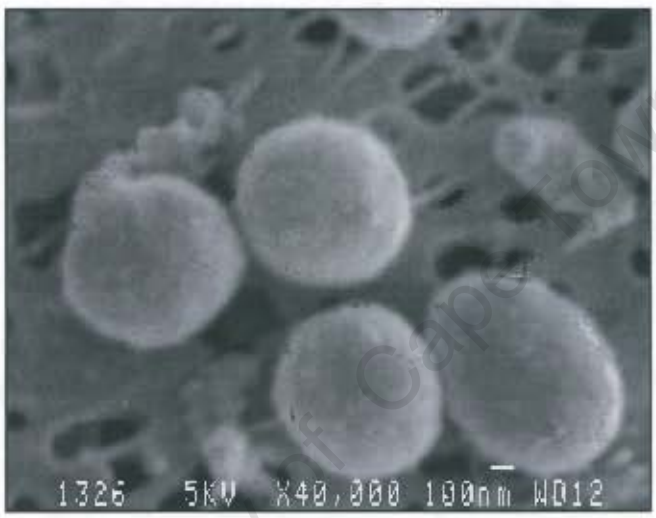


**Figure 5.10:** Scanning electron micrograph of a mid-growth phase *Sulfolobus* culture from a 3 % w/v chalcopyrite slurry (< 22 µm size fraction) operated at 1.97 m $s^{-1}$.

The cells growing under optimal conditions were used as an inoculum for the experimental runs conducted at 0, 12, 15 and 18 % w/v quartzite loadings and an impeller tip speed of 1.97 m $s^{-1}$. Mid-log phase samples from reactors containing 0, 12, 15 and 18% w/v quartzite were prepared by fixing the cells with glutaraldehyde, followed by dehydration and coating (Section 3.5.7.3). The samples were subsequently viewed under the SEM. The sample from the baseline reactor contained mostly round, smooth cells (Figure 5.11) representing type *a* from Figure 5.1. Figure 5.12 shows that most cells sampled from the reactor containing 12 % quartzite appeared damaged or have collapsed. A small number of round, smooth cells were visible (arrow *a*) as were cells of reduced size (arrow *d*). In the micrograph showing cells sampled from the reactor containing 15 % quartzite, collapsed or damaged cells dominated (Figure 5.13). No smooth, round cells were visible. No cells were visible in samples taken from the reactor containing 18 % quartzite (Figure 5.14). Evaluation of the samples by phase microscopy before the fixation step showed only cell clumps and cell debris similar to those observed in Figure 5.7d of Section 5.1.1. It is possible

University of Cape Town

that the highly stressed or damaged cells could not withstand the SEM sample preparation procedure and lysed, thus only cell debris was observed.

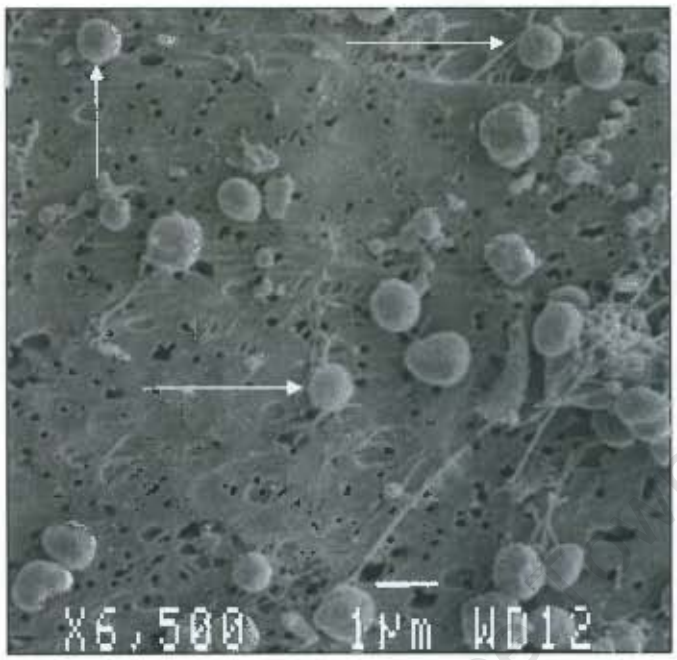


**Figure 5.11:** Scanning electron micrograph of a mid-growth phase *Sulfolobus* culture from a reactor containing 0 % w/v quartzite and operated at 1.97 m $s^{-1}$.

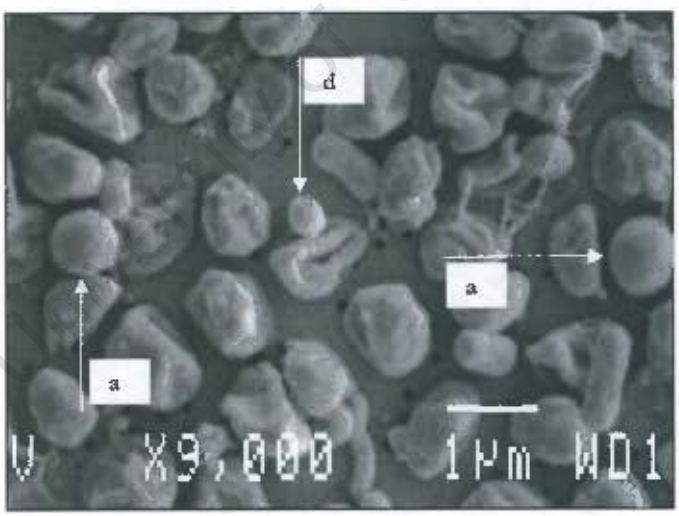


**Figure 5.12:** Scanning electron micrograph of a mid-growth phase *Sulfolobus* culture from a reactor containing 12 % w/v quartzite and operated at 1.97 m $s^{-1}$. a = round, smooth cell; d = small cell.

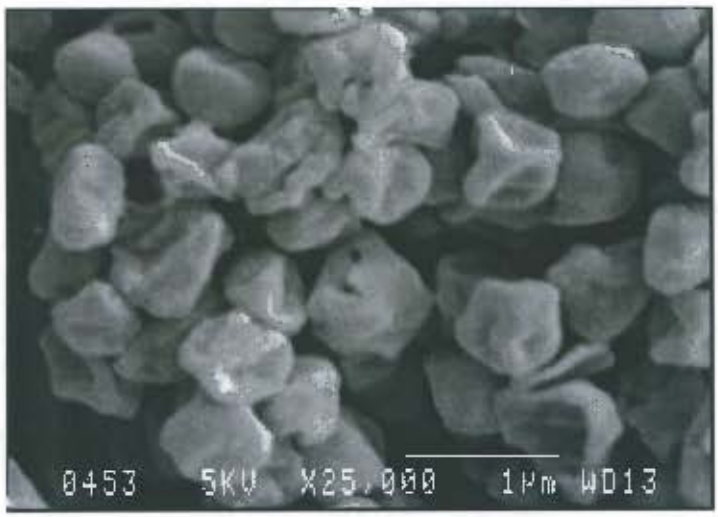


**Figure 5.13:** Scanning electron micrograph of a mid-growth phase *Sulfolobus* culture from a reactor containing 15 % w/v quartzite and operated at 1.97 m $s^{-1}$.

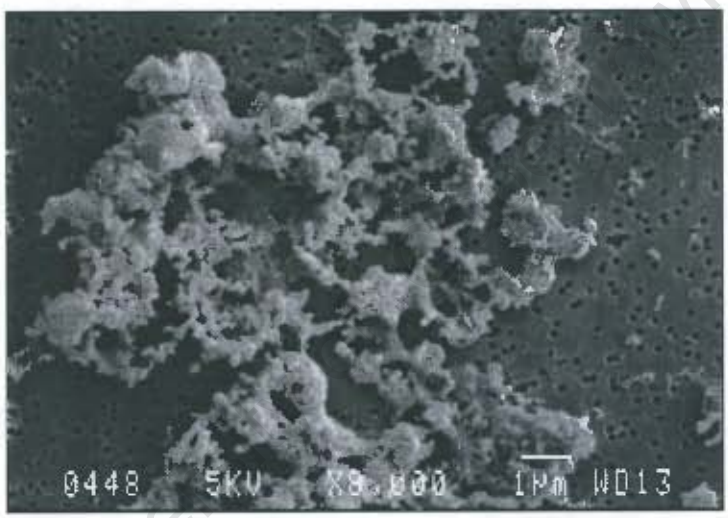


**Figure 5.14:** Scanning electron micrograph of a mid-growth phase *Sulfolobus* culture from a reactor containing 18 % w/v quartzite and operated at 1.97 m $s^{-1}$.

It was difficult to determine whether the collapsed, damaged cells observed in the reactors containing 12 to 18 % quartzite had a similar morphology in the reactor as depicted in Figures 5.12 to 5.14 or whether the damage observed was an artefact of the SEM sample preparation procedure compounded by weakened cell envelopes. Assessment using the light microscope showed damaged cells but detailed morphology could not be determined using the light microscope owing to its resolution limit. However, it is important to note that in Figures 5.12 to 5.14, the intensity of cell damage, collapse and weakening increased with increasing hydrodynamic stress. Furthermore, these morphological types were not observed in samples of cells exposed to conditions of mild hydrodynamic stress (Figure 5.11).

### 5.1.3 QUANTITATIVE ANALYSIS OF CELL SIZE

Section 5.1.1 presented, in part, a qualitative analysis of the effect of hydrodynamic stress on cell size. In this section, a quantitative analysis of the change in cell size with increasing hydrodynamic stress is presented. The experimental protocol was described in Section 4.6. A baseline experiment, in which the particulate phase consisted of only 3 % chalcopyrite and no inert quartzite, was run with each set of experiments. The effect of quartzite concentrations, in the range 0 to 18 % operated at an impeller tip speed of 1.97 m $s^{-1}$, on the cell size distribution was evaluated. Data were normalised as described in Section 4.6.2. As mentioned in Section 3.6, each experiment was repeated to determine whether the size distribution curves were reproducible.

Cell size was analysed using the CellFacts particle size analyser, based on the Coulter principle, to quantify both cell concentration and cell size distribution. The cell size distributions were described by fitting a four parameter Weibull function (Eqn 5.1) to each distribution.

$$y = a\left(\frac{c-1}{c}\right)^{\frac{1-c}{c}}\left[\frac{x-x_0}{b}+\left(\frac{c-1}{c}\right)^{\frac{1}{c}}\right]^{c-1} e^{-\left[\frac{x-x_0}{b}+\left(\frac{c-1}{c}\right)^{\frac{1}{c}}\right]^{c}}+\frac{c-1}{c} \qquad \ldots \text{Eqn. 5.1}$$

The Weibull function was chosen over other bell curves as it best described the shape of the size distribution curves over time and over the range of solids loadings utilised. "Goodness of fit" of the Weibull function to each size distribution was assessed and the three parameters of interest, $a$, $b$ and $X_0$, were obtained. Parameters $a$, $b$ and $X_0$ describe the curve as illustrated in Figure 5.15. Parameter $a$ represents the height of the apex of the peak, $b$ the width of the midpoint of this height and $X_0$, the mode.

University of Cape Town

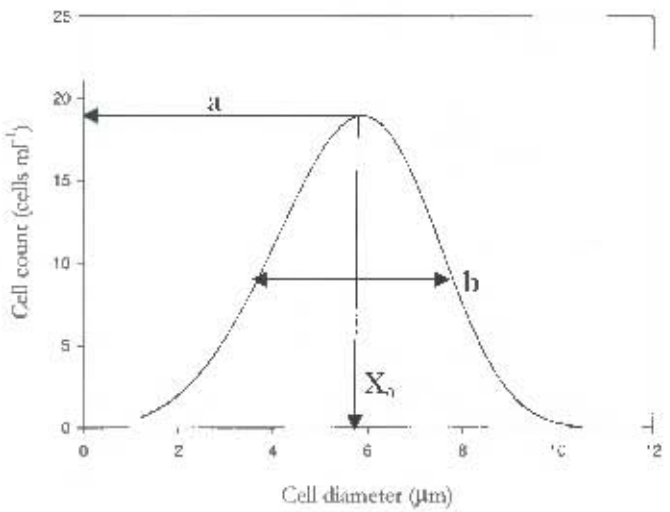


**Figure 5.15:** Description of a, b and $X_0$.

### 5.1.3.1 Sample data

In this section, a set of data representing typical baseline (0 % quartzite) and experimental (18 % quartzite) results is presented to enable comparison between the size distributions and the Weibull function parameters (prior to normalisation) derived from these distributions. These particular quartzite loadings were chosen because they best illustrate the difference between the cell number-based size distributions in the absence and presence of significant hydrodynamic stress. Figures 5.16a and 5.17a show a representative set of cell size distributions as a function of time obtained during a baseline run (0 % quartzite) and an 18 % quartzite run. Figures 5.16b and 5.17b illustrate the change in cell concentration as a function of time at the two quartzite loadings. Furthermore, the Weibull function parameters *a*, *b* and $X_0$ derived from the cell number-based size distributions for the 0 and 18 % quartzite loadings were plotted as a function of time and are presented in Figures 5.18 to 5.20. From these data, the changes in the cell dimensions under optimal conditions (0 % quartzite) and high intensity hydrodynamic stress conditions (18 % quartzite) are analysed.

University of Cape Town

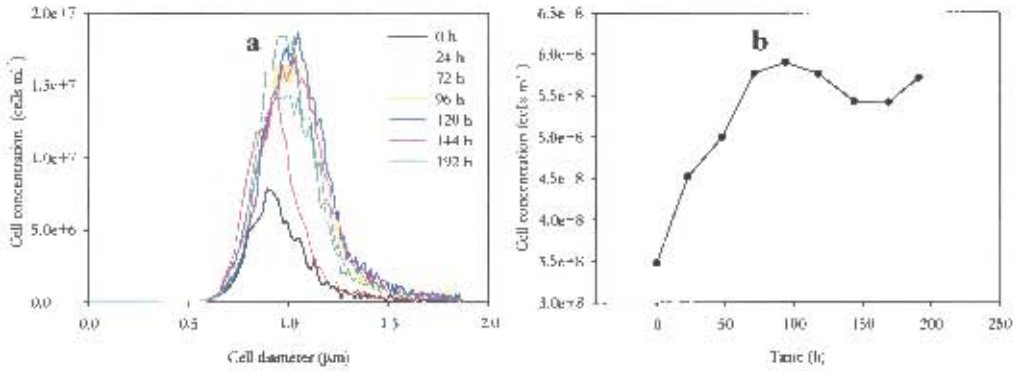


**Figure 5.16:** (a) cell number-based size distribution as a function of time and (b) cell concentration as a function of time, at a 0 % quartzite loading and an impeller tip speed of 1.97 m $s^{-1}$.

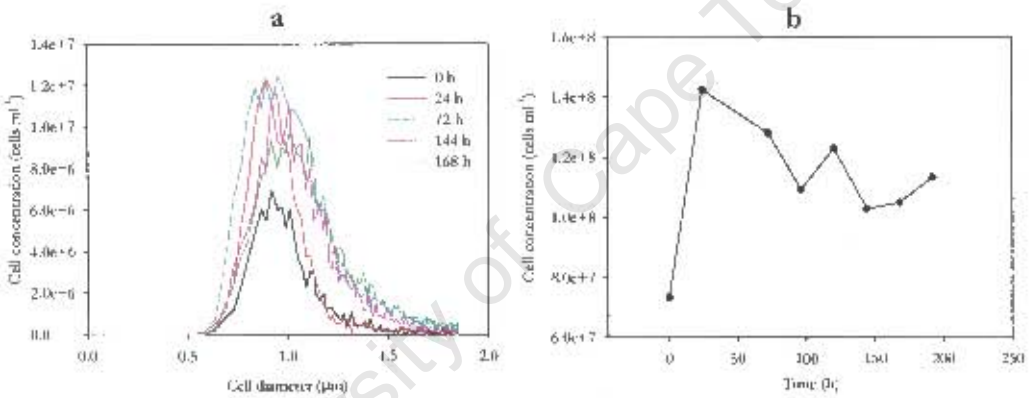


**Figure 5.17:** (a) cell number-based size distribution as a function of time and (b) cell concentration as a function of time at an 18 % quartzite loading and an impeller tip speed of 1.97 m $s^{-1}$.

The cell size distributions for the experiments at 0 h were very similar owing to the absence of quartzite in the inoculum build-up phase and confirming reproducibility of the analysis. At 0 h, characterised by low cell number, the size distributions for 0 and 18 % quartzite loadings were described by a narrow distribution (illustrating uniformity in cell size) with a small area on integration (illustrating a low cell number). As growth progressed, the distribution for the 0 % quartzite loading increased in height and breadth indicating an increase in cell concentration and increased variation in cell diameter. In addition, the distribution curve shifted to the right indicating an increase in average cell diameter with time. At 96h, the culture reached the maximum cell size (Figure 5.16a) and cell concentration (Figure 5.16b). Here the broadest range

University of Cape Town

of particle diameters and maximum peak height were achieved. The size distribution for the 18 % quartzite loading showed an increase in height and breadth over the first 24 h. At 72 h the distribution decreased in height and increased in breadth. The height and breadth of the distribution remained constant up to 144 h whereafter the breath of the curve increased and the height remained constant. During the 72 to 168 h period the distribution shifted to the left indicating a decrease in average cell diameter during this period. The cell concentration (calculated by integration of the distribution) in the absence of quartzite, increased from 0 to 72 h after which the culture entered to stationary phase of growth and the cell number remained constant Figure 5.16b). The cell concentration in the presence of 18 % quartzite decreased after 24 h, the time at which quartzite was added (Figure 5.17b). A minimum cell concentration was attained at 96 h (Figure 5.17b), whereafter the culture remained in stationary phase until the end of the experiment.

Quantitative analysis of the changes the cell size distributions for the 0 and 18 % quartzite loadings were achieved by fitting a Weibull function to the distributions and deriving parameters *a* (apex height), *b* (breadth) and $X_0$ (mode). At a 0 % quartzite loading parameters *a* and *b* (Figures 5.18 and 5.19) followed the shape of the growth curve, being key parameters in determining the area under the curve, proportional to cell concentration. Parameter *a* (Figure 5.18) increased during the growth phase (0 to 72 h) from 6.8 x $10^6$ to 1.8 x $10^7$ cells $ml^{-1}$ and stabilised at approximately 1.7 x $10^7$ cells $ml^{-1}$ between 72 and 168 h which coincided with the stationary phase of growth (Figure 5.16b). Parameter *b* (Figure 5.19) increased during the growth phase from 0.27 to 0.41 μm at 96 h. From 96 to 168 h, *b* remained stable at this value. This increase in the variation in particle diameter of a rapidly-growing healthy culture could be representative of cell doublets preceding completion of cell division. This assumption is validated by the micrographs collected using phase contrast optics, showing doublets during the growth phase of the baseline culture (Figure 5.2). At an 18 % quartzite loading, parameter *a*, describing the height of the distribution, increased from 7.7 x $10^6$ to 1.3 x $10^7$ cells $ml^{-1}$ over the first 24 h during the inoculum build-up phase. After the addition of quartzite to the reactor, *a* declined to 4.9 x $10^6$ cells $ml^{-1}$ and remained close to this value for the remainder of the experiment. Parameter *b* increased from 0.25 to 0.38 μm from 0 to 72 h, and subsequently decreased to 0.34 μm at 144 h and remained at this value till 168 h. It is observed that the size distribution (Figure 5.17a) changed from a normal distribution prior to quartzite addition to be skewed to include an expanded tail on the right hand side owing to the presence of particles of the larger particle diameters. At the high quartzite loading, the larger particles possibly originated from damaged cells becoming 'leaky' and hence 'sticky' and proceeding to clump or aggregate (Section 5.1.1). In addition, because these clumps were of varying diameters and integrities, they may have been partially broken up during the dilution phase of the analysis procedure, causing the noisy signal as observed on the right tail of

University of Cape Town

the size distributions (Figure 5.17a). The presence of these clumps was confirmed using phase contrast optics (images not shown). Similar clumps caused by excessive hydrodynamic stress were seen in impeller tip speed experiments (Section 5.1.1, Figures 5.7c and 5.7d) where the aggregate diameter in the absence of breakage ranged from 2.5 to 3 μm.

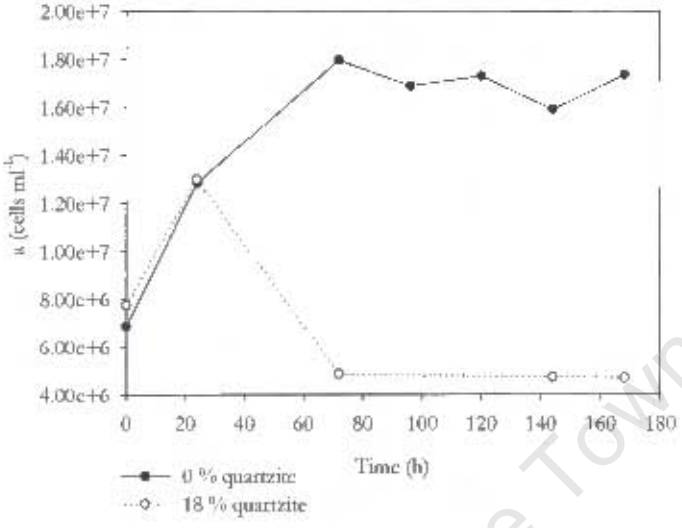


**Figure 5.18:** Time profiles of parameter *a* for 0 and 18 % quartzite loadings operated at an impeller tip speed of 1.97 m $s^{-1}$.

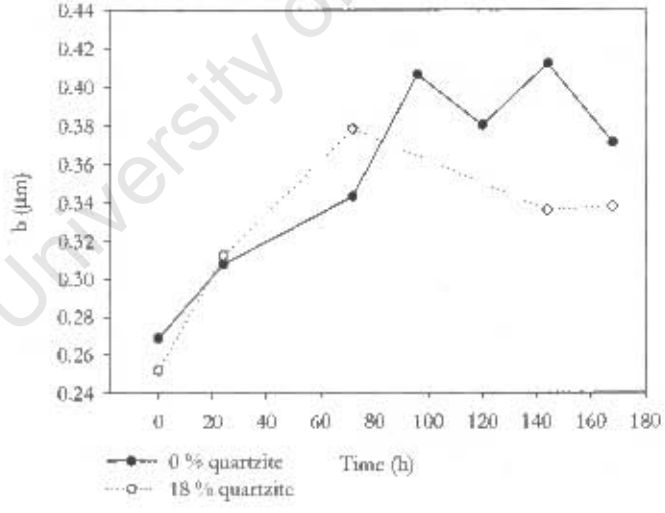


**Figure 5.19:** Time profiles of parameter *b* for 0 and 18 % quartzite loadings operated at an impeller tip speed of 1.97 m $s^{-1}$.

The mode of the cell size distributions for 0 and 18 % quartzite loadings was a function of time as well as solids loading (Figure 5.20). An ANOVA comparing the mode of the distributions over time is presented in Appendix F. This analysis shows that the cell size change on increasing the quartzite loading to 18 % is significant at the 99.99 % level. At the 0 % quartzite loading, the

University of Cape Town

mode increased from 0.90 to 0.97 μm during the growth phase (0 to 72 h). During the stationary phase of growth, the mode remained constant at approximately 1.00 μm over the 96 to 144 h period and decreased to 0.98 μm from 144 to 168 h. At the 18 % quartzite loading, an $X_0$ of 0.91 to 0.92 μm was found in the inoculum build-up phase. At 168 h, the mode declined to 0.83 μm. These results confirm that as the intensity of hydrodynamic stress increased on increasing the quartzite loading from 0 to 18 %, a greater proportion of the cells occurring singly had decreased particle diameters. In addition, the cell diameter decreased as the experiment progressed. As discussed in Section 5.1.1, one of the potential outcomes of hydrodynamic cell damage is a decrease in the average size of the cells. Cell size was postulated to decrease as cells became 'leaky' due to damage to the cell wall and membrane or because smaller cells are more energy efficient in a stressful environment.

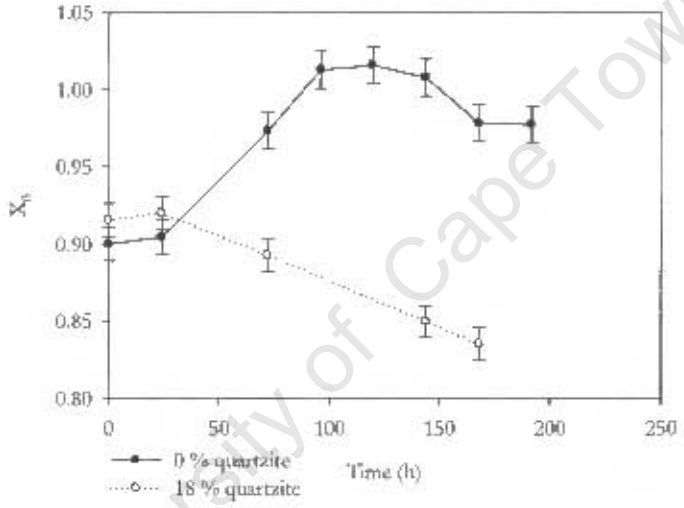


**Figure 5.20:** Time profiles of parameter $X_0$ for 0 and 18 % quartzite loadings operated at an impeller tip speed of 1.97 m s$^{-1}$.

University of Cape Town

### 5.1.3.2 The effect of increasing solids loading across the range 0 to 18 % quartzite

The four parameter Weibull function (Eqn. 5.1) was fitted to the size distribution curve for each sample interval at each solids loading in the range 0 to 18 % quartzite. Parameters $a$, $b$ and $X_0$ were determined. The data for each solids loading over the growth phase of the experiment was averaged and subsequently normalised against the respective 0 % quartzite data (Section 4.6.2) to enable comparison across the range of quartzite loadings tested. These averaged, normalised data are presented in Figure 5.21.

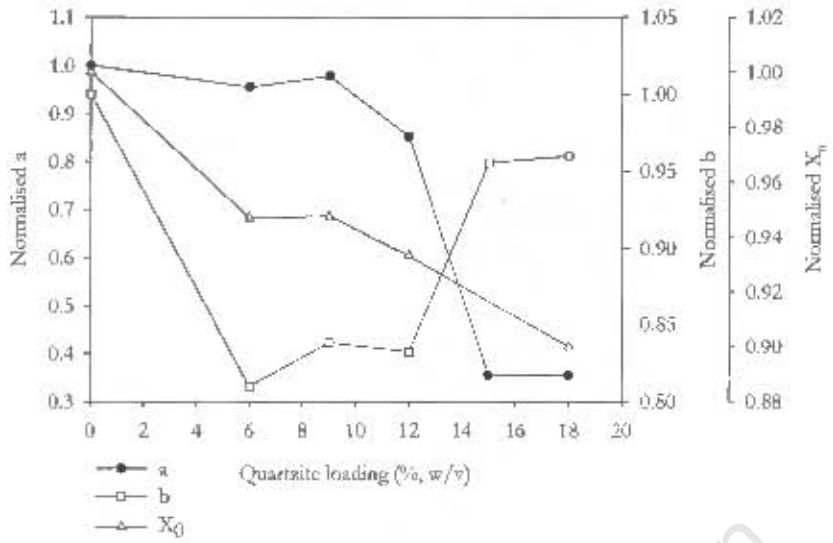


**Figure 5.21:** Change in parameters a, b and $X_0$ with increasing quartzite loading from 0 to 18 % w/v at a constant impellet tip speed of 1.97 m s$^{-1}$.

Parameter *a* (apex) remained constant up to a quartzite loading of 9 %. At a 12 % quartzite loading the average curve apex was 0.85 fold the baseline value and decreased further to 0.35 fold the baseline value at 15 and 18 % quartzite loadings. At 6 and 9 and 12 % quartzite loadings, parameter *b* decreased by approximately 19 % compared to the baseline. On average throughout the experiment parameter *b* was higher at the 15 and 18 % quartzite loading than at the lower loadings of 6, 9 and 12 %. Parameter $X_0$ (mode) decreased with an increase in quartzite loading from 0 to 18 % indicating that there was a decline in the average cell diameter with increasing quartzite loading. There was a decrease in $X_0$ to 0.94 fold that of the baseline reactor on increasing the quartzite loading to 6 and 9 %. Increasing the quartzite loading above 9 % caused the normalised $X_0$ value to decline to 0.89 at an 18 % quartzite concentration. These data are in agreement with the phase contrast micrographs presented in Section 5.1.1.2. The micrographs clearly show a decrease in the average cell diameter with increasing hydrodynamic stress. In addition, combining the results for $X_0$ and *b* with microscope analysis shows that at the 6 to 12 % quartzite loadings the decrease in *b* is due to the presence of small, stressed cells while at the 15 and 18 % quartzite loadings, the increase in the width of the distribution spanning both small and large particle diameters is indicative of a decrease in the average cell size with concomitant aggregation of damaged, 'leaky' cells. The decrease in $X_0$ at the lowest quartzite loading tested (6 %) is an indication of the sensitivity of cell size to the effects of hydrodynamic stress.

### 5.1.3.3 Cell aggregation

In an effort to confirm that at higher pulp densities leaking cells aggregated or clumped, an experiment was conducted at two pulp densities (0 and 18 % quartzite) using the same protocol as

University of Cape Town

in previous solids loading experiments. The cell concentration in the 0 to 5 μm and 2 to 5 μm regions were determined using the CellFacts analyser. It is important to note that a higher proportion (approximately 100 fold) of the cells lay in the 0 to 2 μm range. The percentage of cells in the 2 to 5 μm range was sought using Eqn. 5.2:

$$\%C_{2-5\mu m} = \frac{Cellconc._{2-5\mu m}}{Cellconc._{0-5\mu m}} * 100 \qquad \ldots \text{Eqn. 5.2}$$

where $\%C_{2-5\mu m}$ = percentage of cells in the 2 to 5 μm range

$Cellconc._{2-5\mu m}$ = the concentration of cells in the 2 to 5 μm range (cells $ml^{-1}$)

$Cellconc._{0-5\mu m}$ = the concentration of cells in the 0 to 5 μm range (cells $ml^{-1}$)

Figure 5.22 illustrates the change in the percentage of cells in the 2 to 5 μm range as a function of time for 0 and 18 % quartzite solid loadings. At a 0 % quartzite loading, the percentage of cells in the larger size range decreased over the first 48 h from 3.0 % to 2.0 % and stabilised at approximately 2.5 % for the remainder of the experiment. Conversely, at an 18 % solids loading, the percentage of particles in the larger size range increased from 4.2 on the addition of quartzite to the reactor at 24 h to 7.2 at 144 h whereafter the percentage decreased to 4.0 at 191 h. From 24 to 144 h the cells were in the death phase and hence there was an increase in the degree of clumping. From 144 to 191 h the cell concentration increased marginally possibly due to recovery of the system and resulting in a decline in the degree of clumping. Another possibility is that the cell clumps proceeded to break-up due to their prolonged exposure to mechanical stress.

These data show that the number of cell clumps in suspension was a function of solids loading and time and also corroborate results presented in Section 5.1.1.2. The phase contrast images in Figures 5.7a to 5.7d show an increase in the degree of cell clumping with increasing hydrodynamic stress.

University of Cape Town

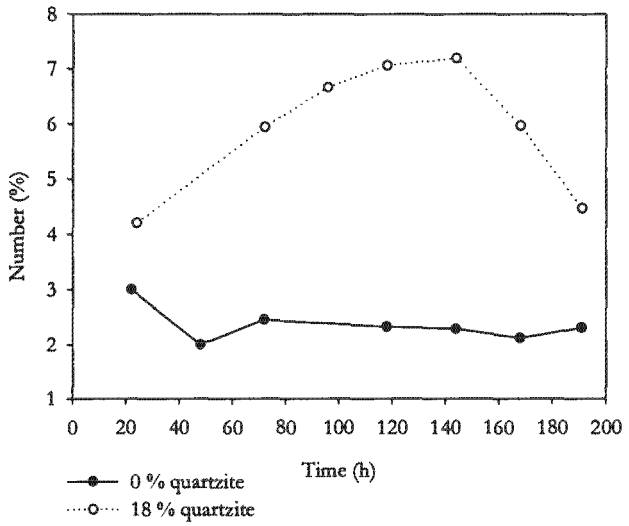


**Figure 5.22:** Percentage of cells in the 2 to 5 μm range as a function of time for 0 and 18% quartzite solid loadings at an impeller tip speed of 1.97 m $s^{-1}$.

### 5.1.3.4 Comparison of results to literature studies

Shuler and Tsuchiya (1975) correlated the size of *Azotobacter vinelandii* to changes in cellular composition, number and morphology. Henrici (1928), cited by Shuler and Tsuchiya (1975), documented that two types of batch growth exist: (i) accumulation of biomass with concomitant increase in cell size and (ii) increase in cell numbers. Figure 5.23 shows the cell size distribution of *Azotobacter vinelandii* and their associated cell shapes at different times during the organism's growth cycle. The size distributions and morphological changes presented by Shuler and Tsuchiya (1975) are similar to the size distributions observed in this study in the absence of quartzite. The most notable similarities in the morphological changes are those observed during exponential phase where the size distribution broadened owing to the increase in cell size prior to division and the height of the distribution increased owing to increased cell number. The shift of the mode of the size distribution to the left observed by Shuler and Tsuchiya (1975) indicated a reduction in the size of intact cells especially during the stationary phase of growth. In the current study this effect is seen in Figure 5.20 where parameter $X_0$ declines during the stationary phase of growth in the absence of quartzite.

University of Cape Town

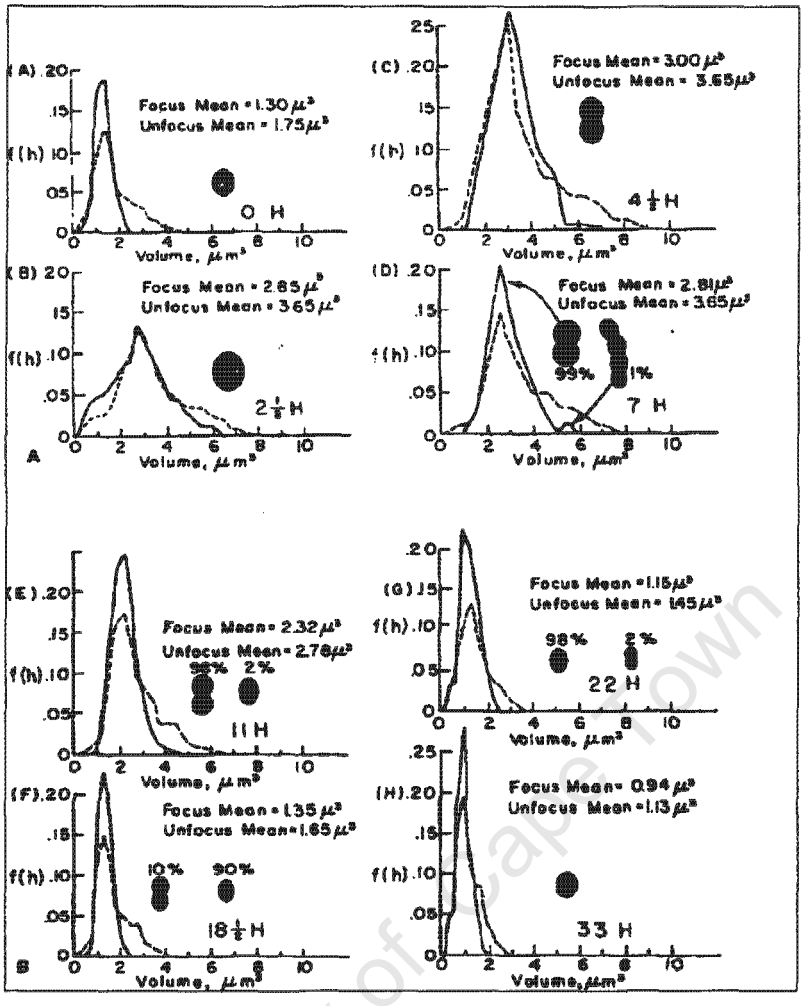


**Figure 5.23:** Cell size distributions featuring different cell shapes during the growth cycle of *Azotobacter vinelandii* (sourced from Shuler and Tsuchiya, 1975).

| | | | |
|---|---|---|---|
| (A) | = start of growth phase | (E) | = 4th quarter of exponential phase |
| (B) | = early exponential phase | (F) | = end of exponential phase |
| (C) | = 2nd quarter of exponential phase | (G) | = early stationary phase |
| (D) | = mid exponential phase | (H) | = mid stationary phase |

The results of cell cycle studies of *Sulfolobus acidocaldarius* by Hjort and Bernander (1999) are in agreement with the results obtained in the present study and those obtained by Shuler and Tsuchiya (1975). The data collected by Hjort and Bernander (1999) from cell size distributions during the exponential and stationary phases of growth of the Archaea showed a reduction in cell size on progression from the exponential growth phase to the stationary phase. In the studies by Hjort and Bernander (1999) and Shuler and Tsuchiya (1975), the cell size distribution changes as the culture growth cycle moves from exponential to stationary phase. In the present study similar time-course based changes were observed at a 0 % quartzite loading (Figure 5.16a). However, on

University of Cape Town

increasing the solids loading to 18 % quartzite, variation in the cell size distribution was observed (Figure 5.17a). This difference indicates that the changes in the cell size distributions at the higher solids loading were possibly due to increased mechanical stress.

A decrease in cell size with increasing stress intensity was observed by Nkosi (2001) who examined the effect of cooling rate on the size of Brewer's yeast cells. Cells were cooled to 4°C at different rates. The control sample was held at 14°C. The predominant cell size decreased with an increase in cooling rate (Figure 5.24). The author found a similar trend to the present study where the mode decreased with increasing stress intensity. In the study by Nkosi (2001), the mode decreased from 6.55 μm for the control sample to 5.88 and 5.13 μm for the slow-cooled and fast-cooled yeast cells respectively. The decrease in yeast size with cooling was attributed to a greater degree of desiccation or a loss of cell contents due to damaged cell membranes.

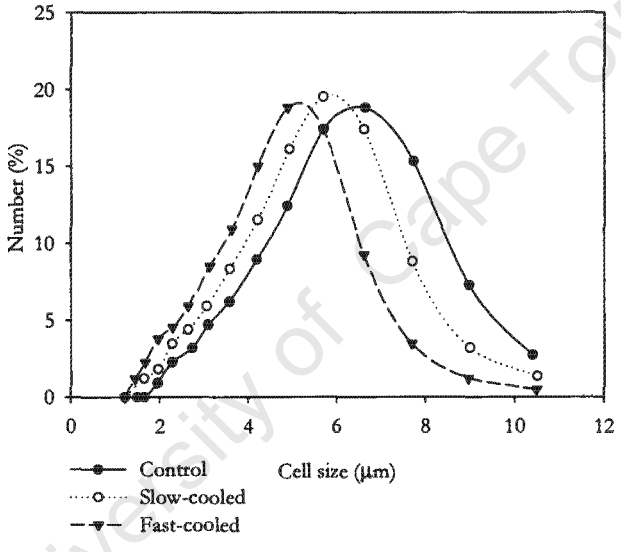


**Figure 5.24:** Comparison of the particle size distribution of yeast as a function of cooling rate (adapted from Nkosi, 2001).

Several physiological changes resulting in, among others, changes in cell morphology occur in the cells under conditions of stress. In terms of morphological changes, cell stress is postulated to induce survival strategies such as the production of smaller cells and thicker cell walls.

As found in the present study (Figure 5.7c and Figure 5.12), Nemati and Harrison (2000) and Sissing (2002) reported that the size of freely suspended cells of *S. metallicus* was smaller in experiments conducted at high intensities of hydrodynamic stress in STRs. Smaller cells have a larger surface area to volume ratio, hence increasing the transfer area available for nutrient transport. Also, smaller cells only interact with small eddies and thus the effective hydrodynamic stress at the cell surface may decrease. Thus, smaller cells are advantageous under sub-optimal

University of Cape Town

conditions. In addition to a reduction in cell size, micro-organisms may repair and re-enforce cell walls in response to stress. Physical evidence of cell wall repair mechanisms was found by Lamaignére (2002). The author showed that the walls of yeast cells grown in the presence of 1 % v/v quartzite in an STR were thicker than the walls of yeast cells grown in the absence of solids. In addition, the percentage of cells with thicker walls increased with time. Klis *et al.* (2002) observed that changes in the morphology of newly formed cell walls of *S. cerevisiae* occurred in response to nutrient limitation. In addition, cell wall construction is strongly regulated and certain pathways are directly involved in signalling cell wall damage.

In order to maintain a diminished size, stressed cells cease synthesis of non-essential cellular components (Shuler and Tsuchiya, 1975). The reduced synthesis of non-essential cellular components under conditions of stress was confirmed by comparison of the protein profiles of healthy cells to those of stressed cells. Furthermore, it is possible that the energy expenditure per unit growth is altered to provide additional maintenance energy to enable resistance to stress and repair of cell injury such as cell wall damage. Illing (1996) stated that hydrodynamic stress may result in the use of the carbon and energy source for maintaining intracellular functioning and repair mechanisms in place of, for example, cell division and product formation. Searby and Hansford (2003) reported kinetic evidence of an increase in the maintenance requirement of a thermoacidophilic archaeon in response to temperature and nutrient stress on analysis of the kinetics of ferrous iron oxidation. They used the constant maintenance Pirt equation (Eqn. 5.3) to describe the dependence of the specific ferrous iron oxidation rate on the growth rate, biomass yield coefficient and the maintenance coefficient.

$$q_{Fe^{2+}} = \frac{\mu}{Y_{SX}^{max}} + m_s \qquad \ldots \text{ Eqn 5.3}$$

where: $q_{Fe^{2+}}$ = the specific iron oxidation rate (mol $Fe^{2+}$ $molC^{-1}$ $h^{-1}$)

$\mu$ = the specific growth rate ($h^{-1}$)

$Y_{SX}^{max}$ = the maximum yield on substrate (mol C (mol $Fe^{2+}$)$^{-1}$)

$m_s$ = the maintenance coefficient (mol $Fe^{2+}$ $molC^{-1}$ $h^{-1}$)

The maintenance coefficient was found to be a function of temperature and increased sharply from 0.39 to 1.26 mol $Fe^{2+}$ $molC^{-1}$ $h^{-1}$ on increasing the temperature from 65 to 70°C. A further increase in the temperature to 75°C resulted in a moderate increase in the maintenance coefficient to 1.31 $Fe^{2+}$ $molC^{-1}$ $h^{-1}$. Furthermore, they established that when the cells were grown under nutrient limiting conditions, the cell maintenance requirements increased.

University of Cape Town

## 5.2 THE EFFECT OF HYDRODYNAMIC STRESS ON CULTURE METABOLIC ACTIVITY

The metabolic activity of a culture is used as a measure of the metabolic activity of the micro-organisms within the culture. The specific oxygen utilisation rate ($q_{O2}$) may be used as an indicator of metabolic activity (Illing, 1996; du Plessis *et al.*, 2001; Kim *et al.*, 2002). The thermoacidophilic Archaea used in the present study utilise oxygen as the terminal electron acceptor in the transport of electrons from ferrous iron and elemental sulphur and thus the oxygen utilisation rate (OUR) and cell concentration were used to determine the metabolic activity of the *Sulfolobus* culture on exposure to increasing levels of hydrodynamic stress during the solids loading experiments. Because the reactors used for the experimental runs were not completely sealed, direct OUR measurements were not possible. Suspensions devoid of mineral but containing growth medium and cells were sampled from the reactors at intermittent time intervals during the experimental runs and inoculated into Schott bottles containing fresh medium and 3 % w/v chalcopyrite fines (Section 3.5.9). The bottles were rotated in an orbital shaker incubator maintained at 68°C. The OUR was measured over a 5 h period. Control samples containing only fresh medium and mineral were tested to determine the extent of decrease in OUR due to the presence of the chalcopyrite fines. The average OUR of the control sample measured over the 5 h period was subtracted from the average OUR measured over the 5 h period for the experimental samples. As described in Section 4.6, the solids loading experiments were conducted in two sets.

The specific OUR data for the two experimental sets are presented in Figure 5.25. The $q_{O2}$ values were obtained by dividing the average OUR over the 5 h period by the total number of cells present in the slurry. The $q_{O2}$ was found to be a function of time and quartzite concentration. For all solids loadings tested, the $q_{O2}$ decreased over the course of the experiment. The extent of decrease was proportional to the solids concentration. The decrease in $q_{O2}$ with time was attributed to a decrease in nutrient availability due to passivation of the chalcopyrite mineral, while the decline in $q_{O2}$ with quartzite concentration was attributed to increased hydrodynamic stress imposed by an increase in the concentration of solid particles present in the reactors. Illing (1996) found that during the normal growth cycle of *Corynebacterium glutamicum*, under conditions of negligible hydrodynamic stress, the specific OUR decreased from 120 mg $O_2$ $h^{-1}g$ dry cell $mass^{-1}$ at the start of the exponential phase to 69 mg $O_2$ $h^{-1}g^{-1}$ in late exponential phase.

In batch culture, as the nutrient supply diminishes, the activity of the system declines leading to a loss of culture metabolic activity. In the present study nutrient limitation occurred early in the chalcopyrite bioleaching system (Section 4.6) due to passivation of the mineral and resulted in a decline in the OUR. At a 0 % quartzite concentration the $q_{O2}$ declined from $1.32 \times 10^{-9}$ to

University of Cape Town

1.21 x $10^{-9}$ µl $O_2$ $cell^{-1}$ $min^{-1}$ over the first 24 hours after the inoculum build-up period (0 to 24 h). The $q_{O2}$ time profile for the 6 % quartzite loading was similar to the profile for the 9 % quartzite loading. Over the first 24 h after the addition of quartzite to the reactors the $q_{O2}$ decreased to a greater extent than at the 0 % quartzite loading. The $q_{O2}$ decreased from 1.28 x $10^{-9}$ and 1.30 x $10^{-9}$ µl $O_2$ $cell^{-1}$ $min^{-1}$ to 9.97 x $10^{-10}$ and 9.46 x $10^{-10}$ µl $O_2$ $cell^{-1}$ $min^{-1}$ for the 6 and 9 % quartzite loadings respectively. The initial sharp decrease in the $q_{O2}$ was followed by a gradual decrease over the remainder of the experiment. At a 12 % quartzite loading the decrease in the $q_{O2}$ over the first 24 h after quartzite addition was more pronounced than at the 6 and 9 % quartzite concentrations. The $q_{O2}$ declined from 1.33 x $10^{-9}$ to 5.57 x $10^{-10}$ µl $O_2$ $cell^{-1}$ $min^{-1}$. However, from 48 to 96 h the system appeared to recover and the $q_{O2}$ increased from 5.57 x $10^{-10}$ to 6.97 x $10^{-10}$ µl $O_2$ $cell^{-1}$ $min^{-1}$. In the second set of experiments, at 15 and 18 % quartzite concentrations, there was a decline in the $q_{O2}$ over the 48 h period after the addition of quartzite to the reactors. The $q_{O2}$ declined from 2.63 x $10^{-9}$ to 8.46 x $10^{-10}$ µl $O_2$ $cell^{-1}$ $min^{-1}$ and from 2.69 x $10^{-9}$ to 6.81 x $10^{-10}$ µl $O_2$ $cell^{-1}$ $min^{-1}$ for 15 and 18 % quartzite concentrations respectively. The $q_{O2}$ subsequently stabilised at approximately 7.5 x $10^{-10}$ µl $O_2$ $cell^{-1}$ $min^{-1}$ for both reactors and remained constant for the remainder of the experiment. The $q_{O2}$ data presented for the 18 % quartzite loading indicates that even though the cells present in the reactor experienced a high intensity of hydrodynamic stress they still remained metabolically active. The results obtained for the OUR experiments are consistent with the kinetic data obtained for the growth, iron and copper data presented in Section 4.6.2.

University of Cape Town

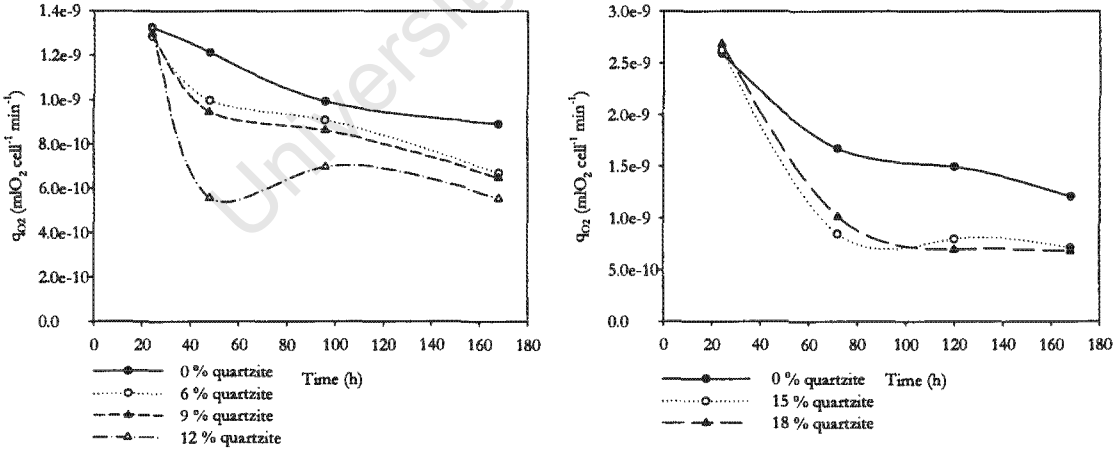


**Figure 5.25:** Specific OUR as a function of time for reactors containing 0, 6, 9 and 12 % quartzite and 0, 15 and 18 % quartzite operated at an impeller tip speed of 1.97 m $s^{-1}$.

## 5.3 THE EFFECT OF HYDRODYNAMIC STRESS ON MEMBRANE INTEGRITY

The cell membrane is vital in several cellular functions including cell division (viability), maintenance of ion gradients and cell energetics. Loss of membrane integrity could result due to mechanical damage of the cell membrane. In the present study, the loss of membrane integrity of the *Sulfolobus* cells on exposure to increasing concentrations of quartzite was measured using a dual fluorescence stain technique. SYTO 13 green and propidium iodide were the fluorochromes of choice (Norris, 2001). Propidium iodide can only diffuse into cells whose membranes have been compromised while SYTO 13 green passes through compromised membranes and uncompromised membranes. Propidium iodide has a higher affinity for nucleic acids than SYTO 13 green. Hence where propidium iodide penetrates cell membranes it replaces SYTO 13 green in the nuclear material. Cells stained with SYTO 13 green produce a green fluorescence when illuminated with blue light while those stained with propidium iodide produce a red fluorescence when illuminated with green light. If propidium iodide only replaces a portion of the SYTO 13 green, then the resultant fluorescence varies in the yellow to orange range. In this way cells with intact membranes can be distinguished from membrane-compromised cells. The amount of propidium iodide that enters the cell is proportional to the level of membrane damage and the time period of staining. If the time period of staining remains consistent between samples, the levels of propidium iodide within the cells can be used as a measure of the membrane integrity. Figures 5.26 to 5.28 present a series of micrographs of dual stained cells sampled from reactors operated across a range of pulp densities at a constant impeller tip speed of 1.97 m $s^{-1}$.

University of Cape Town

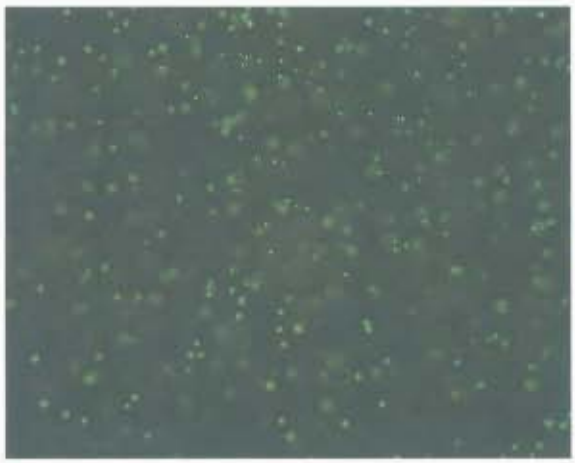

**Figure 5.26:** Dual stained (propidium iodide and SYTO 13 green) *Sulfolobus* cells sampled at 72 h. Reactor conditions: 0 % w/v quartzite; impeller tip speed of 1.97 m $s^{-1}$.

**Figure 5.27:** Dual stained (propidium iodide and SYTO 13 green) *Sulfolobus* cells sampled at 72 h. Reactor conditions: 12 % w/v quartzite; impeller tip speed of 1.97 m $s^{-1}$.

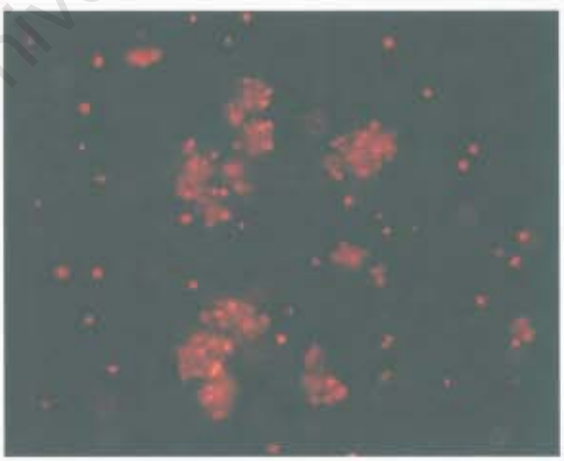

**Figure 5.28:** Dual stained (propidium iodide and SYTO 13 green) *Sulfolobus* cells sampled at 72 h. Reactor conditions: 18 % w/v quartzite; impeller tip speed of 1.97 m $s^{-1}$.

University of Cape Town

Figure 5.26 shows archaeal cells sampled from a reactor containing 0 % quartzite (baseline) in the presence of 3 % chalcopyrite operated at 1.97 m $s^{-1}$ after they were stained with SYTO 13 green and propidium iodide. Comparable images showing only a green fluorescence were retrieved using single and dual band filters. No red fluorescence was visible using either the dual or single band filters, indicating that cells from the baseline reactor showed no visible uptake of propidium iodide. At a 12 % quartzite loading, the proportion of cells fluorescing red and orange increased (Figure 5.27). The percentage of cells in three colour categories of green, red and orange were determined from triplicate images for each solids loading. The fraction of fluorescent green cells was 46.3 % of the total number of cells counted while the fluorescent red and orange cells accounted for 38.7 and 15 % respectively (Table 5.2). The fluorescing cells were enumerated using a manual image analysis tool (analySIS Image Processing software). These results indicate that the cell membranes were compromised due to the presence of solids in the reactor. Propidium iodide was able to penetrate the cells resulting in some cells fluorescing red indicating a high degree of membrane damage and orange indicating a lesser degree of membrane damage. At an 18 % quartzite loading and impeller speed of 1.97 m $s^{-1}$, no green or orange fluorescence was visible (Figure 5.28). All cells fluoresced red, appearing either singly or in clumps indicating that at this solids loading no cell membranes remained intact due to the elevated intensity of mechanical stress. Increasing the solids loading increases the frequency of collisions between cells and quartzite particles and causes increased cellular stress. In Section 5.2 it was shown that at an 18 % quartzite loading the culture was metabolically active. It is possible that although the membranes of these cells were compromised, the cells remained metabolically active.

**Table 5.2:** Proportions of compromised (orange and red) and intact (green) cells for quartzite loadings of 0, 15 and 18 % w/v and an impeller tip speed of 1.97 m $s^{-1}$.

| Quartzite loading (%; w/v) | Colour of fluorescence; % of total cells counted | | | |
|---|---|---|---|---|
| | Green | Orange | Red | |
| 0 | 100 | 0 | 0 | |
| 12 | 46.3 | 15.0 | 38.7 | |
| 18 | 0 | 0 | 29.7 **outside clumps** | 70.3 **inside clumps** |

The loss of cell viability due to compromised membranes resulting from the effects of hydrodynamic and physiological stress has been observed by several investigators (Illing, 1996; Lamaignére, 2002). Lamaignére (2002) observed that increasing solids concentration in the range 0 to 5 % v/v and increasing impeller speed in the range 460 to 850 rpm caused a decrease in the number of viable *S. cerevisiae* cells. The loss of viability was correlated to loss of membrane integrity using used differential methylene blue staining. Nkosi (2001) also utilised methylene blue as an indicator of loss of cell viability through loss of membrane integrity, in the study of nutrient

University of Cape Town

limitation of *S. cerevisiae*. On increasing exposure to starvation stress, the number of membrane damaged cells increased (Table 5.3).

**Table 5.3:** Influence of nutrient limitation on the viability of Brewer's yeast cells (Nkosi, 2001).

| Time (h) | % viability |
|---|---|
| 0 | 94.3 |
| 24 | 88.8 |
| 48 | 81.9 |
| 72 | 75.6 |

Not only is the reproductive capability of micro-organisms affected by a loss of membrane integrity but also the electron transport system and, for acidophilic organisms, the maintenance of a near neutral internal pH may be compromised. Acidophilic micro-organisms need to maintain a larger pH gradient across their membranes compared to neutrophiles and the cell membrane is the only barrier to the low pH environment. The membrane of thermoacidophiles such as *S. acidocaldarius* is capable of proton pumping to maintain a near neutral intracellular pH of approximately 6 pH units (Anemüller *et al.*, 1985). The large resultant pH gradient is not only required for maintaining a near neutral internal pH but has also been linked to cellular respiration. Anemüller *et al.* (1985) proposed that it is unlikely that *S. acidocaldarius* generates ATP exclusively by a fermentative pathway but could also use chemiosmotic means of oxidative phosphorylation. Thus permeabilisation of the membrane of acidophilic micro-organisms through damage caused by mechanical stress not only causes acidification of the cell cytoplasm but also affects the cell energetics. Furthermore, maintaining a large pH gradient under optimal conditions requires considerable maintenance energy. Membrane damage may increase the maintenance energy required to maintain this gradient and it is postulated that this may contribute to the greater maintenance energy requirement during growth of organisms under stressful conditions as discussed in Section 5.1.

## 5.4 THE EFFECT OF HYDRODYNAMIC STRESS ON PROTEIN COMPOSITION

SDS PAGE analysis was used in this study to enable protein profiling and aid the search for stress proteins. The presence of new protein bands or the up- or down-regulation of existing protein bands in the *Sulfolobus* culture exposed to mechanical stress was of interest. Like other organisms, thermoacidophiles have adapted to changing environments and have developed stress responses. It is widely accepted that when cells are stressed, stress proteins may be induced. As stresses such as heat shock, salt stress, ethanol, starvation and oxidative stress have been shown to induce the

University of Cape Town

same set of proteins (Jerez, 1988; Craig *et al.*, 1993; López-García and Forterre, 2000b) it is possible that mechanical stress may induce a similar response from the archaeal culture. Furthermore, evidence of cell wall repair mechanisms in response to hydrodynamic stress has been discussed in Section 5.1.3.4. These repair mechanisms could be facilitated by stress proteins. Using these findings as a basis, it is proposed that stress proteins may be expressed by the archaeal culture in response to hydrodynamic stress in the chalcopyrite slurry system.

A preliminary study was conducted to analyse the protein composition of cells exposed to various impeller tip speeds and solids loadings. The aim of this analysis was to identify changes in protein profiles signalling the appearance of new protein bands, the disappearance of protein bands, or the up- or down- regulation of proteins due to increased hydrodynamic stress conditions. Total protein was extracted from cells in mid-log phase and loaded onto polyacrylamide gels. The samples were prepared as described in Section 3.5.6.1. The protein profiles obtained at higher speeds and solids loadings were compared to the profile of the baseline reactor. Figures 5.29a and 5.30b show a typical set of SDS PAGE gels from a solids loading (a) and an impeller tip speed (b) experiment. The numbered arrows indicate bands of interests. Figure 5.29a shows the protein banding patterns of cells exposed to 0 (lane A and D) and 12 % (lane B and E) quartzite and an impellet tip speed of 1.67 m $s^{-1}$. The intensity of the protein band indicated by arrow 2 is similar in both figures and thus can be used as a reference against which to determine significant changes in the protein profiles. Arrow 1 indicates a possible up-regulated protein of approximately 45 kDa whereas arrow 3 shows a protein of approximately 26 kDa that has been down-regulated on exposure of the cells to a 12 % quartzite concentration. Similarly, Trent *et al.* (1990) and Jerez (1988) reported the down regulation of proteins on exposure of archaeal cells to heat shock. In addition, Jerez (1988) found that there was an increase in the synthesis of two protein bands with molecular weights between 64 and 66 kDa with increasing temperature. Stress proteins found in low concentrations during cell growth under ideal conditions may be up-regulated when the organism is exposed to stressful conditions.

In the present study, under conditions of mild hydrodynamic stress, no difference was observed in the protein profiles. The protein profiles of cells grown in the presence of 0 % quartzite and impeller tip speeds of 1.67 m $s^{-1}$ (lane H), 1.97 m $s^{-1}$ (lane I) and 2.13 m $s^{-1}$ (lane J) were compared (Figure 5.29b). Similar proteins were expressed at all three impeller tip speeds. It is possible that in the up- and down-regulation of the 45 and 26 kDa proteins was in response to increased mechanical stress induced by the presence of quartzite particles. Furthermore, the similar protein profiles observed for the impeller speed experiments served as a control showing that the protein profiles are similar in the absence of high intensities of mechanical stress.

University of Cape Town

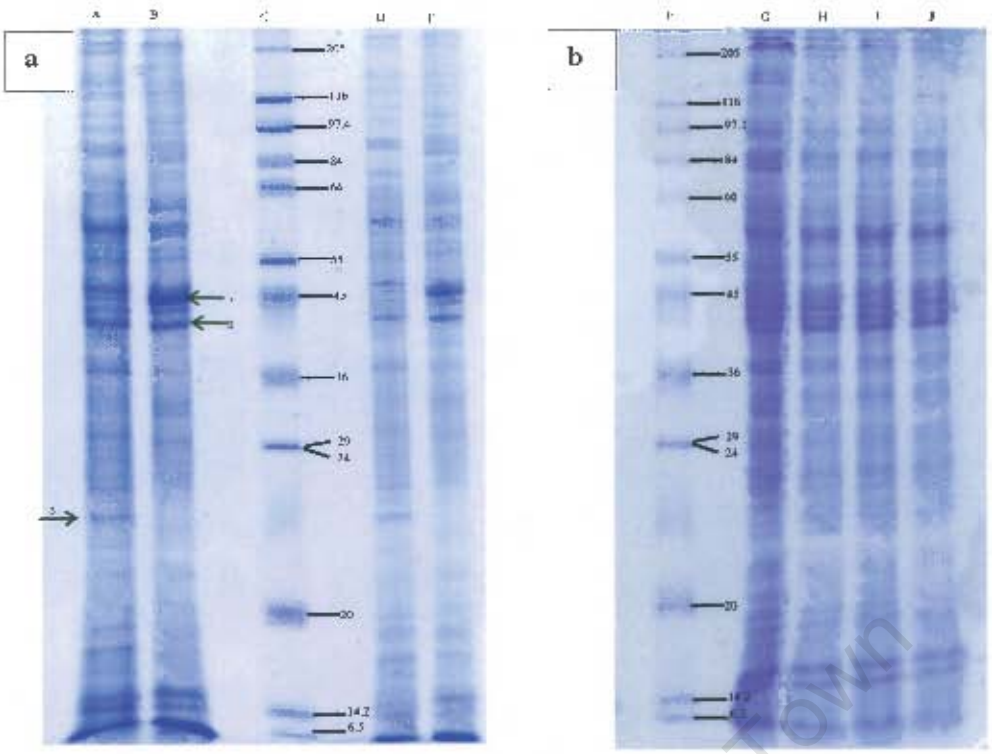


**Figure 5.29:** 15 % SDS PAGE gels of total protein extracted from *Sulfolobus* cells grown in the presence of (a) 0 and 12 % quartzite at an impeller tip speed of 1.97 m $s^{-1}$ and (b) 0 % quartzite at impeller tip speeds of 1.67, 1.97 and 2.13 m $s^{-1}$.

A = 0 % quartzite (100 µl sample)
B = 12 % quartzite (100 µl sample)
C = molecular weight marker (kDa)
D = 0 % quartzite (75 µl sample)
E = 12 % quartzite (75 µl sample)
F = molecular weight marker (kDa)
G = 1.67 m $s^{-1}$ (120 µl sample)
H = 1.67 m $s^{-1}$ (100 µl sample)
I = 1.97 m $s^{-1}$ (100 µl sample)
J = 2.13 m $s^{-1}$ (100 µl sample)

Another phenomenon associated with mechanical damage is the release of proteins into the bulk solution. Proteins liberated into solution due to increased mechanical stress originate from two main sources depending on the level of stress encountered by the cells. These sources are the cell envelope and the cytoplasm.

In the present study, a bulk sample of 300 ml was extracted from each reactor at the end of the experiment, centrifuged to remove mineral and precipitate solids and the supernatant concentrated to 5 ml using a 5 kDa membrane filter (Section 3.5.6.2). In this way all molecules smaller than 5 kDa were excluded from the sample and the protein molecules were concentrated. These samples were used to determine if the protein concentration in the bulk solution increased with increased levels of hydrodynamic stress. After concentration, the samples were analysed for total soluble protein content. The results are presented in Table 5.4. The protein concentration

University of Cape Town

in solution was found to be a function of the intensity of hydrodynamic stress applied. There was an increase in the soluble protein concentration from 10.1 to 27.5 μg $ml^{-1}$ when the solids concentration was increased from 0 to 15 % quartzite at an impeller tip speed of 1.67 m $s^{-1}$. Increasing the impeller tip speed while maintaining a 15 % quartzite concentration, caused a further increase in the protein release from 27 to 39.2 μg $ml^{-1}$ at an impeller tip speed of 1.97 m $s^{-1}$ and 46.2 μg $ml^{-1}$ at an impeller tip speed of 2.13 m $s^{-1}$.

Pearce (1993) and Scholtz-Brown (1998) also found that in STRs, the soluble protein release from *S. cerevisiae* was a function of time and agitation rate. Pearce (1993) investigated the release of the yeast wall-associated protein, invertase. At low impeller speeds and low pulp densities, the outer layer of yeast cell wall was partially damaged, releasing invertase into the bulk solution while intracellular proteins were preserved within the cytoplasm. Similarly, it is possible that in the present study, at low intensities of hydrodynamic stress (0 % quartzite and an impeller speed of 1.67 m $s^{-1}$) the proteins extruded into solution may have originated from the proteinaceous S-layer that surrounds the *Sulfolobus* cells. At high intensities of hydrodynamic stress the proteins in solution may have originated from rupture of the cells and release of cell contents into the medium. Phase contrast images presented in Section 5.1.1 show leakage of the cell contents into the bulk solution confirming the presence of intracellular proteins in the bulk solution.

**Table 5.4:** Solution protein concentrations for 0 and 15 % quartzite loadings at varying impeller tip speeds.

| Sample | Protein concentration in solution (μg $ml^{-1}$) |
|---|---|
| 1.67 m $s^{-1}$, 0 % quartzite | 10.1 |
| 1.67 m $s^{-1}$, 15 % quartzite | 27.5 |
| 1.97 m $s^{-1}$, 15 % quartzite | 39.2 |
| 2.13 m $s^{-1}$, 15 % quartzite | 46.2 |

University of Cape Town

## 5.5 CONCLUSIONS

Although it is important to define the hydrodynamic forces that affect growth and death of cells, it is also vital that a good understanding of the mechanisms by which such forces regulate cellular metabolism, division and survival is attained. In this chapter, the adverse **effects** of hydrodynamic stress on the *Sulfolobus* culture at a cellular level as well as some of the **response** mechanisms of these organisms were discussed.

A range of morphological types was identified on varying the intensity of hydrodynamic stress. These varied from small and tiny cells (Figures 5.7c and Figure 5.12), to damage to the cell

envelope resulting in leaking cells and ghost cells (Figure 5.7d) and complete cell disruption resulting in the presence of cell debris (Figures 5.7d and 5.14). Changes in cell size with increased solids loading were analysed quantitatively using cell-number based cell size distributions. The decrease in the mode of the size distribution with increasing solids loading from 0 to 18 % confirmed that the overall cell size decreased with increased stress. Evidence was also presented to show that cell clumping (in the 2-5 μm cell diameter range) increased with increasing solids loading from 0 to 18 % quartzite. This result corroborated the phase contrast micrographs (Figure 5.7d) showing clumps of cells at the same solids loading.

Oxygen utilisation rate was used to measure the metabolic activity of the culture on exposure to increasing solids loading. It was shown that metabolic activity decreased with time as well as with increasing solids loading. The decrease in metabolic activity with time may have resulted from nutrient limitation due to mineral passivation as discussed in Section 4.6 while the decrease with solids loading was due to increased hydrodynamic stress.

The increased level of propidium iodide uptake by *Sulfolobus* cells demonstrated the loss of membrane integrity as the severity of stress increased. An increase in solids loading was accompanied by a change in the proportions of green, orange and red fluorescence. At a 0 % quartzite loading, no apparent loss of membrane integrity was observed. At a 12 % quartzite loading, more than 50 % of the cells had compromised membranes while at an 18 % quartzite loading, all cell membranes were compromised. Furthermore, cell clumps were visible primarily at an 18 % solids loading.

The possibility of system recovery during long-term exposure to hydrodynamic stress was considered in Section 4.6.2.8. Results showed that at a 15 % quartzite loading the process performance improved over a protracted period of reactor operation. It is postulated that the system recovered due to the intrinsic adaptation and repair mechanisms of the micro-organisms. Several studies have shown possible resistance mechanisms to physiological and hydrodynamic stress. Lamaignére (2002) illustrated the thickening of the yeast cell wall with increasing pulp density and impeller speed in an STR. In addition, kinetic studies by Searby and Hansford (2003) indicated a change in the maintenance energy requirement with stress induced by increased reactor temperature. This increase in maintenance energy requirement can be postulated to result from the diversion of energy from growth to repair mechanisms such as those shown by Lamaignére (2002). Abu-Reesh and Kargi (1991) found that the gradual increase in agitation speed caused minor cell damage to hybridoma cells in comparison to large step changes in agitation speed. The authors proposed that the cells developed some kind of resistance mechanism to shear when the speed was gradually increased. Maintenance energy has also been

University of Cape Town

linked to increased production of stress proteins such as the HSPs. Several investigators have shown increased production of these proteins with increasing stress levels. In Section 5.4 a preliminary investigation yielded SDS PAGE gels showing the down-regulation of a 26 kDa protein and the up-regulation of a 45 kDa protein with increased solids loading. These results suggest that a stress protein may up-regulated under conditions of increased hydrodynamic stress. To determine that the 45 kDa is a typical stress protein, the cross reaction of these bands to known archaeal HSPs is required.

Results presented on the concentrated reactor supernatant showed that the concentration of protein released from the cells into the bulk reactor solution increased on exposure to increased solids loading. Under conditions of mild hydrodynamic stress, proteins released into solution may have originated from damage to the proteinaceous cell wall. At higher intensities of hydrodynamic stress, proteins in solution were sourced from the cytoplasm of ruptured or leaky cells.

In summary, the microbial stress response correlates strongly to cell integrity, viability, and metabolic activity. Furthermore, possible stress proteins are expressed in response to increased hydrodynamic stress. Thus, hydrodynamic stress decreases process performance through changes primarily at the cellular level and not by changing the physicochemical environment. In order to minimise the negative impact of hydrodynamic stress, system conditions favouring maximisation of resilience to decreased cell integrity, viability and metabolic activity are required.

University of Cape Town

# Chapter 6: Conclusions and Recommendations

Slurry reactor systems are widely applied in the bioprocessing industry. In slurry systems hydrodynamic stress, mediated by increased solids loadings and agitation rates, has a major influence on process efficiency. The current study was carried out to determine the effect of hydrodynamic stress on a *Sulfolobus* culture in a chalcopyrite bioleaching slurry system. The effect of hydrodynamic stress was measured at a process performance level as well as at a cellular level. The intensity of hydrodynamic stress was varied by (i) changing the solids concentration using inert quartzite particles while maintaining a constant impeller tip speed, (ii) changing the impeller tip speed while maintaining a constant quartzite loading, and (iii) changing both quartzite concentration and impeller tip speed. The process performance was monitored by measuring the solution pH, redox potential, and cell, iron and copper concentrations. The effect on the micro-organisms at a cellular level as well as the biological response was determined by monitoring changes in culture morphology, metabolic activity, membrane integrity and protein composition.

## 6.1 CONCLUSIONS

The effect of solids loading on process performance was determined by increasing the quartzite loading across the range 0 to 18 % w/v while maintaining a constant 3 % w/v chalcopyrite loading and an impeller tip speed of 1.97 m $s^{-1}$. Using this chalcopyrite-quartzite system, physicochemical stresses such as decreased oxygen availability, associated with increasing the mineral concentration, were avoided. The key findings on varying solids loading across the range were that:

(i) Increasing the quartzite concentration caused a decline in process performance and the extent of the decline was proportional to the quartzite loading applied;

(ii) Passivation of the chalcopyrite caused nutrient limitation and this physiological stress compounded the effect of the hydrodynamic stress; and

(iii) The critical solids loading beyond which process performance was adversely affected was determined to be 9 % w/v quartzite. Increasing the quartzite concentration from 9 to 15 % caused a progressive decline in system performance. At an 18 % quartzite concentration the system approached failure.

Three groups of quartzite loadings with similar levels process performance were identified. These were: 6 and 9 %, 12 and 15 %, and 18 %.

University of Cape Town

The results of the present study were compared to previous studies conducted in the Bioprocess Engineering Group at the University of Cape Town investigating the effect of solids concentration on the bioleaching of pyrite by a *Sulfolobus* culture in pyrite-only (Nemati and Harrison, 2000) and pyrite-quartzite (Sissing, 2002) STRs systems. The comparison showed that the pyrite-only system was most sensitive to the effects of hydrodynamic stress followed by the chalcopyrite-quartzite system and the pyrite-quartzite system. The pyrite system failed at the lowest solids concentration due to factors such as pH of below 1.0 and particle density compounding the effects of hydrodynamic stress. The chalcopyrite-quartzite system used in the present study failed at a lower solids concentration to the pyrite-quartzite system of Sissing (2002) due to nutrient limitation compounding the effect of hydrodynamic stress.

In the present study, the effect of three impeller tip speeds namely, 1.67, 1.97, and 2.13 m $s^{-1}$, on process performance was also determined. Two sets of impeller speed experiments were conducted. In the first set, the solids loading was maintained at 0 % quartzite and 3 % chalcopyrite and the impeller tip speed was varied in the range 1.67 to 2.13 $ms^{-1}$. In the second set, the solids loading was maintained at 9 % quartzite and 3 % chalcopyrite and the impeller tip speed was varied in the range 1.67 to 2.13 m $s^{-1}$. For the second set of experiments, the baseline reactor containing 3 % w/v chalcopyrite and no quartzite and operated at an impeller tip speed of 1.67 m $s^{-1}$ was run simultaneously. The key findings on varying the impeller speed were that:

(i) Increasing the impeller tip speed from 1.67 to 1.97 m $s^{-1}$ at a 0 % quartzite loading resulted in improved mass transfer which caused an increase in the metabolic activity of the culture. This increase however did not improve the ultimate extent of leaching;

(ii) Increasing impeller tip speed at a 9 % quartzite loading caused a decline in the process performance as measured by the change in the extent of iron and copper leaching; and

(iii) At a 9 % quartzite loading the impeller tip speed above which process performance was adversely affected was determined to be the lowest impeller tip speed tested, 1.67 m $s^{-1}$.

A further, significant conclusion was drawn on analysis of the rates of iron and copper solubilisation as a function of time for the solids loading and impeller speed experiments. Results showed that the rate of leaching of the pyrite and chalcopyrite fractions of the mineral was dependent on the redox potential. At low redox potentials (< 500 mV), chalcopyrite leaching dominated while at elevated redox potentials (> 600 mV), pyrite leaching dominated.

University of Cape Town

The growth and redox potential data obtained in the solids loading experiments were analysed further in Section 4.9. Specific death rate constants were derived from the growth data and modelled as a function of solids loading yielding the following model:

$$k_{d1} = 4.61 \times 10^{-5}\Phi^{1.66}$$

Good correlation was found between the measured and predicted values for $k_{d1}$. In addition, the exponent of $\Phi$ was found to be close to 2, corroborating the results of Pearce (1993) and Scholtz-Brown (1998) and showing that the primary mechanism of damage in the slurry reactor is solid-cell-solid collisions. Further analysis of redox potential data was conducted using the method of Rawlings *et al.* (1999) adapted by Petersen and Dixon (2005). The basis of the analysis is that the operating redox potential in a bioleaching system can be predicted if the leaching kinetics, as described by the mineral ferric consumption and the microbial ferric supply, are known. In the present study the analysis method was able to predict the **changes** in the redox potential observed for the solids loading experiments successfully. However, further data is required in order to use the analysis method to predict **actual** operating redox potential data.

On investigating the influence of solids loading and impeller speed on the process performance, a parallel investigation of the effect of hydrodynamic stress at a cellular level was conducted. The results showed that changes in the culture morphology, metabolic activity, membrane integrity and protein composition occurred on increasing solids loading and impeller tip speed. On increasing impeller tip speed, various morphological types were observed using phase contrast microscopy and scanning electron microscopy. These types included, small cells, leaking cells and ghost cells, cell clumps and, at the highest intensity of hydrodynamic stress, cell debris. Quantitative analysis of cell size showed that the average cell size was a function of the phase of growth as well as the solids loading. The culture metabolic activity as measured by the oxygen utilisation rate of the culture was shown to be a function of time as well as solids loading. Metabolic activity decreased with time due to nutrient limitation of the culture early in the growth phase. The membrane integrity of the cells as measured by the uptake of propidium iodide was also found to decline with increasing solids loading. As the intensity of hydrodynamic stress increased, the permeability of the membrane to the fluorescent dye, propidium iodide, increased. An increase in solids loading was accompanied by a change in the proportions of green (intact membranes), orange and red fluorescence (permeabilised membranes). At a 0 % quartzite loading, no apparent loss of membrane integrity was observed as indicated by the green fluorescence. At a 12 % quartzite loading, more than 50 % of the cells had compromised membranes while at an 18 % quartzite loading, all cell membranes were compromised. The protein composition of the cells was determined using SDS PAGE analysis. Protein profiles were analysed for the presence of new protein bands or the up- or down-regulation

University of Cape Town

of existing protein bands with increasing hydrodynamic stress. The preliminary investigation showed that a 26 kDa protein was down-regulated and a 45 kDa protein was up-regulated when the solids loading was increased from 0 to 12 % quartzite.

Possible mechanisms by which the effect of hydrodynamic stress at a cellular level affects the overall process performance may be elucidated on analysis of the bioresponse data. For example, (i) membrane damage, induced by increased solids loading, decreases cell viability, which contributes to a reduction in the extent of growth; (ii) the production of stress proteins or the up-regulation of stress proteins led to a decrease the average cell size as well as a decrease in the yield of cells on substrate due to energy diverted to the stress responses rather than to cell growth.

By integration of the process performance and bioresponse data, four intensities of hydrodynamic stress and four effects were identified:

(i) Negligible hydrodynamic stress with improved process performance owing to improved mass transfer and an adverse effect over time due to nutrient limitation.

(ii) Negligible hydrodynamic stress with adverse effect over time due to nutrient limitation.

(iii) Mild to intermediate hydrodynamic stress. Adverse effect due to increasing hydrodynamic stress and compounded by nutrient limitation over time.

(iv) Intense hydrodynamic stress. The proportion of dead or ruptured cells to viable and/or metabolically active cells increased with increasing the intensity of stress applied.

University of Cape Town

The progressive changes at a process performance level and at a cellular level with increasing intensities of hydrodynamic stress are shown in Table 6.1. Furthermore, the various physiological and metabolic states attained on progression from negligible to intense hydrodynamic stress in the chalcopyrite-quartzite system are illustrated in Figure 6.1. The scheme also shows that the effects observed were not only a function of stress intensity but also of time. The first effect of time is that as the growth phase progressed, nutrient limitation occurred and this compounded the hydrodynamic stress effect. The second effect of time was that over a prolonged period of system operation, adaptation to the stress conditions and hence system recovery was possible.

**Table 6.1:** The effect of increasing intensities of hydrodynamic stress at a process performance and cellular level.

| Stress intensity | Reactor conditions | Process performance | Effect at a cellular level and bio response |
|---|---|---|---|
| Negligible hydrodynamic stress | **Solids loading:** 0 % quartzite **Impeller tip speed:** 1.67, 1.97, 2.13 m $s^{-1}$ -early growth phase | Improved specific growth and solubilisation rates at 1.97 m $s^{-1}$ and improved specific solubilisation rates at 2.13 m $s^{-1}$. No improvement in ultimate extent of leaching | No visible difference in morphological types viewed under phase contrast microscopy |
| Negligible hydrodynamic stress | **Solids loading:** 0 % quartzite **Impeller tip speed:** 1.97 m $s^{-1}$ -mid growth phase to early stationary phase | Decreased growth, iron and copper solubilisation rates | No visible difference in morphological types viewed under phase contrast microscopy |
| Mild to intermediate hydrodynamic stress | **Solids loading:** 0, 6, 9, 12 % quartzite **Impeller tip speed:** 1.97 m $s^{-1}$ | Decreased rate and extent of growth, and iron and copper solubilisation | -Various morphological types observed using phase contrast and SEM: phase dark; round; small; small cell clumps; leaky cells -decreased metabolic activity -increased membrane permeability (12 %) -possible stress protein up-regulated |
| Intense hydrodynamic stress | **Solids loading:** 15 and 18 % quartzite **Impeller tip speed:** 1.97 m $s^{-1}$ | -decreased rate and extent of growth or no growth and cell death -highly reduced rate and extent of iron and copper solubilisation | -Various morphological types observed using phase contrast and SEM: tiny cells; 'leaky' cells; 'ghost' cells; large cell clumps; cell debris (18 %) -all cell membranes permeabilised (18 %) -some degree of metabolic activity measured |

University of Cape Town

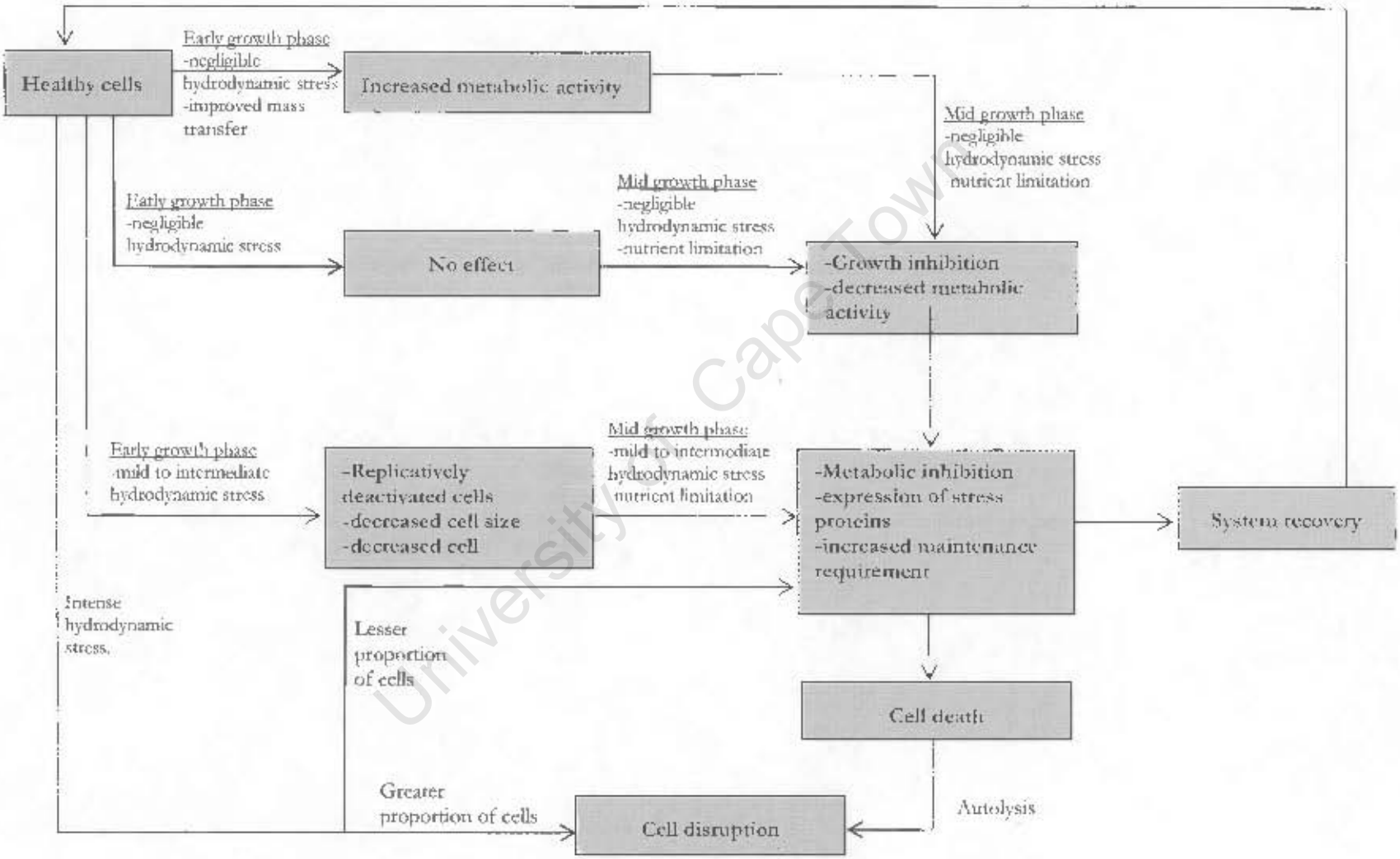


**Figure 6.1**: Proposed scheme for the effect of varying intensities of hydrodynamic stress on the physiology and metabolic state of the *Sulfolobus* culture

University of Cape Town

Thus, in this study, it was demonstrated that the adverse effects of increasing hydrodynamic stress on the bioleaching of chalcopyrite by a *Sulfolobus* culture was due primarily to the presence of solids, and enhanced by increased agitation rates and nutrient limitation, and not due to the oxygen limitation as was proposed by previous studies. Furthermore, the effect of hydrodynamic stress was confirmed at a cellular level where an increase in hydrodynamic stress resulted in changes in cell morphology, metabolic activity, membrane integrity and protein composition.

The indicators investigated in the present study may be used as early warning signals for the detection of system failure. Reduced system performance due to hydrodynamic stress is mediated through (i) a decreased cell concentration which is a function of viability and (ii) decreased metabolic activity of the culture. Thus, in order to develop an early warning system, indicators sensitive to the effects of hydrodynamic stress at a cellular level are required. In the present study, indicators such as the metabolic activity are directly related to microbial performance while indicators such as copper solubilisation are indirectly related to microbial performance. In this study, the most sensitive and practical indicators identified were cell size and metabolic activity. Furthermore, to prevent decreased process performance, conditions favouring increased culture viability and metabolic activity are required. In the chalcopyrite bioleaching system this may be achieved through, for example, minimising the effect of nutrient limitation. In addition, operating conditions that increase the resilience of the cells to stress need to be identified.

University of Cape Town

## 6.2 RECOMMENDATIONS FOR FUTURE WORK

It is proposed that the following areas of research would provide answers to questions that have arisen in the current study, further the understanding of hydrodynamic stress in the chalcopyrite slurry reactor and possibly provide ways to improve the process performance:

1. Identification of the stress proteins induced by hydrodynamic stress is required. Two-dimensional protein electrophoresis is recommended to confirm the presence of new or up-regulated protein bands and the cross-reaction of these proteins with known archaeal stress proteins is proposed. The functional role of these proteins should be sought.
2. The relative contribution of shear damage and collision damage of cells attached to particulates in the reactor requires investigation.
3. This study has investigated the effect of increasing quartzite loading in a chalcopyrite-quartzite system where the concentrations of metal ions did not increase to inhibitory levels. Further, model studies, where the quartzite concentration is increased in the presence of increasing concentrations of iron and copper during the experiment mimicking

a chalcopyrite bioleach, would be useful. Such studies will enable the controlled superimposition of multiple stresses in order to assess their interaction. Ferrous iron and tetrathionate could be used as the nutrient source. In this way the presence of chalcopyrite is not required and passivation effects are negated.

4. In the present study, experiments were conducted in batch culture due to the difficulty of operating the system in a continuous mode at laboratory scale while maintaining accurate solids loadings. However, mode of operation is an important consideration when investigating stress. For example, in a bioleaching system operated in batch mode, non-viable cells remain in the reactor and continue metabolising. Furthermore they have potential for recovery. In a continuous culture system the cell concentration becomes progressively diluted over time due to a loss of reproductive capability and eventually cell washout occurs resulting in system failure. Commercial bioleaching processes are continuous operations and experiments conducted in continuous culture will provide important relevant insights of stress behaviour.
5. Studies on chalcopyrite leaching at reduced cell concentrations (reduced ferric iron supply capacity) and thus reduced redox potentials are required to confirm the hypothesis that over an extended period, the extent of leaching at reduced redox potentials may be higher compared to leaching at elevated redox potentials.

University of Cape Town

# Chapter 7: References

Abrahamson, J. (1975), "Collision rates of small particles in a vigorously turbulent fluid", *Chemical Engineering Science*, **30**, 1371-1379.

Abu-Reesh, I. and F. Kargi. (1991), "Biological responses of hybridoma cells to hydrodynamic shear in an agitated bioreactor", *Enzyme and Microbial Technology*, **13**, 913-919.

Acevedo, F. (2000), "The use of reactors in biomining processes", *Electronic Journal of Biotechnology*, **3**, 184-194.

Allan, E.J., A.H. Scragg and K. Pugh (1988), "Cell suspension culture of *Picrasma quassioides*: the development of rapidly growing, shear resistant cell line capable of quassin formation", *Journal of Plant Physiology*, **132**, 176-183.

Al-Rubeai, M., S.K.W. Oh, R. Musaheb and A.N. Emery (1990), "Modified cellular metabolism in hybridomas subjected to hydrodynamic and other stresses", *Biotechnology Letters*, **12**, 323-328.

Ananta, E., V. Heinz and D. Knorr (2004), "Assessment of high pressure damage on *Lactobacillus rhamnosus* GG by flow cytometry", *Food Microbiology*, **21**, 567-577.

Anemüller, S., M. Lübben and G. Schäfer (1985) "The respiratory system *of Sulfolobus acidocaldarius*, a thermoacidophilic archeabacterium", *FEBS*, **193**, 83-87.

Arce, E.M. and I. González (2002), "A comparative study of electrochemical behaviour of chalcopyrite, chalcocite and bornite in sulphuric acid solution", *International Journal of Mineral Processing*, **67**, 17-28.

Augenstein, D.C., A.J. Sinskey and D.I.C. Wang (1971), "Effect of Shear on the death of two strains of mammalian tissue cells", *Biotechnology and Bioengineering*, **13**, 409-418.

Bailey, A.D. and G.S. Hansford (1993a), "Factors affecting bio-oxidation of sulphide minerals at high concentrations of solids: a review", *Biotechnology and Bioengineering*, **42**, 1164-1174.

Bailey, A.D. and G.S. Hansford (1993b), "Effect of removal of unattached cells on the bio-oxidation rate of pyrite in a fluidised bed reactor", *Biotechnology Letters*, **15**, 543-548.

Bailey, A.D. and G.S. Hansford (1994), "Oxygen mass transfer limitation of batch bio-oxidation at high solids concentration", *Minerals Engineering*, **7**, 293-303.

Bakker, A. and H.E.A. van den Akker (1990), "The use of profiles axial flow impellers in gas-liquid reactors", *Institute of Chemical Engineers Symposium Series*, **121**, 153-166.

Bangaru, B. (2004), "A detailed investigation of microbial cell disruption by hydrodynamic cavitation for selective product release", *Ph.D. Dissertation*, University of Cape Town, South Africa.

University of Cape Town

Barr, D.W., M.A. Jordan, P.R. Norris and C.V. Phillips (1992), "An investigation into bacterial cell, ferrous iron, pH and $E_h$ interactions during thermophilic leaching of copper concentrates", *Minerals Engineering*, **5**, 557-567.

Basson, L., A. (1996), "Loss of yeast quality during mechanical handling in a brewery: an investigation of cropping", *MSc. Dissertation*. University of Cape Town, South Africa.

Basson, L., A. Robinson, T.A. Godfrey, E. O'Connor-Cox, B. Axcell and S.T.L. Harrison (1997), "Mechanical handling of brewers' yeast during cropping and its effect on yeast quality", *Proceedings of the Institute of Brewers Convention (Central and Southern African Sections)*, **6**, 55-60.

Baumeister, W. and G. Lembcke (1992), "Structural features of archaebacterial cell envelopes", *Journal of Bioenergetics and Biomembranes*, **24**, 567-575.

Beck, P. and R. Huber (1997), "Detection of cell viability in cultures of hyperthermophiles", *FEMS Microbiology Letters*, **148**, 11-14.

Beyer, M., H.G. Ebner, H.G. and J. Klein (1986), "Influence of pulp density and bioreactor design on microbial desulphurization of coal", *Applied Microbiology and Biotechnology*, **24**, 342-346.

Boon, M. (1996), "Theoretical and experimental methods in the modelling of biooxidation kinetics of sulphide minerals", *Ph.D. Dissertation*, Delft University of Technology, The Netherlands.

Boon, M., T.A. Meeder, J.J. Heijnen and A.M. Luyben (1992), "Influence of oxygen adsorption on the dynamic $k_La$ measurement in three-phase slurry reactors", *Biotechnology and Bioengineering*, **40**, 1097-1106.

Boulton-Stone, J.M. and J.R. Blake (1993), "Gas bubbles at the free surface", *Journal of Fluid Mechanics*, **254**, 437-466.

Bourret, R. B., K.A. Borkovich and M.I. Simon (1991), "Signal transduction pathways involving protein phosphorylation in prokaryotes", *Annual Review of Biochemistry*, **60**, 401-41.

Brandl, H. (2001), "Microbial leaching of metals" In *Biotechnology, Volume 10*, H.J. Rehm (Ed.), Wiley-VCH, Weinheim.

Brierley, C.L. (1976), "Thermophilic microorganisms in extraction of metals from ores", *Developments in Industrial Microbiology*, **18**, 273-283.

Brierley, C.L. and J.A. Brierley (1973), "A chemoautotrophic and thermophilic micro-organism isolated from an acid hot spring", *Canadian Journal of Microbiology*, **19**, 183-8.

Brierley, J.A. (1966), "Contribution of chemoautotrophic bacteria to the acid thermal waters of the Geyser Spring Group in Yellowstone National Park", *Ph.D. Dissertation*, Montana State University, U.S.A.

Brierley, J.A. (1978), "Thermophilic iron-oxidizing bacteria found in copper leaching dumps", *Applied and Environmental Microbiology*, **36**, 523-525.

University of Cape Town

Brierley, J.A. (1986), "Microbial mining using thermophilic organisms" In *Thermophiles: General, Molecular and Applied Microbiology*, T.D. Brock (Ed.), John Wiley and Sons, New York. Pp. 280-305.

Brierley, J.A.. (1990), "Acidophilic thermophilic archaebacteria: potential application for metals recovery", *FEMS Microbiology Reviews*, **75**, 287-292.

Brierley, J.A., and C.L. Brierley (1978), "Microbial leaching of copper at ambient and elevated temperatures", In *Metallurgical Applications of Bacterial Leaching and Related Microbiological Phenomena*, L.E. Mire, A.E. Torma and J.A. Brierley (Eds.), Academic Press, New York .

Bronnenmeier, R. and H. Märkl (1982), "Hydrodynamic stress capacity of microorganisms", *Biotechnology and Bioengineering*, **24**, 553-578.

Brock, T.D. (1978), "Thermophilic Microorganisms and Life at High Temperatures", Springer-Verlag, New York.

Brock, T.D., K.M. Brock, R.T. Belly and R.L. Weiss (1972), "*Sulfolobus*: a new genus of sulphur-oxidizing bacteria living at low pH and high temperature", *Archiv fur Mikrobiologie*, **84**, 54-68.

Brock, T.D. and M.T. Madigan (1991), "Biology of Microorganisms, 6th ed., Prentice-Hall, New Jersey.

Burton, N.P., T.D. Williams and P.R. Norris (1995), "A potential anti-oxidant protein in a ferrous iron-oxidising *Sulfolobus* species", *FEMS Microbiology Letters*, **134**, 91-95.

Chalmers, J.J. and F. Bavarian (1991), "Microscopic visualisation of insect cell-bubble interactions. II: the bubble film and bubble rupture", *Biotechnology Progress*, **7**, 151-158.

Chattopadhyay, D., J.F. Rathman and J.J. Chalmers (1995), "The protective effect of specific medium additives with respect to bubble rupture", *Biotechnology and Bioengineering*, **45**, 473-480.

Cherry, R.S. and E.T. Papoutsakis (1986), "Hydrodynamic effects on cells in agitated tissue culture reactors", *Bioprocess Engineering*, **1**, 21-41.

Cherry, R.S. and E.T. Papoutsakis (1988), "Physical mechanisms of cell damage in microcarrier cell culture bioreactors", *Biotechnology and Bioengineering*, **32**, 1001-1004.

Chisti, Y. and M. Moo-Young (1996), "Bioprocess intensification through bioreactor engineering", *Trans IChemE*, **74**, 575-583.

Chong, N., D.G. Karamanev and A. Margaritis (2002), "Effect of particle-particle shearing on the bioleaching of sulphide minerals", *Biotechnology and Bioengineering*, **80**, 349-357.

Clark, D.A. and P.R. Norris (1996), "Oxidation of mineral sulphides by thermophilic micro-organisms", *Minerals Engineering*, **9**, 1119-1125.

Colmer, A.R. and M.E. Hinkel (1947), "The role of micro-organisms in acid mine drainage: a preliminary report", *Science*, **106**, 253-256.

University of Cape Town

Comas, J. and J. Vives-Rego (1998), "Enumeration, viability and heterogeneity in *Staphylococcus aureus* cultures by flow cytometry", *Journal of Microbiological Methods*, **32**, 45-53.

Craig, E.A. , B.D. Gambill and R.J. Nelson (1993), "Heat shock proteins: molecular chaperones of protein biogenesis", *Microbiological Reviews*, **57**, 402-414.

Croughan, M.S., J-F. Hamel and D.I.C. Wang (1987), "Hydrodynamic effects on animal cells grown in microcarrier cultures", *Biotechnology and Bioengineering*, **29**, 130-141.

Croughan, M.S., J-F. Hamel and D.I.C. Wang (1988), "Effects of microcarrier concentration in animal cell culture", *Biotechnology and Bioengineering*, **32**, 975-982.

Das, T., S. Ayyappan and G.R. Chaudhury (1999), "Factors affecting bioleaching kinetics of sulphide ores using acidophilic microorganisms", *Biometals*, **12** 1-10.

Derksen, J.J., K. Buist, G. van Weert and M.A. Reuter (2000), "Oxygen transfer in agitated silica and pyrite slurries", *Minerals Engineering*, **13**, 25-36.

Deveci, H. (2001), "Bacterial leaching of complex zinc/lead sulphides using mesophilic and thermophilic bacteria, *PhD. Dissertation*, Camborne School of Mines, University of Exeter.

Deveci, H. (2002), "Effect of solids on viability of acidophilic bacteria", *Minerals Engineering*, **15**, 1181-1189.

Deveci, H. (2004), "Effect of particle size and shape of solids on the viability of acidophilic bacterial during mixing in stirred tank reactors", *Hydrometallurgy*, **71**, 385-395.

Dew, D.W., C. van Buuren, K. McEwan and C. Bowker (1999), "Bioleaching of Base metal sulphide concentrates: a comparison of mesophile and thermophile bacterial cultures", In *Proceedings of the International Biohydrometallurgy Symposium. Biohydrometallurgy and the Environment Toward the 21st Century*, R. Amils and A. Ballester (Eds.), Elsevier, Amsterdam.

Dinnbier, U., E. Limpinsel, E. Schmid and E. Bakker (1988), "Transient accumulation of potassium glutamate and its replacement by trehalose during adaptation of growing cells of *Escherichia coli* K-12 to elevated sodium chloride concentrations", *Archives of Microbiology*, **150**, 348-357.

Dispirito, A.A., P.R. Dugan and O.H. Tuovinen (1981), "Inhibitory effects of particulate materials in growing cultures of *Thiobacillus ferroxidans*", *Biotechnology and Bioengineering*, **23**, 2761-2769.

Doran, P. (1997), "Bioprocess Engineering Principles", Academic Press, London.

Dunlop, E.H. and P. K. Namdev (1994), "Effect of fluid shear forces on plant cell suspensions", *Chemical Engineering Science*, **49**, 2263-2276.

Einsele, A. (1978), "Scaling up bioreactors", *Process Biochemistry*, **13**, 13-14.

Finley, D., A. Crechanover and A. Varshavsky (1984), "Thermolability of ubiquitin-activating enzyme from the mammalian cell cycle mutant ts85", *Cell*, **37**, 43-55.

Galinski, E.A. (1995), "Osmoadaptation in bacteria", *Advances in Microbial Physiology*, **37**, 273-328.

Garcia-Briones, M.A. and J.J. Chalmers (1994), "Flow parameters associated with hydrodynamic cell injury", *Biotechnology and Bioengineering*, **44**, 1089-1098.

University of Cape Town

Garduno, R.A., G. Faulkner, M.A. Trevors, N. Vats and P.S. Hoffman (1998), "Immumolocalisation of Hsp60 in *Legionella pneumophilia*", *Journal of Bacteriology*, **180**, 505-513.

Gericke, M., A. Pinches and J.V. van Rooyen (2001), "Bioleaching of a chalcopyrite concentrate using an extremely thermophilic culture", *International Journal of Mineral Processing*, **62**, 243-255.

Gómez, E., M.L. Blázquez, A. Ballester and F. González (1996), "Study by SEM and EDS of chalcopyrite bioleaching using a new thermophilic bacteria", *Minerals Engineering*, **9**, 985-999.

Gómez, E., I. Marin, A. Ballester, F. González, R. Amils and M.L. Blázquez (1994), "Previous studies of characterization and bioleaching of a novel thermophilic microorganism", In *Minerals Bioprocessing II.* D.S. Holmes and R.W. Smith (Eds.), The Minerals, Metals and Materials Society.

Gormely, L.S. and R.M.R. Branion (1989), "Engineering design of microbiological leaching reactors", *Proceedings of the International Biohydrometallurgy Symposium*, J Salley, R.G.L. McCready and P.L. Wichlacz (Eds.). Canmet, Canada.

Grima, E.M., Y. Chisti and M. Moo-Young (1997), "Characterisation of shear rates in airlift bioreactors for animal cell culture", *Journal of Biotechnology*, **54**, 195-210.

Gunasekera, T. S., D.A.Veal and P.V. Attfield (2003), "Potential for broad applications of flow cytometry and fluorescence techniques in microbiological and somatic cell analyses of milk", *International Journal of Food Microbiology*, **85**, 269-279.

Hamill, O.P. and B. Martinac (2001), "Molecular basis of mechanotransduction in living cells", *Physiology Reviews*, **81**, 685-740.

Han, C.J., S.H. Park and R.M. Kelly (1997), " Acquired thermotolerance and stressed-phase growth of the extremely thermoacidophilic archaeon *Metallosphaera sedula* in continuous culture", *Applied and Environmental Microbiology*, **63**, 2391-2396.

Harahuc, L., H.M. Lizama and I. Suzuki (2000), "Selective inhibition of the oxidation of ferrous iron or sulphur in *Thiobacillus ferrooxidans*", *Applied Environmental Microbiology*, **66**, 1031–1037.

Harrison, S.T.L., A. Sissing, S. Raja, S.J.A. Pearce, V. Lamaignére and M. Nemati (2003), "Solids loading in the biotech slurry reactor: mechanisms through which particulate parameters influence slurry bioreactor performance", *Proceedings of the International Biohydrometallurgy Symposium*, Greece, Sept 2003.

Hei, D.J. and D.S. Clark (1994), "Pressure stabilisation of proteins from extreme thermophiles", *Applied and Environmental Microbiology*, **60**, 932-939.

University of Cape Town

Hiroyoshi, N., S. Kuroiwa, H. Miki, M. Tsunekawa and T. Hirajima (2004), "Synergistic effect of cupric and ferrous ions on active-passive behaviour in anodic dissolution of chalcopyrite and sulphuric acid solutions", *Hydrometallurgy*, **74**, 103-116.

Hjort, K. and R. Bernander (1999), "Changes in cell size and DNA content in *Sulfolobus* cultures during dilution and temperature shift experiments", *Journal of Bacteriology*, **181**, 5669-5675.

Holden, J.F. and J.A. Baross (1993), "Enhanced thermotolerance and temperature-induced changes in protein composition in the hyperthermophilic archaeon ES4", *Journal of Bacteriology*, **175**, 2839-2843.

Horváth, I., A. Glatz, V. Varvasovszki, Z. Török, T. Páli, G. Balogh, E. Kovács , L. Nádasdi, S. Benkö, F. Joó and L. Vígh (1998), "Membrane physical state controls the signalling mechanism of the heat shock response in *Synechocystis* PCC 6803: identification of *hsp17* as a "fluidity gene"", *Proceedings of the National Academy of Science*, USA, **95**, 3513-3518.

Holtje, J.-V and B. Glaune (1990), "Structure and metabolism of the murein sacculus", *Research in Microbiology*, **141**, 75-89.

Howard, D. and F.K. Crundwell (1999), "A kinetic study of the leaching of chalcopyrite with *Sulfolobus metallicus*". In *Proceedings of the International Biohydrometallurgy Symposium. Biohydrometallurgy and the Environment Toward the 21st Century*, R. Amils and A. Ballester (Eds.), Elsevier, Amsterdam.

d'Hugues, P., P. Cezac, T. Cabral, F. Battaglia, X.M. Truong-Meyer and D. Morin (1997), "Bioleaching of a cobaltiferous pyrite: a continuous laboratory-scale study at high solids concentration", *Minerals Engineering*, **10**, 507-527.

d'Hugues, P., S. Foucher, P. Gallé-Cavalloni and D. Morin (2002), "Continuous bioleaching of chalcopyrite using a novel extremely thermophilic mixed culture", *International Journal of Mineral Processing*, **66**, 107-119.

Illing, S. (1996), "An investigation of the effect of hydrodynamic stress on the growth, morphology and metabolism of microorganisms", *Ph.D. Dissertation.*, University of Cape Town, South Africa.

Illing, S. and S.T.L. Harrison (1999), "The kinetics and mechanisms of *Corynebacterium glutamicum* aggregate breakup in bioreactors", *Chemical Engineering Science*, **54**, 441-454.

Itoh, T. (2003), "Taxonomy of nonmethanogenic hyperthermophilic and related thermophilic archaea", *Journal of Bioscience and Bioengineering*, **96**, 203-212.

Iwahashi, H., K. Obuchi, S. Fujii and Y. Komatsu (1995), "The correlative evidence suggesting that trehalose stabilised membrane structure in the yeast *Saccharomyces cerevisiae*", *Cellular and Molecular Biology*, **41**, 763-769.

Jerez, C.A. (1988), "The heat shock response in meso- and thermoacidophilic chemolithotrophic bacteria", *FEMS Microbiology Letters*, **56**, 289-294.

University of Cape Town

Jobin, M-P, F. Delmas, D. Garmyn, C. Diviès and J. Guzzo (1997), "Molecular characterisation of the gene encoding an 18-kilodalton small heat shock proteins associated with the membrane of *Leuconostoc oenos*", *Applied and Environmental Microbiology*, **63**, 609-614.

Jones, R.P. (1987), "Measures of yeast death and deactivation and their meaning: Part I.", *Process Biochemistry*, **22**, 118-128.

Jordan, M.A., D.W. Barr and C.V. Phillips (1993), "Iron and sulphur speciation and cell surface hydrophobicity during bacterial oxidation of a complex copper concentrate", *Minerals Engineering*, **6**, 1001-1011.

Junker, B.H., M. Stanik, C. Barna, P. Salmon and B.C. Buckland (1998), "Influence of impeller type on mass transfer in fermentation vessels", *Bioprocess Engineering*, **19**, 403-413.

Karamanev, D., A. Margaritis and N. Chong (2001), "The application of ore immobilisation to the bioleaching of refractory gold concentrate", International Journal of Mineral Processing, **62**, 231-241.

Kelly, D. P. and C.A. Jones (1978), "Factors affecting metabolism and ferrous iron oxidation in suspensions and batch cultures of *Thiobacillus ferrooxidans*: Relevance to ferric iron leach solution regeneration", In *Proceedings of the International Symposium on Metallurgical Applications of the Bacterial Leaching and Related Microbiological Phenomena.*

Kim, H.J., J.H. Kim, H.J. Oh and C.S. Shin (2002), "Morphology control of *Monascus* cells and scale-up of pigment fermentation", *Process Biochemistry*, **38**, 649-655.

Klauber, C., A. Parker, W. van Bronswijk and H. Watling (2001), "Sulphur speciation of leached chalcopyrite surfaces as determined by X-ray photoelectron spectroscopy", *International Journal of Minerals Processing*, **62**, 65-94.

Klis, F.M., P. Mol, K. Hellingwerf and S. Brul (2002), "Dynamics of cell wall structure in *Saccharomyces cerevisiae*", *FEMS Microbiology Reviews*, **26**, 239-256.

König, H. (1988), "Archaeobacterial cell envelopes", *Canadian Journal of Microbiology*, **34**, 395-406.

Konishi, Y., S. Asai and M. Tokushige (1999), "Kinetics of the bioleaching of chalcopyrite concentrate by acidophilic thermophile *Acidianus brierleyi*", *Biotechnology Progress*, **15**, 681-688.

Konishi, Y., M. Tokushige and S. Asai (2001a), "Bioleaching of chalcopyrite concentrate by acidophilic thermophile *Acidianus brierleyi*", *Proceedings of the International Biohydrometallurgy Symposium. Biohydrometallurgy: Fundamentals, technology and Sustainable Development*, held 16-19 September 2001 in Minas Gerais, Brazil. Pp. 367-376.

Konishi, Y., M. Tokushige, S. Asai and T. Suzuki (2001b), "Copper recovery from chalcopyrite concentrate by acidophilic thermophile *Acidianus brierleyi* in batch and continuous-flow stirred tanks", *Hydrometallurgy*, **59**, 271-282.

Konishi, Y., S. Yoshida and S. Asai (1995), "Bioleaching of pyrite by acidophilic thermophile *Acidianus brierleyi*", *Biotechnology and Bioengineering*, **48**, 592-600.

University of Cape Town

Krahe, M., G. Antranikian and H. Märkl (1996), "Fermentation of extremophilic microorganisms", *FEMS Microbiology Reviews*, **18**, 271-285.

Kubek, D.J. and M.L. Shuler (1978), "Electronic measurement of plant cell number and size in suspension culture", *Journal of Experimental Botany*, **29**, 511-523.

Kunas, K.T. and E.T. Papoutsakis (1990), "Damage mechanisms of suspended animal cells in agitated bioreactors with and without bubble entrainment", *Biotechnology and Bioengineering*, **36**, 476-483.

Kusters, K.A., J.G. Wijers and D. Thoenes (1997), "Aggregation kinetics of small particles in agitated vessels", *Chemical Engineering Science*, **52**, 107-121.

LaPaglia, C. and P. Hartzell (1997), "Stress-induced production of biofilm in the hyperthermophile *Archaeoglobus fulgidus*", *Applied and Environmental Microbiology*, **63**, 3158-3163.

Lakhotia, S. and E.T. Papoutsakis (1992), "Agitation induced cell injury in microcarrier cultures. Protective effect of viscosity is agitation intensity dependent: experiments and modelling", *Biotechnology and Bioengineering*, **39**, 95-107.

Laksanalamai, P., D.L. Maeder and F.T. Robb (2001), "Regulation and mechanism of action of the small heat shock protein from the hyperthermophilic Archaeon *Pyrococcus furiosus*", *Journal of Bacteriology*, **183**, 5198-5202.

Lamaignére, V (2002), "Effects of hydrodynamic stress on growing *Saccharomyces cerevisiae* in a slurry reactor", *MSc. Dissertation*, University of Cape Town, South Africa.

Lamosa, P., L.O. Martins, M.S. Da Costa and H. Santos, (1998), "Effects of temperature, salinity, and medium composition on compatible solute accumulation by *Thermococcus* spp.", *Applied and Environmental Microbiology*, **64**, 3591-3598.

Lawrence, R. W and R. Poulin (1996), "Biooxidation of copper sulphides", 1996, In *Proceedings of Sessions and Symposia of the EPD Congress held at the TMS Annual Meeting*, Anaheim, California.

Le Roux, N.W., D.S. Wakerley and S. D. Hunt (1977), "Thermophilic thiobacillus-type bacteria from Icelandic thermal areas", *Journal of General Microbiology*, **100**, 197-201.

Le Roux, N.W. and D.S. Wakerley (1988), "Leaching of chalcopyrite ($CuFeS_2$) at 70°C using *Sulfolobus*", In *Proceedings of the International Biohydrometallurgy Symposium*. P.R. Norris and D.P. Kelly (Eds.), Science and technology Letters, Kew Surrey, U.K..

Lindquist, S. and E.A. Craig (1988), "The heat-shock proteins", *Annual Review of Genetics*, **22**, 631-677.

Lindström, E.B., S. Wold, N. Kettaneh-Wold and S. Sääf (1993), "Optimisation of pyrite bioleaching using *Sulfolobus acidocaldarius*", *Applied Microbiology and Biotechnology*, **38**, 702-707.

University of Cape Town

Liu, M.S., R.M.R. Branion, D.W. Duncan (1987), "Oxygen mass transfer to *Thiobacillus* cultures", In *Proceedings of the International Biohydrometallurgy Symposium*. P.R. Norris and D.P. Kelly (Eds.), Science and technology Letters, Kew Surrey, U.K..

Loia, G., A. Mura, P. Trois and G, Rossi (1994), "Bioreactor performance versus solids concentration in coal biodepyritization", *Fuel Processing Technology*, **40**, 251-260.

López-García, P. and P. Forterre (2000a), "DNA topology and the thermal stress response, a tale from mesophiles and hyperthemrophiles", *BioEssays*, **22**, 738-746.

López-García, P. and P. Forterre (2000b), "Thermal stress in hyperthermophiles" In *Bacterial Stress Responses*. G. Storz and R. Hengge-Aronis (Eds.), ASM Press, Washington, D.C.

Lotter, S. and J. Büchs (2004), "Utilisation of specific power input measurements for optimisation of culture conditions in shaking flasks", *Biochemical Engineering Journal*, **17**, 195-203.

Lu, G. Z., B.G. Thompson and M.R. Gray (1992), "Physical modelling of animal cell damage by hydrodynamic forces in suspension cultures", *Biotechnology and Bioengineering*, **40**, 1277-1281.

Lu Chau, T., A. Guillan, E. Roca, M.J. Nunez and J.M. Lema (2001), "Population dynamics of a continuous fermentation of recombinant *Saccharomyces cerevisiae* using flow cytometry", *Biotechnology Progress*, **17**, 951-957.

de Macario E.C. and A.J.L. Macario (2003), "Molecular biology of stress genes in methanogens: potential for bioreactor technology", *Advances in Biochemical Engineering and Biotechnology*, **81**, 95-150

Macario, A.J.L., M. Lange, B.K. Ahring and E. Conway de Macario (1999), "Stress genes and proteins in the archaea", *Microbiology and Molecular Biology Reviews*, **63**, 923-967.

Mandl, M. (1984), "Growth and respiration kinetics of *Thiobacillus ferrooxidans* limited by carbon dioxide and oxygen", *Biologia*, **39**, 429-34.

Märkl, H., R. Bronnenmeier and B. Wittek (1991), "The resistance of microorganisms to hydrodynamic stress", *International Journal of Chemical Engineering*, **31**, 185-197.

Marsh, R.M. and P.R. Norris (1983), "The isolation of some thermophilic, autotrophic, iron- and sulphur-oxidising bacteria", *FEMS Microbiology Letters*, **17**, 311-315.

Martinac, B. and A. Kloda (2003), "Evolutionary origins of mechanosensitive ion channels", *Progress in Biophysics and Molecular Biology*, **82**, 11-24.

Martins, L.O., R. Huber, H. Huber, K,O, Stetter, M.S. Da Costa and H. Santos (1997), "Organic solutes in hyperthermophilic archaea", *Applied and Environmental Microbiology*, **63**, 896-902.

May, N., D.E. Ralph and G.S. Hansford (1997), "Dynamic redox potential measurement for determining the ferric leaching kinetics of pyrite", *Minerals Engineering*, **10**, 1279-1290.

Mehta, A.P. and L.E. Murr (1982), "Kinetic study of sulfide leaching by galvanic interaction between chalcopyrite , pyrite and sphalertie in the presence of *T. ferrooxidans* (30°C) and a thermophilic microorganism (55°C)", *Biotechnology and Bioengineering*, **24**, 919-940.

University of Cape Town

Messner, P. (1996), "Chemical composition and biosynthesis of S-layers", In *Crystalline Bacterial Cell Surface Proteins*. U.B. Sleytr,P. Messner, D. Pum and M. Sára (Eds.), R. G. Landes/Academic Press Inc., Austin, Texas.

Michel, H., D.-Ch. Neugebauer and D. Oesterhelt (1980), "The 2-D crystalline cell wall of *Sulfolobus acidocaldarius*: structure, solubilisation and reassembly", In *Electron Microscopy at Molecular Dimension*, W. Baumeister and V.W. Vogell (Eds.), Springer-Verlag, Berlin.

Michaels, J.D., A.K. Mallik and E.T. Papoutsakis (1996), "Sparging and agitation-induced injury of cultures animal cells: do cell-to-bubble interactions in the bulk liquid injure cells?", *Biotechnology and Bioengineering*, **51**, 399-409.

Mills, D.B., R. Bar, D.J. Kirwan (1987), "Effect of solids on oxygen transfer in agitated three-phase systems", *AIChe Journal*, **33**, 1542-1549.

Montealegre, R. and S. Bustos (1991), "Industrial application of thin layer process (BTL)", In *Bioleaching from Molecular Biology to Industrial Applications*, R. Badilla, T. Vargas and L. Herrera (Eds.), Universitaria, Santiago, Chile.

Mukhopadhyay, B., E.F. Johnson and R.S. Wolfe (1999), "Reactor-scale cultivation of hyperthermophilic methanarchaeon *Methanococcus jannaschii* to high cell densities", *Applied and Environmental Microbiology*, **65**, 5059-5065.

Murr, L. E (1980), "Theory and practice of copper sulphide leaching in dumps and *in situ*", *Minerals Science and Engineering*, **12**, 121-89.

Myers, K.J. and A. Bakker (1998), "Solids suspension with up-pumping pitched-blade high-efficiency impellers", *Canadian Journal of Chemical Engineering*, **76**, 433-440.

Namdev, P.K., E.H. Dunlop, K. Wenger and P. Villeneuve (1994), "Role of turbulence in Fermentations", In *Advanced in Bioprocess Engineering*, E. Galindo and O.T. Ramírez (Eds.), Kluwer Academic Publishers, Dordrecht, The Netherlands.

Natarajan, K.A. (1990), "Electrochemical aspects of bioleaching of base-metal sulphides". In *Microbial Mineral Recovery*, H.L. Ehrlich and C.L. Brierley, (Eds.), McGraw-Hill, New York.

Nemati, M. and S.T.L. Harrison (2000), "Effect of solid loading on thermophilic bioleaching of sulphide minerals", *Journal of Chemical Technology and Biotechnology*, **75**, 526-532.

Nemati, M., J. Lowenadler and S.T.L. Harrison (2000), "Particle size effects in bioleaching of pyrite by acidophilic thermophile *Sulfolobus metallicus* (BC)", *Applied Microbiology and Biotechnology*, **53**, 173-179.

Nkosi, J. C. (2001), "The effect of cooling on brewer's yeast quality", *MSc. Dissertation*. University of Cape Town, South Africa.

Norris, P.R. (2001). Personal Communication.

Norris, P.R. and D.W. Barr (1988), "Bacterial oxidation of pyrite in high temperature reactors", *Proceedings of the International Biohydrometallurgy Symposium*. P.R. Norris and D.P. Kelly (Eds.), Science and Technology Letters, Kew Surrey, U.K.. Pp. 532-536.

University of Cape Town

Olsen, G.J., J.A. Brierley and C.L. Brierley (2003), "Bioleaching review part B: Progress in bioleaching: applications of microbial processes by the minerals industries", *Applied Microbiology and Biotechnology*, **63**, 249-257.

Osorio, G. and C.A. Jerez (1996), "Adaptive response of the archaeon *Sulfolobus acidocaldarius* BC65 to phosphate starvation", *Microbiology*, **142**, 1531-1536.

Otomo, N., W. Bujalski, A.W. Nienow and K. Takahashi (2003), "Gassed power consumption and gas hold-up for a dual hollow blade impeller systems in a stirred vessel", *Journal of Chemical Engineering of Japan*, **36**, 905-911.

Parsell, D.A. and S. Lindquist (1993), "The function of heat-shock proteins in stress tolerance: degradation and reactivation of damaged proteins", *Annual Review of Genetics*, **27**, 437-496.

Peacey, J., X.J. Guo and E. Robles. "Copper hydrometallurgy – current status, preliminary economics, future direction and positioning versus smelting", www.hatch.ca/Non_Ferrous/ articles/copper_hydrometallurgy.pdf, accessed: 23 June 2005.

Pearce, S.J.A. (1993), "Disruption of microorganisms due to agitation in slurries of fine particles", *MSc. Dissertation*, University of Cape Town, South Africa.

Peeples , T.L. and R.M. Kelly (1995), "Bioenergetic response of the extreme thermoacidophile *Metallosphaera sedula* to thermal and nutritional stresses", *Applied and Environmental Microbiology*, **61**, 2314-2321.

Peillex, J-P., M-L. Fardeau, R. Boussand, J-M. Navarro and J-P. Belaich (1988), "Growth of *Methanococcus thermolithotrophicus* in batch and continuous culture on $H_2$ and $CO_2$: influence of agitation", *Applied Microbiology and Biotechnology*, **29**, 560-564.

Pelham, H.R.B. (1986), "Speculations on the functions of the major heat-shock and glucose-regulated proteins", *Cell*, **46**, 959-961

Petersen, J. and D.G. Dixon (2005), "Competitive bioleaching of pyrite and chalcopyrite", Accepted for publication in the Proceedings of the *16th International Biohydrometallurgy Symposium*, September 2005.

du Plessis, C.A., P. Barnard, K. Naldrett and S.H. de Kock (2001), "Development of respirometry methods to assess the microbial activity of thermophilic bioleaching archaea", *Journal of Microbiological Methods*, **47**, 189-198

Plumb, J.J., B. Gibbs, M.B. Stott, W.J. Robertson, J.A.E. Gibson, P.D. Nichols, H.R. Watling and P.D. Franzmann (2002), "Enrichment and characterisation of thermophilic acidophiles for the bioleaching of mineral sulphides", *Minerals Engineering*, **15**, 787-794.

Potgieter, T. (2002), "Retention of fermentation biomass for extended L-Lysine fermentations", *Ph.D. Dissertation*, University of Cape Town, South Africa.

Prokop, A. and R.K. Bajpai (1992), "The sensitivity of biocatalysts to hydrodynamic shear stress", *Advances in Applied Biochemistry*, **37**, 165-233.

University of Cape Town

Pum, D., A. Neubauer, E. Gyoervary, M. Sára and U.B. Sleytr (1999), "S-layer proteins as basic building blocks in a biomolecular construction kit", *Proceedings of the Seventh Foresight Conference on Molecular Nanotechnology*, Santa Clara, California.

Quain, D.E. (1991), "Stress and the yeast cell", *Fermentation*, **4**, 155-156.

Rao, M.A. and R.S. Brodkey (1972), "Continuous flow stirred tank turbulence parameters in the impeller stream", *Chemical Engineering Science*, **27**, 137-156.

Rawlings, D.E. (2002), "Heavy metal mining using microbes", *Annual Review of Microbiology*, **56**, 65-91.

Rawlings, D.E., D.W. Dew and C.A. du Plessis (2003), "Biomineralisation of metal-containing ores and concentrates", *Trends in Biotechnology*, **21**, 38-44.

Rawlings, D.E., H. Tributsch and G.S. Hansford (1999), "Reasons why '*Leptospirillum*'-like species rather than *Thiobacillus ferrooxidans* are the dominant iron-oxidising bacteria in many commercial processes for the biooxidation of pyrite and related ores", *Microbiology*, **145**, 5-13.

Reis, A., T.L. da Silva, C.A. Kent, M. Kosseva, J.C. Roseiro and C.J. Hewitt (2004), "Monitoring population dynamics of the thermophilic *Bacillus licheniformis* CCMI 1034 in batch and continuous cultures using multi-parameter flow cytometry", *Journal of Biotechnology*, **115**, 199-210.

Rivera-Santillán, A. Ballester Pérez, M.L. Blázquez Izquierdo and F. González González (1999), "Bioleaching of a copper sulphide flotation concentrate using mesophilic and thermophilic microorganisms", In *Proceedings of the International Biohydrometallurgy Symposium. Biohydrometallurgy and the Environment Toward the 21st Century*, R. Amils and A. Ballester (Eds.), Elsevier, Amsterdam.

Rohwerder, T., T. Gehrke, K. Kinzler and W. Sand (2003), "Bioleaching review part A: progress in bioleaching: fundamentals and mechanisms of bacterial and metal sulphide oxidation", *Applied Microbiology and Biotechnology*, **63**, 239-248.

Rossi, G. (2001), "The design of bioreactors", *Hydrometallurgy*, **59**, 217-231.

Rubio, A. and F.J. García Frutos (2002), "Bioleaching capacity of an extremely thermophilic culture for chalcopyritic material", *Minerals Engineering*, **15**, 689-694.

Ruepp, A., C. Eckerskorn, M. Bogyo and W. Baumeister (1998), "Proteasome function is dispensable under normal but not under heat shock conditions in *Thermoplasma acidophilum*", *FEBS Letters*, **425**, 87-90.

Sadowski, Z., E. Jazdzyk and H. Karas (2003), "Bioleaching of copper ore flotation concentrates", *Minerals Engineering*, **16**, 51-53.

Sales, K., W. Brandt, E. Rumbak and G. Lindsey (2000), "The LEA-like protein HSP 12 in *Saccharomyces cerevisiae* has a plasma membrane location and protects membranes against desiccation and ethanol-induced stress", *Biochimica et Biophysica Acta*, **1463**, 267-278.

University of Cape Town

Sampson, M.I. and R.C. Blake (1999), "The cell attachment and oxygen consumption of two strains of *Thiobacillus ferrooxidans*", *Minerals Engineering*, **12**, 671–686.

Sand, W., T. Gehrke, P-G. Jozsa and A. Schippers (2001), "(Bio)chemistry of bacterial leaching – direct vs. indirect bioleaching", *Hydrometallurgy*, **59**, 159-175.

Sand, W., K. Rhode, B. Sobotke and C. Zenneck (1992), "Evaluation of *Leptospirillum ferroxidans* for leaching", *Applied and Environmental Microbiology*, **58**, 85-92.

Schlegel, H.G. 1993. General Microbiology, 7th ed., Cambridge University Press, New York. 1993.

Scholtz-Brown, N.J. (1998), "The Effect of non-biological particulates on microbial cell disruption in a slurry bioreactor", *Ph.D. Dissertation*, University of Cape Town, South Africa.

Scholtz, N. J., A.B. Pandit and S.T.L. Harrison (1997), "The effect of solids suspension on microbial cell disruption", *BHR Group Conference Series Publication*, **25**, 199-215.

Schuster, B. and U.B. Sleytr (2000), "S-layer-supported lipid membranes", *Reviews in Molecular Biotechnology*, **74**, 233-254.

Schwarzentruber, P. (2002), "CellFacts II – single cell analysis in real time", *Macromolecule Symposium*, **187**, 543-552.

Searby, G.E. and G.S. Hansford (2003), "The kinetics of thermophilic ferrous-iron oxidation", In *Proceedings of the International Biohydrometallurgy Symposium*, September 2003, Athens, Greece.

Searby, G.E. (2005), Unpublished data.

van Scherpenzeel, D.A. (1997), " The kinetics of ferrous iron oxidation by *Leptospirillum*-like bacteria", *MSc. Dissertation*, University of Cape Town, South Africa.

Shuler, M.L. and H.M. Tsuchiya (1975), "Cell size as an indicator of changes in intracellular composition of *Azotobacter vinelandii*", *Canadian Journal of Microbiology*, **21**, 927-935.

Sissing, A. (2002), "An investigation into the effect of solid particulate phase on the bioleaching of *Sulfolobus Metallicus*", *MSc. Dissertation*, University of Cape Town, South Africa.

Sissing, A. and S.T.L. Harrison (2003), "Thermophilic mineral bioleaching performance: A compromise between maximizing mineral loading and maximizing microbial growth and activity", *The Journal of the South African Institute of Mining and Metallurgy*, **103**, 139-142.

Slaninová, I., S. Šesták, A. Svoboda and V. Farkaš (2000), "Cell wall and cytoskeleton reorganisation as the response to hyperosmotic shock in *Saccharomyces cerevisiae*", *Archives of Microbiology*, **173**, 245-252.

Stathopoulos, N.A. and J.D. Hellums (1985), "Shear stress effects on human embryonic kidney cells *in vitro*", *Biotechnology and Bioengineering*, **27**, 1021-1026.

Stock, J. B., A.J. Ninfa and A.M. Stock (1989), "Protein phosphorylation and regulation of adaptive responses in bacteria", *Microbiological Reviews*, **53**, 450-90.

University of Cape Town

Stott, M.B., D.C. Sutton, H.R. Watling and P.D. Franzman (2003), "Comparative leaching of chalcopyrite by selected acidophilic bacteria and archaea", *Geomicrobiology Journal*, **20**, 215-230.

Stott, M.B., H.R. Watling, P.D. Franzmann and D. Sutton (2000), "The role of iron-hydroxy precipitates in the passivation of chalcopyrite during bioleaching", *Minerals Engineering*, **13**, 1117-1127.

Temple, K.L. and A.R. Colmer (1951), "The autotrophic oxidation of iron by a new bacterium: *Thiobacillus ferroxidans*", *Journal of Bacteriology*, **62**, 605-611.

Third, K.A., R. Cord-Ruwisch and H.R. Watling (2000), "The role of iron-oxidising bacteria in stimulation or inhibition of chalcopyrite bioleaching", *Hydrometallurgy*, **57**, 225-233.

Toma, M.K., M.P. Ruklisha, J.J. Vanags, M.O. Zeltina, M.P. Leite, N.I. Galinina, U.E. Viesturs and R.P. Tengerdy (1991), "Inhibition of microbial growth and metabolism by excess turbulence", *Biotechnology and Bioengineering*, **38**, 552-556.

Torma, A. E., C.C. Walden and R.M.R Branion (1970), "Microbiological leaching of a zinc sulphide concentrate", *Biotechnology and Bioengineering*, **12**, 501-17.

Török, Z., Horvath, I., Goloubinoff, P., Kovacs, E., Glatz, A., Balogh, G. and L. Vigh (1997), "Evidence for a lipochaperonin: association of active protein-folding GroESL oligomers with lipids can stabilize membranes under heat shock conditions", *Proceedings of the National Academy of Sciences*, USA.

Trent, J.D., J. Osipiuk and T. Pinkau (1990), "Acquired thermotolerance and heat chock in the extremely thermophilic archaebacterium *Sulfolobus* sp. Strain B12", *Journal of Bacteriology*, **172**, 1478-1484.

Trent, J.D. (2000), "Extremophiles in Astrobiology", *Gravitational and Space Biology Bulletin*, **13**, 5-11.

van Uden, N. (1969), " Kinetics of nutrient-limited growth", *Annual Review of Microbiology*, **23**, 473-485.

Valencia, P., J.C. Gentina and F. Acevedo (2003), "Effect of pulp density and particle size on the biooxidation rate of a pyritic gold concentrate by *Sulfolobus metallicus*", In *Proceedings of the International Biohydrometallurgy Symposium*, September 2003, Athens, Greece.

Vígh, L., B. Maresca and J.L. Harwood (1998), "Does the membrane's physical state control the expression of heat shock and other genes?", *Trends in Biochemical Sciences*, **23**, 369-374.

Vogel, A.I. (1989), "A Textbook of Quantitative Chemical Analysis", 5th ed., Longman Group, London.

van de Vossenberg, J.L.C.M. (1999), "Borders of life: bioenergetics and cation permeability of the cytoplasmic membrane in extremophiles", *PhD Dissertation*, University of Groningen, The Netherlands. WWW reference: http://irs.ub.rug.nl/ppn/183471504

University of Cape Town

van de Vossenberg, J.L., A.J.M. Driessen, W. Zillig and W.N. Konings (1998), "Bioenergetics and cytoplasmic membrane stability of the extremely acidophilic, thermophilic archaeon *Picrophilus oshimae*", *Extremophiles*, **2**, 67-74.

Walker, G.M. (1998), "Yeast physiology and biotechnology", 1st ed., John Wiley and Sons.

Wang, J.-Y. and M. Syvanen (1992), "DNA twist is a transcriptional sensor for environmental changes", *Molecular Microbiology*, **6**, 1861-1866.

Warhurst, A. and G. Bridge (1996), "Improving environmental performance through innovation: recent trends in the mining industry", *Minerals Engineering*, **9**, 907-921.

Wase, D.A. and E.R. Patel (1985), "Variations in the volumes of microbial cells with change in the agitation rates of chemostat cultures", *Journal of General Microbiology*, **131**, 725-736.

van Weert, G., D. van der Werff and J.J. Derksen (1995), "Transfer of $O_2$ from air to mineral slurries in a Rushton turbine agitated tank", *Minerals Engineering*, **8**, 1109-1124.

Wiemken, A. (1990), "Trehalose in yeast, stress protectant rather than reserve carbohydrate", *Antonie van Leeuwenhoek*, **58**, 209-217.

Witne, J.Y. and C.V. Phillips (2001), "Bioleaching of OK Tedi copper concentrate in oxygen-and carbon dioxide-enriched air", *Minerals Engineering*, **14**, 25-48.

Yang, J-D. and N.S. Wang (1992) "Cell inactivation in the presence of sparging and mechanical agitation", *Biotechnology and Bioengineering*, **40**, 806-816.

Zhang, Z., Y. Chisti and M. Moo-Young (1995) "Effects of the hydrodynamic environment and shear protectants on survival of erythrocytes in suspension", *Journal of Biotechnology*, **43**, 33-40.

**WWW references:**

http://www.escondida.cl/english/copper_uses.htm, BHP Billiton, Minera Escondida. Date of access: 10 September 2002.

http://web.pdx.edu/~clore/EM%20pics.html, Maria Harutunian, Date of access: 10 February, 2005.

http://web.pdx.edu/~clore/EM%20pics.html, Maria Harutunian, Date of access: 10 February, 2005.

University of Cape Town

# Appendix A: Analytical methods

## A.1 SDS PAGE PROTOCOL

A 25 cm vertical PAGE unit VG/01 purchased from Omeg Scientific (Cape Town) was used to cast the polyacrylamide gels. The unit consisted of 2, 200 mm (h) by 160 (w) mm glass plates, 2 plastic spacers, a gel caster, a gel stand, a plastic comb, 8 binder clips and a power pack unit were used to cast and run the gel. Upper and lower buffer chambers were created when the glass plates were secured to the gel stand using binder clips. The resolving gel was made up according to Table A.1. The gel components were mixed and the gel was cast to a height of 5 mm below the level of the combs (Figure A.1).

**Table A.1:** Volumes of the components of the 15 % resolving gel.

| Compound | Volume |
|---|---|
| Acrylamide /bisacrylamide | 16 ml |
| 4 X Tris-HCl / SDS pH 8.8 | 8 ml |
| Distilled Water | 8 ml |
| 10% w/v APS | 108 µl |
| TEMED | 20 µl |

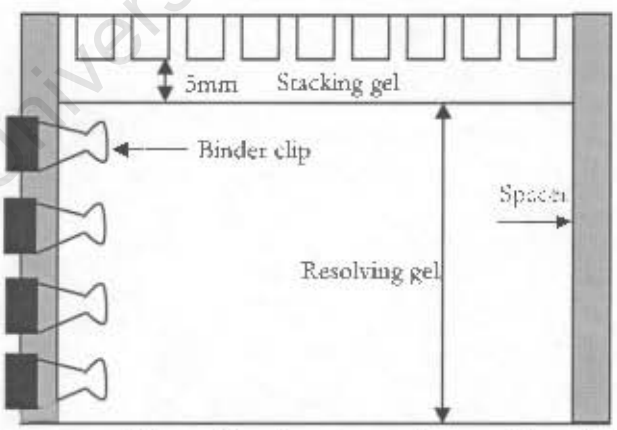


**Figure A.1:** Schematic representation of the glass plate setup used to cast the SDS PAGE gels.

The resolving gel was levelled with water-saturated butanol and left to polymerise for 1 h. When the separating gel had set, the butanol was decanted and the unpolymerised material was washed with distilled water. The excess distilled water on the gel surface was removed using filter paper. The stacking gel was mixed according to Table A.2 and cast over the resolving gel and allowed to polymerize for 30 min.

University of Cape Town

**Table A.2:** Volumes of the components of the stacking gel.

| Compound | Volume |
|---|---|
| Acrylamide/bisacrylamide | 1.6 ml |
| 4 X Tris-HCl / SDS pH 6.8 | 3 ml |
| Distilled Water | 7.32 ml |
| 10 % APS | 120 µl |
| TEMED | 12 µl |

## A.1.1 STOCK SOLUTIONS USED FOR SDS PAGE ANALYSIS

### A.1.1.1 5 % Acetic acid

A 1 litre stock solution was prepared by adding 50 ml of acetic acid to 950 ml of distilled water.

### A.1.1.2 Acryl / Bisacrylamide

A 200 ml stock solution was prepared by adding 60 g Acrylamide and 1.6 g Bisacrylamide 100 ml distilled water. The solution was mixed and made up to 200 ml using distilled water.

### A.1.1.3 4 X Tris-HCl /SDS – pH 8.8

36.4 g Tris base and 0.8 g SDS were added to 150 ml of distilled water. The pH was adjusted to pH 8.8 with HCl. The solution was the diluted to 200 ml with distilled water.

### A.1.1.4 4X Tris-HCl /SDS – pH 6.8

12.08 g Tris base and 0.8 g SDS were added to 150 ml distilled water. The pH was adjusted pH 6.8 with HCl. The solution was the diluted to 200 ml with distilled water.

### A.1.1.5 10 X Electrophoresis Buffer

A 1 litre stock solution of electrophoresis buffer was made up by adding 30.25 g Tris base , 144 g glycine and 10 g SDS to 900 ml distilled water. The pH was adjusted to pH 8.3 with HCl. The volume of the solution was then adjusted to one litre using distilled water.

### A.1.1.6 2 X SDS Sample Buffer (Loading buffer)

The sample buffer was prepared by adding 3.04 g Tris base, 8 g SDS, 20 ml mercaptoethanol, 40 ml glycerol and 0.02 g bromophenol blue to 170 ml distilled water. The pH was adjusted to pH 6.8 with HCl. The volume of the solution was adjusted to 200 ml with distilled water.

### A.1.1.7 APS (Ammonia persulphate)

A 0.1 g aliquot of APS was dissolved in 1 ml distilled water.

University of Cape Town

### A.1.1.8 Stain

The stain solution was prepared by dissolving 1.2 g Coomassie Blue R250 in a mixture containing 500 ml methanol, 400 ml distilled water and 100 ml acetic acid.

### A.1.1.9 Destain I

The destain I solution was a mixture of 150 ml acetic acid, 250 ml methanol and 1600 ml distilled water.

### A.1.1.10 Destain II

The destain II solution was a mixture of 140 ml acetic acid, 800 ml methanol and 1060 ml distilled water.

### A.1.1.11 50mM Tris-HCl pH 8

1.2 g of Tris base was dissolved in 180 ml distilled water. The pH was adjusted to pH 8 with HCl. The final solution was made up to 200 ml with distilled water.

### A.1.1.12 Protein marker

A wide range SigmaMarker™ with proteins of known molecular weights ranging from 6.5 to 205 kDa was used as the molecular weight marker standard (Figure A.2). This size range was chosen because it spanned the range of molecular weights of interest in this study.

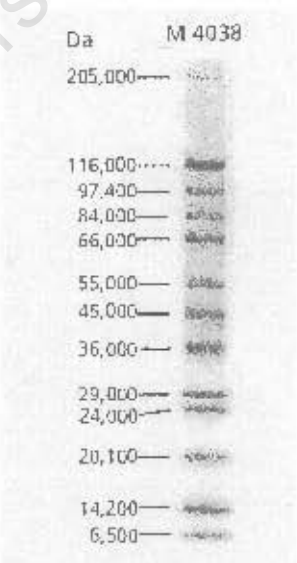


**Figure A.2:** Banding pattern of the wide range SigmaMarker™.

University of Cape Town

## A.2 BRADFORD PROTEIN ASSAY

The Bradford protein method was used to determine the concentration of soluble protein extruded from the archaeal cells upon damage and lysis. The basic principle of the Bradford protein assay is a protein-dependent colour change of the Coomassie Brilliant Blue G-250 dye. The assay is based on the equilibrium between two forms of the Coomassie dye. Under strongly acid conditions, the dye is most stable as a doubly-protonated red form. Upon binding to protein, however, it is most stable as the un-protonated, blue form which has a characteristic absorption maximum at 595 nm. The analytical error was calculated to be 9.8 %.

### A.2.1 BRADFORD REAGENT

The Bradford reagent was prepared by dissolving 100 mg of Coomassie Brilliant Blue G-250 in 95 % ethanol. To this solution, 100 ml of 85 % (w/v) phosphoric acid was added followed by dilution to a volume of 1 litre.

### A.2.2 PROTEIN STANDARD

Protein standard solutions were prepared using bovine serum albumin (BSA). A stock solution of 1 mg $ml^{-1}$ was prepared and diluted in the 1000 to 10 $\mu g\ ml^{-1}$ range.

### A.2.3 PROCEDURE

A 0.1 ml aliquot of sample (protein sample, standard or blank) was added to a 2 ml plastic cuvette. One millilitre of the Bradford reagent was then added to the cuvette. The cuvette was inverted twice to ensure complete mixing and incubated for 2 to 5 min at room temperature. The absorbance of the solutions was measured at 595 nm against a blank (Norris 0K medium pH 1.6).

## A.3 FERROUS IRON TITRATION SOLUTIONS

### A.3.1 POTASSIUM DICHROMATE

Potassium dichromate powder was heated for 30 to 60 min at 150°C followed by cooling in a dessicator. The 0.017 M solution of $K_2Cr_2O_7$ was prepared by adding 4.9 g of dry potassium dichromate to a litre of distilled water.

University of Cape Town

### A.3.2 BARIUM DIPHENYLAMINE SULFONATE (INDICATOR)

1 g of barium diphenylamine sulfonate was added to 100 ml concentrated sulphuric acid. The solution was agitated until the salt had completely dissolved.

## A.4 STANDARD CURVES FOR IRON AND COPPER DETERMINATIONS BY AAS

Standard copper and iron curves were generated using solutions of known concentration. Standard solutions were prepared by diluting the pre-prepared standards solutions (Merck NT) to the desired concentrations. Typical standard curves for iron and copper are presented in Figures A.3 and A.4.

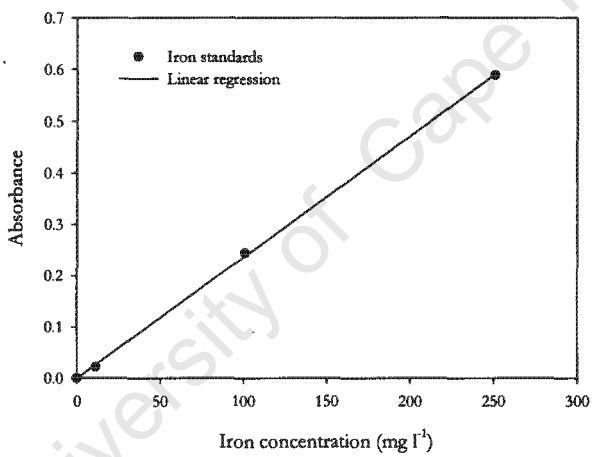


**Figure A.3:** Standard curve for iron determinations using the AAS.

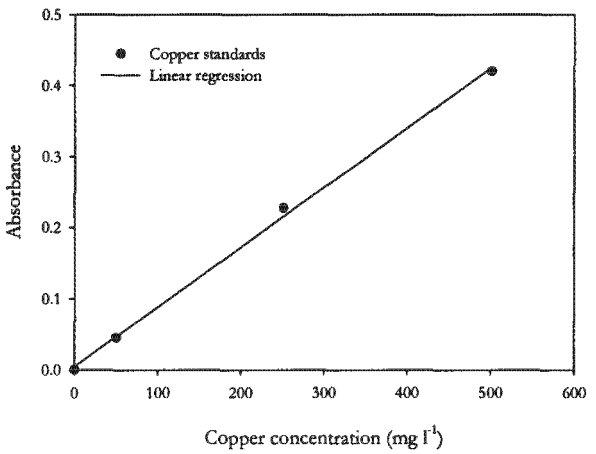


**Figure A.4:** Standard curve for copper determinations using the AAS.

University of Cape Town

## A.5 RESPIROMETER CALIBRATION

The Micro Oxymax Respirometer was calibrated using the following gas blends:

(i) 4.5 – 4.9 % $CO_2$;

(ii) 19.5 – 20.0 % $O_2$; balance $N_2$

(iii) $N_2$ for zero point calibration

## A.6 ANALYTICAL ERROR

The error of each analytical method used was determined by conducting replicate analyses. Triplicate samples were measured and the standard deviation (stdev) and standard error (%) were calculated using the following equations:

$$\text{Stdev } (\sigma) = \sqrt{\frac{n\sum x^2 - \left(\sum x\right)^2}{n(n-1)}} \qquad \ldots\text{Eqn. A.1}$$

$$\text{Standard error} = \frac{\sigma}{\bar{x}} * 100 \qquad \ldots\text{Eqn. A.2}$$

Where $x$ = measurement

n = number of observations

$\bar{x}$ = average of n measurements

University of Cape Town

# Appendix B: Calculations

## B.1 RATES

Growth, and iron and copper solubilisation rates were calculated either by linear regression or by calculating the rate between each sample point.

### B.1.1 LINEAR REGRESSION

A typical iron solubilisation curve is used as an example to illustrate the method used to determine growth, iron and copper solubilisation rates (Figure B.1). A straight line was fitted to the data and only correlation coefficients above 0.98 were accepted. The slope of the curve was the average iron solubilisation rate over the specified time period.

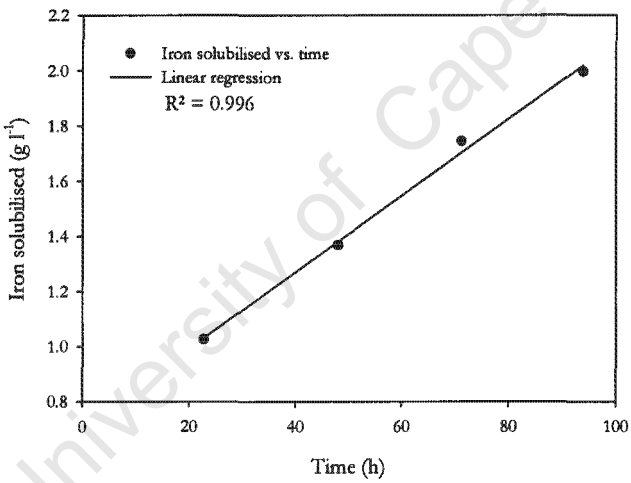


**Figure B.1:** Typical iron solubilisation curve with a linear regression fit.

### B.1.2 DETERMINING RATES BY CALCULATION

The alternative way of calculating rates was using the following equation:

$$\frac{x_2 - x_1}{t_2 - t_1} \qquad \text{...Eqn. B.1}$$

where $x_1$ = the cell, iron or copper concentration at time $t_1$

$x_2$ = the cell, iron or copper concentration at time $t_2$

University of Cape Town

The rate was calculated between each sampling point and averaged to give an average rate over the time period selected.

## B.2 SPECIFIC RATES

Apparent specific growth, specific death, specific OUR and iron and copper solubilisation rates were determined by dividing the rate (calculated using either of the methods detailed in Section B.1) by the average cell concentration over the specified time period (Eqn. B.2).

$$\frac{(x_{t2} - x_{t1})}{(t_2 - t_1)} * \frac{1}{\overline{C}_{t1-t2}} \qquad \ldots \text{Eqn.B.2}$$

Where $x_1$ = the cell, OUR, iron or copper concentration at time $t_1$

$x_2$ = the cell, OUR, iron or copper concentration at time $t_2$

$\overline{C}_{t1-t2}$ = the average cell concentration over the time period $t_1$ to $t_2$

## B.3 BIOMASS YIELD ON FERROUS IRON SOLUBILISED

The biomass yield on ferrous iron was calculated as follows:

$$Y_{X/Fe} = \frac{X_{t2} - X_{t1}}{Fe_{t2} - Fe_{t1}} \qquad \ldots \text{Eqn. B3}$$

where $X_{t1}$ = the concentration of cells at time $t_1$

$X_{t2}$ = the concentration of cells at time $t_2$

$Fe_{t1}$ = the concentration of iron at time $t_1$

$Fe_{t2}$ = the concentration of iron at time $t_2$

University of Cape Town

# Appendix C: Raw data

## C.1 RAW DATA FOR GRAPHS FROM CHAPTER 4

### C.1.1. CULTURE VARIABILITY

Chalcopyrite bioleaching at a 3 % w/v solids loading of chalcopyrite (38-75 μm) and an agitation rate characterised by an impeller tip speed of 1.67 m $s^{-1}$. Experiments 1 and 2 were conducted two months apart.

**Table C.1**: Culture variability (Figure 4.1).

| Experiment 1 | | | Experiment 2 | | |
|---|---|---|---|---|---|
| Time (h) | Redox potential (mV; Ag/AgCl) | Copper solubilised (%; w/w) | Time (h) | Redox potential (mV; Ag/AgCl) | Copper solubilised (%; w/w) |
| 0 | 513 | 0.0 | 0 | 514 | 0.0 |
| 24 | 602 | 13.4 | 23 | 606 | 10.4 |
| 48 | 630 | 16.8 | 48 | 621 | 15.2 |
| 72 | 644 | 19.3 | 71 | 636 | 18.9 |
| 96 | 648 | 25.4 | 94 | 645 | 23.4 |
| 120 | 649 | 26.1 | 118 | 650 | 25.9 |
| 144 | 649 | 29.0 | 144 | 643 | 28.3 |
| 192 | 648 | 37.6 | 169 | 644 | 31.2 |
| 240 | 649 | 46.4 | 192 | 655 | 36.2 |
| 264 | 648 | 55.0 | 216 | 653 | 40.8 |
| | | | 261 | 648 | 53.1 |

### C.1.2 REPRODUCIBILITY OF THE EXPERIMENTS

Reproducibility data for chalcopyrite bioleaching at a solids loading of 6 % w/v quartzite (38-75 μm) and 3 % chalcopyrite (38-75 μm) and an agitation rate characterised by an impeller tip speed of 1.67 m $s^{-1}$

**Table C.2**: Reproducibility of the experiments (Figure 4.2).

| | Run1 | | Run 2 | |
|---|---|---|---|---|
| Time (h) | Redox potential (mV; Ag/AgCl) | Copper solubilised (%; w/w) | Redox potential (mV; Ag/AgCl) | Copper solubilised (%; w/w) |
| 23 | 605 | 10.6 | 600 | 9.29 |
| 48 | 607 | 16.2 | 608 | 17.3 |
| 71 | 618 | 17.5 | 620 | 19.0 |
| 94 | 629 | 21.9 | 632 | 22.4 |
| 118 | 637 | 27.0 | 635 | 27.2 |
| 144 | 640 | 30.2 | 641 | 30.9 |
| 192 | 640 | 34.3 | 644 | 35.0 |
| 216 | 639 | 35.5 | 643 | 35.9 |

University of Cape Town

## C.1.3 ABIOTIC CONTROL

Time profiles of pH and redox potential for a 3 % w/v chalcopyrite solids loading in the absence of micro-organisms. Experiments were run at a pH of 1.6, temperature of 68°C, aeration rate of 2 vvm and an impeller tip speed of 1.97 m $s^{-1}$

**Table C.3**: Abiotic control. pH and redox potential data (Figure 4.3).

| Time (h) | pH | Error | Redox potential (mV; g/AgCl) | Error |
|---|---|---|---|---|
| 0 | 1.57 | 0.0111 | 498 | 0.4490 |
| 4 | 1.57 | 0.0111 | 420 | 0.3787 |
| 6 | 1.68 | 0.0119 | 393 | 0.3543 |
| 22 | 1.71 | 0.0121 | 397 | 0.3580 |
| 28 | 1.74 | 0.0124 | 391 | 0.3525 |
| 31 | 1.73 | 0.0123 | 390 | 0.3516 |
| 49 | 1.76 | 0.0125 | 392 | 0.3534 |
| 52 | 1.78 | 0.0126 | 390 | 0.3516 |
| 56 | 1.82 | 0.0129 | 392 | 0.3534 |
| 74 | 1.79 | 0.0127 | 393 | 0.3543 |

Time profiles of ferric and ferrous iron concentrations for a 3 % w/v chalcopyrite solids loading in the absence of micro-organisms. Experiments were run at a pH of 1.6, temperature of 68°C, aeration rate of 2 vvm and an impeller tip speed of 1.97 m $s^{-1}$

**Table C.4:** Abiotic control. Ferrous and ferric iron data (Figure 4.4).

| Time (h) | Ferrous iron (g $l^{-1}$) | Error | Ferric iron (g $l^{-1}$) | Error |
|---|---|---|---|---|
| 0 | 0.00 | 0.0000 | 0.00 | 0.0000 |
| 22 | 0.25 | 0.0034 | 0.00 | 0.0000 |
| 49 | 0.25 | 0.0051 | 0.17 | 0.0021 |
| 74 | 0.42 | 0.0058 | 0.25 | 0.0106 |

University of Cape Town

## C.1.4 THE BASELINE EXPERIMENT

Leaching of the chalcopyrite concentrate in the baseline reactor characterised by a solids loading of 3 % chalcopyrite and an impeller tip speed of 1.97 m $s^{-1}$. Changes in pH, redox potential, cell concentration and iron and copper solubilisation are shown.

**Table C.5**: Baseline reactor: (Figure 4.5).

| Time (h) | pH | Redox potential (mV; Ag/AgCl) | Cell concentration (cells $ml^{-1}$) | Iron solubilised (%; w/w) | Copper solubilised (%; w/w) |
|---|---|---|---|---|---|
| 0 | 1.68 | 514 | 3.48E+08 | 0.00 | 0.00 |
| 23 | 1.64 | 606 | 4.52E+08 | 14.9 | 10.4 |
| 48 | 1.56 | 621 | 5.00E+08 | 18.3 | 19.2 |
| 71 | 1.49 | 636 | 5.76E+08 | 25.8 | 20.4 |
| 94 | 1.47 | 645 | 5.90E+08 | 28.4 | 24.1 |
| 118 | 1.43 | 650 | 5.76E+08 | 33.9 | 29.2 |
| 144 | 1.41 | 648 | 5.42E+08 | 36.0 | 32.0 |
| 169 | 1.39 | 650 | 5.41E+08 | 38.7 | 33.0 |
| 192 | 1.38 | 655 | 5.71E+08 | 40.7 | 36.2 |
| 216 | 1.38 | 653 | 4.50E+08 | 40.0 | 40.8 |

University of Cape Town

## C.1.5 SOLIDS LOADING EXPERIMENTS

Raw data for graphs from Section 4.6.2.

**Table C.6**: Normalised pH data for solids loading experiments: (Figure 4.13).

| Time (h) experimental set 1 | Relative pH; experimental set 1 | | | | Time (h) experimental set 2 | Relative pH; experimental set 2 | | |
|---|---|---|---|---|---|---|---|---|
| | 0 % quartzite | 6 % quartzite | 9 % quartzite | 12 % quartzite | | 0 % quartzite | 15 % quartzite | 18 % quartzite |
| 23 | 1 | 1.00 | 1.00 | 1.00 | 24 | 1 | 1.00 | 1.00 |
| 48 | 1 | 1.04 | 1.08 | 1.07 | 48 | 1 | 1.01 | 1.08 |
| 71 | 1 | 1.07 | 1.09 | 1.11 | 72 | 1 | 1.04 | 1.14 |
| 94 | 1 | 1.08 | 1.10 | 1.10 | 96 | 1 | 1.02 | 1.18 |
| 118 | 1 | 1.10 | 1.13 | 1.11 | 120 | 1 | 1.05 | 1.18 |
| 144 | 1 | 1.10 | 1.13 | 1.13 | 144 | 1 | 1.04 | 1.19 |
| 169 | 1 | 1.12 | 1.14 | 1.14 | 168 | 1 | 1.03 | 1.21 |
| 192 | 1 | 1.13 | 1.16 | 1.16 | 192 | 1 | 1.02 | 1.21 |
| 216 | 1 | 1.14 | 1.14 | 1.13 | 216 | 1 | 1.02 | 1.22 |

**Table C.7**: Normalised redox potential data for solids loading experiments: (Figure 4.15).

| Time (h) experimental set 1 | Relative redox potential; experimental set 1 | | | | Time (h) experimental set 2 | Relative redox potential; experimental set 2 | | |
|---|---|---|---|---|---|---|---|---|
| | 0 % quartzite | 6 % quartzite | 9 % quartzite | 12 % quartzite | | 0 % quartzite | 15 % quartzite | 18 % quartzite |
| 23 | 1 | 1.00 | 1.00 | 1.00 | 24 | 1 | 1.00 | 1.00 |
| 48 | 1 | 0.98 | 0.96 | 0.91 | 48 | 1 | 0.91 | 0.82 |
| 71 | 1 | 0.97 | 0.96 | 0.94 | 72 | 1 | 0.92 | 0.80 |
| 94 | 1 | 0.98 | 0.97 | 0.94 | 96 | 1 | 0.92 | 0.78 |
| 118 | 1 | 0.98 | 0.98 | 0.95 | 120 | 1 | 0.93 | 0.77 |
| 144 | 1 | 0.99 | 0.99 | 0.96 | 144 | 1 | 0.94 | 0.75 |
| 169 | 1 | 0.98 | 0.98 | 0.97 | 168 | 1 | 0.94 | 0.74 |

University of Cape Town

| Time (h) experimental set 1 | Relative redox potential; experimental set 1 | | | | Time (h) experimental set 2 | Relative redox potential; experimental set 2 | | |
|---|---|---|---|---|---|---|---|---|
| | 0 % quartzite | 6 % quartzite | 9 % quartzite | 12 % quartzite | | 0 % quartzite | 15 % quartzite | 18 % quartzite |
| 192 | 1 | 0.98 | 0.98 | 0.96 | 192 | 1 | 0.95 | 0.72 |
| 216 | 1 | 0.98 | 0.98 | 0.97 | 216 | 1 | 0.95 | 0.71 |

**Table C.8**: Normalised cell concentration data for solids loading experiments: (Figure 4.17).

| Time (h) experimental set 1 | Relative cell concentration; experimental set 1 | | | | Time (h) experimental set 2 | Relative cell concentration; experimental set 2 | | |
|---|---|---|---|---|---|---|---|---|
| | 0 % quartzite | 6 % quartzite | 9 % quartzite | 12 % quartzite | | 0 % quartzite | 15 % quartzite | 18 % quartzite |
| 23 | 1 | 1.00 | 1.00 | 1.00 | 24 | 1 | 1.00 | 1.00 |
| 48 | 1 | 0.93 | 0.93 | 0.91 | 72 | 1 | 0.79 | 0.40 |
| 71 | 1 | 0.89 | 0.88 | 0.82 | 96 | 1 | 0.71 | 0.32 |
| 94 | 1 | 0.88 | 0.87 | 0.78 | 120 | 1 | 0.79 | 0.33 |
| 118 | 1 | 0.88 | 1.01 | 0.83 | 144 | 1 | 0.66 | 0.30 |
| 144 | 1 | 0.92 | 1.09 | 0.89 | 168 | 1 | 0.79 | 0.28 |
| 169 | 1 | 1.00 | 1.08 | 0.92 | 192 | 1 | 0.76 | 0.38 |
| 192 | 1 | 0.93 | 0.89 | 0.78 | | | | |

**Table C.9**: Normalised maximum cell concentration and apparent specific growth rate data for solids loading experiments: (Figure 4.18).

| Quartzite loading (%; w/v) | Relative maximum cell concentration at 72 h | Error | Apparent specific growth rate ($h^{-1}$) | Error |
|---|---|---|---|---|
| 0 | 1.00 | 0.0320 | 0.0050 | 0.0002 |
| 6 | 0.89 | 0.0284 | 0.0039 | 0.0001 |
| 9 | 0.88 | 0.0281 | 0.0034 | 0.0001 |
| 12 | 0.82 | 0.0263 | 0.0022 | 0.0001 |
| 15 | 0.79 | 0.0254 | 0.0007 | 0.0000 |
| 18 | 0.40 | 0.0128 | -0.0016 | -0.0001 |

University of Cape Town

**Table C.10:** Normalised percentage iron solubilised data for solids loading experiments: (Figure 4.20).

| Time (h) experimental set 1 | Relative percentage iron solubilised; experimental set 1 | | | | Time (h) experimental set 2 | Relative percentage iron solubilised; experimental set 2 | | |
|---|---|---|---|---|---|---|---|---|
| | 0 % quartzite | 6 % quartzite | 9 % quartzite | 12 % quartzite | | 0 % quartzite | 15 % quartzite | 18 % quartzite |
| 23 | 1 | 1.00 | 1.00 | 1.00 | 24 | 1 | 1.00 | 1.00 |
| 48 | 1 | 1.07 | 0.93 | 0.89 | 48 | 1 | 0.94 | 0.44 |
| 71 | 1 | 0.95 | 0.92 | 0.81 | 72 | 1 | 0.75 | 0.41 |
| 94 | 1 | 0.89 | 0.86 | 0.84 | 96 | 1 | 0.69 | 0.34 |
| 118 | 1 | 0.90 | 0.88 | 0.80 | 120 | 1 | 0.73 | 0.29 |
| 144 | 1 | 0.89 | 0.89 | 0.77 | 144 | 1 | 0.70 | 0.28 |
| 169 | 1 | 0.86 | 0.89 | 0.77 | 168 | 1 | 0.74 | 0.28 |
| 192 | 1 | 0.81 | 0.88 | 0.71 | 192 | 1 | 0.76 | 0.21 |
| 216 | 1 | 0.85 | 0.86 | 0.74 | 216 | 1 | 0.70 | 0.20 |

**Table C.11**: Normalised extent and rate of iron solubilisation data for solids loading experiments: (Figure 4.21).

| Quartzite loading (%; w/v) | Relative extent of iron solubilisation | Error | Relative rate of iron solubilisation | Error |
|---|---|---|---|---|
| 0 | 1.00 | 0.0286 | 1.00 | 0.0286 |
| 6 | 0.81 | 0.0231 | 0.82 | 0.0234 |
| 9 | 0.88 | 0.0252 | 0.86 | 0.0246 |
| 12 | 0.71 | 0.0204 | 0.71 | 0.0203 |
| 15 | 0.76 | 0.0217 | 0.72 | 0.0206 |
| 18 | 0.21 | 0.0060 | 0.29 | 0.0083 |

University of Cape Town

**Table C.12**: Normalised percentage copper solubilised data for solids loading experiments: (Figure 4.23).

| Time (h) experimental set 1 | Relative percentage copper solubilised; experimental set 1 | | | | Time (h) experimental set 2 | Relative percentage copper solubilised; experimental set 2 | | |
|---|---|---|---|---|---|---|---|---|
| | 0 % quartzite | 6 % quartzite | 9 % quartzite | 12 % quartzite | | 0 % quartzite | 15 % quartzite | 18 % quartzite |
| 23 | 1 | 1.00 | 1.00 | 1.00 | 24 | 1 | 1.00 | 1.00 |
| 48 | 1 | 0.85 | 0.79 | 0.77 | 48 | 1 | 0.81 | 0.71 |
| 71 | 1 | 0.86 | 0.93 | 0.82 | 72 | 1 | 0.68 | 0.55 |
| 94 | 1 | 0.91 | 0.97 | 0.80 | 96 | 1 | 0.80 | 0.55 |
| 118 | 1 | 0.92 | 0.89 | 0.87 | 120 | 1 | 0.71 | 0.47 |
| 144 | 1 | 0.94 | 0.88 | 0.80 | 144 | 1 | 0.79 | 0.48 |
| 169 | 1 | 0.85 | 0.99 | 0.83 | 168 | 1 | 0.76 | 0.50 |
| 192 | 1 | 0.95 | 0.99 | 0.73 | 192 | 1 | 0.71 | 0.47 |
| 216 | 1 | 0.87 | 0.98 | 0.72 | 216 | 1 | 0.76 | 0.47 |

**Table C.13**: Normalised extent and rate of copper solubilisation data for solids loading experiments: (Figure 4.24).

| Quartzite loading (%; w/v) | Relative extent of copper solubilisation | Error | Relative rate of copper solubilisation | Error |
|---|---|---|---|---|
| 0 | 1.00 | 0.0062 | 1.00 | 0.0062 |
| 6 | 0.95 | 0.0058 | 1.01 | 0.0057 |
| 9 | 0.99 | 0.0061 | 1.01 | 0.0062 |
| 12 | 0.73 | 0.0045 | 0.73 | 0.0045 |
| 15 | 0.71 | 0.0043 | 0.69 | 0.0042 |
| 18 | 0.47 | 0.0029 | 0.32 | 0.0019 |

University of Cape Town

**Table C.14**: Recovery data 0 to 216 h: (Figure 4.32).

| Time (h) | pH | Redox potential (mV; Ag/AgCl) | Cell concentration (cells $ml^{-1}$) | Percentage iron solubilised (%; w/w) | Percentage copper solubilised (%; w/w) |
|---|---|---|---|---|---|
| 24 | 1.78 | 604 | 1.53E+08 | 6.11 | 7.86 |
| 48 | 1.69 | 565 | 2.54E+08 | 10.9 | 11.4 |
| 72 | 1.71 | 584 | 2.43E+08 | 12.2 | 13.2 |
| 96 | - | 596 | 2.88E+08 | 13.2 | 15.8 |
| 120 | 1.72 | 604 | 2.25E+08 | 16.3 | 16.8 |
| 144 | 1.71 | 610 | 2.94E+08 | 17.6 | 21.0 |
| 168 | 1.70 | 613 | 2.22E+08 | 19.0 | 21.5 |
| 192 | 1.70 | 616 | - | 21.0 | 21.6 |
| 216 | 1.71 | 618 | - | 20.4 | 23.7 |

**Table C.15**: Recovery data 216 to 456 h: (Figure 4.33).

| Time (h) | pH | Redox potential (mV; Ag/AgCl) | Cell concentration (cells $ml^{-1}$) | Percentage iron solubilised (%; w/w) | Percentage copper solubilised (%; w/w) |
|---|---|---|---|---|---|
| 216 | 1.71 | 618 | - | 20.4 | 23.7 |
| 240 | 1.72 | 617 | 1.90E+08 | 21.3 | 26.9 |
| 264 | 1.74 | 619 | 1.87E+08 | 22.4 | 27.2 |
| 288 | 1.74 | 623 | 1.75E+08 | 24.4 | 27.2 |
| 408 | 1.73 | 631 | 2.11E+08 | 25.8 | 33.4 |
| 456 | 1.72 | 632 | | 26.0 | 35.5 |

University of Cape Town

## C.1.6 IMPELLER SPEED EXPERIMENTS

Raw data for graphs from Section 4.7.

**Table C.16**: pH data for impeller speed experiments: (Figure 4.34).

| Time (h) | 0 % quartzite; 1.67 m s$^{-1}$ | 9 % quartzite | | |
|---|---|---|---|---|
| | | 1.67 m s$^{-1}$ | 1.97 m s$^{-1}$ | 2.13 m s$^{-1}$ |
| 0 | 1.63 | 1.61 | 1.61 | 1.63 |
| 48 | 1.8 | 1.85 | 1.77 | 1.81 |
| 72 | 1.45 | 1.47 | 1.49 | 1.48 |
| 96 | 1.46 | 1.58 | 1.61 | 1.6 |
| 120 | 1.48 | 1.65 | 1.68 | 1.75 |
| 144 | 1.44 | 1.62 | 1.65 | 1.76 |
| 168 | 1.44 | 1.63 | 1.68 | 1.79 |
| 192 | 1.45 | 1.67 | 1.69 | 1.8 |

**Table C.17**: Redox potential data for impeller speed experiments: (Figure 4.35).

| Time (h) | 0 % quartzite; 1.67 m s$^{-1}$ | 9 % quartzite | | |
|---|---|---|---|---|
| | | 1.67 m s$^{-1}$ | 1.97 m s$^{-1}$ | 2.13 m s$^{-1}$ |
| 0 | 460 | 456 | 459 | 456 |
| 48 | 548 | 541 | 551 | 532 |
| 72 | 577 | 546 | 528 | 499 |
| 96 | 603 | 565 | 529 | 487 |
| 120 | 610 | 577 | 527 | 484 |
| 144 | 615 | 588 | 535 | 481 |
| 168 | 613 | 597 | 538 | 478 |
| 192 | 610 | 601 | 540 | 470 |

**Table C.18**: Cell concentration data for impeller speed experiments: (Figure 4.36).

| Time (h) | 0 % quartzite; 1.67 m s$^{-1}$ | 9 % quartzite | | |
|---|---|---|---|---|
| | | 1.67 m s$^{-1}$ | 1.97 m s$^{-1}$ | 2.13 m s$^{-1}$ |
| 0 | 7.60E+07 | 7.50E+07 | 7.50E+07 | 7.25E+07 |
| 48 | 1.84E+08 | 1.75E+08 | 1.85E+08 | 1.75E+08 |
| 72 | 2.35E+08 | 1.72E+08 | 9.37E+07 | 9.25E+07 |
| 96 | 3.56E+08 | 2.38E+08 | 1.20E+08 | 7.81E+07 |
| 120 | 4.35E+08 | 2.98E+08 | 1.40E+08 | 7.50E+07 |
| 144 | 4.23E+08 | 2.88E+08 | 1.83E+08 | 7.50E+07 |
| 168 | 3.85E+08 | 2.75E+08 | 1.75E+08 | 2.19E+07 |
| 192 | 4.00E+08 | 1.84E+08 | 1.44E+08 | 2.03E+07 |

University of Cape Town

**Table C.19**: Percentage iron solubilised data for impeller speed experiments: (Figure 4.37).

| Time (h) | 0 % quartzite; 1.67 m $s^{-1}$ | 9 % quartzite | | |
|---|---|---|---|---|
| | | 1.67 m $s^{-1}$ | 1.97 m $s^{-1}$ | 2.13 m $s^{-1}$ |
| 0 | 0.0 | 0.0 | 0.0 | 0.0 |
| 48 | 11.8 | 11.5 | 8.6 | 10.7 |
| 72 | 15.9 | 12.6 | 9.7 | 9.6 |
| 96 | 18.4 | 15.9 | 13.5 | 12.5 |
| 120 | 24.2 | 20.4 | 14.0 | 10.4 |
| 144 | 30.6 | 25.5 | 14.1 | 9.4 |
| 168 | 33.3 | 28.4 | 15.9 | 12.4 |
| 192 | 35.7 | 28.4 | 16.6 | 12.0 |

**Table C.20**: Average specific rate and extent of iron solubilised at a 9 % quartzite loading. Data for impeller speed experiments: (Figure 4.38).

| Impeller tip speed (m $s^{-1}$) | Average specific rate of iron solubilisation (g Fe $cell^{-1}$ $h^{-1}$) | Extent of iron solubilisation (%; w/v) |
|---|---|---|
| 1.67 | 5.7E-14 | 24.0 |
| 1.67 | 4.9E-14 | 14.0 |
| 1.97 | 3.5E-14 | 8.04 |
| 2.13 | 1.4E-14 | 1.80 |

**Table C.21**: Percentage copper solubilised data for impeller speed experiments: (Figure 4.39).

| Time (h) | 0 % quartzite; 1.67 m $s^{-1}$ | 9 % quartzite | | |
|---|---|---|---|---|
| | | 1.67 m $s^{-1}$ | 1.97 m $s^{-1}$ | 2.13 m $s^{-1}$ |
| 0 | 0.0 | 0.0 | 0.0 | 0.0 |
| 48 | 16.5 | 15.9 | 14.7 | 16.1 |
| 72 | 22.9 | 20.3 | 18.4 | 18.1 |
| 96 | 29.6 | 26.4 | 23.5 | 20.8 |
| 120 | 31.5 | 27.1 | 25.6 | 21.2 |
| 144 | 35.7 | 30.5 | 26.2 | 19.5 |
| 168 | 36.5 | 34.2 | 25.2 | 21.5 |
| 192 | 36.7 | 33.2 | 27.6 | 21.2 |

**Table C.22**: Average specific rate and extent of copper solubilised at a 9 % quartzite loading. Data for impeller speed experiments: (Figure 4.40).

| Impeller tip speed (m $s^{-1}$) | Average specific rate of copper solubilisation (g Cu $cell^{-1}$ $h^{-1}$) | Extent of copper solubilisation (%; w/v) |
|---|---|---|
| 1.67 | 7.2E-14 | 28.8 |
| 1.67 | 6.8E-14 | 24.7 |
| 1.97 | 7.8E-14 | 18.4 |
| 2.13 | 4.5E-14 | 7.7 |

University of Cape Town

**Table C.23**: Average specific rate of iron solubilised and apparent specific growth rate at a 0 % quartzite loading. Data for impeller speed experiments: (Figure 4.41).

| Impeller tip speed ($m\ s^{-1}$) | Average specific rate of iron solubilisation ($g\ Cu\ cell^{-1}\ h^{-1}$) | Apparent specific growth rate ($h^{-1}$) |
|---|---|---|
| 1.67 | 6.2E-11 | 0.0103 |
| 1.97 | 8.2E-11 | 0.0184 |
| 2.13 | 8.3E-11 | 0.0120 |

### C.1.7 FURTHER ANALYSIS OF GROWTH DATA

Raw data for graphs from Section 4.9.

**Table C.24**: Measured and modelled specific death rate constant for solids loading experiments: (Figure 4.47).

| Quartzite loading (%, w/w) | $k_{d1\ measured}$ ($h^{-1}$) | $k_{d1\ modelled}$ ($h^{-1}$) |
|---|---|---|
| 6 | 0.0011 | 0.0010 |
| 9 | 0.0016 | 0.0020 |
| 12 | 0.0028 | 0.0031 |
| 15 | 0.0043 | 0.0046 |
| 18 | 0.0066 | 0.0063 |

## C.2 RAW DATA FROM CHAPTER 5

### C.2.1 THE EFFECT OF HYDRODYNAMIC STRESS ON CULTURE MORPHOLOGY

**Table C.25**: Change in normalised Weibull parameters a, b and $X_0$ describing the cell size distribution as a function of solids loading: (Figure 5.21).

| Quartzite loading (%, w/v) | Parameter | | |
|---|---|---|---|
| | a | b | $X_0$ |
| 0 | 1.00 | 1.00 | 1.00 |
| 6 | 0.95 | 0.81 | 0.95 |
| 9 | 0.98 | 0.84 | 0.95 |
| 12 | 0.85 | 0.83 | 0.93 |
| 15 | 0.35 | 0.96 | - |
| 18 | 0.35 | 0.96 | 0.90 |

University of Cape Town

## C.2.2 THE EFFECT OF HYDRODYNAMIC STRESS ON CULTURE METABOLIC ACTIVITY

**Table C.26**: Specific OUR as a function of time for reactors containing 0 to 18 % w/w quartzite and operated at 1.97 m $s^{-1}$: (Figure 5.24).

| Time (h) | Specific OUR ($\mu lO_2$ $cell^{-1}$ $min^{-1}$); experimental set 1 | | | |
|---|---|---|---|---|
| | 0 % quartzite | 6 % quartzite | 9 % quartzite | 12 % quartzite |
| 24 | 1.3E-09 | 1.3E-09 | 1.3E-09 | 1.3E-09 |
| 48 | 1.2E-09 | 1.0E-09 | 9.5E-10 | 5.6E-10 |
| 96 | 9.9E-10 | 9.1E-10 | 8.6E-10 | 7.0E-10 |
| 168 | 8.9E-10 | 6.7E-10 | 6.5E-10 | 5.5E-10 |

| Time (h) | Specific OUR ($\mu lO_2$ $cell^{-1}$ $min^{-1}$); experimental set 2 | | |
|---|---|---|---|
| | 0 % quartzite | 15 % quartzite | 18 % quartzite |
| 24 | 2.6E-09 | 2.6E-09 | 2.7E-09 |
| 48 | 1.7E-09 | 8.5E-10 | 1.0E-09 |
| 96 | 1.5E-09 | 8.0E-10 | 7.0E-10 |
| 168 | 1.2E-09 | 7.1E-10 | 6.8E-10 |

University of Cape Town

# Appendix D: Power measurements

**Table D.1**: Power input per unit volume corresponding to impeller tip speeds and solids loadings utilised in Section 4.7

| Solids loading (%, w/w) | P/V (W $m^{-3}$) | | |
|---|---|---|---|
| | 1.67 m $s^{-1}$ | 1.97 m $s^{-1}$ | 2.13 m $s^{-1}$ |
| 0 | 605 | 1097 | 1386 |
| 3 | 686 | 1097 | 1489 |
| 9 | 686 | 1287 | 1592 |

University of Cape Town

# Appendix E: t-Test: paired two sample for means for normalised process data presented in Section 4.6.2

**Table E.1:** t-Test comparing normalised redox potential for 0 and 6 % quartzite and 0 and 9 % quartzite (data presented in Figure 4.15).

| t-Test: Paired Two Sample for Means | | | t-Test: Paired Two Sample for Means | | |
|---|---|---|---|---|---|
| | Quartzite concentration | | | Quartzite concentration | |
| | *0 %* | *6 %* | | *0 %* | *9 %* |
| Mean | 1 | 0.980851 | Mean | 1 | 0.977344 |
| Variance | 0 | 7.01E-05 | Variance | 0 | 0.000129 |
| Observations | 9 | 9 | Observations | 9 | 9 |
| Hypothesized Mean Difference | 0 | | Hypothesized Mean Difference | 0 | |
| df | 8 | | df | 8 | |
| t Stat | **6.859713** | | t Stat | **5.994642** | |
| P(T<=t) one-tail | 6.49E-05 | | P(T<=t) one-tail | 0.000163 | |
| t Critical one-tail | 1.859548 | | t Critical one-tail | 1.859548 | |
| P(T<=t) two-tail | 0.00013 | | P(T<=t) two-tail | 0.000325 | |
| t Critical two-tail | **2.306006** | | t Critical two-tail | **2.306006** | |

**Table E.2:** t-Test comparing normalised redox potential for 0 and 12 % quartzite and 0 and 15 % quartzite (data presented in Figure 4.15).

| t-Test: Paired Two Sample for Means | | | t-Test: Paired Two Sample for Means | | |
|---|---|---|---|---|---|
| | Quartzite concentration | | | Quartzite concentration | |
| | *0 %* | *12 %* | | *0 %* | *15 %* |
| Mean | 1 | 0.955642 | Mean | 1 | 0.940789 |
| Variance | 0 | 0.000612 | Variance | 0 | 0.00069 |
| Observations | 9 | 9 | Observations | 9 | 9 |
| Hypothesized Mean Difference | 0 | | Hypothesized Mean Difference | 0 | |
| df | 8 | | df | 8 | |
| t Stat | **5.379142** | | t Stat | **6.763141** | |
| P(T<=t) one-tail | 0.000331 | | P(T<=t) one-tail | 7.16E-05 | |
| t Critical one-tail | 1.859548 | | t Critical one-tail | 1.859548 | |
| P(T<=t) two-tail | 0.000662 | | P(T<=t) two-tail | 0.000143 | |
| t Critical two-tail | **2.306006** | | t Critical two-tail | **2.306006** | |

University of Cape Town

**Table E.3:** t-Test comparing normalised redox potential for 0 and 18 % quartzite (data presented in Figure 4.15).

| t-Test: Paired Two Sample for Means | | |
|---|---|---|
| | Quartzite concentration | |
| | *0 %* | *18 %* |
| Mean | 1 | 0.788163 |
| Variance | 0 | 0.007402 |
| Observations | 9 | 9 |
| Hypothesized Mean Difference | 0 | |
| df | 8 | |
| t Stat | **7.386452** | |
| P(T<=t) one-tail | 3.86E-05 | |
| t Critical one-tail | 1.859548 | |
| P(T<=t) two-tail | 7.72E-05 | |
| t Critical two-tail | **2.306006** | |

**Table E.4:** t-Test comparing normalised cell concentration for 0 and 6 % quartzite and 0 and 9 % quartzite (data presented in Figure 4.17).

| t-Test: Paired Two Sample for Means | | | t-Test: Paired Two Sample for Means | | |
|---|---|---|---|---|---|
| | Quartzite concentration | | | Quartzite concentration | |
| | *0 %* | *6 %* | | *0 %* | *9 %* |
| Mean | 1 | 0.929613 | Mean | 1 | 0.975534 |
| Variance | 0 | 0.002068 | Variance | 0 | 0.007218 |
| Observations | 9 | 9 | Observations | 9 | 9 |
| Hypothesized Mean Difference | 0 | | Hypothesized Mean Difference | 0 | |
| df | 8 | | df | 8 | |
| t Stat | **4.64389** | | t Stat | **0.863923** | |
| P(T<=t) one-tail | 0.000829 | | P(T<=t) one-tail | 0.206391 | |
| t Critical one-tail | 1.859548 | | t Critical one-tail | 1.859548 | |
| P(T<=t) two-tail | 0.001658 | | P(T<=t) two-tail | 0.412782 | |
| t Critical two-tail | **2.306006** | | t Critical two-tail | **2.306006** | |

**Table E.5:** t-Test comparing normalised cell concentration for 0 and 12 % quartzite and 0 and 15 % quartzite (data presented in Figure 4.17).

| t-Test: Paired Two Sample for Means | | | t-Test: Paired Two Sample for Means | | |
|---|---|---|---|---|---|
| | Quartzite concentration | | | Quartzite concentration | |
| | *0 %* | *12 %* | | *0 %* | *15 %* |
| Mean | 1 | 0.852867 | Mean | 1 | 0.7703 |
| Variance | 0 | 0.006773 | Variance | 0 | 0.011344 |
| Observations | 9 | 9 | Observations | 8 | 8 |
| Hypothesized Mean Difference | 0 | | Hypothesized Mean Difference | 0 | |
| t Stat | **5.363262** | | t Stat | **6.099848** | |
| P(T<=t) one-tail | 0.000338 | | P(T<=t) one-tail | 0.000246 | |
| t Critical one-tail | 1.859548 | | t Critical one-tail | 1.894578 | |
| P(T<=t) two-tail | 0.000675 | | P(T<=t) two-tail | 0.000491 | |
| t Critical two-tail | **2.306006** | | t Critical two-tail | **2.364623** | |

University of Cape Town

**Table E.6:** t-Test comparing normalised cell concentration for 0 and 18 % quartzite (data presented in Figure 4.17).

| t-Test: Paired Two Sample for Means | | |
|---|---|---|
| | Quartzite concentration | |
| | *0 %* | *18 %* |
| Mean | 1 | 0.424444 |
| Variance | 0 | 0.055845 |
| Observations | 8 | 8 |
| Hypothesized Mean Difference | 0 | |
| df | 7 | |
| t Stat | **6.888749** | |
| P(T<=t) one-tail | 0.000117 | |
| t Critical one-tail | 1.894578 | |
| P(T<=t) two-tail | 0.000234 | |
| t Critical two-tail | **2.364623** | |

**Table E.7:** t-Test comparing normalised percentage iron solubilised for 0 and 6 % quartzite and 0 and 9 % quartzite (data presented in Figure 4.20).

| t-Test: Paired Two Sample for Means | | | t-Test: Paired Two Sample for Means | | |
|---|---|---|---|---|---|
| | Quartzite concentration | | | Quartzite concentration | |
| | *0 %* | *6 %* | | *0 %* | *9 %* |
| Mean | 1 | 0.912747 | Mean | 1 | 0.901573 |
| Variance | 0 | 0.006804 | Variance | 0 | 0.001858 |
| Observations | 9 | 9 | Observations | 9 | 9 |
| Hypothesized Mean Difference | 0 | | Hypothesized Mean Difference | 0 | |
| df | 8 | | df | 8 | |
| t Stat | **3.173267** | | t Stat | **6.850304** | |
| P(T<=t) one-tail | 0.006565 | | P(T<=t) one-tail | 6.55E-05 | |
| t Critical one-tail | 1.859548 | | t Critical one-tail | 1.859548 | |
| P(T<=t) two-tail | 0.01313 | | P(T<=t) two-tail | 0.000131 | |
| t Critical two-tail | **2.306006** | | t Critical two-tail | **2.306006** | |

**Table E.8:** t-Test comparing normalised percentage iron solubilised for 0 and 12 % quartzite and 0 and 15 % quartzite (data presented in Figure 4.20).

| t-Test: Paired Two Sample for Means | | | t-Test: Paired Two Sample for Means | | |
|---|---|---|---|---|---|
| | Quartzite concentration | | | Quartzite concentration | |
| | *0 %* | *12 %* | | *0 %* | *15 %* |
| Mean | 1 | 0.813152 | Mean | 1 | 0.778291 |
| Variance | 0 | 0.007671 | Variance | 0 | 0.012601 |
| Observations | 9 | 9 | Observations | 9 | 9 |
| Hypothesized Mean Difference | 0 | | Hypothesized Mean Difference | 0 | |
| t Stat | **6.400178** | | t Stat | **5.92505941** | |
| P(T<=t) one-tail | 0.000105 | | P(T<=t) one-tail | 0.000175843 | |
| t Critical one-tail | 1.859548 | | t Critical one-tail | 1.85954832 | |
| P(T<=t) two-tail | 0.000209 | | P(T<=t) two-tail | 0.000351685 | |
| t Critical two-tail | **2.306006** | | t Critical two-tail | **2.306005626** | |

University of Cape Town

**Table E.9:** t-Test comparing normalised percentage iron solubilised for 0 and 18 % (data presented in Figure 4.20).

| t-Test: Paired Two Sample for Means | | |
|---|---|---|
| | Quartzite concentration | |
| | *0 %* | *18 %* |
| Mean | 1 | 0.382881 |
| Variance | 0 | 0.060292 |
| Observations | 9 | 9 |
| Hypothesized Mean Difference | 0 | |
| t Stat | **7.539789** | |
| P(T<=t) one-tail | 3.34E-05 | |
| t Critical one-tail | 1.859548 | |
| P(T<=t) two-tail | 6.67E-05 | |
| t Critical two-tail | **2.306006** | |

**Table E.10:** t-Test comparing normalised percentage copper solubilised for 0 and 6 % quartzite and 0 and 9 % quartzite (data presented in Figure 4.23).

| t-Test: Paired Two Sample for Means | | | t-Test: Paired Two Sample for Means | | |
|---|---|---|---|---|---|
| | Quartzite concentration | | | Quartzite concentration | |
| | *0 %* | *6 %* | | *0 %* | *9%* |
| Mean | 1 | 0.920812 | Mean | 1 | 0.930448 |
| Variance | 0 | 0.003041 | Variance | 0 | 0.00449 |
| Observations | 9 | 9 | Observations | 9 | 9 |
| Hypothesized Mean Difference | 0 | | Hypothesized Mean Difference | 0 | |
| t Stat | **4.307886** | | t Stat | **3.113743** | |
| P(T<=t) one-tail | 0.001294 | | P(T<=t) one-tail | 0.007182 | |
| t Critical one-tail | 1.859548 | | t Critical one-tail | 1.859548 | |
| P(T<=t) two-tail | 0.002588 | | P(T<=t) two-tail | 0.014364 | |
| t Critical two-tail | **2.306006** | | t Critical two-tail | **2.306006** | |

**Table E.11:** t-Test comparing normalised percentage copper solubilised for 0 and 12 % quartzite and 0 and 15 % quartzite (data presented in Figure 4.23).

| t-Test: Paired Two Sample for Means | | | t-Test: Paired Two Sample for Means | | |
|---|---|---|---|---|---|
| | Quartzite concentration | | | Quartzite concentration | |
| | *0 %* | *12 %* | | *0 %* | *15 %* |
| Mean | 1 | 0.815935 | Mean | 1 | 0.780718 |
| Variance | 0 | 0.006777 | Variance | 0 | 0.008751 |
| Observations | 9 | 9 | Observations | 9 | 9 |
| Hypothesized Mean Difference | 0 | | Hypothesized Mean Difference | 0 | |
| t Stat | **6.707493** | | t Stat | **7.032333** | |
| P(T<=t) one-tail | 7.58E-05 | | P(T<=t) one-tail | 5.45E-05 | |
| t Critical one-tail | 1.859548 | | t Critical one-tail | 1.859548 | |
| P(T<=t) two-tail | 0.000152 | | P(T<=t) two-tail | 0.000109 | |
| t Critical two-tail | **2.306006** | | t Critical two-tail | **2.306006** | |

University of Cape Town

**Table E.12:** t-Test comparing normalised percentage copper solubilised for 0 and 18 % quartzite (data presented in Figure 4.23).

| t-Test: Paired Two Sample for Means | | |
|---|---|---|
| | Quartzite concentration | |
| | *0 %* | *18 %* |
| Mean | 1 | 0.578217 |
| Variance | 0 | 0.031049 |
| Observations | 9 | 9 |
| Hypothesized Mean Difference | 0 | |
| df | 8 | |
| t Stat | **7.181021** | |
| P(T<=t) one-tail | 4.71E-05 | |
| t Critical one-tail | 1.859548 | |
| P(T<=t) two-tail | 9.42E-05 | |
| t Critical two-tail | **2.306006** | |

University of Cape Town

# Appendix F: ANOVA two-factor with replication for cell size data presented in Figure 5.20

**Table F.1:** Cell size data as a function of time for 0 and 18 % quartzite loadings operated at an impeller tip speed of 1.97 m $s^{-1}$.

| Sample | Time (h) | Quartzite loading | |
|---|---|---|---|
| | | 0 % | 18 % |
| | | $X_0$ (μm) | |
| 1 | 0 | 0.900 | 0.915 |
| 2 | | 0.906 | 0.921 |
| 3 | | 0.894 | 0.921 |
| 1 | 24 | 0.904 | 0.920 |
| 2 | | 0.910 | 0.926 |
| 3 | | 0.910 | 0.914 |
| 1 | 72 | 0.973 | 0.892 |
| 2 | | 0.967 | 0.887 |
| 3 | | 0.967 | 0.898 |
| 1 | 144 | 1.008 | 0.850 |
| 2 | | 1.001 | 0.844 |
| 3 | | 1.015 | 0.856 |
| 1 | 168 | 0.978 | 0.835 |
| 2 | | 0.984 | 0.840 |
| 3 | | 0.972 | 0.829 |

**Table F.2:** ANOVA for cell size data presented in Table F.1 (significant at the 99.99 % level).

| ANOVA | | | | | | |
|---|---|---|---|---|---|---|
| *Source of Variation* | *SS* | *df* | *MS* | *F* | *P-value* | *F crit* |
| Sample | 0.002976 | 4 | 0.000744 | 25.43808 | 1.34E-07 | 4.43069 |
| Columns | 0.036116 | 1 | 0.036116 | **1234.981** | 1.88E-19 | **8.095958** |
| Interaction | 0.041794 | 4 | 0.010448 | 357.2795 | 2.72E-18 | 4.43069 |
| Within | 0.000585 | 20 | 2.92E-05 | | | |
| | | | | | | |
| Total | 0.081471 | 29 | | | | |

University of Cape Town